Investigation of CT Dosimetry Techniques for Use in Optimisation of Automatic Tube Current Modulation (ATCM) Performance

Supawitoo Sookpeng
BSc (Hons), MSc (Radiation Science)

Submitted in fulfilment of the requirements for the Degree of PhD

School of Medicine
College of Medical, Veterinary & Life Sciences
University of Glasgow

June 2014

Abstract

The PhD project aimed to develop methodologies for optimisation of automatic tube current modulation (ATCM) performance for the four most important computed tomography (CT) scanner manufacturers (Toshiba, GE, Philips and Siemens scanners). Since the human body to which ATCM response is elliptical in shape, the project started with an investigation of differences between dosimetry in cylindrical and elliptical phantoms. The ATCM systems modulate the tube current in both the x-y plane and z-axis, therefore phantoms made from multiple sections of different size ellipses were designed for quality control of the ATCM performances and evaluated by comparing with a conical phantom developed by imaging performance and assessment of CT (ImPACT) evaluation centre, UK. In order to link the project into patient dose optimisation, CT scanners in which patient doses were high were identified and the link with patient size evaluated. Since the large variations in patient dose may be influenced by scan parameters, the phantom developed was used to carry out measurements on CT scanners and investigate some factors and attribute reasons for the high doses. Finally changes in CT scanner protocols were recommended.

The results from the elliptical phantom showed that the doses in the centre and anterior were larger than in the cylinder, while doses in the lateral periphery were similar. Differences in ratios of doses between the two phantoms for different CT scanners are linked to the beam profiles produced by the individual bow tie filters. Phantoms made from multi elliptical sections demonstrated similar trends for the Philips and Siemens ATCM systems. However, the abrupt changes in attenuation provoked the ATCMs to increase tube current aggressively with the GE and Toshiba systems. A phantom like a wedding cake with broader sections and smaller differences in attenuation circumvented these effects. The volume weighted CT dose index ($CTDI_{vol}$) increased significantly with patient size for Toshiba and GE scanners whilst the changes for Siemens and Philips scanners were less marked. However, the use of Philips the D-DOM ATCM option led to a significant increase in patient dose. The reconstruction filter and image thickness are major factors influencing patient dose for the Toshiba CT scanner.

Table of Content

List of Tables

List of Figures

Acknowledgement

I would like to express my deepest appreciation to my supervisor Dr Colin J Martin, who has shown the attitude and the substance of a genius. He continually and persuasively conveyed a spirit of adventure in regard to this research. Without his supervision and knowledge this thesis would not have been possible. I would also like to give special gratitude to my co-supervisor, Dr David J Gentle, whose contribution, stimulating suggestions and encouragement helped me to coordinate my project especially in collecting data from CT scanners.

Besides my supervisors, I would like to thank the external advisors, Prof. David Keating, Prof. Alex Elliot, Mr Martin Glegg, and the rest of my thesis committee: Dr David Sutton, Dr John Foster and Prof. David Keating.

I would like to thank my partner, Mr Narin Aiummongkol, for his love, kindness and support he has shown during the past several years it has taken me to finalize this thesis. I would also like to thank my aunt, Mrs Renu Sookpeng, and my late uncle, Mr Mongkol Sookpeng, for their endless love and unconditional support. My sincere thanks also go to Mrs Marian Martin and the Martin family for the warm welcome during my stay in Glasgow.

Furthermore I would also like to acknowledge with much appreciation the staff of Glasgow Health Physics, who gave the permission to use all required equipment and the necessary materials to complete the thesis. I would also like to thank Mr Matthew J Carter, Mr David Robertson for their assistance in operating CT scanners and Dr Gurpreet Singh and Mrs Margaret Campbell for their help.

The success of the project depends largely on the encouragement and guidelines of others. I take this opportunity to express my gratitude to the people who have been instrumental in the successful completion of this thesis. I wish to acknowledge the assistance of Dr Maris Rosario Lopez Gonzalez, Deptartment of Clinical Physics, College of Medical, Veterinary and Life Sciences, University of Glasgow, for her assistance in the Matlab, Mr Douglas Alexander, a friendly

Toshiba engineer, to help operate the scanner in service mode for the bow-tie filter dose profile measurement, Ms Sue Edyvean for loan of the ImPACT conical Phantom, Mr Robin Sayer, Mr Alan McIntyre and Mr Ramsay Thompson, Mechanical Engineering Service, for developing CT phantoms. I wish to thank Ms Amy Pedvin (Philips CT applications specialist), Mr Mark Thomas, Mr Neil Baker, Mr Mark Condron and Mr Roy Irwan (Toshiba CT applications specialists) for information of CT ATCM systems.

I would like to express my gratitude to radiographers for their help with the scans of abdomen and pelvis phantom for chapter 6 and the patient dose survey completion for chapter 7. I wish to thank Dr Jen Dennis for her analysis of patient dose survey, 2011 and Mr Ron Corrigall for his help in collecting patient dose data, 2013. Also I would like to express my appreciation to 'Image Owl©' for the Catphan®600 phantom QA analysis software and Ms Audrey Trotter for her assistant for gaining access the CT scanner at Stobhill hospital.

Last but not least, I would also like to thank to the Royal Thai Government and the Ministry of Science and Technology, Thailand for their financial support granted through PhD fellowship.

Author's declaration

I declare that this dissertation is the result of my own work and has not been submitted for any other degree at the University of Glasgow or any other institution. Matlab programming contributing to the analysis was performed by Dr Maria del Rosario Lopez-Gonzalez, and an Auto mA plugin written by Dr David J Gentle was used in the analysis, and explicit reference is made to these contributions in the text at the appropriate places.

Signature _____

Printed name Supawitoo Sookpeng

Publications arising from this work

1. Sookpeng S, Martin J C and Gentle J D 2013 A study of dose distribution and image quality under an automatic tube current modulation (ATCM) system for a Toshiba aquilion 64 CT scanner using a new design of phantom [published conference paper] Available at http://www.waset.org/journals/waset/v73/V73-17.pdf

2. Sookpeng S, Martin J C and Gentle J D 2013 A study of CT dose distribution in an elliptical phantom and the influence of automatic tube current modulation in the x-y plane*. J. Radiol. Prot.* 33 (2013) 461-83

3. Sookpeng S, Martin J C and Gentle J D 2013 Comparison of different phantom designs for CT scanner Automatic Tube Current Modulation (ATCM) system test *J. Radiol. Prot.* 33 (2013) 735-761

4. Sookpeng S, Martin J C, Gentle J D and M R Lopez-Gonzalez Relationships between patient sizes, doses and image noise under automatic tube current modulation (ATCM) systems *J. Radiol. Prot.* 34 (2014) 103-123

Permissions to reproduce published papers had been granted by institute of physics (IOP) publishing and world academy of science, engineering and technology publishing.

Definitions/Abbreviations

ATCM	Automatic tube current modulation
AK	Air Kerma
AP	Anteroposterior
CAP	Chest, abdomen and pelvis
CTDI	Computed tomography dose index
$CTDI_w$	Weighted computed tomography dose index
$CTDI_{vol}$	Volume weighted computed tomography dose index
DICOM	Digital imaging and communications in medicine
DLP	Dose length product
D_{eq}	Cumulative equilibrium dose
ESAK	Entrance surface air kerma
KERMA	Kinetic energy released per unit mass
ℓ	Chamber length
L	Scan length
mAs	Tube current times product
NI	Noise index
PACS	Picture Archiving and Communications System
QRM	Quality reference mAs
ROI	Region of interest
SSDP	Single scan dose profile
SPR	Scanned projection radiography

1 Introduction

1.1 Rationale

Computed Tomography (CT) scanner technology has been developed significantly since the first CT scanner was constructed in early 1970s (Kalender, 2005). Initial CT scanners were single slice axial, but technological development has seen the introduction of helical and multi-slice models. Modern scanners are capable of imaging simultaneously 64, 128 or even 320 parallel slices in one rotation (Geleijns *et al.*, 2009). Beam width has increased significantly from a standard of 10 mm to current beam widths of up to 160 mm. The use of CT has been increasing rapidly; there have been 12-fold and 20-fold increases in CT in European countries and the United States over the last 20 years (Hall and Brenner, 2008). Moreover CT is a high radiation dose examination and makes the largest contribution to the patient radiation dose from medical exposures. CT now accounts for 50% , 68% and 70 % of the collective dose in European countries, the United Kingdom and the United States, respectively (Martin, 2008; Hart *et al.*, 2010). Because the use of CT has been increasing rapidly, there has been growing concern about potential heath effects from the high doses that can be delivered (Amis *et al.,* 2007; Berrington de Gonzalez *et al.,* 2009; Smith-Bindman *et al.,* 2009), and patient dose from CT examinations has become a cause for concern among radiological professionals.

The standard method for CT dosimetry measurement has been the CT dose index (CTDI). This is designed to measure the output for a single CT slice or a limited number of slices, but is also used for measurements inside phantoms simulating parts of the body for the purpose of patient dose assessment. Scans with an axial slice include most of the radiation within the length of the standard 100 mm pencil chamber used for the measurement. However the advent of multi-slice systems with 64, 128 or more slices when used to irradiate a phantom result in a significant amount of scatter beyond the 100 mm length of the chamber (Boone, 2007; Brenner *et al.*, 2006; Dixon *et al.*, 2005 ; Dixon, 2003; Geleijns *et al.*, 2009; Morgan and Luhta, 2004; Nakonechny *et al.*, 2005). Moreover, in this case, a typical CTDI phantom which is only 150 mm long is not of sufficient length since it is unable to include contributions from radiation scattered beyond its length. Thus the link between the standard CT dosimetry

methodology and patient dose begins to break down. At the present time, there is no consensus on the technique for measuring the dose from helical scan series or the most suitable phantom. Systems that more accurately reflect the true dose require large phantoms that are impractical for routine measurements.

A literature survey of papers published in the last ten years has shown many studies (AAPM Task Group, 2010; Boone, 2007; Brenner *et al.*, 2006; Dixon, 2003; Dixon and Ballard, 2007; Morgan and Luhta, 2004; Nakonechny *et al.*, 2005) that have proposed alternative techniques for CT dosimetry. These have focused on CT dosimetry for longer body scans to measure a cumulative dose at the centre of the phantom, $D_L(0)$ and to identify an equilibrium scanning length, L_{eq}, which is the length that scatter radiation is sufficiently remote to make negligibly small additional contribution. Several studies have aimed to evaluate the relationship between patient size and CT dose in order to minimize patient dose (Israel *et al.*, 2010; Zarb *et al.*, 2010; Meeson *et al.*, 2010). However, there is no study that links together practical CT dosimetry and patient dose, and tackles the dosimetry investigation required to establish the relative performance of the options available on the scanners that can be used in optimisation of dose. Health Physics has primary responsibility for carrying out routine patient dose measurements as well as providing CT users with scientific advice on optimisation on a substantial number of CT scanners of different types. Objectives of the first phase of this PhD project were to investigate alternative techniques and phantoms for assessment of CT dose and scanner performance. These will be used to investigate the reasons why doses for patients on certain scanners are high and determine changes that might be implemented to minimize the high doses while maintaining an acceptable level of image quality. Finally, the practical application of different methods proposed for scanner dose assessment will be investigated.

Automatic tube current modulation (ATCM) systems are now available on CT scanners (Kalra *et al.*, 2004b; Lee *et al.*, 2008; Rizzo *et al.*, 2006; Söderberg and Gunnarsson, 2010) and used in the majority of patient examinations, so failure to test them is to omit a major component of the imaging system. At the present time, the routine quality control of CT scanners carried out by Health Physics does not include ATCM testing because there is no evaluation method and

standard phantom. With the ATCM system, although different CT manufacturers work on slightly different bases, the tube current is modulated while scanning according to the patient size, shape and attenuation. Therefore, the ideal phantom for testing these systems should be able to support evaluating how tube current, image quality as well as dose vary according to changes in patient size and shape. ImPACT developed a phantom for ATCM system assessment, that is a conical in shape increasing in size along the z-axis. The diameters in the x and y axis have a ratio of 3:2, which is approximately for an abdomen (Keat *et al.*, 2005). The phantom has been used by several studies (Field, 2010; Keat, 2006). However, phantoms of this type are difficult for a workshop to construct and are expensive to manufacture. The second phase of the project aimed to develop and investigate new phantoms for ATCM system testing. The ATCM systems of different CT manufacturers were then tested using the developed phantoms and the phantoms were evaluated by comparing to the ImPACT conical phantom.

Audit of CT patient dose data accessed from Radiology Information Systems (RIS) by Health Physics has revealed high doses for some patients on a number of CT scanners in the West of Scotland. CT chest abdomen pelvis (CAP) is one of the more popular CT examinations and the patient doses for this were high in some scanners, although ATCM systems had been implemented. It was uncertain whether these high doses related to the size of the patient or to other factors, so it was necessary to study how dose varied with patient size. There have been a number of studies of relationships between patient size and radiation dose received under ATCM systems (Israel *et al.*, 2010; Meeson *et al.*, 2010; Zarb *et al.*, 2010) and on the optimisation of image noise and dose as a function of patient size (Siegel *et al.*, 2004; Verdun *et al.*, 2004; Li *et al.*, 2012). The patient diameter and cross sectional area provide better estimates of patient size (AAPM, 2011) for study of the relationship with $CTDI_{vol}$ and DLP (Meeson *et al.*, 2010; Zarb *et al.*, 2010) since weight ignores more subtle differences in a patient's build and symptoms such as distended abdomen (Israel *et al.*, 2010). There have been a number of studies evaluating relationships between radiation dose and image noise in phantoms or patients of different size in single CT scanners (Meeson *et al.*, 2010; Schindera *et al.*, 2008; Siegel *et al.*, 2004). But none have investigated and compared these relationships for studies on patients with CT scanners from different manufacturers.

The ATCM systems have options for users to set the desired image quality levels and other scanning options. Individual CT users can set up their own protocols. Variation from site to site in the user selected scanning parameters had a substantial influence on the radiation doses and image quality for patients. Knowing how to use the ATCM system correctly and efficiently is very important for dose and image quality optimisation. Efficient use of the ATCM system needs a knowledge of ATCM options available on the scanner and an understanding of how all user selectable parameters including, for example, tube voltage (kVp), pitch factor, rotation time, slice thickness and reconstruction filter as well as the output value for image quality interact and change image quality and exposure factors. The last phase of the project focused on the study of relationships between patient dose, image noise and patient size under ATCM and investigating the effect of changing scan parameters and image quality settings on ATCM system operation. Since ATCM systems for individual CT scanner manufacturers aim to achieve a constant image noise for patients of differing size and shape. They define the noise as the standard deviation of the CT number in a uniform water phantom, this PhD project measured the image noise as the primary image quality indicator.

1.2 Project Goals

The PhD project has final goals to identify options for future CT dosimetry in order to devise methodologies which will fulfil the requirement of quality assurance measurement and investigate methods of optimising patient dose in CT examinations

1.3 Thesis structure

The thesis is comprised of nine chapters. The introduction and literature review are in chapters 1 and 2. Results and discussions of individual components are in chapters 3-8, while the summary of the project is shown in chapter 9. The main work of the project can be divided into three major parts. Overall picture of the project is shown in figure 1-1, parts 2 and 3 are summarised in a form of a chart shown in figure 1-2.

- Part 1: Investigation of methodologies for CT dosimetry – details are shown in chapter 3.
- Part 2: Development and evaluation of phantoms of different designs for ATCM system tests - details are shown in chapters 4-5
- Part 3: CT optimisation of patient dose and image quality – details are shown in chapters 6-8.

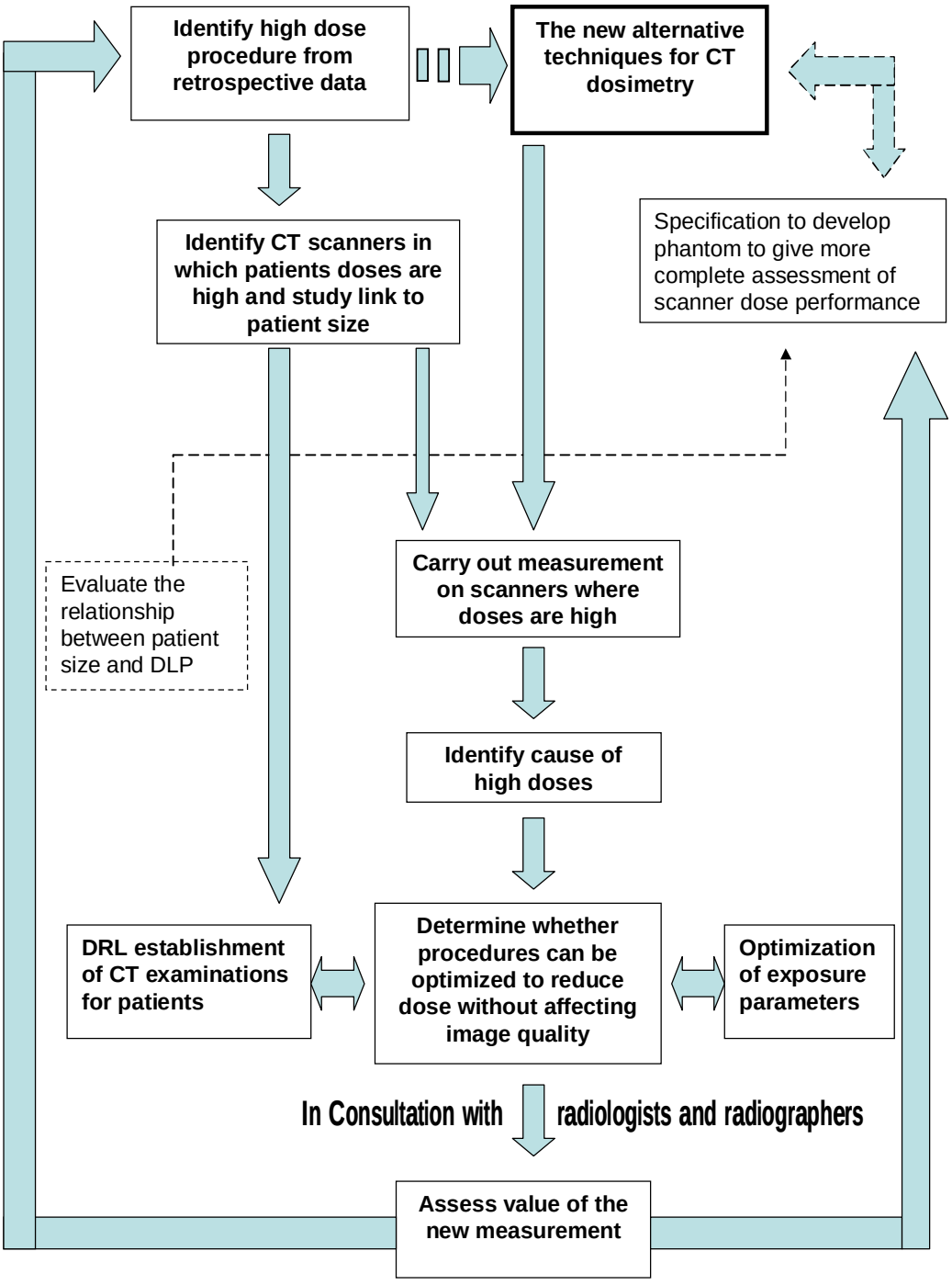

Figure 1-1 Research Idea

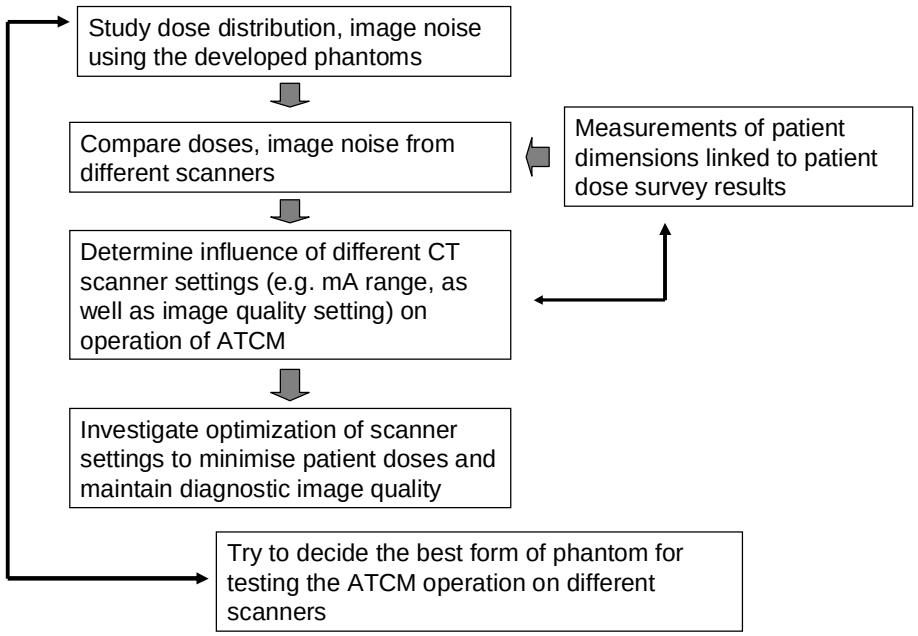

Figure 1-2 Summary of works for the second and third parts of the project

1.4 Overview

Chapter 2 provides details regarding basic knowledge of physics in CT, CT image quality, CT dosimetry, limitation of traditional CTDI measurement and alternative dosimetry techniques. The chapter also contains details for principles of different ATCM systems employed by individual CT scanners and custom made phantoms for the ATCM system tests.

Chapter 3 focused on the development of methodologies for practical implementation of proposed alternative CT dosimetry techniques. Single Scan Dose Profile (SSDP) on CT scanners were measured using Gafchromic film in cylindrical and elliptical phantoms, these were used to simulate and calculate the cumulative dose at the centres $D_L(0)$ of phantoms for various scan lengths (L). This was to confirm concerns that the current CTDI measurement using a 100 mm pencil chamber and a 150 mm long phantom length significantly underestimated the total dose. The central cumulative doses from helical scans measured by a 20 mm chamber were investigated at different scan lengths. Responses of the ATCM systems for the simple elliptical phantom were evaluated.

Chapters 4 and 5 aimed to understand responses of the ATCM systems for different CT scanner manufacturers. Alternative designs of phantom had been developed, which comprised multiple elliptical sections of different dimensions. The concept of the design is to reflect the varying dimensions along the length of the human body. The ImPACT phantom has been compared with multi-ellipse phantoms for assessing ATCM systems in terms of the dynamic changes in tube current and the image noise. The study was performed on CT scanners from four different manufacturers; Philips, Siemens, GE and Toshiba. The aims were to evaluate options for the design of phantoms, suitable for checking that ATCM systems are functioning correctly and to investigate the modes of operation of the ATCMs on different scanners, in order to gain knowledge on optimisation of image quality and patient dose.

Chapter 6, responses for ATCM systems were tested in an arthopomorphic phantom. A study carried out by scanning an abdomen pelvis phantom on different CT scanners. Entrance surface air kerma (ESAK) and image noise levels from CT abdomen pelvis examinations were measured. Routine protocols of individual CT scanners were evaluated in order to identify reasons for any high patient doses. Dose reduction potentials from the ATCM techniques were compared to fixed tube current techniques used by individual scanners.

In chapter 7, data on the patient DLPs received from CT CAP examinations within hospitals in the West of Scotland has been reviewed and reasons for high doses for a small proportion of patients on a number of CT scanners were investigated. In order to determine how different factors affect patient dose it is necessary to study how dose varies with patient size. This study involved measurement of dimensions from cross sectional patient images generated for patients with a range of different doses identified using the accession number in order to establish relationships between dose and patient size for different scanners. A detailed understanding of the interaction between scanner settings, patient dose and image quality were required, based on which recommendations for optimised scanning protocols could be made. Results were linked with those from chapter 5.

Chapter 8 focused on optimising exposure parameters. Variations from site to site in the user selected scanning parameters, identified from the results obtained from chapter 7, had shown that exposure parameters selected had a substantial influence on the radiation doses and image quality for patients under ATCM. Knowing how to use the ATCM system correctly and efficiently is very important for dose and image quality optimisation. Efficient use of the ATCM system needs knowledge of ATCM options available on the scanner and an understanding of how all user selectable parameters interact. Effects of changes in scan parameters on tube currents, dose, image noise and image quality were investigated in this chapter. Finally, strategies for CT optimisation in the West of Scotland, as an outcome of this study, were concluded.

2 Background and Related Work

The Computed Tomography (CT) scanner has been of outstanding benefit to medicine, through creating cross sectional images of the human body based on x-ray attenuation properties from computer processing of the data collected.

2.1 Development of CT scanner Technology

2.1.1 Design of CT Scanners

The first CT scanner was developed in the early 1970s by Hounsfield, a computer engineer in England (Kalender, 2005). The first generation used a pencil beam having only one detector acquired image data by a 'translate-rotate' method. The combination of the x-ray tube and detector moved in a linear motion across the patient (translate) and this was followed by a one degree rotation and this procedure repeated for 180 degree. The total scan time was more than 24 hour in the first generation of CT.

The second generation of the CT was introduced in 1972. The x-ray source was changed from the pencil beam to a narrow fan shaped beam, together with multiple detectors. The principle of the second generation CT was still 'translate and rotate'. The beam irradiated a line of detectors, so the number of translation step could be reduced and this gave a significant decrease in total scan time.

Instead of sampling a transmission profile from the pencil and the narrow fan beam, a larger fan beam coupled with a large array of detector arc in the third generation was installed in 1975. These are able to measure a complete projection, the translation motion becomes obsolete and the systems are operated with only a rotation. The x-ray tube and detector array rotates as one through 360 degree. In the fourth generation of CT, the detector configuration was changed into a stationary circular array of fixed detectors completely surrounding the patient. With the third and fourth generations of CT scanners, data accumulation times as short as 1 second are achievable. However, there is a disadvantage in the fourth generation CT scanner, since there is a need for many more detector elements, and also the x-ray tube is closer to the patient than the

detectors, a geometric magnification and also scatter artefact are large (Hendee and Ritenour, 2003).

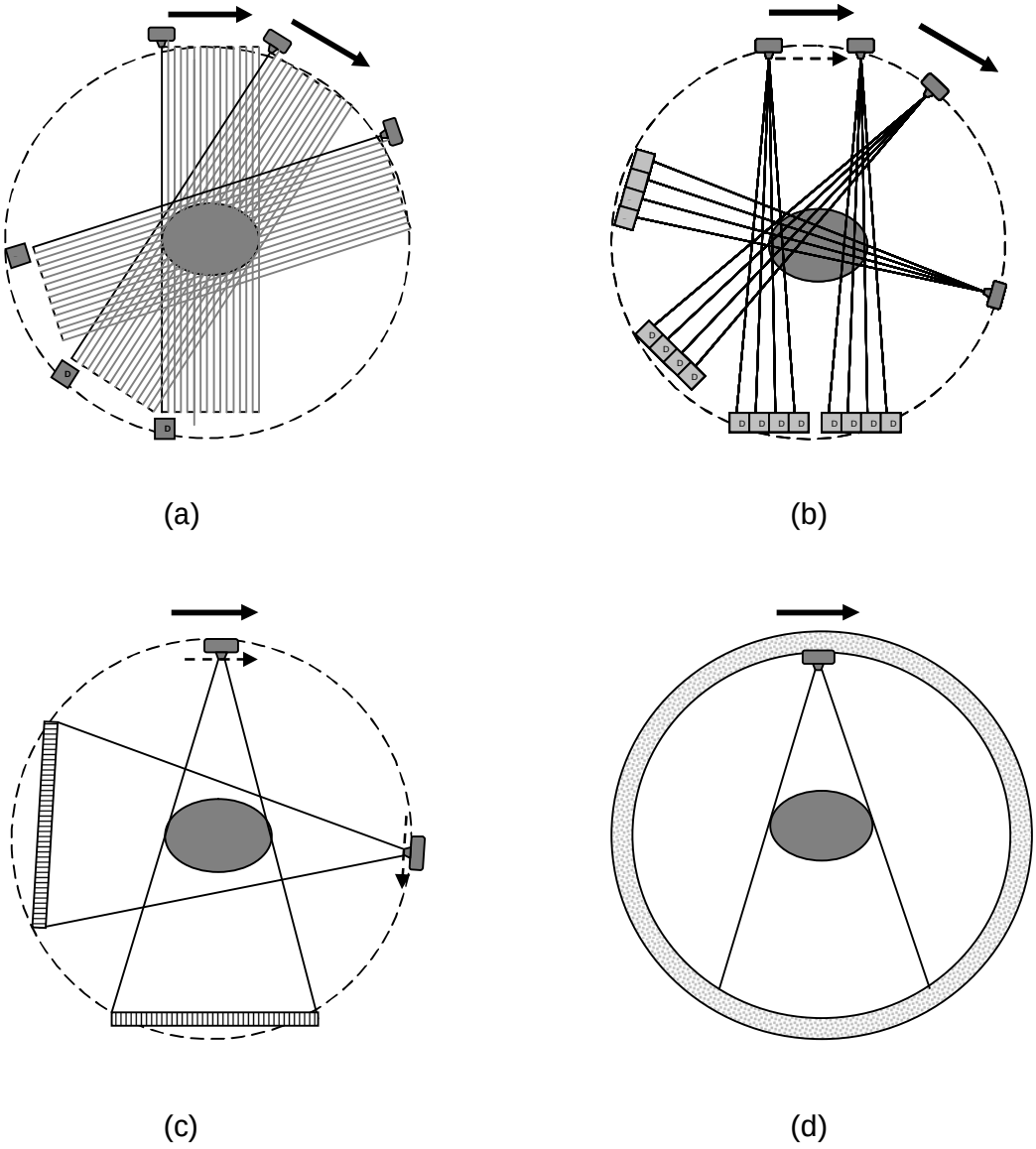

Figure 2-1 CT scanners in the (a) first, (b) second, (c) third and (d) fourth generations

After the year 1975 CT scanners have been developed from the concept of the third CT generation and were single slice axial with the detector array containing long elements along z-axis. Both of the x-ray tube and the detectors which are opposite to each other rotate around the patient, the scan is taken slice by slice and after each slice the scan stops and moves to the next slice and information is obtained. This is called conventional or sequential CT.

2.1.2 Helical CT

In 1989, technological development has seen the introduction of helical CT, with slip-ring technology invention in 1988. Slip rings are electro-mechanical devices. The design consists of sets of parallel conductive rings concentric to the gantry axis which connect to the x-ray tube, detectors and control circuit by sliding contactors. The x-ray source detector assembly is allowed to rotate continuously and a continuous scan is taken. The patient is moved continuously through the scan field in the z-direction while the gantry performs multiple 360^{o} rotations in the same direction in a spiral fashion. The helical CT is referred to as 'volume scanning', a potential advantage of the helical CT technique is a reduction of patient motion as it is a much quicker process.

In a conventional CT scanner, as discussed earlier, the slice would be moved into a particular z position, and the gantry rotated through 360 degrees to acquire all projections. However, for spiral scanning, new projections are interpolated from those available at z-positions different from that of the reconstructed slice. The simplest approach is to estimate a value at a certain position using known data from nearby points of 360^{o} linear interpolation algorithm to derive an interpolated. A slightly more sophisticated approach is to recognise that points repeat every 180 degrees, half the fan angle, and interpolate new rays from projections in opposite directions (Keat, 2005a, Keat, 2005b and Peter, 2002)

2.2 Multi Slice CT

Multi-slice CT (MSCT) has been introduced by Elscint since 1992 (Kalender 2005). The MSCT can be called in other terms such as multi row CT, multi detector row CT (MDCT). Because a helical CT scan covering the patient body is a high workload for an x-ray tube, a limitation is imposed by x-ray tube heating. Solutions to this heat issue are to develop x-ray tubes with higher heat capacities or more effectively widen the x-ray beam in the z-direction. When multiple detector rows can be used, CT can collect data from several slices at the same time. Therefore, the scan time and the heat requirement of x-ray tube is reduced. Under these conditions, the projections are not collected on a slice-by-slice basis. However, virtual projections can be constructed for each required reconstructed slice by suitable interpolation from the adjacent projections.

2.2.1 MSCT Detector

MSCT is different from single slice CT (SSCT) in terms of the detector configuration as illustrated in figure 2-2a, the detectors of MSCT are in an array segmented in the z axis which means there are more rows of detectors next to each other allowing for simultaneous acquisition of multiple images in the scan plane with one rotation (Goldman, 2008 ; Bongartz *et al.,* 2004).

An early detector design of the first modern MSCT from GE scanner consists of 16 rows of equal 1.25 mm elements in z axis (figure 2-2b), for the acquisition of 4 slices, the combinations of slice widths that can be acquired simultaneously are: , 4 × 1.25 mm, 4 × 2.5 mm, 4 × 3.75 mm and 4 × 5 mm. These can acquire up to 4 images per rotation with the maximum beam width of 20 mm. The results from thin slices can be combined to get thicker slices (ImPACT, 2002). Another detector configuration used at the beginning of the MSCT era from a Siemens scanner is called an adaptive array detector which consists of detector elements of different sizes. Individual elements of the adaptive array can be linked to acquire four slices simultaneously.

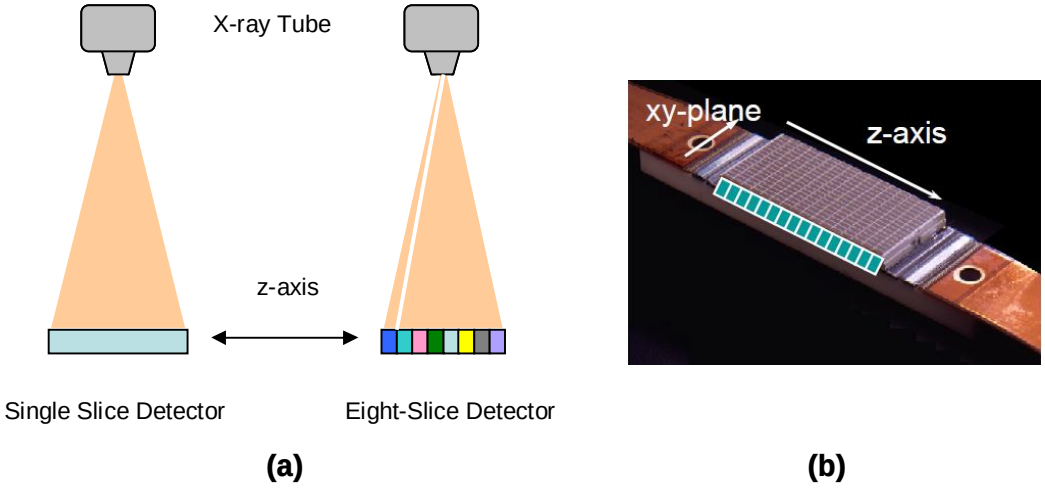

Figure 2-2 (a) Single and eight-slice detector scanners and (b) multi detector of 16 rows, 4-slice from GE scanner

16-slice GE CT scanners were introduced in 2002, detector element arrays are in the form of an adaptive array which consists of 16 x 0.625 millimetre inner detector elements, and eight outer elements which are double the size of the inner elements. This allows the simultaneous recording of 16 thin slices. Alternatively, the inner 16 elements can be linked to get thicker slices.

By 2005, 64 slice CT scanners were announced. Detector array configurations of some manufacturers are shown in figure 2-3. The design of Siemens scanner is different. They use a periodic motion of the focal spot in the longitudinal direction (z-flying focal spot) to double the number of simultaneously acquired slices. Each of the 32 detectors collects two measurements separated by 0.3 mm, therefore the net result gives a total of 64 slices (Goldman, 2008). At the present time, modern CT scanners are capable of imaging simultaneously 128 or even 320 parallel slices in one rotation (Geleijns *et al.*, 2009). Beam width has increased significantly from a standard of 10 mm to current beam widths of up to 160 mm.

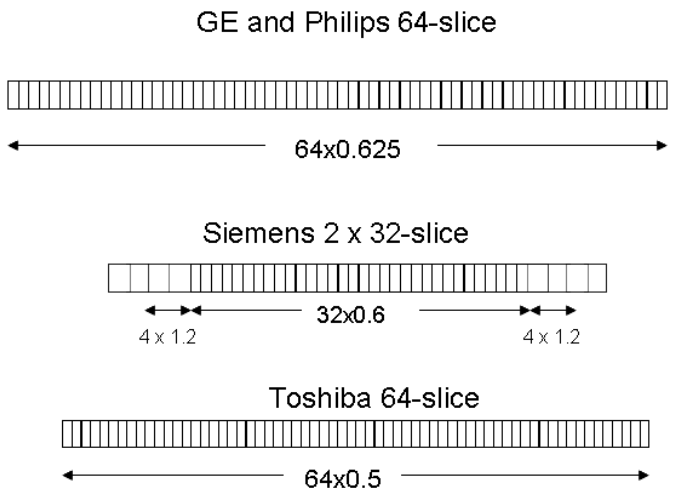

Figure 2-3 Diagrams of 64-slice detector designs in *z*-direction for different CT scanner manufacturers

2.2.2 CT scanner collimation and filtration

Collimation reduces unnecessary radiation to patients and improves the quality of the images. A distinction can be made between two types of collimator in CT scanners, pre-patient and post-patient collimators. The pre-patient collimator effectively limits the amount of x-radiation that reaches the patient. The post-patient collimator which is positioned directly in front of the detectors is used to block scattered photons from reaching the detectors, thus preventing image artefacts.

There are two major types of filtration utilized in CT scanner; mathematical and physical filters. The physical filter is discussed in this section. Beside an inherent filtration provided by the x-ray tube, there are two filters inserted for CT scanners. The common filter is a flat filter which is made from aluminium or copper. This filter is used to remove low energy photons that will be absorbed in the patient or reduce the beam-hardening artefact (Bongartz *et al*., 2004). The other type is a bow-tie filter or beam shaping filter which is made from polytetrafluoroethylene (PTFE), aluminium or Teflon. Because the human body shape is elliptical, the radiation passing through such a shape is not uniform. The bow tie filter is used for shaping the beam in the x-y plane; it absorbs off axis the radiation at the edge of field of view. The advantages of using the bow-tie filter are maintaining a more uniform x-ray field at the detector (Mahesh, 2009). Modern CT scanners have two or three different bow-tie filters which are implemented automatically for clinical scan protocols. Some scanner manufacturers provide bow-tie filters based on field of view. Therefore, choosing the appropriate protocol or scan field of view (FOV) that matches the body part being scanned can introduce the correct bow tie filter. The GE scanners have two bow-tie filters which are used for head and body scans (ImPACT, 2009). For the Toshiba Aquilion scanner, there are two bow-tie filters, small and large filters, depending on the scanning field size. The small filter is used for extra small (SS), small (S) and medium (M) FOVs. The large filter is used for large (L) and extra large (LL) FOVs. The filter movement motor is a stepping motor. This motor rotates to set the appropriate filter position (ImPACT, 2009; personal communication from a Toshiba CT scanner Engineer, June 13 2012).

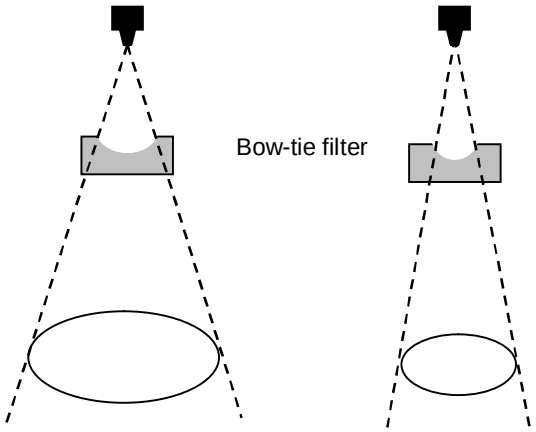

Figure 2-4 Different sizes of bow-tie filter or beam shaping filter

2.2.3 Definition of helical pitch

Currently, manufacturers of multi-slice systems employ two different definitions of pitch; detector pitch and beam pitch. The beam pitch is determined solely by the x-ray collimation and table speed, whereas the detector pitch will also depend on the number of slices acquired per rotation. The detector pitch is similar to the beam pitch on a single slice scanner.

$$Beam\ Pitch = \frac{Table\ movement\ \ per\ \ rotation}{X-ray\ beam\ width} \quad \text{.....Equation 2-1}$$

For the beam pitch, a pitch of less than 1 and a pitch of greater than 1 imply overlaps and gaps between the x-ray beams from adjacent rotations.

$$Detector\ Pitch = \frac{Table\ movement\ \ per\ \ rotation}{Detector\ acquisition\ width} \quad \text{.....Equation 2-2}$$

Therefore,

$$Detector\ Pitch = Beam\ Pitch \times No.\ of\ \ slice\ acquired \quad \text{.....Equation 2-3}$$

2.3 CT image and display

Each CT slice represents a specific plane in the patient's body. The thickness of the slice is referred to the z-axis. The data that form the CT slice are divided into elements, each one of these two dimensional squares is a pixel (picture element) with the width indicated by x and height by y. The CT image is displayed on the monitor composed of pixels. If the z-axis is taken into account, this element is referred to as a voxel (volume element). Image displayed from CT scanners is normally 512x512 in size at 16 bits per pixel therefore they contain 65,536 shades of grey scale or brightness. The level of brightness can be called various names such as pixel value, grey scale value, digital number or Hounsfield unit. The CT image does not show the linear attenuation coefficient (μ) values directly but values used are called CT numbers in Housefield units. A viewer can adjust how grey levels are to be allocated by specifying a window width or a range of CT numbers (maximum - minimum) that are distributed over the viewable grey scale, for example −100 to 200, and a window level or the CT number in the centre of the viewable grey scale.

CT number contains the μ-value of the underlying tissue in every volume element with respect to the μ-value of water. For elements having μ-values less than that of water, CT number is negative, air is a good example. Conversely, for substances having μ-values greater than that of water, CT number is positive, for example the bone (Dendy and Heatson ,2012 ; Kalender 2005).

CT number is calculated by the equation 2-4,

$$CT\ number = \frac{(\mu - \mu_{water}) \times 1000}{\mu_{water}} \quad \text{.....Equation 2-4}$$

Some typical values for CT numbers are given in table 2-1

Table 2-1 Typical CT number for different biological tissues

Tissue	Hounsfield Units Range
Air	-1000
Lung	-200 to -500
Fat	-50 to -200
Water	0
Muscle	+25 to +40
Bone	+200 to +1000

Source: Dendy and Heaton (2012)

2.3.1 Image Reconstruction

There are two major steps for image processing. The first step is data acquisition or record of projections and the second step is image reconstruction from projection. There are two major groups of reconstruction methods; analytic reconstruction, filtered back projection (FBP) and iterative reconstruction (IR) (Dendy and Heaton, 2012). CT reconstruction has traditionally been performed by FBP. It is fast but dose reduction is difficult with this technique, as reduction results in a readily perceived increase in noise. It is a modification of an older technique, called back projection or simple back projection in which an individual sample is back projected along the ray pointing to the sample to the same value. A back projected image is very blurred. Filtered back projection is a technique to correct the blurring; each view is filtered before the back projection. The procedure is to first convolve each projection with a selected filter function before back projecting convolution result to form an image. The selection of the proper filter is the key to obtaining a good reconstruction from filter (convolution) back projection (Smith, 1997).

Iterative reconstruction is more versatile but is a slower process. Commercial names for individual CT scanners are iterative Dose (iDose) in Philips, Iterative Reconstruction in Image Space (IRIS) and Sinogram Affirmed Iterative Reconstruction (SAFIRE) in Siemens, Adaptive Iterative Dose Reduction (AIDR) in Toshiba, and Adaptive Statistical Iterative Reconstruction (ASiR) in GE scanners. In principle, iterative reconstruction is an algorithm whereby image data are

modified through the use of advanced mathematical models. The principle of the iterative technique algorithm is to find a solution by successive estimates. In each cycle, the projections of the current estimate are compared with the measured projections. It can either subtract or divide the corresponding projection in order to obtain correction factors. The result of the comparison is used to modify the current estimate, thereby creating a new estimate and is used to update the original image.

2.3.2 Image reconstruction filter

The images produces by direct back-projection of attenuation profiles are unsharp, and to counteract this the profiles are convolved with a high pass filter. The choice of convolution filter kernel affects the image characteristics. A sharper filter will increase spatial resolution or edge enhancement, but also increased image noise.

There are five different types of kernels for basic protocols of the Siemens scanner; H, B, C, S and T which refer to Head, Body, Child Head, Special Application and Topogram (Siemens medical solution 2004). The image sharpness is defined by numbers, the higher the number the sharper the image, while the lower the number, the smoother the image. The endings ‘s’ ‘f’ and ‘h’ indicate standard, fast and high resolution modes. For the body scans, standard kernels B30s or B40s are recommended. Smoother images are obtained with B20s.

The Filter convolution (FC) for the Toshiba scanners can be split into two major groups, with and without beam hardening correction (BHC). For the body scan, they can also divided into body and soft tissue filters; FC01-FC05 (Body filter with BHC), FC11-FC15 (Body filter without BHC), FC07-FC09 (Soft tissue filter with BHC) and FC17-FC19 (Soft tissue filter without BHC), the lower the number of FC the smoother image and the higher the number of FC the sharper image (Toshiba’s CT user manual). The first number after FC indicates whether the BHC is used or not, e.g. FC01 and FC11 are the same reconstruction algorithm and the difference is whether BHC is used or not.

The filter for the Philips scanner has two major groups; for the body scan and cardiac scan. There are various kernels for the body scan, for example filter A,

B, C, D refer to very smooth, smooth, sharp and very sharp. The filter A is recommended for large patients, while filters B and C are recommended for the routine abdomen and pelvis. Filter D is for edge enhancement and the bone. (Philips's CT user manual). They also have other filters, for example F and L which are sharp and very sharp for scans of the lungs, knee and shoulder. Selections of resolution which are standard, high and ultra high can be made with each filter. The GE algorithm consists of soft, standard, detail, lung (chest), Bone, edge and bone plus (GE's CT user manual).

2.4 Automatic Tube Current Modulation

The Automatic Tube Current Modulation (ATCM) or automatic exposure control (AEC) systems have been another recent development in modern CT scanners. Tube current can be reduced while scanning regions of lower attenuation and increased with those of higher attenuation; the attenuation level depends on patient body size, body shape, and anatomic location. Results from many studies have shown that use of ATCM systems reduced patient dose by about 35%-60% for the body and 18% for the neck, across all sizes of patient, compared with the traditional fixed tube current techniques. These dose reductions vary between different studies and depend on the tube current being used for the fixed technique and the size of the patient. (Lee *et al.*, 2011; Soderberg & Gunnarsson, 2010; Rizzo *et al.*, 2006; Lee *et al.*, 2009; Peng *et al.*, 2009; Papadakis *et al.*, 2008).

2.4.1 Principles of ATCM system for different CT manufacturers

With the ATCM system, the traditional tube current selection is replaced by an input value which is on the basis of the required image quality. For ATCM systems, the tube current is automatically adjusted to the X-ray attenuation of the patient cross section being scanned leading to a potential for a reduction in radiation dose, while obtaining images with a consistent level of image quality (Kalender, 2005). The principles of ATCM systems for different CT scanner manufacturers and differences in translation of terms used for different manufacturers are shown in table 2-4. ATCM can be divided into angular and longitudinal modulations which adjust the tube current as the X-ray tube rotates around the patient and along the longitudinal axis, respectively.

Table 2-2 Comparison of 64 slice CT scan parameters from 4 CT scanners: Translation of terms for different manufacturers

	Toshiba Aquilion	**GE Lightspeed**	**Philips Brilliance**	**Siemens Sensation**
User interface	eXam Plan	Exam Rx	Scan Procedure	Examination
CT localizer scan projection radiograph	Scanogram	Scout	Surview	Topogram
Tube Current				
Tube current	mA	mA	-	-
Tube current time product	mAs	-	mAs	mAs
Effective Tube current time product	Effective mAs (mAs/Pitch)	-	mAs/slice (=mAs/Pitch)	Effective mAs (mAs/Pitch)
Pitch	CT Pitch Factor	Pitch	Pitch	Pitch
Automatic Tube Current Modulation (ATCM)	Sure Exposure	AutomA/Smart mA	DoseRight Automatic Current selection (ACS)	CareDose4D
Principle of ATCM	Constant target noise by varying the tube currents within the minimum and maximum limits, according to patient attenuation		Keep image quality similar to that of a reference image	Use effective mAs level by comparing to a standard patient size
Angular tube current modulation	Not as a separate item	-	D-DOM	Care Dose
Longitudinal tube current modulation	Sure Exposure	Auto mA	Z-DOM	Not as a separate item
Angular and Longitudinal tube current modulation	Sure Exposure 3D	Smart mA	-	CareDose4D
Image quality reference parameter	Standard deviation	Noise Index	Reference Image	Quality Reference mAs (QRM)
Image reconstruction property	Filter Convolution (FC)	Algorithm	Reconstruction filter	Kernel

2.4.1.1 Toshiba scanner

The Toshiba ATCM system 'SureExposure 3D' modulates the tube current by patient size, shape and attenuation and the tube current is modulated along the longitudinal (z-direction) and axial (x,y) plane (figure 2-5) (Angel, 2009; Kalra *et al*., 2004a). If a single scanned projection radiograph (SPR) is used, SureExposure will modulate the tube current in the z-direction but if a dual AP and lateral SPR is used SureExposure will modulate the tube current in all three dimensions as the tube rotates and transverses the patient. SureExposure determines the relative attenuation of a patient from SPRs and converts them into a water equivalent thickness. For z-axis modulation, the water equivalent diameter at each level of the patient is calculated and compared to the maximum attenuation. The tube current required to achieve the selected standard deviation for the maximum water equivalent diameter is applied. Tube current is then modulated to maintain the target standard deviation throughout the examination. The image quality level can be automatically set for the clinical examination. Different target image standard deviation modes are available on the Toshiba Aquilion 64. These correspond to the selection of different pre-selected image noise levels; a) high quality (standard deviation (SD) =7.5 HU), b) quality (SD=10 HU), c) standard (SD=12.5 HU), d) low dose (SD =15 HU), e) ultra low dose (SD=17.5 HU), or f) low dose ++ (SD=20.0 HU). The system also allows the user to set any standard deviation of pixel value (in Hounsfield unit) and a minimum and maximum (range) of the tube current.

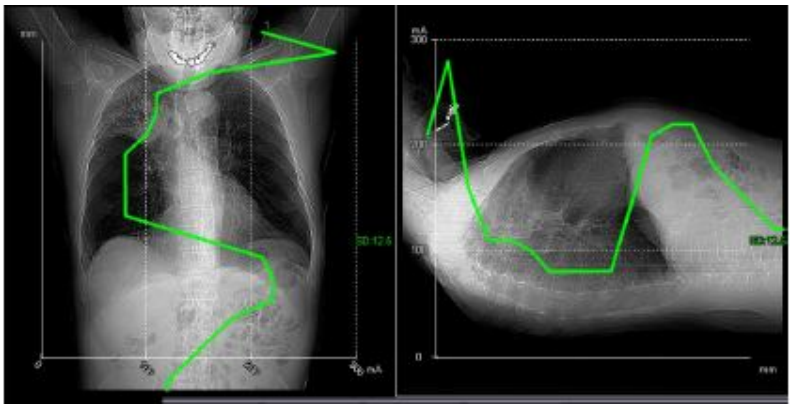

Figure 2-5 Tube current (mA) modulation pattern in x-y plane and z-axis shown on the scanner monitor prior to the scan

SureExposure aims to maintain the image quality. It is not a stand alone tube current modulation algorithm. It incorporates the selected imaging and reconstructing parameters. The primary acquisition parameters affecting image noise are pitch factor, rotation time and kVp. For example, a higher pitch can reduce the scan time but increase image noise. SureExposure counteracts this effect by adjusting the tube current to achieve the target image quality regardless of the selected pitch value.

Sure Exposure can also be incorporated with noise reduction tools. One of the noise reduction tools available on the Aquillion scanner is Quantum Denoising Software (QDS). QDS applies a combination of smoothing and enhancing filters for lower mA imaging, the image areas of soft tissue or with little edge are smoothed while sharper image areas are processed with edge enhancing filters. When QDS is used in a protocol, SureExposure decreases the tube current to account for the benefits gained from QDS (Boedeker 2010).

2.4.1.2 General Electric (GE) scanner

There are two elements of the GE ATCM system; Auto mA and Smart mA. The Auto mA provides longitudinal (z) axis modulation, whereas SmartmA enables both longitudinal and angular modulations. The quality of image depends on a selected noise index (NI). The reference NI which is a default or baseline NI for a given protocol is provided. The NI is defined as the standard deviation of pixel values in the central region of an image of a uniform water phantom (Mahesh 2009 p.121, General Electric Company 2008). The system allows the user to set the new NI value by changing the NI value itself or adjusting dose steps. The dose step value of 0 indicates that the prescribed NI is equal to the reference NI for the protocol. When the dose step is decreased by 1, the mA decreased by 10% and the NI increased by 5%. The NI value is used for estimating the tube current.

Only a SPR image is required for AutomA. A table of tube current values can be previewed before scanning. For SmartmA, the system estimates the attenuation level and the oval ratio from SPR images. The attenuation level reflects the density and size of the patient. The oval ratio reflects how circular or elliptical the patient is at that level and is estimated from brightness and width information in the scout image. To determine the appropriate tube current, the

system interpolates between the targeted NI relating noise to attenuation level and oval ratio. Using the relationships between image noise and mAs, slice thickness, and pitch factor, the mA required to achieve the prescribed noise index is calculated. For this, the tube-current is modulated four times for each rotation along the angular and longitudinal directions (Bruesewitz *et al.,* 2008). There are two tube current values in the mA table information for the Smart mA, one for the y-axis (AP) and the other for the x-axis (lateral) directions. For Auto mA, the tube current is kept constant during each rotation and only changes along the longitudinal direction. Since Smart mA reduces the mA along the axis with less attenuation (typically the AP direction), the radiation dose is reduced by an additional amount relative to Auto mA.

2.4.1.3 Philips scanner

Philips is the only one manufacturer that is not able to operate the tube current in both x-y plane and z-axis at the same time. The dose modulation for the Philips scanner is Automatic Current Selection (ACS) (Philips, 2008). Philips uses a reference image concept to modulate tube current. After a protocol is selected and a SPR is processed, the system calculates the attenuation coefficient of the patient, compares this to a tube current table stored for a reference average patient, and suggests suitable mAs values to produce CT scans with image noise similar to that of the reference image. For every 5-6 cm the patient is above the reference size the mAs is double, while the mAs is halved for each 7-8 cm smaller the patient is than the reference size.

Table 2-3 Reference size of patient for different body part, Philips scanners

	Reference Size (cm)		
Body Part	Infant	Child	Adult
Body	16	20	33
Extremity	8	12	16
Knee	8	12	16
Wrist	8	12	16

The system needs only one SPR (surview), either AP or lateral. When a dual SPR is performed only the first data is used for the ATCM system. There are two dose saving methods for the Philips scanner which are angular and z–axis dose

modulations (DOM). The angular or dynamic modulation (D-DOM) can be used independently with the ACS. It works best on eccentric body areas, for example the shoulders. The system boosts the tube current laterally and reduces the tube current in the AP direction where there is less beam attenuation, based on attenuation data received from the previous rotation. The Z-DOM differs from D-DOM; it plans the applied tube current before the X-rays are switched on. Z-DOM can only be used in conjunction with the ACS, and then the dose is modulated depending on body thickness along the z direction. The system determines the tube current time products (mAs), which will be used to achieve an appropriate image quality per slice for a particular clinical task, and increases or decreases the mAs base on the tube current table mentioned above. The system suggests the maximum mAs/slice, minimum mAs/slice and average mAs/slice. The users can review the suggested mAs and set the new values for the reference image. The older systems had a facility to learn from previous patient scans, but this meant that the average patient size changed when the operator changed the mAs from what the DoseRight ACS had suggested. The latest software versions of the Philips scanners calculate the tube current for the same reference patient size (personal communication from Philips CT application specialist, December 13 2012).

2.4.1.4 Siemens scanner

The 'CareDose 4D' ATCM system of the Siemens scanner is the combined modulation technique (xyz). It combines three different adaptation methods to optimize image quality; automatic adaptation of the tube current to patient size, to the attenuation of patient longitudinal axis and to the angular attenuation profile measured online for each single tube rotation (angular modulation).

Based on a single AP or lateral topogram, CareDose 4D determines the suitable mAs level for every section of the patient. For the z modulation component of the combined modulation technique, the attenuation profile is estimated, using a mathematical algorithm, based on patient SPR and the tube current adjusted using these data. The correlation between attenuation and tube current is defined by an analytical function which results in the optimum dose and image noise in every section of the scan. This correlation is based on a clinical

assessment of diagnostic image quality. The result is designed to give good diagnostic image quality at reasonable dose levels. The image noise is not necessarily constant for all body sizes and regions. Tube current changes less than for constant noise - for large and small patients. For every protocol, an x-ray attenuation of a standard patient size (75 kg patient) is stored and a default QRM value is related to this reference x-ray attenuation.

With angular modulation, based on the above described for z-axis modulation, the tube current is modulated automatically during the scan or in real time to achieve an optimum distribution of the x-ray intensity for every viewing angle. Tube currents reduced as a function of attenuation profile (The tube current in the AP projection is reduced when compared to the lateral projection). It estimates the attenuation profile online in real-time, and data are analysed and relayed to adapt the tube current with a 180° delay. Therefore, after the SPR has been performed the effective mAs value in the routine tab card displays the mean effective mAs estimated by CareDose4D based on the topogram. After the scan has been completed this value is updated to the mean value and it may differ from the original value because of the online modulation according to the angular attenuation profile.

The scanner specifies a quality reference mAs (QRM) for each protocol. It is expressed in term of effective mAs and is used for determining the image quality level for a standard-sized patient. After a SPR, an effective mAs is estimated and adjusted during the scan based on real time measurement of patient attenuation (Rego *et al., 2*007). CareDose4D automatically adapts the effective mAs to patient size and attenuation changes within the scan region based on a QRM. Users can change the QRM value and also modify the "strength" of the tube current modulations which determines the rate of decrease in tube current for slim patients and increase for larger patients before SPR for an advanced adjustment (Bredenhöller and Feuerlein, 2005). There are three 'strengths' of tube current adjustment; weak (low), average (medium) or strong (high). The strong increase of the tube current in obese patients and the weak decrease of the tube current in slim patients results in a higher dose and a lower noise, when compared to the average strength (figure 2-6).

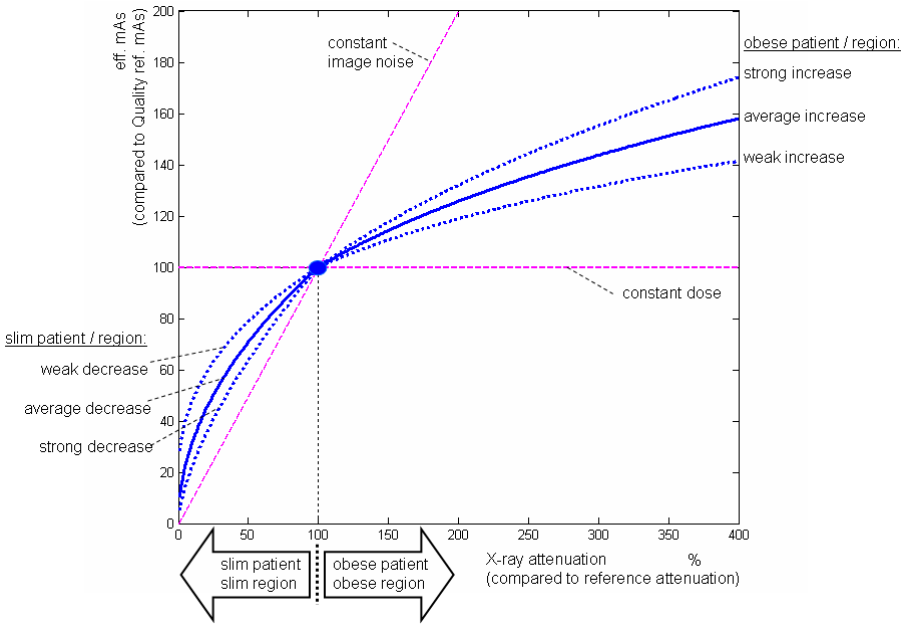

Figure 2-6 Effect of Effect of Modulation Strengths on Radiation Dose for Slim and Obese Patients
(Source: Kalra and Brady 2006)

2.5 CT Dosimetry

2.5.1 CTDI

The CTDI is the primary dose measurement concept in CT. CTDI represents the average air kerma, along the z-axis, from a series of contiguous irradiations. This is defined for axial scanning and is measured during a single rotation using a pencil ionization chamber aligned parallel to the z-axis of the CT scanner. CTDI is not patient dose but used to measure output and used to compare the radiation output levels between different CT scanners. This concept was introduced over thirty years ago in the era of single slice CT scanners with beam widths of 10 mm or less (Brenner *et al*., 2006).

$$CTDI = \frac{1}{nT}\int_{-\infty}^{+\infty} D(z)dz \quad \text{.....Equation 2-5}$$

where n is the number of slices acquired, T is the slice thickness and $D(z)$ is the radiation dose measured at position along the scanner's main axis

2.5.2 $CTDI_{100}$, $CTDI_{\ell}$, and $CTDI_{\infty}$

The methods employed for CT dosimetry in phantoms comprise a summation of contributions from the primary and scattered radiations along a given length within a phantom, as explained above. CT pencil chambers measure the integral of the dose along the length of an ionisation chamber placed across a CT slice. Thus, for a chamber of length ℓ (normally ℓ= 100 mm), the recorded measurement d_{ℓ} is given by:

$$d_{\ell} = \int_{-\frac{\ell}{2}}^{+\frac{\ell}{2}} f(z)dz \qquad \text{.....Equation 2-6}$$

where *f(z)* is the dose profile along the scan *z* axis and the unit of d_{ℓ} is dose × length.

The CTDI is expressed in air kerma and is given by:

$$CTDI_{l} = \frac{d_{l}}{nT} \qquad \text{.....Equation 2-7}$$

for a single rotation of a beam for *n* slices each of nominal width *T*. An assessment of the $CTDI_{\ell}$ with a chamber of length ℓ = 100 mm is given by:

$$CTDI_{100} = \frac{1}{nT}\int_{-50}^{+50} D(z)dz \qquad \text{..... Equation 2-8}$$

$CTDI_{250}$ refers to the CTDI measurement using a 250-mm-long ionization chamber that is integrated over ±125 mm and $CTDI_{\infty}$ refers to the CTDI measurement using an infinitely long ionization chamber, as shown in equations 2-9 and 2-10 (the $CTDI_{250}$ and $CTDI_{\infty}$ will be referred to in chapter 3).

$$CTDI_{250} = \frac{1}{nT}\int_{-125}^{+125} D(z)dz \qquad \text{.....Equation 2-9}$$

$$CTDI_{\infty} = \frac{1}{nT}\int_{-\infty}^{+\infty} D(z)dz \qquad \text{.....Equation 2-10}$$

For this project, a $CTDI_{450}$ is used as $CTDI_{\infty}$. Calculations were made of the CTDI for chambers of different lengths up to 2 metres for a Toshiba Aquillion 64 scanner at 120 kVp for a 16 mm wide beam. It showed that a chamber length of 450 mm is sufficiently long, that extending the chamber further makes negligibly small additional contributions to the scattered radiation recorded, as shown in figure 2-7. Values for $CTDI_{450}$ and $CTDI_{2000}$ were 0.2% different. Therefore it has been assumed that the measured dose for a 450 mm long chamber would be similar to that measured for an infinitely long chamber.

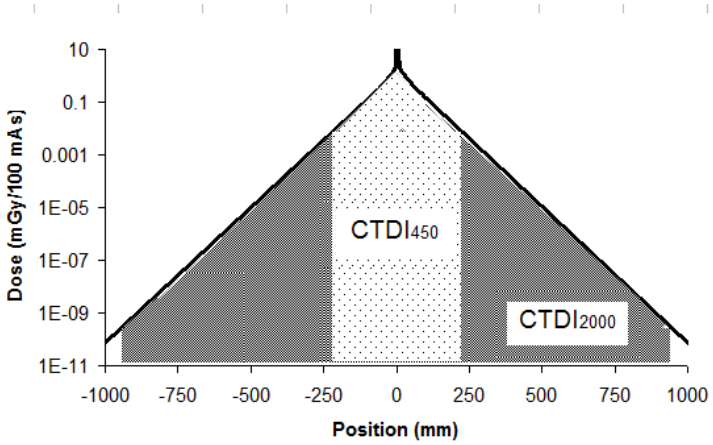

Figure 2-7 Comparisons of the intregration areas of the dose profile between $CTDI_{450}$ and $CTDI_{2000}$

(Note: The profile is measured at the anterior periphery within a cylindrical phantom, from the Toshiba Aquillion scanner for a 16 mm wide beam. Dose data for scatter tails were derived from extrapolations of the dose profile between 50-100 mm from the middle of the phantom)

2.5.3 Weighted CTDI ($CTDI_w$)

The CTDI varies across the field of view (FOV). Typically, the dose distribution within the body cross section imparted by a CT scan is much more homogeneous than that imparted by radiography, but is still somewhat larger near the skin than in the body centre. Therefore, a third measure, the weighted CTDI is introduced. $CTDI_{100}$ at the centre and periphery of standard PMMA phantoms either a 16 cm (head) or 32 cm (body) diameters are combined to give a measure relating to patient dose. The $CTDI_w$ is employed as a standard measure relating to patient dose (IEC 2003) and this is given by,

$$CTDI_w = \frac{1}{3} CTDI_{100,centre} + \frac{2}{3} CTDI_{100,periphery} \quad \text{.....Equation 2-11}$$

2.5.4 Volume-weighted CT dose index ($CTDI_{vol}$)

To represent dose for a specific scan protocol, which almost always involves a series of scans, it is essential to take into account any gaps or overlaps between the x-ray beams from consecutive rotations of the x-ray source. $CTDI_{vol}$ is a standardized parameter to measure scanner radiation out put and is an index to track across protocols for quality control purposes. The dose received from CT examinations is recorded in the Digital Imaging and Communications in Medicine (DICOM) header and displayed on the scanner screen in term of $CTDI_{vol}$ and dose length product (DLP). The $CTDI_{vol}$ is based on dose measurements in a standard CTDI phantom and a correction factor applied for pitch as explained earlier.

$$CTDI_{vol} = \frac{CTDI_{w}}{Pitch\ Factor} \quad \text{.....Equation 2-12}$$

2.5.5 Limitation of concept for CTDI measurement

The suitability of the CTDI method for measurements in phantoms particularly for the assessment of doses from helical scans has been questioned (Boone 2007, Brenner *et al*., 2006, Dixon *et al*., 2005; Dixon 2003, Nakonechny *et al*., 2005). The CTDI measurement is based on the assumption that the level of scattered radiation falls to zero within the defined distance used. However, a significant amount of the incident radiation is scattered beyond the end of the 100 mm long chambers used in practice. In addition, the advent of multi-slice systems which are capable of imaging simultaneously 64, 128 or even 320 parallel slices in one rotation present a significant issue for the 100 mm long chamber (Boone 2007; Brenner *et al.*, 2006; Dixon *et al*., 2005; Dixon 2003, Geleijns *et al.*, 2009; Nakonechny *et al*., 2005). Several studies have concluded that current techniques and phantoms are not suitable for dose measurement in MSCT (AAPM Task Group, 2010; Dixon and Ballard 2007; Nakonechny *et al*., 2005). A 150 mm long polymethymethacrylate (PMMA) cylindrical phantom used for CTDI measurement together with a 100 mm pencil chamber are not of sufficient length for wide radiation beams. Consequently the tail of scattered radiation that would contribute to the patient dose is lost and patient dose is underestimated (Geleijns *et al.*, 2009; McNitt-Gray *et al.*, 1999; Nakonechny *et al.*, 2005 ; Mori *et al.*, 2005).

2.5.6 Dose length product (DLP)

To represent the overall energy delivered by a given scan protocol, the air kerma can be integrated along the scan length and Dose-Length Product (DLP) is computed. The DLP reflects the total energy (and thus the potential biological effect) attributable to the complete scan acquisition. The DLP is the product of the $CTDI_{vol}$ and the length of scan (slice thickness × number of slices) in centimetres. DLP can be linked to the effective dose for different parts of the body (Huda *et al.,* 2008). It should be noted that the DLP is independent of patient size and age. In other words, the reported DLP is the same whether a child or an adult is scanned if the scan length and other scan parameters are the same. The relationship between patient size and effective dose is also a topic of interest. Recently, AAPM published a report on size-specific dose estimates (SSDE) it is not specific organ dose and effective dose but is a size dependent conversion factor to allow estimation of patient dose based on $CTDI_{vol}$ and patient size. For the same $CTDI_{vol}$, a smaller patient will tend to have a higher patient dose than a larger patient (AAPM, 2011) since the mean dose in the center of the scanned volume is higher.

There is a difference between the DLP and the product of the $CTDI_{vol}$ and the total imaged length. Typically, a scanner will need 1 or 2 extra rotations beyond the nominal imaged volume to gather sufficient data to reconstruct all images. An exposure time can be converted to a scan length with knowledge of a total collimation, spiral pitch and rotation time.

$$Irradiated\ length = \frac{Col\lim ation \times pitch \times \exp osure\ time}{Rotation\ time} \quad \textbf{.....Equation 2-13}$$

DLP can be calculated by multiplying this by the $CTDI_{vol}$. This will be slightly higher than the $CTDI_{vol}$ x the total imaged length since this includes overranging which is an extended scan length beyond the planed image boundaries to reconstruct the first and last sections of a helical CT scan, as mention earlier.

2.5.7 Multi scan average dose (MSAD)

CTDI can be used as a dose index for multiple rotations scanning. The average dose along the z-axis from multiple slices is known as the multiple scan average dose (MSAD). It represents the average dose across the central slice from a series of N slices (each of thickness T) when there is a constant increment between successive slices

$$MSAD = \frac{Nx\,T}{I} xCTDI \quad \text{.....Equation 2-14}$$

where *N* is the number of scans, *T* is the nominal scan width (mm), and *I* is the distance between scans (mm).

For MSCT systems, $N \times T$ is the total beam width, and *I* corresponds to the patient table advance during 1 gantry rotation. Therefore, given the definition of the pitch above, the MSAD for spiral scans can be expressed as

$$MSAD = {}^{1}\!/_{Pitch}\ xCTDI \quad \text{.....Equation 2-15}$$

Theoretically the CTDI is equivalent to the MSAD where pitch is equal to 1 (Edyvean *et al*., 2003). This means that all of the scatter tails are included and the scan interval (I) equals the nominal thickness (T).

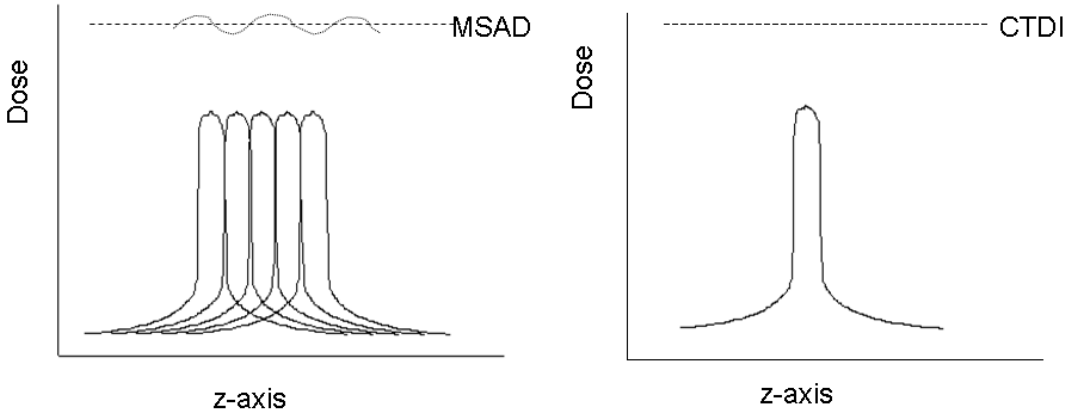

Figure 2-8 MSAD and CTDI

2.5.8 Alternative CT Dosimetry Techniques

Several alternative methodologies for CT dosimetry have been suggested; using arrays of Thermo luminescence Dosimeter (TLD) (Kyriakou *et al.*, 2008; McNitt-Gray *et al.*, 1999; Perisinakis *et al.*, 2007; Tsai *et al.*, 2003); small ionisation chambers (Nakonechny *et al.*, 2005 ; Mori *et al.*, 2005); a 300 mm long pencil chamber (Geleijns *et al.*, 2009); and simulations using Monte Carlo (MC) models (Boone, 2007; Zhou and Boone, 2008). However, each of these approaches has limitations. The use of TLD is an accurate method, but it is time consuming and large numbers of TLD are required (Nakonechny *et al.*, 2005). MC modelling is a possible alternative technique but the conversion factors used in MC are specific to the model of CT scanner and require detailed information which may not be available. Direct measurement by an ionization chamber seems to be the best choice for CT dosimetry, but there are difficulties as discussed below.

There are two major issues that must be considered with regard to the use of an ionization chamber to measure radiation dose in CT scanners. Since the trend in modern CT scanners is to have wider longitudinal collimations and longer scanning lengths, there have been a few studies suggesting the use of longer phantoms and ionization chambers e.g. a 300 mm or a 450 mm long phantom, with a 300 mm long ionization chamber (Geleijns *et al.*, 2009; Mori *et al.*, 2006; Mori *et al.*, 2005). However, such equipment might be suitable for use in a standard laboratory, but would be difficult to transport and use for routine scanner performance tests. The phantom proposed would be too heavy to lift and so present significant practical problems for routine dosimetry measurements. An alternative dosimetry method that has been proposed is the use of a short chamber in the middle of a long helical scan to establish a cumulative dose (AAPM Task Group, 2010; Dixon and Ballard, 2007).

Dixon and Ballard (2007) conducted measurements to compare results from a small ion chamber and a 100 mm pencil chamber in a 400 mm long PMMA phantom. The results showed that a small Farmer-type ionization chamber and 100 mm pencil chamber are good agreement (±2%) for the accumulated dose and $CTDI_{100}$ value at a scan length equal to the active length of the pencil chamber. This conclusion is similar to Nakonechny *et al.* (2005) who measured single scan dose profiles (SSDPs) of several slice thickness using a PTW diamond detector

and compared these results with measurement of $D_L(0)$ using an IC-10 small volume ion chamber.

For scan lengths longer than 100 mm, values for the $CTDI_{\infty}$ are higher than the $CTDI_{100}$. Boone (2007) simulated the relative air kerma along the longitudinal distance away from the edge of the primary beam by using MC simulation and also performed direct measurement, and found that at 75 mm away from the edge of the primary beam, relative air kerma is approximately 10% and 30 % of the value of the peak in head and body phantoms, respectively. Mori *et al*. (2005) carried out a longitudinal dose profile measurement of a 256 slice CT scanner in a 900 mm long PMMA cylindrical body phantom using a silicon diode detector. The scatter tails dropped off exponentially with distance from the edge of the primary beam. The magnitude relative to the peak dose is more than 1% at distances of 313 mm and 270 mm from the centre of primary beam for 138 mm and 20 mm beam widths, respectively. They concluded that scatter tails extend significantly and a minimum phantom length of 300 mm is required to collect more than 90% of the dose profile for beam widths of greater than 20 mm in body phantoms.

2.5.9 Concept of cumulative dose

An alternative dosimetry measurement proposed by the American Association of Physics in Medicine (AAPM) is the cumulative dose $D_L(0)$ in the middle of a dosimetry phantom from a helical scan of length L using a short chamber (AAPM task group 2011; Nakonechny *et al*., 2005).

The cumulative dose $D_L(z)$ at longitudinal position z within a phantom from a scan of length L can be calculated by convolving a single axial rotation with rectangular functions of varying scanning length L (AAPM Task group 2010), as shown in equation 2-16.

The distribution is smoothed by taking the averaging over an interval $z \pm \frac{b}{2}$ at each value of z.

$$D_L(z) = \frac{1}{b} f(z) \otimes \prod(z/L) = \frac{1}{b} \int_{-L/2}^{L/2} f(z - z')dz' \text{.....Equation 2-16}$$

where b is the scan interval, $\prod(z/L)$ is the rectangular function of unit height and length L, f(z) is the associated dose profile resulting from a single axial rotation, b is the midpoint-to-midpoint spacing betweenscans. The cumulative dose at the midpoint of the scanning range (z = 0) is given by:

$$D_L(0) = \frac{1}{b} \int_{-L/2}^{L/2} f(z')dz' \text{.....Equation 2-17}$$

As the scan length is extended, the cumulative dose at the midpoint of the scanning range increases due to the contributions of scatter tails from adjacent profiles. The contribution from an X-ray beam at infinity is negligible, so the cumulative dose eventually approaches an equilibrium value, or cumulative equilibrium dose as the scan length increases. This is given by:

$$D_{eq} = \frac{1}{b} \int_{-\infty}^{\infty} f(z')dz' \text{.....Equation 2-18}$$

The scanning length for which the difference between $D_L(0)$ and D_{eq} becomes negligible is called the 'equilibrium scanning length'. The quantities $D_L(0)$ and D_{eq} for an axial scan can be calculated by recording a dose profile for a single tube rotation, and combining results from sequential rotations spaced at the appropriate distance along the scanner axis.

2.5.9.1 Equilibrium length of scan

Nakonechny *et al.* (2005) concluded that dose equilibrium is only achieved at scan lengths > 300 mm suggesting that the standard CTDI phantom is not long enough. The difference in $D_L(0)$ values at the central axis for a scan length around 250 mm and 14 times the beam width ($CTDI_{14nT}$) are 25%-30% higher than $CTDI_{100}$ for nominal beam widths ranging from 3 mm to 20 mm and up to 50% for

small beam widths. $CTDI_{\infty}$ are 1.75 and 1.22 times the values of $CTDI_{100}$ in the central and peripheral positions in a body phantom, respectively (Dixon and Ballard, 2007).

2.5.10 Measurement of the dose distribution with Gafchromic film

Gafchromic film provides a method for measuring dose profiles of CT scanners. It is a self-developing radio-chromic film which has been developed for use in quality assurance in diagnostic radiology over the last few years (Gorny *et al.*, 2005; Rampado *et al.*, 2006). It has been used in a range of dosimetry applications including the assessment of skin doses in interventional radiology procedures (Giles and Murphy, 2002; Guibelalde *et al.*, 2003; Morrell and Rogers, 2004) and for carrying out CT dose profile measurements in a 320 detector row CT scanner using Gafchromic XR-QA film (Denaro and Bregant, 2011). This film has the potential for measuring CT dose distributions and responses could be derived for different lengths of detector or scans of varying length based on assessments of dose profiles. It has several advantages over other techniques for practical measurement. It has a reasonable energy response range, develops in real time, is tissue equivalent and can be handled in room light.

Gafchromic film XR-QA (International Specialty Products, Wayne, NJ) has been developed for radiology QA applications. It has an operational dose response range up to 200 mGy and energy range between 20 kVp and 200 kVp (Gorney *et al*., 2005). Investigations of the feasibility of using Gafchromic XR-QA films in dose measurement, and comparing with others dosimetry methods, has been carried out in some studies. Martin *et al* (2011) used Gafchromic XR-QA to measure the dose distribution for various CT scanners from different manufacturers, head and body CT phantoms. The results of the dose profiles can be used to simulate CTDI with ionization chamber and cumulative dose from different length of detector or scans of varying length. Gafchromic film measurements have been compared with a 20 mm ionization chamber and showed close agreement. The method for Gafchromic film calibration is discussed in chapter 3.

2.6 CT image quality

2.6.1 CT Image Quality Parameters

Factors influencing how well a CT image represents the actual object scanned are image contrast, spatial resolution, image noise, and artifacts (Goldman 2007). However, in order to assess how well an image represents patient anatomy, two main features: *detail*—or high-contrast resolution—and *contrast detectability*—or low-contrast resolution are employed.

2.6.1.1 Image noise

CT image noise is associated with the number of photons contributing to each detector measurement, increasing the number of photons will result in a smaller percentage variation between pixels. The pixel noise, designated σ is determined as the standard deviation of the values P_i from N pixels of a region of interest (ROI) in a homogeneous image section relative to their value P. It is normally measured in a water phantom (Kalender, 2005).

$$\sigma^2 = \frac{1}{N-1}.\sum_{i=1}^{N}\left(P_i - P\right)^2 \quad \text{.....Equation 2-19}$$

Noise limits low contrast resolution and may hide anatomy similar to surrounding tissue. The noise level is influenced by many parameters including tube voltage, mA, exposure time, collimation, reconstructed slice thickness, reconstruction algorithm and helical pitch (McNitt-Gray, 2013; Kalendar 2005; Brooks and DiChiro 1976). The correlation between these quantities can be formulated:

$$\sigma = f_A \cdot \sqrt{\frac{I_0 / I}{\varepsilon . mAs \ . S}} \quad \text{.....Equation 2-20}$$

where σ = standard deviation of the pixel value or CT number (noise), I_0 / I = attenuation factor of the object, ε = efficiency of the entire system, mAs = tube current scan time products, S = slice thickness. The f_A takes account the

effect of the reconstruction algorithm; sharp algorithms (high pass filter) increase the noise level while smooth algorithms (low pass filters) reduce the noise level.

When focusing on slice thickness, noise and mAs

$$S \times \sigma^2 \alpha \frac{1}{mAs} \quad \text{.....Equation 2-21}$$

From the equation; the noise increases by $\sqrt{2}$ if the mAs is reduced by half when slice thickness is kept constant and mAs doubled if slice thickness is cut by half when the noise is kept constant.

There are several recommendations for the ROI size being used for noise measurement, as shown in table 2-4. A size of selected ROI for noise measurement is also capable of measuring the standard deviation (Edyvean, 2004), use of larger ROI size results in less uncertainties of the noise measurement

Table 2-4 Recommendations for ROI sizes and Range and SD of measured noise with ROI size
(Note: Range and SD of measured noise were from the phantom having 340 diameter, the values obtained from Edyvean, 2004)

Organisation	**Recommendation**	Phantom 340 mm diameter	
		Average SD (%)	Range SD (%)
Imaging Performance Assessment of CT scanner (ImPACT)	500 mm^2 and average values from more than 10 rotations	3%	12%
Institute of Physics and Engineering in Medicine (IPEM) Report 32 (second edition)	10% -20% diameter of phantom and average values from more than 10 images	1%-2%	6%-12%
Radiological Society of North America (RSNA)	Greater than 10 mm diameter ROI	8%	34%

Source: Edyvean 2004

2.6.1.2 High contrast resolution

High-contrast resolution or spatial resolution is the level of detail that is visible on the image. It is the parameter determining the system's ability to resolve high contrast objects of small sizes that are very close together (Lois, 2013).
Spatial resolution can be measured using two methods; measured directly, or calculated. To measure the spatial resolution directly, a *line pair phantom* is used. A module inside the Catphan®600 phantom having closely spaced metal strips imbedded in it is commonly used. Each bar plus adjacent space is referred to as a line-pair (lp). The phantom is scanned, and the numbers of strips that are visible are counted. The spatial frequency in line-pairs per centimeter, defined as in equation 2-16, where bar width is in centimeters (Goldman, 2007)

$$Spatial\ Frequency = \frac{1}{2 \times bar\ width} \quad \text{.....Equation 2-22}$$

Spatial resolution can be defined in terms of using the modulation transfer function (MTF). Several quantitative methods have been described for measuring MTF such as scanning a wire, bead or bar pattern (Keat, 2005). In theory, MTF is calculated using the Fourier transform of the line spread function (Akbari *et al.,* 2010). The MTF depends on the size or spatial frequency of the object. A smaller object of higher spatial frequency is not accurately depicted on the CT image. The MTF scale is normally from 0 to 1. If the image reproduces the object exactly, the MTF would have a value of 1. If the image contained no information about the object, the MTF would be zero. An MTF curve that extends farther to the right indicates higher spatial resolution and better ability to reproduce small objects (Joseph and Rose, 2013). Sharp convolution kernels preserve higher spatial frequencies but the smooth convolution kernels reduce the higher frequency contribution. As shown in figure 2-9, at 10% value, the smooth, standard and sharp kernels obtain values at 12 $lp.cm^{-1}$, 15.5 $lp.cm^{-1}$ and 18 $lp.cm^{-1}$, respectively.

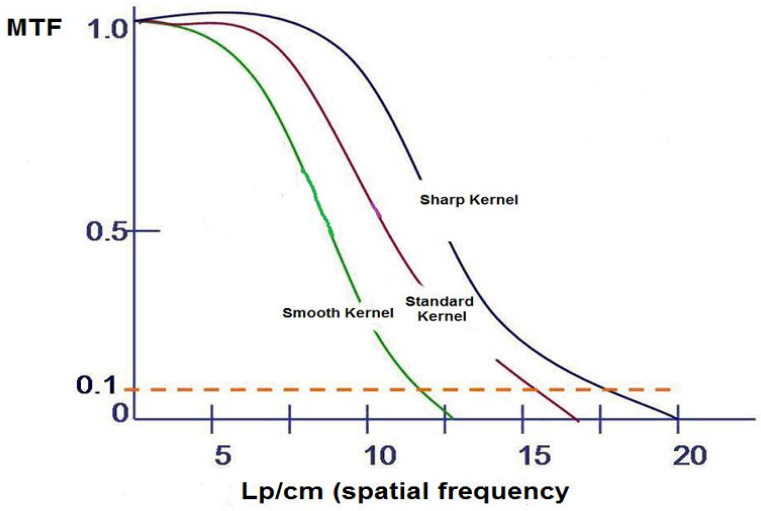

Figure 2-9 Comparison of spatial resolution for various convolution kernels

2.6.1.3 Low contrast resolution

Low-contrast resolution is the ability of the system to differentiate between objects with similar densities. It is often determined using objects having a very small difference from the background. The visibility of low contrast objects is constrained mainly by the contrast level, image noise and window setting of the display (Morin, 2004). High noise in the image will cause a decrease in low-contrast resolution. Typically, low contrast detectability can be evaluated by subjective and objective methods using phantoms containing low contrast targets of different diameters and contrasts. The subjective method requires an observer to detect objects as distinct. Several objective or quantitative methods have been proposed (Image owl, 2013) these are based on calculations of the difference in contrast to noise ratio of objects and background using mathematical algorithms. Image owl software used for this project couples with an image obtained from a scan of Catphan®600 phantom, at each target size (2-9 mm and 15 mm), circular ROIs are generated in the background. The mean CT number and SD for the sets of ROIs are calculated. A detection level for each target size is calculated, with a detectability factor of 4, as 4 times the SD.

2.6.2 Catphan®600 Phantom

Catphan®600 is widely used in the UK for testing the performance of CT scanners. The phantom consists of five modules to check the image quality which are CTP404 (slice width, sensitometry and pixel size), CTP591 (bead geometry), CTP528 (line pair resolution and point source), CTP515 (sub slice and supra slice low contrast) and CTP486 (image uniformity) (figure 2-10). Details regarding application of each module are available in the Catphan®600 manual (The Phantom Laboratory, 2006).

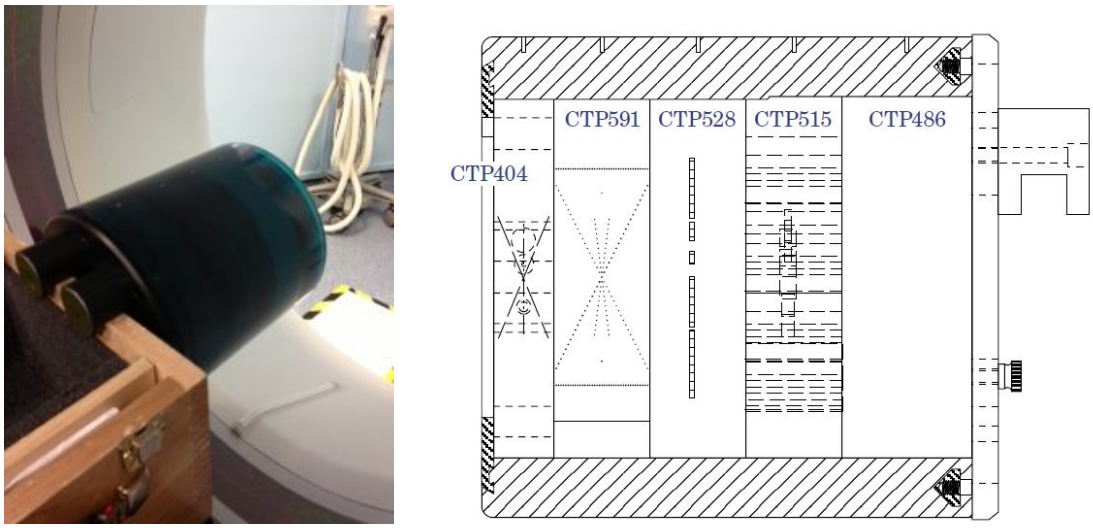

Figure 2-10 Catphan® 600 phantom and different modules
(A permission to use the image from the Phantom Laboratory)

The following modules are used in this study; CTP 258 is high resolution module with 21 line pair per cm and two bead point sources (figure 2-11). The beads are tungsten carbide having diameter of 0.28 mm positioned along the y axis 20 mm above or below the phantom's centre and 2.5 and 10 mm past the centre of the gauge in the Z-direction. CTP515 is sub slice and supra slice low contrast. It consists of cylindrical supra-slice and sub-slice targets. The series of supra-slice contrast targets are 40 mm long in the z-direction having diameters of 2, 3, 4, 5, 6, 7, 8, 9 and 15 mm at three contrast levels of 0.3%, 0.5% and 1.0% (or 3HU, 5HU and 10HU) (figure 2-11). CTP 591 is bead geometry module containing 3 pairs of opposed ramps to measure slice width, and 2 individual beads 0.28 mm and 0.18 mm in diameter.

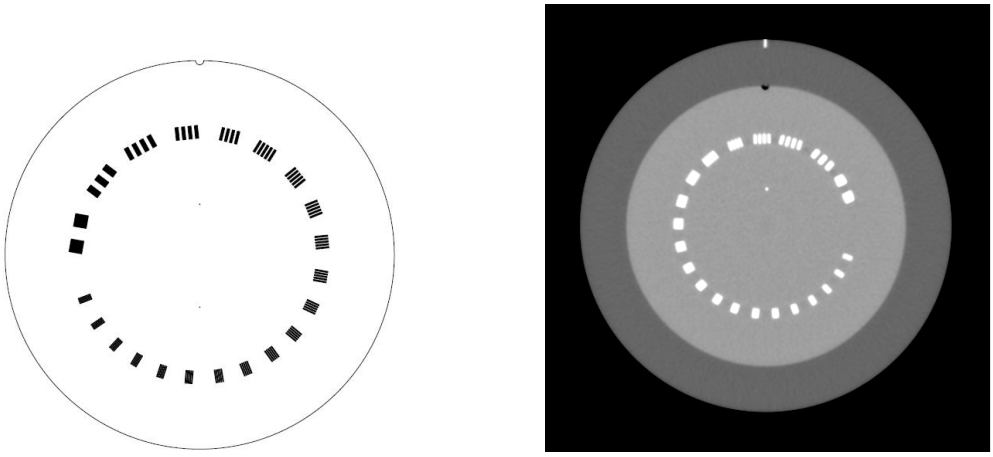

(a)

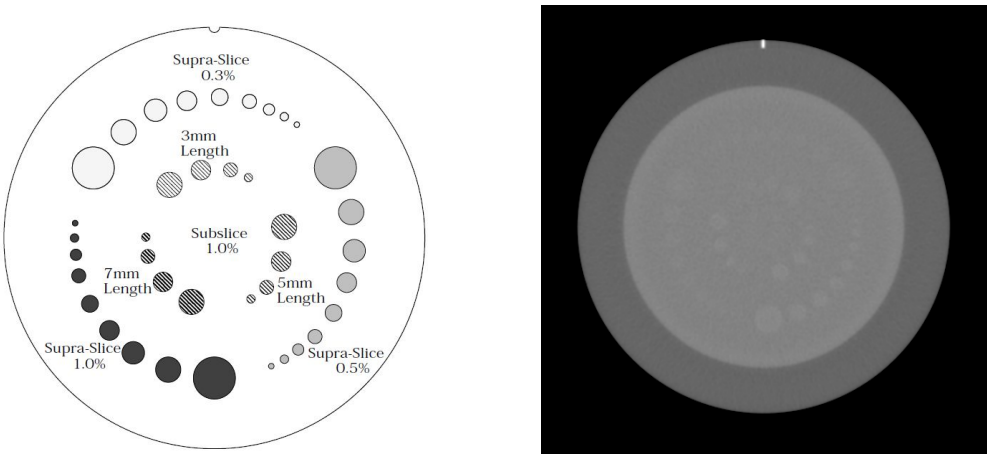

(b)

Figure 2-11 Modules (a) CTP 258 for high contrast resolution with 21 line pair and (b) CTP515 for low contrast resolution assessments
(A permission to use the images from the Phantom Laboratory)

2.7 Custom made phantoms for ATCM system test

At the present time, there is no agreed method for ATCM system evaluation. The standard CT phantoms which are cylindrical in shape are not suitable for measuring dose profiles in ATCM systems. They will therefore not give an actual estimation of radiation distribution in a real patient. In order that full use can be made of these facilities in optimisation, there is a need to develop phantoms and test methods to investigate and record the performance of ATCM systems. Such devices need to be based on elliptical phantoms of different sizes that closely resemble human anatomy. However, there is no consensus currently for specification of phantom material, dimension and shape for measuring CT dose

(AAPM Task Group, 2010). Some studies used a commercial anatomical phantom for ATCM system test (Soderberg & Gunnarsson2010; Papadakis *et al*., 2008), while other studies have developed their own custom made phantoms for ATCM test. Majority of these are uniform phantoms having a range of sizes and eccentricities.

Fisher R F (2006) has proved that a urethane based compound is human tissue equivalent material and constructed ellipsoid-shaped phantoms of five different sizes using the urethane-based material. Each of the five phantoms fits around a 16 cm CTDI head phantom for use in CT imaging and dose measurement. The major axis lengths are 26 cm, 28.5 cm, 31.25 cm, 32.6 cm, and 37.25 cm, while the minor axis length for five phantoms remains at 16 mm. These phantoms can only be used for evaluating the modulation systems in the x-y plane in any single scan.

Muramatsu *et al* (2007) have developed a series of CT-ATCM phantoms which consist of a cone, an ellipse, a variable-shaped ellipse and stepped phantoms. These phantoms have been evaluated using ATCM systems of the major CT manufacturers and it has been shown that they reflect the performance of CT ATCM systems.

In the UK, ImPACT has developed a conical elliptical phantom that is placed parallel to the z-axis of the scanner (Keat *et al*., 2005). It was developed from a similar design of 'Apollo' phantom from Y Muramatsu, national cancer centre, Tokyo, Japan. The phantom is 300 mm long, increases from 61.2 X 40.8 to 428.7 x 285.8 mm. The diameters of the x and y axes are in the ratio of 3:2, which is approximately equal to that for an abdomen. It is designed to attach to the carrying case of a Catphan®600 phantom, and is suspended in air. The phantom has been used for ATCM system tests in the UK (Field 2010, Keat 2006).

Bateman and Hiles (2008) have developed a simple anthropomorphic phantom used to demonstrate ATCM system. The phantom represents a human thorax filled with air representing both lungs. It can be used to ensure systems are working as specified and to compare tube current modulation for different scanners and protocols. A multi elliptical phantom called CT elliptical test (CelT) phantom has been developed by Hiles *et al*, North Wales Medical Physics

Department, (2011). The phantom consists of four stepped elliptical sections and, for the first version, has to be filled with water. In 2012, a second version of the phantom has been developed using a solid material. It is patent pending and they present that the phantom can be used for CT dose and image quality assessment (Bateman *et al*.,2012).

2.8 Relationship between patient size and CT dose on ATCM systems

Since modern CT scanners have the ability to modulate the X-ray tube current, patient radiation exposure can be kept as low as possible. However, the way in which these options are implemented varies not only from one scanner manufacturer to another but also between models. As part of a strategy to reduce patient dose, it is necessary to investigate the relationship between patient size and patient dose.

Some studies (Israel *et al*., 2010; Meeson *et al*., 2010; Zarb *et al*., 2010) aimed to identify the relationship between patient size and CT dose in CT scanners utilising ATCM. This relationship could be useful in optimising scans for individual patients. Many patient size parameters such as weight, cross sectional diameters and cross sectional area can be used. Israel *et al*. (2010) conclude that the weight of patient determines radiation dose used in CT examinations of chest, abdomen and pelvis (CAP) of ATCM scanners. The patient weight is also used in a study by Castellano (2013). The amount of radiation used for a 100 kg patient was three times and organ doses were two times higher than those of 60 kg patients. Zarb *et al* (2010) carry out a retrospective study to identify the relationship between CT dose and the patient size parameters (weight, AP and lateral diameters) for patients who had undergone CT chest and abdomen and show that the patient's AP diameter has the strongest relationship with CTDI and DLP. Meeson *et al*. (2010) carry out a study in the same way as Zarb *et al* (2010) but using patient cross sectional area at the level of the third lumbar vertebra to represent the patient size and find that CTDI increased with patient cross sectional area. There are high coefficient of determination (R^2) values between CTDI and DLP obtained from CT abdomen examinations and patient cross sectional area.

3 Single scan dose profile and cumulative dose measurement in cylindrical and elliptical phantoms and the influence of the ATCM system

3.1 Introduction

As a phantom made of different size ellipse was to be used to investigate performance of ATCMs, tests were first undertaken as a simple elliptical phantom to understand effect of dose distribution. The elliptical phantom is more representative of a patient than the standard cylindrical CTDI phantom. The suitability of the CTDI method for measurements in phantoms particularly for the assessment of doses from helical scans has been questioned, as detailed in chapter 2 (Boone 2007; Brenner *et al.,* 2006; Dixon *et al.,* 2005; Dixon 2003; Nakonechny *et al.,* 2005). Proposals have been made for the development of alternative systems for CT dosimetry using chambers of different lengths in longer phantoms (Dixon and Ballard 2007). If an alternative system for CT dosimetry is to be developed, then it is worthwhile considering whether the shape of the phantom used currently is appropriate (Nakonechny *et al.,* 2005; Kallendar 2005).

The $CTDI_{100}$ measurement is based on the assumption that all the radiation contributing to the patient dose is recorded and so the level of scattered radiation falls to zero within the defined distance used, whereas in practice a significant amount of the incident radiation is scattered beyond the end of the 100 mm long chambers used. Thus, such chambers only record 60%-70% of the radiation dose delivered at the centre of a standard body dosimetry phantom (Mori *et al.,* 2005; Boone 2007; Martin *et al.,* 2011). An alternative method is to measure the cumulative dose $D_L(0)$ in the middle of a dosimetry phantom from a helical scan of length *L* using a short chamber (AAPM Task group 2010; Nakonechny *et al.,* 2005).

Bow-tie shaped filters are used in CT scanners to attenuate parts of the x-ray beam passing through the edge of the body to both minimising the dose to the periphery of the patient and ensure that the beam quality incident on all detectors is similar. Since the human body has an elliptical cross-section, any differences in the bow-tie filter shape between CT scanners will modify the

dose distribution within the body. In particular they will affect the doses to the peripheral aspects of the elliptical torso in different ways, and this will not be apparent for cylindrical phantoms. The automatic tube current modulation systems that are incorporated into current CT scanner models modify the air kerma incident on the body according to orientation in the x-y plane to compensate for variations in attenuation, as well as along the z-axis, and these will also modify the distribution of dose within the body. Moreover, since differences in the bow-tie filter shape between CT scanners will modify the dose distribution within the body, the way the ATCMs change there will not be identified in measurements made on cylindrical phantoms. Therefore, it will be necessary to employ elliptical phantoms to take full account of the influence of these systems on patient dose distribution.

In this chapter, distributions of air kerma (AK) in elliptical and cylindrical phantoms have been measured using Gafchromic film in order to gain a better understanding of the dependence of CT dosimetry measurements on phantom shape, the influence of the ATCM on dose distribution which were linked to the shape of the bow-tie filters have been investigated.

3.2 Materials and Methods

3.2.1 Material

3.2.1.1 Elliptical and Cylindrical phantoms

Dose distributions were measured in a standard cylindrical CT dosimetry phantom which is 320 mm in diameter, as defined in the IEC standard (figure 3-1a), and in a custom built elliptical phantom (figure 3-1b), both are 150 mm long and made from Polymethyl methacrylate (PMMA). The elliptical phantom had major and minor axes of 330 and 220 mm, respectively. The size chosen was based on the average size of cross sectional images of CT chest, abdomen and pelvis (CAP) for 30 randomly selected patients measured at the level of mid chest (seventh thoracic vertebrae), measured by Health Physics in August 2010 (prior this project). The antero posterior (AP) diameter of the thorax was taken to be the distance between the skin surface at the level of mid sternum and the skin surface at the level of mid body of vertebra. The transverse diameter was

measured between the two widest points along a line at right angles to the AP diameter. The elliptical phantom contained a hole along the central axis and four holes at depths of 10 mm at either end of the ellipse axes for CT dosimetry. The cross sectional areas of the cylindrical and elliptical phantoms are 804 cm^2 and 570 cm^2 respectively. Diagrams of the phantoms are also shown in Appendix I.

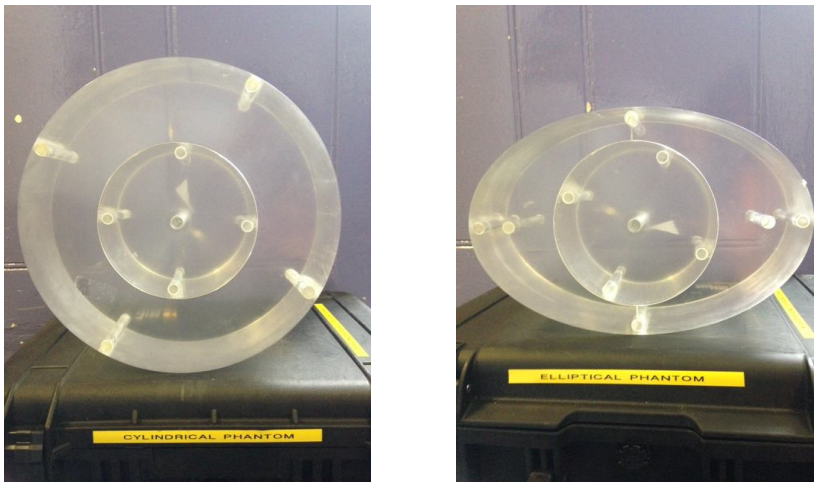

(a) **(b)**

Figure 3-1 (a) Cylindrical Phantom and (b) Elliptical Phantom

3.2.1.2 Gafchromic film

Gafchromic XR-QA film has been developed for patient dosimetry and is sensitive over the dose range from 1 to 200 mGy (Alnawaf *et al* 2010b; Ruiz *et al* 2010; Boivin *et al.,* 2011; Martin *et al.,* 2011). Differences in measurements of CTDI between Gafchromic XR-QA film and a pencil ionization chamber have been reported to be less than 9% (Rampado *et al.,* 2010). Measurements of the film response at different angles were carried out prior to the study and these found that it was almost independent of irradiation angle. The optical densities (ODs) varied by about 1% between the two orientations perpendicular to the x-ray beam and at an angle of 45° this was similar to reports by Giaddui *et al*., 2012; Rampado *et al.,* 2006., however the ODs of films exposed parallel to the x-ray beam were 20% lower (Martin *et al.,* 2011). Exposures have also been carried out both free in air and in the centre of a 125 mm thick PMMA slab phantom where radiation scattered contributed to the air kerma, and the results found that the two calibration conditions gave optical densities within ±2% (Martin *et al.,* 2011).

In this study, the film was calibrated using a Gulmay superficial therapy unit at 110 kV with Al sheets added to achieve a total filtration equivalent to 8 mm of aluminium in order to match those of CT scanners. Pieces of film 20 mm square were irradiated with exposures covering the full dose range (figure 3-2). The materials and methods for Gafchromic XR-QA film calibration which was prepared by Health Physics (2009) is detailed in Appendix II.

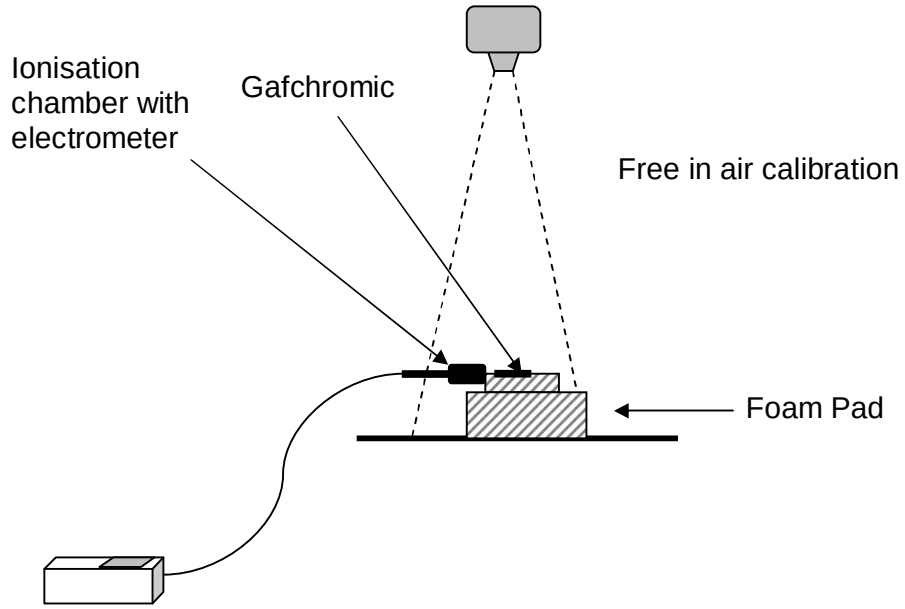

Figure 3-2 setting of experiment for calibration of Gafchromic film

The OD variation of the film increases progressively in the first 24 h after exposure, therefore the exposed film was left for at least 24 hours post exposure, in order for the optical density to reach the equilibrium value (Giaddui *et al* .,2012; Rampodo *et al*., 2006). All pieces of film were scanned in the reflection mode using an Epson V700 flat-bed colour scanner at 72 dpi resolution (pixel spacing ≈0.352778 mm) and 48 bit colour (16 bits per channel), and saved in .tiff format, as explained in Martin *et al* (2011). The film is positioned at the centre of the scanner rather than the edges for consistency of the polarization effect, since there are variations of 2%-4% in reflectance with distance away from the centre (Giaddui *et al.,* 2012; Alnawaf *et al.,* 2010a).

ImageJ was used for analysis of the film. The scanned film data were split into three channels (red, green and blue), using the Image command of imageJ. Only the signal from the red channel was used for interpretation of the result since the main absorption peak which contains most of the dose information for the Gafchromic XR-QA film is located at 636 nm (Alnawaf *et al.,* 2010b; Delvic, 2011), within the wavelength range of the red channel. A square ROI approximately equal to 18 mm x 18 mm was created to make red pixel value measurements for individual pieces of film. The optical density (OD), which is normally used for measurement of changes in film blackening (Alnawaf *et al* 2010b, Rampodo *et al*., 2006) for each piece of film was calculated by comparing the red pixel value (RPV) from that piece of film to the RPV of the unexposed film, from the same batch. The OD values were plotted against the known exposed dose to form a calibration curve. The formula to convert RPV to OD is shown in equation 3-1 below.

$$OD = \log_{10}\left[\frac{RPV_{unexposed}}{RPV_{exposed}}\right] \quad \text{.....Equation 3-1}$$

For this study, a command written by Loveland (2009) which is run on imageJ was used for the Gafchromic film calibration. The software automatically selects the red channel after the calibration image of the Gafchromic film has been opened. Users are instructed to enter the total number of square films in the calibration image. The square ROI is prompted to measure the pixel value which is converted to the OD automatically, the users then are asked to enter the known exposed doses in milligray for individual pieces of the film. Finally, a text window of the OD values for each dose value is shown.

The result for the individual OD values and doses was fitted to a Rodbard equation using a curve fitting tool on ImageJ (Rasband 2011). The form of Rodbard equation and individual equation parameters are shown below in equation 3-2 (DeLean 1978). The calibration curve for the batches of film used is shown in figure 3-3. The reproducibility of Gafchromic film calibration of the same batch was tested and found to be within ±5%. The Gafchromic film optical

density (OD) curve was calibrated over a dose range of 1 mGy to 200 mGy and resulted in ODs of up to 0.5.

$$Y = d + \frac{(a-d)}{1+(X/c)^b} \;;\; X = c \times \left[\frac{(a-d)}{(Y-d)} - 1 \right]^{\frac{1}{b}} \quad \text{.....Equation 3-2}$$

Where a = 'y'; when 'x'=0

b = slope factor that determines the steepness of the curve

c = 'x'; when 'y' is at the half way between a and d

d = 'y'; when 'x'=∞

Table 3-1 Parameters A, B and C values obtained from different batches of the Gafchromic film XR-QA

parameter	Lot#A10071002A	Lot#A10071003B	Lot#A10071003A
a	-0.0007	0.0011	0.0009
b	0.91201	0.898	0.9059
c	71.2813	80.5099	63.9401
d	0.67102	0.669	0.642

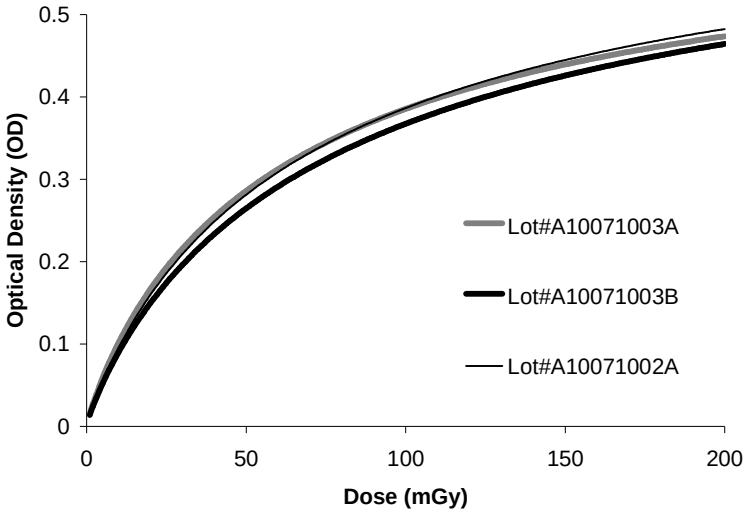

Figure 3-3 Calibration curve of Gafchromic XR-QA film from different batches

The $CTDI_{100}$ and central cumulative dose were measured with ionisation chambers to compare results with the Gafchromic film, and results are shown in table 3-2, the differences for the measurements of $CTDI_{100}$ were within ±10%, while those for the cumulative measurement were up to 35%.

Table 3-2 Comparison of CTDI100 and central cumulative doses for complete scans of the 150 mm long phantom measured with ionisation chambers and Gafchromic film measurements. Measured from the Toshiba scanner
(Note : Central cumulative doses were measured with a helical scan using 200 mAs, 120 kV, 0.938 Pitch factor, 16 mm beam width)

Phantom/ Position	$CTDI_{100}$ (mGy/100mAs)		Cumulative dose* (mGy/100mAs)		
	Chamber (100 mm Radcal)	Film	Chamber (20 mm Unfors)	Chamber (20 mm Radcal)	Film
Ellipse					
Centre	11.2	10.9	14.1	14.5	15.6
Anterior	20.1	21.4	23.5	23	23.0
Posterior	16.9	18.3	20.5	20.5	20.4
Lateral	15.0	14.8	17.3	17.3	17.2
Cylinder					
Centre	7.1	6.5	9.1	9.3	9.6
Anterior	15.2	16.7	16.8	15.6	14.6
Posterior	13.1	13.5	16.2	15.0	12.0
Lateral	14.8	15.3	17	15.7	14.7

3.2.2 Methods

The main CT scanner used was a Toshiba Aquillion 64 model (64 slices). Some measurements were also made on a GE Lightspeed16 multi- slice (16 slices) CT scanner and a Philips Brilliance multi –slice (64 slices) CT scanner, in order to compare the SSDP results. Dose measuring under ATCM was carried out on the Toshiba Aquilion 64, GE Discovery 64 and Philips Brilliance 64 scanners.

3.2.2.1 Measurement of effect of Bowtie filter

The distribution of X-ray intensity within the fan beam in the x-y plane of a CT scanner is determined by the characteristics of the bow-tie filter. Measurements were made of the fan beam profiles in the x-y plane produced by the bow-tie filters for the different scanners to aid in interpretation of dosimetry results.

The X-ray tube was positioned so that the beam was directed horizontally. A pencil ionization chamber was supported in air by the patient couch, but with the couch retracted so that it was not within the beam. The scan projection radiograph (SPR) mode, in which the tube remains stationary as the couch moves through the gantry to create a simple radiographic image for planning purposes, was used with a large field of view selected. The exposure settings were 120 kV, 150 mA, 200 mm scan length for all scanners. Output measurements were made across the scan field (distance 'd' in figure 3-4) by raising and lowering the couch in 10 mm increments. Three CT scanners were involved in this experiment; Toshiba Aquilion 64, GE Discovery 64 and Philips Brilliance 64 scanners. Each scanner has different bow tie filters depending on FOV. The Large FOV is selected in this study since it is used routinely for body scans. However, it is uncertain whether the bow-tie filter employed in SPR mode are the same as those employed for the scan mode. Later on in this study, for the Toshiba scanner Aquilion CXL, which has the same wedge filter unit configuration as the Toshiba Aquilion 64, the scanner was put into service mode, stopping the rotation and the x-ray tube was fixed at 90°. Individual FOVs such as extra small (SS), small (S), medium (M), large (L) and extra large (LL) can be selected to investigate the bow tie filter profile.

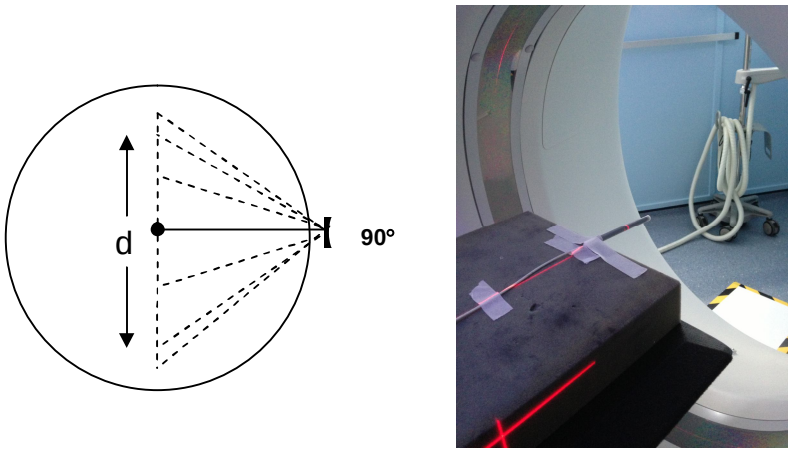

Figure 3-4 Bow-tie filter dose profile measurement

3.2.2.2 Single scan dose profile and cumulative dose measurement

Scans were performed with the phantom on the couch to represent the supine position. Measurements at the top and bottom will be referred to as anterior and posterior (figure 3-5). Strips of Gafchromic film 8 mm wide were placed in each hole of the phantom. The PMMA rods were inserted into the holes that were not used for measurements. Measurements were made for single scan dose profiles (SSDPs), taken as single axial scan rotations.

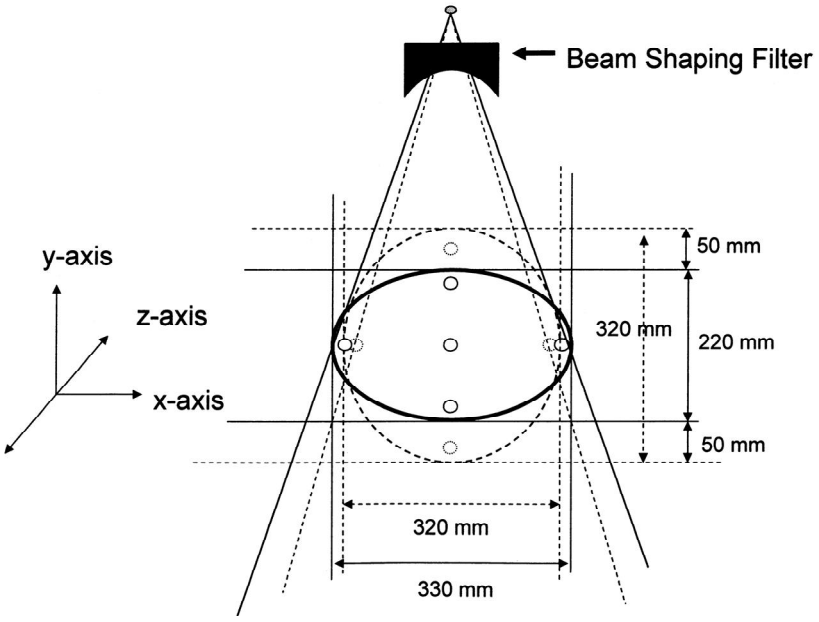

Figure 3-5 Experimental set up and dimensions for the elliptical and cylindrical phantoms

As explained earlier, the Gafchromic film OD curve was calibrated over a dose range of up to 200 mGy which resulted in ODs of up to 0.5. However, above around 110 mGy the film begins to saturate at OD of 0.4 (figure 3-4). Since the slope of the curve determines the precision with which the OD can be determined, the uncertainties will be significantly higher at doses above 110 mGy. In this study exposure factors were chosen to enable the resultant dose to parts of the film from which results were recorded to be less than 100 mGy and consequently an OD of less than 0.4. Multiple rotations were used to record low doses far from the primary beam.

SSDPs were measured by positioning the primary beam either at the longitudinal midpoint of the phantom (mid point beam profile) or 25 mm from one end of the phantom (edge beam profile) (figure 3-6). The positions near the ends of the phantoms were selected to allow contributions from scattered radiation to be measured to a greater distance from the primary X-ray beam (Martin *et al.,* 2011). In order to reduce noise signal, a smoothing filter was applied to derive the results, pixel values were replaced by a weighted average of the nearest five points.

For the Toshiba scanner, measurements were made for a 16 mm beam width, with 1 s axial rotations. One set of films was exposed using twelve rotations, at 300 mA (3600 mAs) and a second set with six rotations at 100 mA (600 mAs). Multiple rotations were employed to reduce the variations in air kerma level around the phantom circumference due to overscan with the Toshiba scanner (Martin *et al.,* 2011). For GE and Philips scanners 1 s rotations were used with 20 mm and 25 mm beam widths respectively, and measurements were made for a set of twelve 600 mA (7200 mAs) rotations and a set of two 600 mA (1200 mAs) ones. The two different exposure levels were employed to derive film ODs suitable for assessment of both the peak dose level and the low densities in the scatter tails (Martin *et al.,* 2011). The pairs of measurements were combined to derive beam profiles with the higher exposure films being used to calculate dose levels below 2 mGy per 100 mAs, diagrams illustrating the two profiles are shown in figure 3-7. Experiments with similar exposure settings were performed for both the elliptical and cylindrical phantoms. All results were normalized to 100 mAs. Values for the $CTDI_{100}$ in the 150 mm long phantoms were calculated by summing the doses recorded by the Gafchromic film for the SSDPs over 100 mm lengths through the mid point of the phantoms.

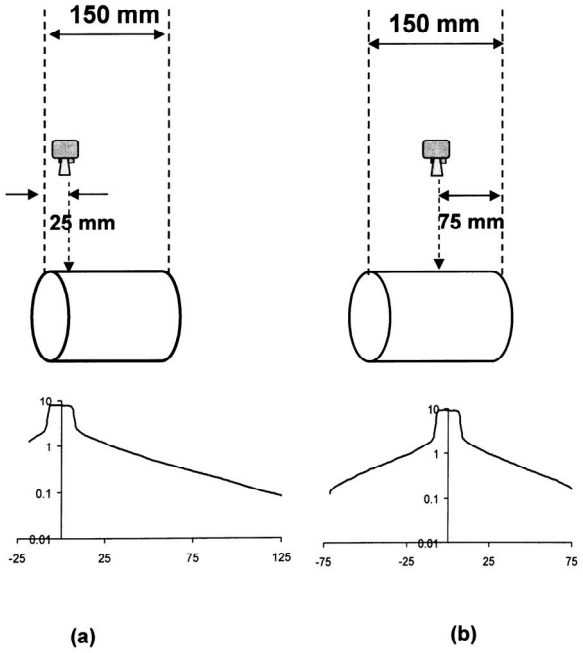

Figure 3-6 Positions of primary beam used for recording of SSDPs at (a) edge beam profile and (b) mid point beam profile

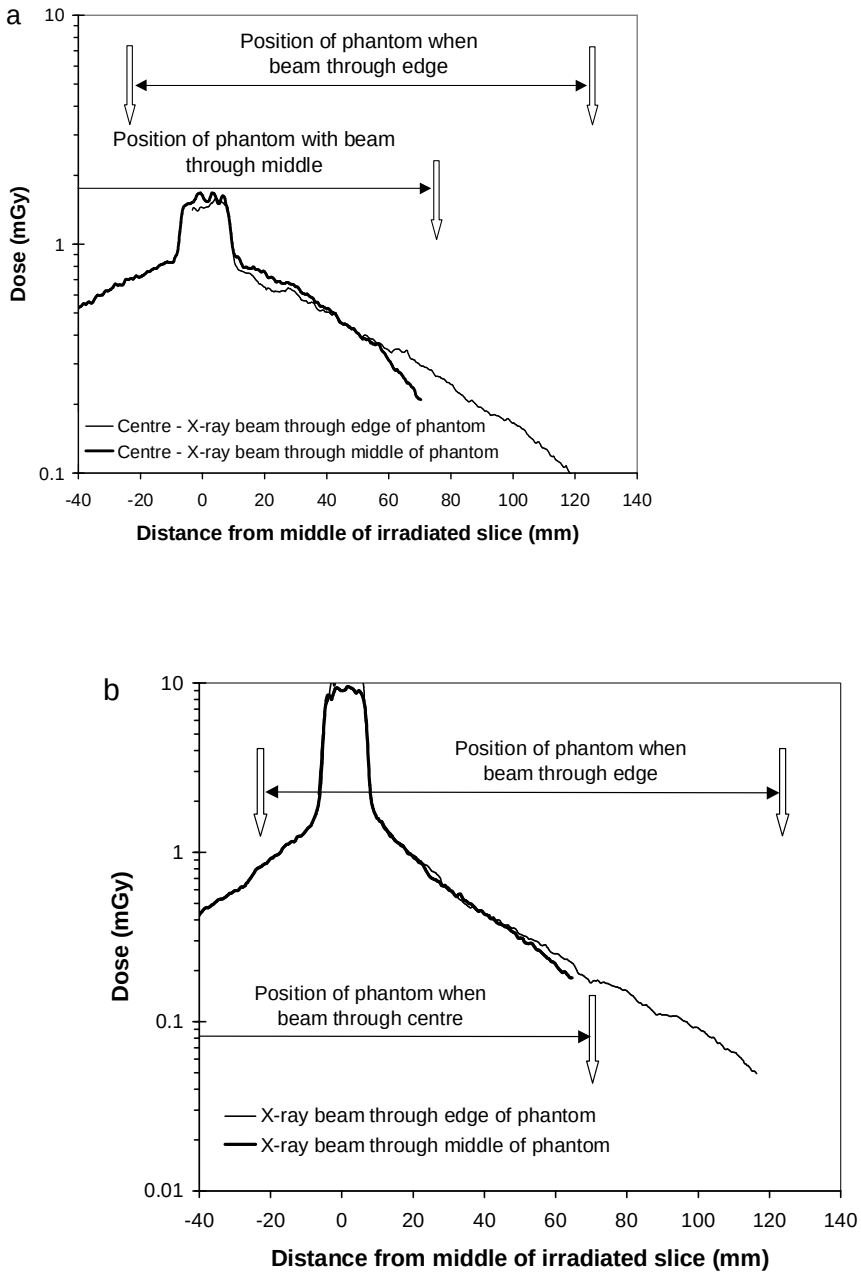

Figure 3-7 Examples of SSDPs obtained at the middle and at the 25 mm from the edge of the body phantom (a) the centre and (b) the periphery of the phantom
(The figures have been published in Martin *et al*., 2011)

3.2.2.3 Calculation of $CTDI_{\ell}$ and simulation of central z-axis cumulative dose

Dose levels and values of $CTDI_{100}$ at the centre and periphery within the 150 mm long elliptical and cylindrical phantoms were calculated from scans with the X-ray beam through the mid points of the phantoms. Values of $CTDI_{\ell}$ for chambers of various lengths ℓ in phantoms 450 mm long were derived from the extrapolated data and integrals of the dose profile over length ℓ.

As explained, the dose profile data sets from positioning the primary beam at the longitudinal midpoint and near the longitudinal edge of the phantom were combined. The mid point beam profiles were used to represent the main beam and the surrounding region to a distance of 40 mm from the middle and the scan profiles with the beam near the edge were deployed to represent the scatter tails at distances of 40 mm to 110 mm from the middle of the beam. In order to derive assessments of cumulative doses and CTDIs in longer phantoms, SSDPs were required that would be representative of profiles in longer phantoms. The dose level in the scatter tails declines exponentially with distance from the beam, but falls more rapidly within 10 mm of the edge, where there is little back scatter (Martin *et al.,* 2011). An exponential fit of the tails of the SSDPs recorded with the beam near the end of the phantom between 50 mm and 100 mm from the middle of the beam was used to estimate the scatter levels at greater distances from the primary beam.

The exponential curve fitting and the extrapolation function of Matlab R2010a (Mathworks, Natick, MA, USA) was used to extrapolate the data set beyond the measured range. Matlab programming was performed by Dr Maria del Rosario Lopez-Gonzalez. The dose starts to drop near the edge of the phantom at around 100 mm from the middle of the peak. Therefore, the dose beyond 100 mm was not used for the extrapolation as it could result in underestimation of the scatter dose. Different ranges of the raw data were investigated in order to choose the most appropriate curve fitting; 50-80 mm, 50-90 mm, 60-90 mm and 60-100 mm from the middle of the primary beam were used and evaluated. Percentage differences among the four extrapolation options were within ±2% of the mean. The fits gave coefficient of determination (R^2) of 0.99 and better. Data in the range having the highest R^2 was selected, exponential curves were fitted to

scatter tail data and are shown as dotted lines, as an example for the elliptical phantom in the Toshiba scanner in figure 3-8.

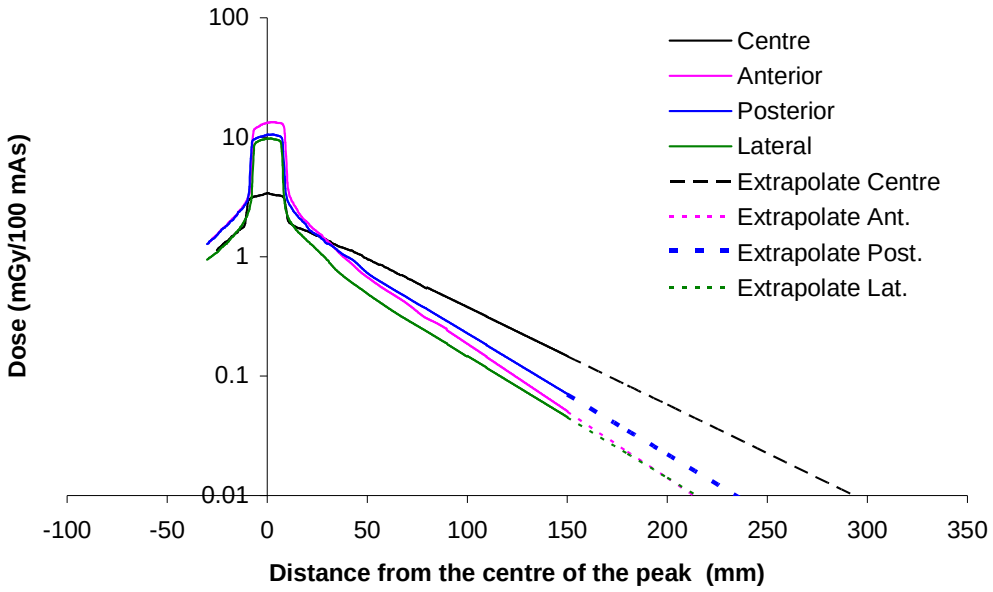

Figure 3-8 Exponential extrapolation of SSDP from each position within the elliptical phantom, measured from Toshiba Aquillion 64 scanner at 120 kVp for a 16 mm wide beam

The central cumulative dose $D_L(z)$ at longitudinal position z within a phantom from a scan of length L can be calculated theortically by convolving single axial rotations of varying scanning length (L) (Dixon *et al.,* 2010), as explained in chapter 2. For this study, helical scans were simulated by combining a series of axial scans in order to build up cumulative dose distributions along the central axis of the phantom using the method described in Martin *et al.,* 2011. The central cumulative doses for scans with lengths up to 450 mm were calculated by summing contributions to the dose in the middle of a phantom from SSDPs for a series of single axial rotations along the axis of the phantom. The Matlab program was applied in this study. The central cumulative curve was smoothed by replacing each z value with average value over an interval $z \pm \frac{b}{2}$, as discussed in equation 2-16, chapter 2 (AAPM task group 2011). Dose distributions were measured for complete helical scans of the cylindrical and elliptical phantoms, and results compared with assessments derived from simulations constructed from SSDPs. Measurements undertaken are summarised in table 3-3.

Table 3-3 Summary of methods employed for dosimetry measurements

Method	Measurement				
	SSDP	$CTDI_{100}$	$CTDI_{\ell}$	Cumulative Dose Profile	Central Z-axis cumulative dose
Gafchromic	yes	yes	yes	yes (simulated)*	yes
100 mm Chamber	-	yes	-	-	-
20 mm chamber	-	-	-	-	yes

*except for the data in table 3-10, they were obtained from helical scan measurements

3.2.2.4 Automatic tube current modulation (ATCM) dose measurement

Measurements were made with the ellipsoidal phantom on different image quality settings of the ATCM. A routine CAP protocol was used and details of the exposure parameter settings, and ATCM options for three scanners are shown in table 3-4. All measurements were done using 120 kV. For the Toshiba scanner, three target noise settings were selected from a drop down list available on Aquilion scanners; a) high quality (standard deviation (SD)=7.5 HU), b) standard (SD=12.5 HU), c) very low dose (SD=17.5 HU). For the GE scanner, the reference NI value used for the CAP protocol of 11.57 and two other NI values of 6.94 and 16.20 were selected. For the Philips scanner the maximum mAs values selected were 162 mAs/slice (value recommended by the software), 300 mAs/slice and 410 mAs/slice. The Toshiba and GE scanners modulate the tube current to account for variations in attenuation in both the x-y plane and along the z-axis, while the x-y and z axis modulations are separate for the Philips scanner and the ATCM option recommended for body scans only makes adjustments along the z-axis. The ATCM uses a constant tube current during each rotation and changes the tube current value for the next rotation, as explained in chapter 2. However, measurements were made in order to compare the ATCM operation for the three scanners. In this study, tube current time products of 240 mAs, 390 mAs and 410 mAs were used as fixed mAs techniques for Toshiba, GE and Philips scanners, respectively since they are the maximum values applied by the ATCM systems for the CAP protocols.

The helical scans for the ATCM measurements were each 100 mm long. For each, average air kerma doses were measured along 100 mm lengths in the middle of the elliptical phantom with strips of Gafchromic film. Measurements were made along the central axis of the phantom and in the four peripheral holes, and ESAKs were measured along the anterior and the left and right lateral surfaces of the phantom. The results are shown in the form of bar charts depicting changes with ATCM settings.

Table 3-4 Routine Chest, Abdomen and Pelvis (CAP) Protocols which are used in ATCM systems testing

CT scanner	mA range	Rotation time (sec)	Collimation	Pitch	Recon Filter	Image quality (ATCM Option)	Fixed Technique
Toshiba Aquilion 64	100-480	0.5	64x0.5	0.828	FC13	SD=7.5, 12.5*, 17.5	480x0.5 mAs
GE Discovery 64	100-650	0.6	16x1.25	1.375	Standard	NI=6.94, 11.57*, 16.20	650x0.6 mAs
Philips Brilliance 64	-	0.75	64x0.625	0.921	B	162*, 300, 410 mAs/slice	410 mAs

*** standard or recommended setting for ATCM**

3.3 Results

3.3.1 Bow- tie filter measurement

The fan beam profiles of the three scanners measured in SPR mode are shown in figure 3-9. The central regions in the GE and Philips scanners were broader, the relative air kerma being within 10% of the maximum at ±65 mm and ±50 mm from the isocentre respectively. However, the fan beam profile of the Toshiba scanner was narrower with the beam falling below 90% of the maximum value by ±30 mm from the isocentre and by ±50 mm from the isocentre, the relative air kerma dropped to around 70% of the maximum value. A CT application specialist from GE has confirmed that the bow-tie filter used in the GE Lightspeed 16 is similar to that in the Discovery 64. The Toshiba's bow tie filter profiles for scan mode have been measured using the engineer service mode operated by a scanner engineer for a Toshiba Aquilion CXL scanner. The fan beam profiles used for scanning are the same as the SPR one, as suspected (figure 3-10).

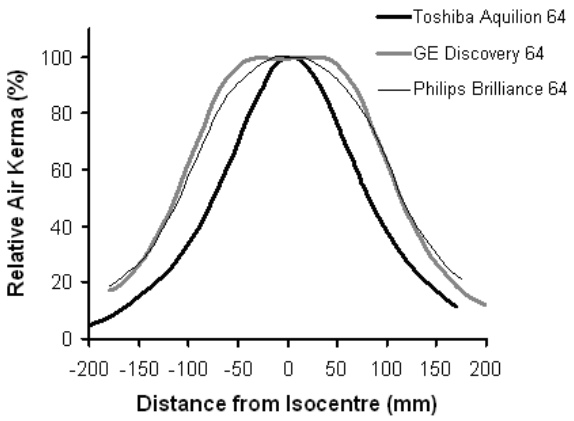

Figure 3-9 Relative Air kerma (%) measured from different bow tie filters for each manufacturer

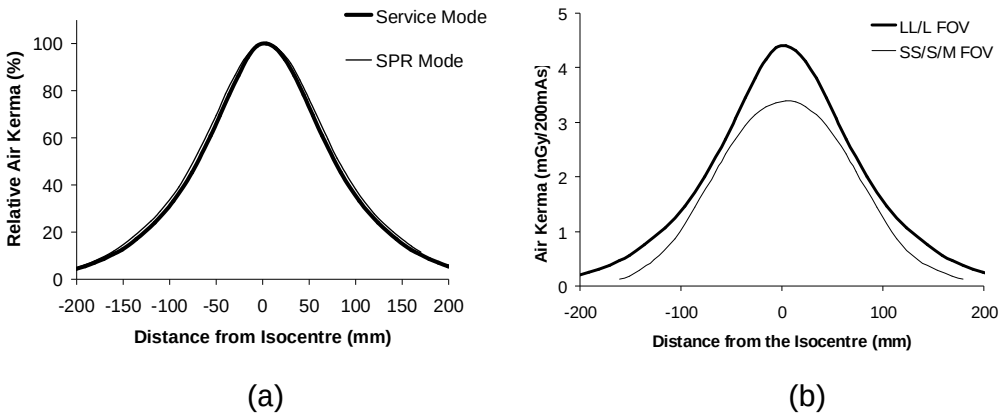

Figure 3-10 (a) comparison of relative air kerma (%) between SPR and Service modes and (b) Air kerma (mGy/200mAs) for different FOV settings, measured from Toshiba scanner

3.3.2 Measurement of dose profiles

SSDPs measured at the centre and periphery in the elliptical and cylindrical phantoms were measured from the Toshiba, Philips and GE scanners (figures 3-11 to 3-13). Within the primary beam measured in the elliptical phantom, the doses to the anterior periphery were higher than those at the sides or lateral periphery and the beams were wider. The doses at the anterior and lateral positions were similar, for the cylinder. The doses in the primary beam at the centre for the two phantoms were the lowest, but the dose in the scatter tails did not decline as rapidly with distance from the primary beam and the centre scatter tail dose was higher than the dose at the periphery beyond 30 mm and 25 mm from the edge of the beam for the cylinder and ellipse phantoms respectively. SSDPs at similar positions in the elliptical and cylindrical phantoms recorded with the same exposure factors and scanning options are compared in figures 3-14 to 3-16. The doses shown are for the anterior positions, centre and average for left and right lateral positions. The doses at the centre of the elliptical phantom were substantially higher than those in the cylinder (1.7-2.0 times), the doses at the anterior periphery were also higher (1.2-1.3 times), while the doses at the lateral positions were similar to those in the cylindrical phantom. The posterior peripheral doses were lower than the anterior ones because of attenuation by the couch particularly for oblique orientations.

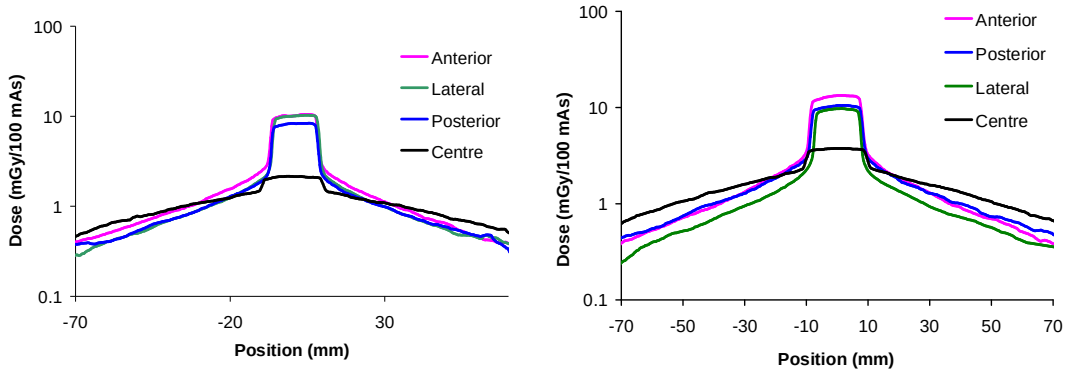

(a) (b)

Figure 3-11 SSDPs measured at the centre and peripheral positions when the beam is at the middle of the phantom, measured from a Toshiba Aquillion 64 scanner at 120 kVp for a 16 mm wide beam in (a) cylindrical and (b) elliptical phantoms

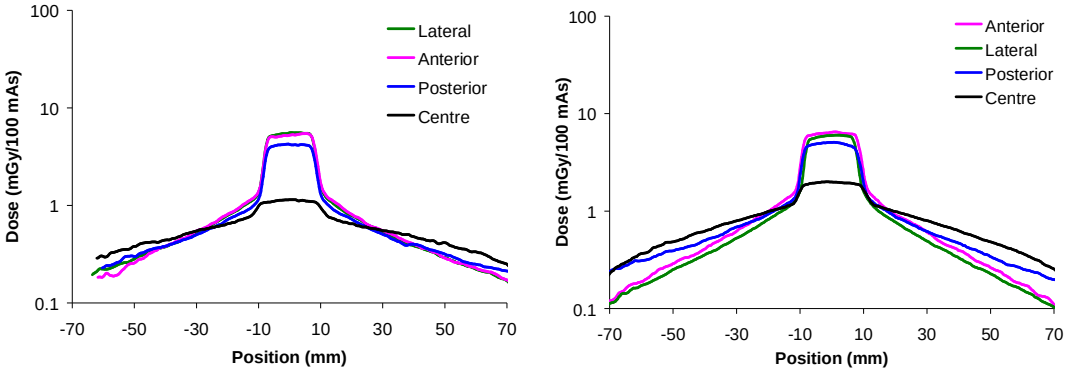

(a) (b)

Figure 3-12 SSDPs measured at the centre and peripheral positions when the beam is at the middle of the phantom, measured from a GE Lightspeed scanner at 120 kVp for a 20 mm wide beam in (a) cylindrical and (b) elliptical phantoms

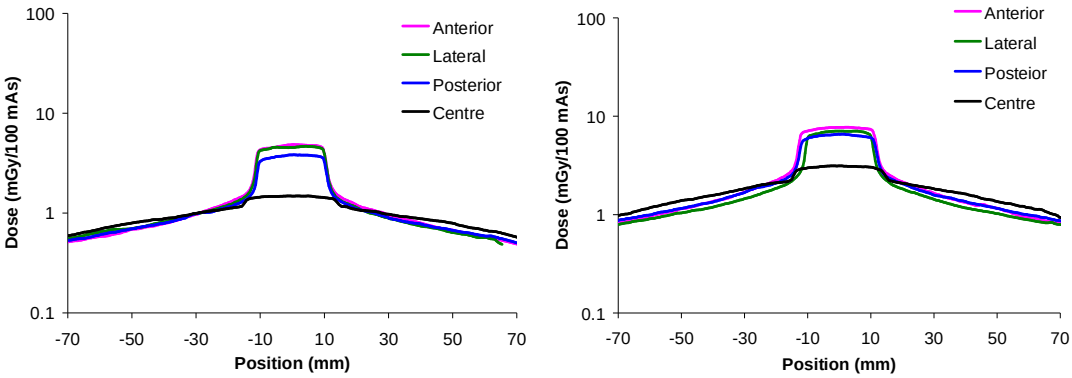

(a) (b)

Figure 3-13 SSDPs measured at the centre and peripheral positions when the beam is at the middle of the phantom, measured from a Philips Briliance 64 scanner at 120 kVp for a 25 mm wide beam in (a) cylindrical and (b) elliptical phantoms

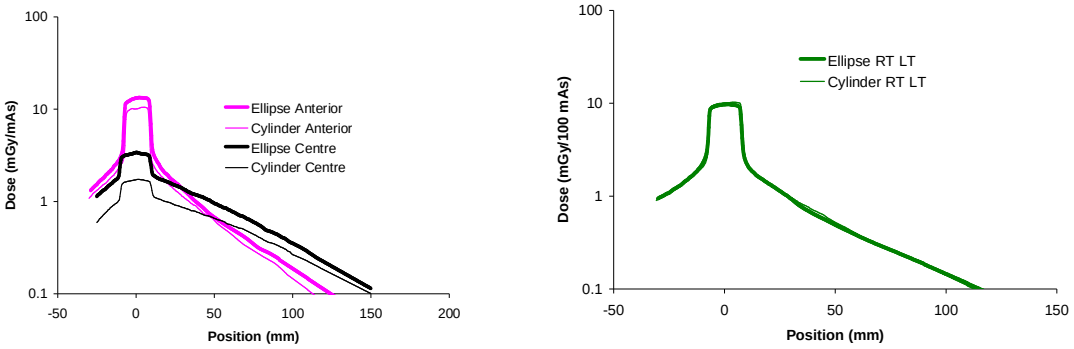

(a) (b)

Figure 3-14 Comparisons of dose profiles measured in 150 mm long phantoms (a) at the centre and the anterior periphery and (b) at the right and left laterals, measured from a Toshiba Aquillion 64 scanner at 120 kVp for 16 mm wide beam

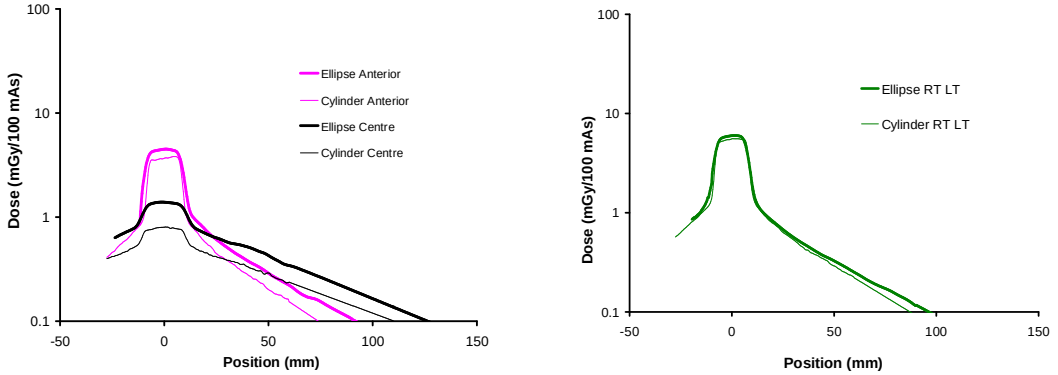

(a) (b)

Figure 3-15 Comparisons of dose profiles measured in 150 mm long phantoms (a) at the centre and the anterior periphery and (b) at the right and left laterals, measured from a GE Lightspeed 16 scanner at 120 kVp for 20 mm wide beam

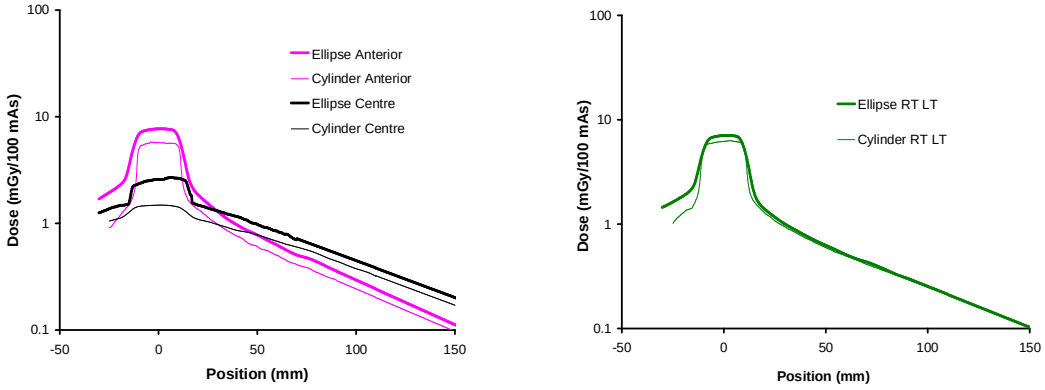

(a) (b)

Figure 3-16 Comparisons of dose profiles measured in 150 mm long phantoms (a) at the centre and the anterior periphery and (b) at the right and left laterals, measured from a Philips Briliance 64 scanner at 120 kVp for 25 mm wide beam

3.3.3 Evaluation and measurement of $CTDI_{\ell}$

Values for the $CTDI_{100}$ and $CTDI_{\ell}$ at the centre and periphery within the elliptical and cylindrical phantoms are presented in table 3-5. These varied significantly between different scanners with the Toshiba scanner having larger values at the centre and lower values at the lateral periphery than the other scanners. For the Toshiba scanner the $CTDI_{100}$ in the centre in the elliptical phantom was 68% higher than that in the cylindrical phantom and the dose at the centre within the primary beam was almost double that in the cylindrical phantom. The anterior and posterior periphery $CTDI_{100}$ values in the elliptical phantom for the three scanners were 19%-36% higher than the equivalent measurements in the cylindrical phantom, while the $CTDI_{100}$ in the lateral position was similar to that in the cylinder.

CTDI values at the centre of the elliptical phantom were about 50% higher than for the cylindrical phantom for the GE and Philips scanners and about 75% higher within the primary beam. Values calculated for the $CTDI_{\ell}$ in a phantom 450 mm long were derived from integrals of the dose profile over length ℓ obtained from Gafchromic film measurements. $CTDI_{\infty}$ was $CTDI_{450}$ as explained in section 2.5.2, chapter 2.

Table 3-5 $CTDI_{\ell}$ (mGy/100 mAs) values for chambers of different lengths ℓ , simulated using SSDPs measured with Gafchromic film in 150 mm long elliptical and cylindrical phantoms

(Note: All measurements were done using 120 kV. The beam widths for the Toshiba, GE and Philips scanners were 16, 20 and 25 mm)

Model	Phantom Length	$CTDI_{\ell}$ (mGy/100mAs)							
		$CTDI_{100}$	$CTDI_{100}$	$CTDI_{200}$	$CTDI_{250}$	$CTDI_{300}$	$CTDI_{\infty}$ *	$\frac{CTDI_{100}}{CTDI_{\infty}}$	$\frac{CTDI_{250}}{CTDI_{\infty}}$
		150	∞	∞	∞	∞	∞		
Toshiba	**Elliptical Phantom**								
Aquillion64	Centre	10.90	11.04	14.96	15.87	16.43	17.23	0.64	0.92
	Anterior Periphery	21.40	23.53	25.90	26.26	26.44	26.65	0.88	0.99
	Posterior Periphery	18.30	18.91	21.59	22.08	22.34	22.67	0.83	0.97
	Lateral Periphery	14.80	15.39	17.15	17.46	17.62	17.83	0.86	0.98
	Cylindrical Phantom								
	Centre	6.50	6.51	9.32	10.01	10.44	11.07	0.59	0.90
	Anterior Periphery	16.70	18.04	20.03	20.28	20.39	20.50	0.88	0.99
	Posterior Periphery	13.50	14.72	16.74	17.12	17.34	17.63	0.84	0.97
	Lateral Periphery	15.30	16.53	18.33	18.63	18.79	18.99	0.87	0.98

* Note : $CTDI_{\infty}$ was derived from integrals of the dose profile over length 450 mm (section 2.5.2)

Table 3-5 (Cont.) $CTDI_{\ell}$ (mGy/100 mAs) values for chambers of different lengths ℓ, simulated using SSDPs measured with Gafchromic film in 150 mm long elliptical and cylindrical phantoms

(Note: All measurements were done using 120 kV. The beam widths for the Toshiba, GE and Philips scanners were 16, 20 and 25 mm)

Model	Phantom Length	$CTDI_{\ell}$ (mGy/100mAs)							
		$CTDI_{100}$	$CTDI_{100}$	$CTDI_{200}$	$CTDI_{250}$	$CTDI_{300}$	$CTDI_{\infty}$ *	$\frac{CTDI_{100}}{CTDI_{\infty}}$	$\frac{CTDI_{250}}{CTDI_{\infty}}$
		150	∞	∞	∞	∞	∞		
GE LightSpeed	**Elliptical Phantom**								
16	Centre	5.23	5.47	7.42	7.88	8.17	8.58	0.64	0.92
	Anterior Periphery	8.78	9.30	10.45	10.65	10.76	10.88	0.85	0.98
	Posterior Periphery	7.47	7.72	9.13	9.42	9.61	9.86	0.78	0.96
	Lateral Periphery	7.46	7.74	8.66	8.81	8.89	8.98	0.86	0.98
	Cylindrical Phantom								
	Centre	3.40	3.40	4.75	5.09	5.31	5.64	0.60	0.90
	Anterior Periphery	7.40	7.43	8.19	8.28	8.32	8.36	0.89	0.99
	Posterior Periphery	6.00	6.03	6.98	7.16	7.26	7.39	0.82	0.97
	Lateral Periphery	7.40	7.40	8.18	8.29	8.33	8.38	0.88	0.99

* Note : $CTDI_{\infty}$ was derived from integrals of the dose profile over length 450 mm (section 2.5.2)

Table 3-5 (Cont.) $CTDI_{\ell}$ (mGy/100 mAs) values for chambers of different lengths ℓ , simulated using SSDPs measured with Gafchromic film in 150 mm long elliptical and cylindrical phantoms

(Note: All measurements were done using 120 kV. The beam widths for the Toshiba, GE and Philips scanners were 16, 20 and 25 mm)

Model	Phantom Length	$CTDI_{\ell}$ (mGy/100mAs)							
		$CTDI_{100}$	$CTDI_{100}$	$CTDI_{200}$	$CTDI_{250}$	$CTDI_{300}$	$CTDI_{\infty}$ *	$\frac{CTDI_{100}}{CTDI_{\infty}}$	$\frac{CTDI_{250}}{CTDI_{\infty}}$
		150	∞	∞	∞	∞	∞		
Philips	**Elliptical Phantom**								
Brilliance 64	Centre	6.50	6.74	9.46	10.18	10.66	11.44	0.59	0.89
	Anterior Periphery	10.90	11.51	13.47	13.91	14.20	14.62	0.79	0.95
	Posterior Periphery	10.20	10.12	12.26	12.78	13.12	13.65	0.74	0.94
	Lateral Periphery	9.70	9.65	11.28	11.66	11.91	12.29	0.78	0.95
	Cylindrical Phantom								
	Centre	4.40	4.38	6.67	7.35	7.85	8.74	0.50	0.84
	Anterior Periphery	8.30	8.39	9.97	10.34	10.58	10.94	0.77	0.95
	Posterior Periphery	7.70	7.43	9.11	9.54	9.82	10.28	0.72	0.93
	Lateral Periphery	8.50	8.67	10.25	10.63	10.87	11.26	0.77	0.94

* Note : $CTDI_{\infty}$ was derived from integrals of the dose profile over length 450 mm (section 2.5.2)

3.3.4 Ratios of doses from elliptical and cylindrical phantoms

Comparisons of the dose distributions in the elliptical and cylindrical phantoms and the variations that result from different bow-tie filters are demonstrated more readily by considering the ratios in the two phantoms and they are given in table 3-6. The ratios for the CTDI, cumulative dose and peak doses at the centre of the elliptical and cylindrical phantoms in the Toshiba scanner were higher than those of the GE and Philips scanners while those for the lateral periphery were lower. In other words the Toshiba scanner gave relatively higher doses in the centre of the elliptical phantom and lower doses at the lateral periphery. These results are thought to be linked to the shape of the fan beam produced by the bow-tie filter (figure 3-9), with the central region of the beam for the GE and Philips being broader and so increasing the dose to the periphery of the cylinder.

Table 3-6 Ratios of doses in the primary beam, $CTDI_{\ell}$ and central cumulative doses values for elliptical and cylindrical phantoms
(Note: All measurements were done using 120 kV. The beam widths for the Toshiba, GE and Philips scanners were 16, 20 and 25 mm)

Model	Position of measurement	Ratio of doses	Ratio of CTDI					Ratio of Cumulative dose			
		At the peak	$CTDI_{100}$	$CTDI_{100}$	$CTDI_{250}$	$CTDI_{300}$	$CTDI_{\infty}$ *	L=100 mm	L=250 mm	L=300 mm	L=∞ mm
	Phantom Length		150	∞	∞	∞	∞	∞	∞	∞	∞
Toshiba Aquillion 64	Centre	1.98	1.68	1.70	1.60	1.57	1.56	1.71	1.59	1.58	1.57
	Anterior Periphery	1.31	1.28	1.30	1.29	1.30	1.30	1.31	1.29	1.30	1.30
	Posterior Periphery	1.26	1.36	1.28	1.29	1.29	1.29	1.36	1.35	1.35	1.35
	Lateral Periphery	0.96	0.97	0.93	0.94	0.94	0.94	0.96	0.96	0.96	0.96
GE Light Speed 16	Centre	1.73	1.54	1.61	1.56	1.54	1.52	1.61	1.55	1.54	1.53
	Anterior Periphery	1.22	1.19	1.25	1.28	1.29	1.30	1.29	1.32	1.33	1.34
	Posterior Periphery	1.20	1.24	1.28	1.31	1.32	1.33	1.31	1.35	1.35	1.36
	Lateral Periphery	1.07	1.01	1.04	1.06	1.07	1.07	1.07	1.08	1.09	1.09
Philips Brilliance 64	Centre	1.75	1.48	1.54	1.42	1.36	1.31	1.53	1.38	1.36	1.32
	Anterior Periphery	1.34	1.31	1.37	1.35	1.34	1.34	1.37	1.35	1.34	1.34
	Posterior Periphery	1.33	1.32	1.36	1.35	1.34	1.33	1.38	1.35	1.35	1.34
	Lateral Periphery	1.13	1.14	1.11	1.10	1.10	1.09	1.11	1.10	1.10	1.09

* Note : $CTDI_{\infty}$ was derived from integrals of the dose profile over length 450 mm (section 2.5.2)

3.3.5 Evaluation of central z-axis cumulative dose

Helical scans within the two phantoms were simulated using the SSDP results with exponential extrapolation within an 450 mm long phantom. The AAPM reported that a phantom 450 mm long was sufficient to achieve an equilibrium value for the cumulative dose D_{eq} (AAPM Task group 2010). Cumulative dose profiles along the central axis of the elliptical phantom were modelled by summation of SSDPs for several scan lengths between 80 mm and 450 mm and the results normalized with respect to the maximum dose $D_L(0)$ in the middle of a 450 mm long scan (figure 3-17). The absolute central cumulative doses that would be measured by a 20 mm long chamber in the central and peripheral positions at the middle of the elliptical phantom calculated by summation of SSDPs are plotted against scan length and normalised with respect to the cumulative equilibrium dose, D_{eq}, of the anterior peripheral position in the elliptical phantom for all CT scanners in figures 3-18 to 3-20. Values for the central cumulative dose for scans of different lengths of 150 mm and 450 mm for both phantoms are given in Table 3-7 and results quoted as a percentage of the equilibrium dose.

Values for the elliptical phantom were substantially higher than those for the cylindrical one. The central cumulative doses for a 150 mm scan at the anterior peripheries of the ellipse phantom are 20% to 47% higher than the lateral values. However, the doses at the sides attained D_{eq} within a shorter length of phantom (table 3-7). Thus while the central cumulative doses at the lateral periphery of the elliptical phantom are 18% to 27% greater than those at the centres for a 150 mm long scan, the values for D_{eq} were only 1%-9% higher than in the centre. Central cumulative doses at the centre of an elliptical phantom for a 150 mm long scan were within 21% to 25% of the equilibrium value, compared to 24% to 32% for a cylindrical phantom. The ratio of the cumulative doses at the centre of the elliptical and cylindrical phantoms was larger for the Toshiba scanner, than for the GE and Philips scanners. As with the peak dose and CTDI, the ratio for the lateral periphery was less than 0.97 for the Toshiba scanner, but 1.09 and 1.11 for the GE and Philips scanners respectively (table 3-6) due to the bow-tie filter as explanined in section 3.3.1.

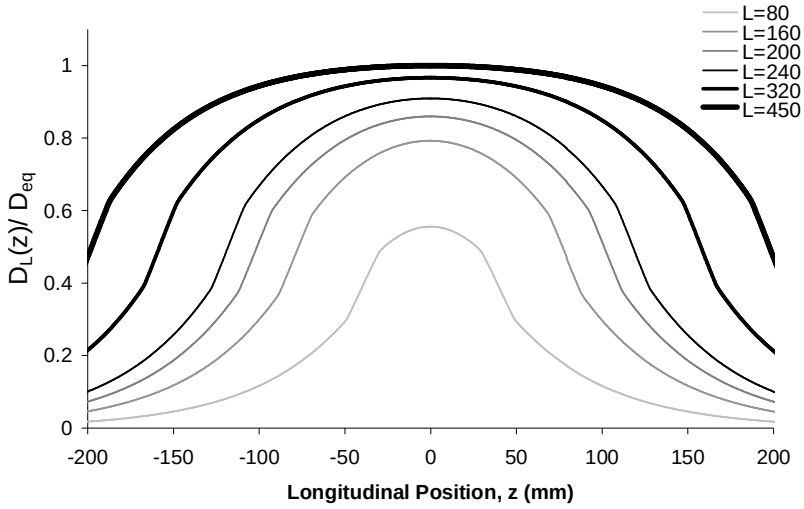

Figure 3-17 Simulated central cumulative dose distribution along central axis in an infinitely long elliptical phantom for various scanning lengths (L), simulated using Gafchromic film profile measurements taken from Toshiba Aquillion 64 scanner at 120 kVp for a 16 mm wide beam

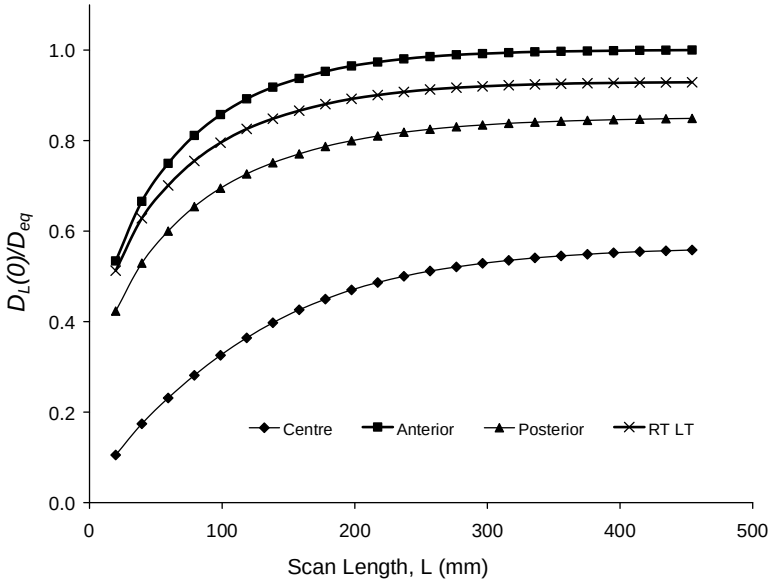

(a)

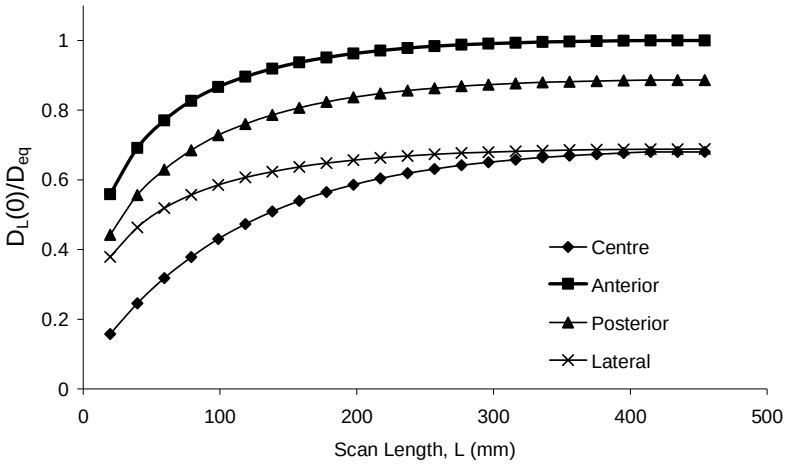

(b)

Figure 3-18 Calculations of central cumulative dose $D_L(0)$ at the central and peripheral positions as a function of scan length derived from SSDPs for scans using 120 kV and 16 mm wide beam on a Toshiba Aquillion 64 scanner for (a) the cylindrical and (b) the elliptical phantoms

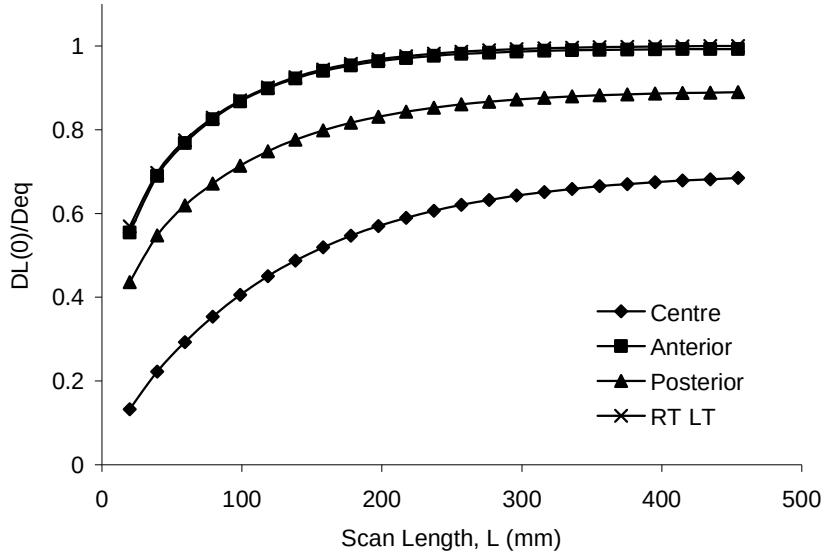

(a)

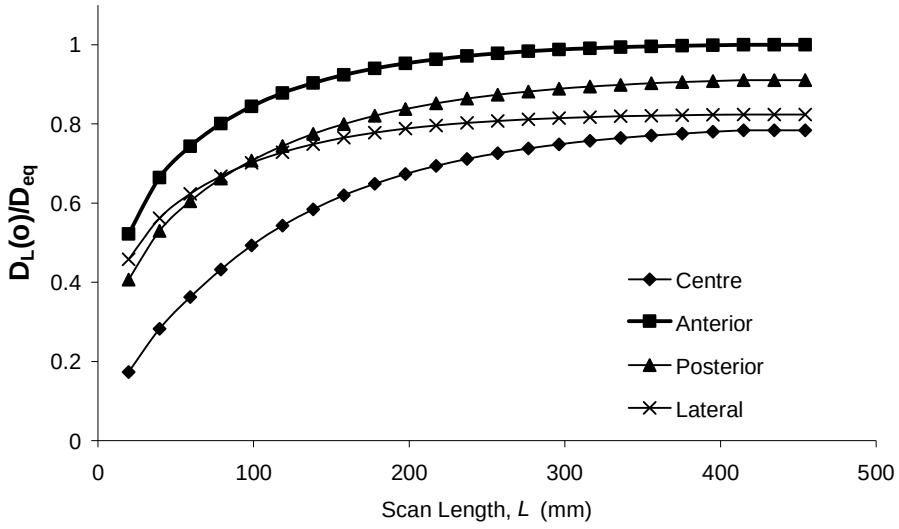

(b)

Figure 3-19 Calculations of central cumulative dose $D_L(0)$ at the central and peripheral positions as a function of scan length derived from SSDPs for scans using 120 kV and 20 mm wide beam on a GE Lightspeed scanner for (a) the cylindrical and (b) the elliptical phantoms

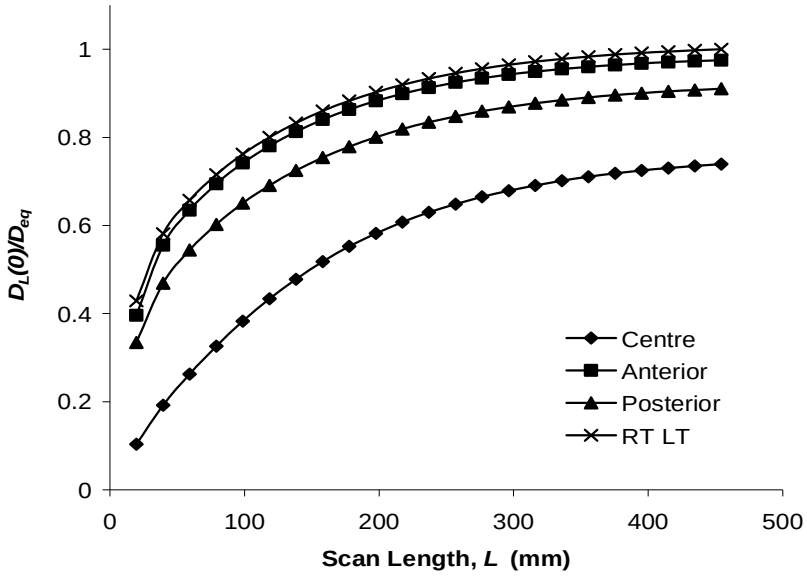

(a)

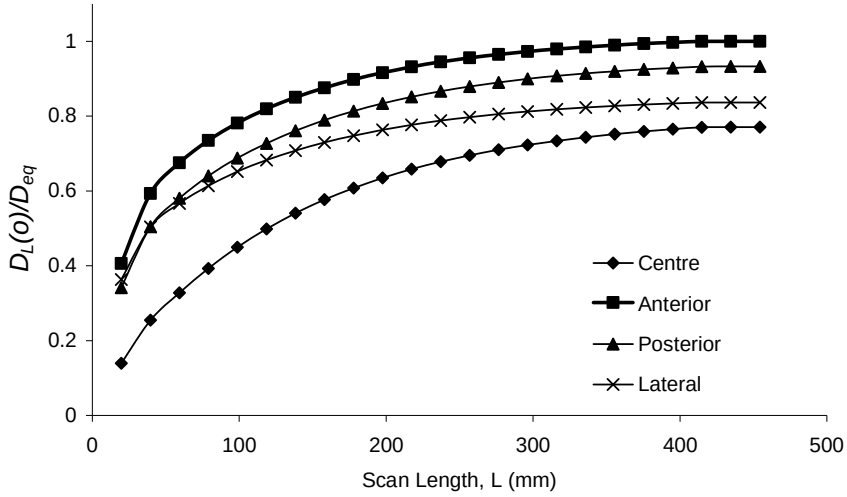

(b)

Figure 3-20 Calculations of central cumulative dose $D_L(0)$ at the central and peripheral positions as a function of scan length derived from SSDPs for scans using 120 kV and 25 mm wide beam on a Philips Briliance 64 scanner for (a) the cylindrical and (b) the elliptical phantoms

Table 3-7 Central cumulative doses of 450 mm long phantoms simulated from Gafchromic film measurements for various scan lengths, using 20 mm beam widths. Results are expressed as percentages of the cumulative equilibrium dose (D_{eq}) from an infinitely long scan
(Note: Central cumulative doses were simulated from SSDP, using 120 kV, the beam width for the Toshiba, GE and Philips scanner were 16, 20 and 25 mm)

Model	Position of measurement	Cumulative Dose (mGy/100mAs)					%of the equilibrium dose*			Ratio of Ellipse and Cylinder phantoms		
		Scan Length					Scan Length				Scan Length	
		150 mm	200 mm	300 mm	400 mm	∞	150 mm	200 mm	300 mm		150 mm	∞
Toshiba Aquillion 64	**Elliptical Phantom**											
	Centre	10.88	11.82	13.12	13.72	13.72	79.3	86.2	95.6	Centre	1.64	1.57
	Anterior Periphery	18.89	19.40	19.98	20.16	20.16	93.7	96.2	99.1	Anterior Periphery	1.29	1.30
	Lateral Periphery	12.84	13.23	13.70	13.88	13.88	92.5	95.3	98.7	Lateral Periphery	0.96	0.97
	Cylindrical Phantom											
	Centre	6.64	7.32	8.29	8.76	8.76	75.8	83.6	94.6			
	Anterior Periphery	14.61	15.01	15.42	15.52	15.52	94.1	96.7	99.4			
	Lateral Periphery	13.35	13.75	14.22	14.38	14.38	92.8	95.6	98.9			
GE LightSpeed 16	**Elliptical Phantom**											
	Centre	6.94	7.55	8.39	8.79	8.79	79.0	85.9	95.4	Centre	1.58	1.53
	Anterior Periphery	10.36	10.68	11.07	11.21	11.21	92.4	95.3	98.8	Anterior Periphery	1.30	1.34
	Lateral Periphery	8.58	8.83	9.13	9.23	9.23	93.0	95.7	98.9	Lateral Periphery	1.08	1.09
	Cylindrical Phantom											
	Centre	4.39	4.82	5.44	5.75	5.75	76.3	83.8	94.6			
	Anterior Periphery	7.95	8.15	8.34	8.39	8.39	94.8	97.1	99.4			
	Lateral Periphery	7.98	8.18	8.40	8.46	8.46	94.3	96.7	99.3			

***** the cumulative equilibrium dose (D_{eq}) was derived from 450 mm long phantom

Table 3-7 (Cont.) Central cumulative doses of 450 mm long phantoms simulated from Gafchromic film measurements for various scan lengths, using 20 mm beam widths. Results are expressed as percentages of the cumulative equilibrium dose (D_{eq}) from an infinitely long scan
(Note: Central cumulative doses were simulated from SSDP, using 120 kV, the beam width for the Toshiba, GE and Philips scanner were 16, 20 and 25 mm)

Model	Position of measurement	Cumulative Dose (mGy/100mAs)					% of the equilibrium dose*			Ratio of Ellipse and Cylinder phantoms		
		Scan Length					Scan Length				Scan Length	
		150 mm	200 mm	300 mm	400 mm	∞	150 mm	200 mm	300 mm		150 mm	∞
Philips	**Elliptical Phantom**											
Brilliance 64	Centre	10.53	12.02	13.21	14.07	14.07	74.8	85.4	93.9	Centre	1.45	1.32
	Anterior Periphery	16	17.02	17.77	18.27	18.27	87.6	93.2	97.3	Anterior Periphery	1.36	1.34
	Lateral Periphery	13.33	14.19	14.84	15.28	15.28	87.2	92.9	97.1	Lateral Periphery	1.11	1.09
	Cylindrical Phantom											
	Centre	7.26	8.58	9.372	10.68	10.68	68.0	80.3	87.8			
	Anterior Periphery	11.77	12.60	13.23	13.68	13.68	86.2	92.3	96.9			
	Lateral Periphery	12.05	12.89	13.53	13.97	13.97	86.3	92.3	96.9			

***** the cumulative equilibrium dose (D_{eq}) was derived from 450 mm long phantom

3.3.6 Measurements from ATCM system using Gafchromic film

The mean ESAKs, peripheral doses and central doses along 100 mm lengths in the middle of the elliptical phantom from helical scans of the whole phantom are shown in figure 3-21 in the form of bar charts depicting changes with ATCM settings. Ratios of the dose in each position relative to that at the centre are given in table 3-8 to demonstrate differences in the distribution of air kerma. The doses adjacent to the anterior of the phantom were the largest with the peripheral dose for the anterior being 1.3-1.7 times that to the laterals of the phantom with a fixed mA, while the peripheral dose at the sides was 1.2-1.3 times that at the centre. The dose distribution changed with the ATCM in operation. From the Toshiba scanner the ratio of the peripheral doses at the anterior and the side was 1.3 with the high quality option and the standard option. The change from a fixed tube current to the high quality ATCM mode reduced the anterior dose to 68% of the original and that at the side to 86%. The change from high quality to standard mode gave similar reductions for all parts of the phantom reducing the anterior further to 35% of the fixed mA value and the side dose to 47%. Further reductions for this phantom achieved by changing to the very low dose option were only 10% or less due to the minimum mAs setting limiting the level of dose reduction possible. The air kerma at the periphery are up to 14% larger than ESAKs at corresponding positions, but the pattern of reduction as the ATCM was implemented was similar in both. For the Philips scanner, the change from the fixed tube current technique to the recommended setting (162 mAs/slice) reduced the doses at all positions to 30% of the original, but the ratios of doses in different positions within the phantom remained virtually constant as expected. For the GE scanner, the change from fixed mAs to the recommended value of NI 11.57 reduced the dose to 82%-87%. However, the change from NI 11.57 to NI 16.20 reduced the doses further to 47%-56% for the different positions. The relative differences in the changes in dose at different positions within the phantom were slightly smaller than for the Toshiba.

As shown in figure 3-21, for the fixed mAs technique, peripheral dose at the anterior was 70% higher than at the lateral position for the Toshiba scanner, while anterior peripheral doses for the GE and Philips scanners were 40% and 27% higher, respectively. Comparisons of doses for the recommended setting from each scanner (SD = 12.5 for the Toshiba, NI = 11.57 for the GE and 162 mAs/slice for the Philips scanner) showed that doses at all positions for the Philips scanner were around 50-60% less than those for the other scanners. The central dose in the GE scanner was 4% less than that of the Toshiba scanner and doses in the peripheral positions were up to 10% less.

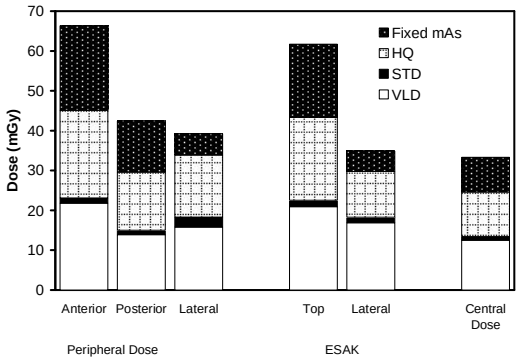

(a)

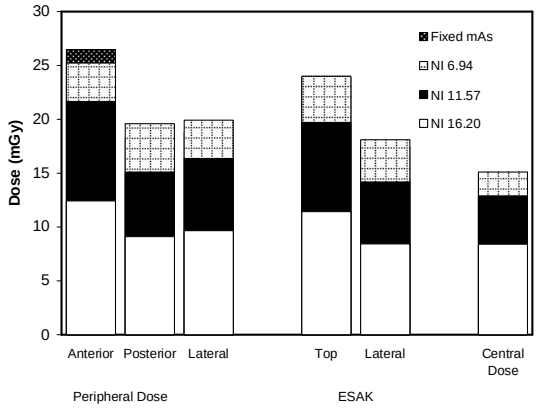

(b)

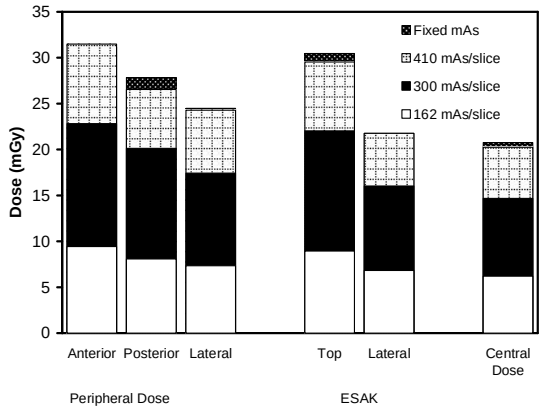

(c)

Figure 3-21 Mean results for peripheral, ESAK and central dose along 100 mm lengths in the middle of the elliptical dosimetry phantom, using different ATCM options, (a) Toshiba Aquilion 64, (b) GE Discovery 64 scanner and (c) Philips Brilliance 64. The recommended settings are standard option for the Toshiba, NI value of 11.57 for the GE and 162 mAs/slice for the Philips scanners (HQ=high quality, STD=standard and VLD=very low dose Toshiba ATCM options)

Table 3-8 Central axis doses along 100 mm lengths in the middle of the elliptical dosimetry phantom, and ratios of peripheral doses and ESAKs to the dose along the central axis

CT scanner		ATCM option			
		Fixed mAs	**HQ**	**STD**	**VLD**
Toshiba Aquilion 64	Centre Dose (mGy)	33.3	24.6	13.4	12.5
	Ratio of Periphery Dose				
	$\frac{Ant.Peri.}{Lat.Peri}$	1.69	1.33	1.26	1.38
	Ratio of ESAK				
	$\frac{Ant.ESAK}{Lat.ESAK}$	1.77	1.46	1.23	1.24
	Ratio of Periphery dose to Centre dose				
	$\frac{Ant.Peri.}{CentreDose}$	1.99	1.83	1.72	1.74
	$\frac{Post.Peri.}{CentreDose}$	1.27	1.20	1.12	1.11
	$\frac{Lat.Peri.}{CentreDose}$	1.18	1.38	1.37	1.26
Philips Brilliance 64		**Fixed mAs**	**410 mAs/slice**	**300 mAs/slice**	**162 mAs/slice**
	Centre Dose (mGy)	20.76	20.25	14.68	6.20
	Ratio of Periphery Dose				
	$\frac{Ant.Peri.}{Lat.Peri}$	1.27	1.30	1.31	1.29
	Ratio of ESAK				
	$\frac{Ant.ESAK}{Lat.ESAK}$	1.40	1.36	1.37	1.31
	Ratio of Periphery dose to Centre dose				
	$\frac{Ant.Peri.}{CentreDose}$	1.50	1.55	1.56	1.52
	$\frac{Post.Peri.}{CentreDose}$	1.34	1.31	1.37	1.30
	$\frac{Lat.Peri.}{CentreDose}$	1.18	1.20	1.19	1.18
GE Discovery 64		**Fixed mAs**	**NI=6.94**	**NI=11.57**	**NI=16.20**
	Centre Dose (mGy)	15.04	15.10	12.90	8.40
	Ratio of Periphery Dose				
	$\frac{Ant.Peri.}{Lat.Peri}$	1.40	1.27	1.32	1.29
	Ratio of ESAK				
	$\frac{Ant.ESAK}{Lat.ESAK}$	1.37	1.33	1.39	1.36
	Ratio of Periphery dose to Centre dose				
	$\frac{Ant.Peri.}{CentreDose}$	1.76	1.67	1.68	1.48
	$\frac{Post.Peri.}{CentreDose}$	1.21	1.30	1.17	1.08
	$\frac{Lat.Peri.}{CentreDose}$	1.25	1.32	1.27	1.15

3.4 Discussion

3.4.1 Dose distributions in elliptical and cylindrical phantoms

Dose distributions within elliptical and cylindrical phantoms with similar cross-sectional dimensions to the human body have been analysed using measurements based on Gafchromic film. There are significant differences in the dose levels and distributions within the two designs of phantom (figures 3-14 to 3-16, tables 3-6 and 3-7). The dose level within the peak at the centre of the elliptical phantom was between 70% and 100% higher for a single tube rotation than for the scans performed with the cylindrical phantom using similar exposure factors. This occurs because of the higher transmission of the x-ray beam through the thinner AP phantom dimension. The dose at the anterior periphery in the elliptical phantom was between 20% and 30% higher than for the cylindrical phantom, primarily because the anterior surface in the elliptical phantom is nearer to the isocentre. As a result x-ray beams incident obliquely on the phantom periphery pass through a section closer to the middle of the bow-tie filter, where the primary beam attenuation is lower. The central z-axis cumulative dose at the anterior periphery of the ellipse was 45% higher than the lateral periphery dose in the Toshiba scanners for the same reason, although the differences were less for the Philips and GE scanners which were 20%, (figures 3-18 to 3-20, table 3-8). The differences in results between scanners can be explained by differences in the shapes of the bow-tie filters (figure 3-9). The shape of the bow-tie filter for the Toshiba scanner with scans using the large field of view is significantly narrower than those for the other scanners, this could explain the result observed. Values for the X-ray beam, fan angle for the different manufacturers of 49.2°, 56° and 57° have been reported for Toshiba, GE and Philips scanners respectively (Mahesh 2009, p.46), which supports the differences observed in this study.

The doses at the laterals of the elliptical phantom are within ±10% greater than those for the cylindrical phantom (table 3-6). There is more attenuation along the lateral axis of the elliptical phantom (330 mm in diameter) compared with the cylindrical phantom (320 mm in diameter), so the contribution to the dose at the lateral periphery of the elliptical phantom when the beam is directed horizontally will be slightly lower than that for the cylindrical phantom. But

when the x-ray beam is incident on the anterior and posterior of the phantom and for the majority of oblique orientations the contribution to the lateral periphery dose from the outer part of the fan beam will be larger, because the thickness of PMMA attenuating the radiation is less than for the cylindrical phantom, as can be seen from figure 3-5.

3.4.2 Dose variables for practical measurements

The $CTDI_{100}$ and central z-axis cumulative dose at 150 mm scan length for the ellipse were 50% to 70% higher than for the 320 mm cylinder in the centre, and 20%-40% higher in the anterior periphery (figures 3-14 to 3-16, tables 3-6 and 3-7). The differences in $CTDI_{100}$ and central z-axis cumulative dose at the centre between the elliptical and cylindrical phantoms are less than those for the peak dose values within the main beam (table 3-5) because of the more rapid decline in the doses in the central scatter tails within the ellipse than in the cylinder. The $CTDI_{100}$ values in the elliptical phantom at the centre are about 40% to 50% less than that at the anterior periphery and 26% to 33% less than that at the laterals. For comparison, the $CTDI_{100}$ in the cylindrical phantom at the centre were 47% to 61% less than that at the periphery.

These results show that the shape of a phantom has a significant influence on both the dose level and the dose distribution. The elliptical phantom has a higher dose in the centre because of the lower attenuation due to the smaller depth of tissue along the shorter axis. It also has a higher dose at the anterior periphery which is nearer to the isocentre. The larger cylindrical phantom does not take into account the different distances of the anterior and lateral surfaces of the body from the isocentre. Thus the elliptical phantom will give a better representation for the dose to a human trunk and takes more account of differences in bow tie filters which are relevant to clinical practice.

3.4.3 Influence of lengths of phantoms on practical measurements

Many studies have been written about the underestimation of dose by the $CTDI_{100}$ in dosimetry phantoms because the contribution in the scatter tails beyond z = ± 50 mm is not negligible. Similar arguments apply to cylindrical and elliptical phantoms. The central z-axis cumulative dose varies with the scan length in different ways within the two types of phantom, as shown in figures 3-21 to 3-23. This is because the dose level within the primary beam is higher and the contribution from scatter is lower for the thinner elliptical phantom. The peripheral doses in both phantoms approach an equilibrium value earlier. The central cumulative dose at the centre of the 150 mm long elliptical phantom reaches a higher proportion of D_{eq} than in the cylindrical phantom (figures 3-18 to 3-20, table 3-7). The central cumulative dose for the ellipse is within 3% of D_{eq} for a phantom of length *L* > 355 mm and within 1% for a 400 mm long phantom (figures 3-18 to 3-20). This result is similar to that found by Nakonechy *et al* (2005) who concluded that the central axis dose reached equilibrium for *L* > 350 mm. The central cumulative dose in the cylindrical phantom, D_{eq} reached the equilibrium value for a slightly longer scan.

3.4.4 Measurements from ATCM system

Gafchromic film was used to assess the variation in dose resulting from operation of the ATCM. Doses were calculated along 100 mm lengths in the middle of the elliptical dosimetry phantom for comparison. The doses near the anterior of the phantom are largest (figure 3-21, table 3-8) because of the lower attenuation in the AP direction and the anterior surface being closer to the isocentre. The peripheral doses were greater than the ESAKs at corresponding positions because of larger components of scattered radiation from within the phantom. These differences were larger for the Toshiba scanner than the other scanners which is thought to result from a narrower fan beam profile associated with the shape of the bow-tie filter (figure 3-9). When the high quality mode was implemented for the Toshiba scanner, the anterior and posterior doses declined substantially, as the tube current was reduced in the AP direction to take account of the lower attenuation, making the peripheral dose distributions more uniform. For the GE

and Philips scanners the differences in anterior and peripheral doses with a fixed tube current were less (figure 3-21) and this is thought to be linked to the broader fan beam profiles for these scanners (figure 3-9). There were no differences between the doses of the fixed tube current technique and the high quality image settings. Thus the Toshiba scanner ATCM operates to equalise larger differences in peripheral dose resulting from use of a narrow bow-tie filter, but such differences are less significant in the other scanners.

3.4.5 Shape for a practical CT dosimetry phantom

The view has been expressed in recent years that the use of the $CTDI_{100}$ is no longer appropriate, because it underestimates the dose received by the patient (Brenner *et al.,* 2006; Dixon 2003; Dixon 2006; Dixon *et al.,* 2005). If the practical measurement is required to provide an assessment of dose that is closely linked to that of a patient, then the cross-sectional shape of the phantom used should also be considered. This study has shown that $CTDI_{\ell}$ and central cumulative dose measured in the elliptical phantom with dimensions close to that of a human torso are up to 70% higher than those in the standard cylindrical phantom depending on position of measurements and scan length. The elliptical phantom has a higher dose in the centre and at the anterior periphery. The cylindrical phantom does not take into account the different distances of the anterior and lateral surfaces from the isocentre and the resulting influence of the bow tie filters that are relevant to clinical practice on dose.

Whether or not these differences are important depends on how measurements of CTDI and cumulative dose are to be used. If the measurements are primarily for quality assurance (QA), allowing performance of different scanners to be compared, then the underestimation of dose may not be too important.

Whether or not elliptical phantoms might be used for standard CT dosimetry measurements, it is important to develop a knowledge of dose distributions within elliptical bodies in order to interpret the influence of the automatic tube current modulation systems on current CT scanners.

3.5 Conclusions

Dose distributions in an elliptical PMMA phantom for scans on three CT scanners have been measured using Gafchromic film which replicates the effect of the thinner A-P dimension for an average UK patient. CTDIs for chambers of different lengths and central cumulative doses for scans of different lengths have been determined from simulations using SSDP data. Dosimetry measurements with an elliptical phantom demonstrate differences in dose distribution with various CT scanners due to beam shape. The $CTDI_{100}$ and central cumulative doses at the centre of the phantom from a 150 mm long scan in the elliptical phantom were 50%-70% higher than those in the cylindrical phantom for the same scan parameters. The differences are less marked for the GE and Philips scanners because of the narrower fan beam profile in the x-y plane for the Toshiba scanner linked to the shape of the bow-tie filter.

The elliptical phantom enabled differences when the ATCM was implemented in x-y plane to be investigated. The ATCM reduced the anterior dose substantially more for the Toshiba scanner, related to the bow-tie filter, bringing doses around the elliptical phantom to a similar level. Such differences will have an important influence on doses to different organs in scans of patients and should be taken into account when evaluating patient doses distribution under ATCM operation. Since the human body is elliptical in shape with varying sizes, a phantom of multiple elliptical sections has been developed for the ATCM system test in both x-y plane and z-axis. Details are shown in the next chapter.

4 A prelimary study exploring the use of a multi section phantom for Toshiba Aquilion 64 CT scanners

4.1 Introduction

In order to gain a better understanding of the dependence of dose distribution on body shape, a phantom comprising a single ellipse had been used to study the variation in dose with ATCM operation in the x-y plane as discussed in chapter 3. For this chapter, initial studies of distributions of air kerma in a multi section elliptical phantom, enabled tube current modulation in both x-y plane and z-axis to be assessed, using Gafchromic XR-QA film. Initial investigations were undertaken for Toshiba Aquilion 64 CT scanners.

In an effort to address concerns about high doses that are received from CT scans, manufacturers have introduced the capability to modulate the tube current to reduce the radiation exposure for regions of lower attenuation (Kalra *et al.,* 2004a; Soderberg and Gunnarsson 2010). The ATCM systems automatically adjust the tube current to take into account the X-ray attenuation of the section of the patient being scanned. The aim is to obtain images with a consistent image quality or quantum noise level. Options available may vary the tube current with both the tube orientation in the x-y plane and the z-axis position. Several investigators have published data relating to the efficiency of ATCM systems in reducing dose for patient examinations. However, there is little published information explaining how ATCM changes the mA for different patient sizes, how this is related to the distribution of dose within a patient or phantom, and how the image noise varies.

One of the challenges facing CT users is to determine how modifications to scan protocols using ATCM will affect image quality and patient dose. In order that full use can be made of these facilities in optimisation, there is a need to develop phantoms and test methods to investigate and record the performance of ATCM systems. There have been some studies developing phantoms for the ATCM system test. Such devices would ideally be based on elliptical phantoms of different size that more closely resemble human anatomy, in order that the

performance of the ATCM can be determined under conditions akin to those used in clinical practice. The purpose of this study is to investigate the variation in tube current, dose across the surface and within elliptical phantoms of differing dimensions as well as image quality in terms of image noise produced by different ATCM options.

4.2 Materials and Methods

4.2.1 Materials

4.2.1.1 CT scanner

Measurements were made for helical scans on two Toshiba Aquillion 64 scanners (scanners A and B). In the Aquilion scanners, the ATCM (Sure exposure) allows users to set a target standard deviation in pixel value and to define a minimum and maximum (range) of tube current in mA that can be used. Sure exposure uses data obtained from SPRs to determine the z-axis modulation (Lee *et al.,* 2009). The water equivalent diameter at each level of the patient is calculated and compared to the maximum attenuation. The tube current required at the maximum water equivalent diameter to achieve the selected standard deviation is then modulated to maintain the standard deviation throughout the examination, as the patient diameter varies.

4.2.1.2 Multi section elliptical phantom (Torso phantom)

In order to investigate the operation of the ATCM along the z-axis as well as in the x-y plane, a phantom comprising five elliptical segments of differing dimensions has been constructed from polyethylene (density 0.95 g/cm^3) (figure 4-1). Each section of the torso phantom is 80 mm in length and the diameters of the major and minor axes respectively for the five sections are: 1) 220 mm × 310 mm, 2) 240 mm × 330 mm, 3) 270 mm × 350 mm, 4) 200 mm × 400 mm and 5) 120 mm × 180 mm. The sizes were chosen to reflect the varying dimensions along the length of the trunk. Section 4 had a longer major axis, but the minor axis was smaller than section 3 in order to simulate the cross section at the shoulders. The sections were held together by two polyethylene rods each 10 mm in diameter running the length of the phantom through holes 140 mm apart on the long axes of the ellipses. The rods passed through 2 mm thick polycarbonate endplates that supported the phantom in a horizontal position on the patient couch. The ends of the rods were threaded and polyethylene nuts and washers were used to hold the sections in close contact. A hole 12 mm in diameter along the central axis allowed measurements of dose within the phantom. The phantom was laid on the couch so as to represent a patient lying supine with the central axis horizontal, supported by the polycarbonate end plates, which were shaped to fit into the curvature of the couch. The phantom was positioned so that the central axis was at the isocentre and the upper and lower surfaces will be referred to as anterior and posterior respectively.

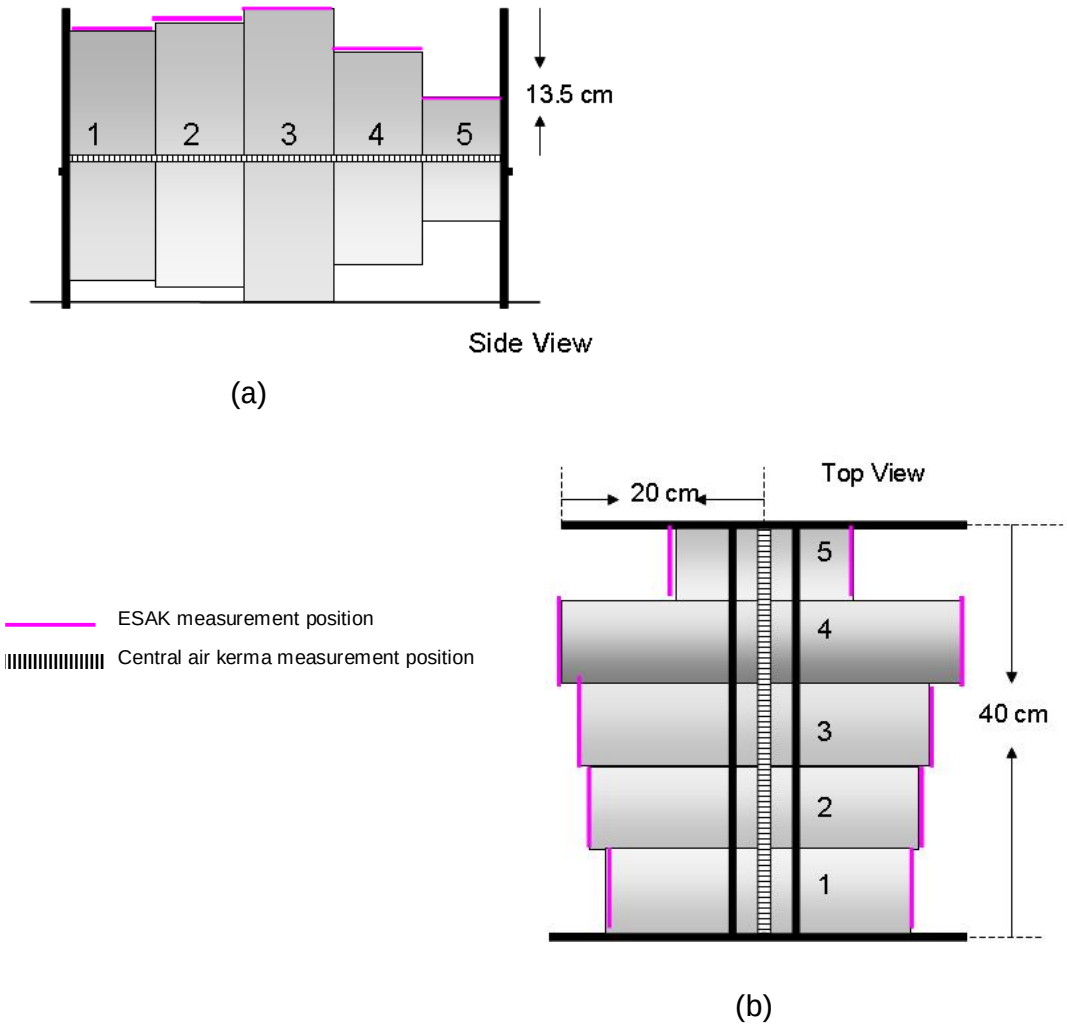

Figure 4-1 Prototype ATCM torso phantom (a) the side view (b) the top view of phantom and positions for ESAK and central air kerma measurements

4.2.2 Methods

4.2.2.1 Dose quantities measurement

Dose distributions were recorded using strips of Gafchromic XR-QA film 8 mm wide, equal in length to the section of phantom being studied. The calibration of the film and methods used for the analysis of the dose data has been described in chapter 3.

ESAKs and central dose were chosen for measurements in the torso phantom.

- ESAKs were measured using strips of Gafchromic film 80 mm long, placed along the surfaces of each elliptical section on the anterior of the phantom at the upper end of the minor axes, and at the left and right hand sides of the phantom on the major axes.

- Air kerma along the central axis of the phantom was measured with a single strip of Gafchromic film placed in the central hole.

The mean ESAK along each section of the phantom was calculated from the average Gafchromic film data along the relevant section for the range of settings (figure 4-2).

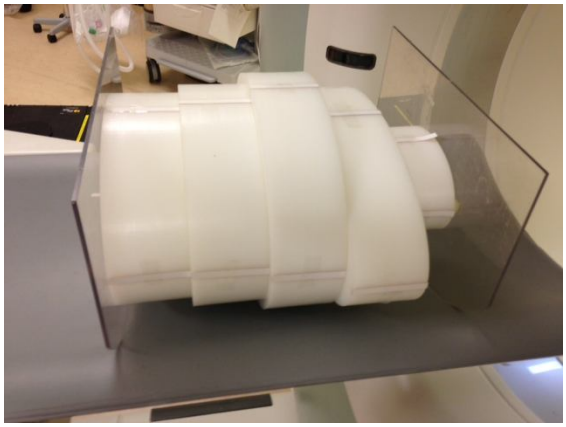

Figure 4-2 Position of torso phantom on the CT scanner couch for ESAK measurements
(Note: the ratios of lateral and AP diameters of all sections are 3:2 except section 4 for which the ratio is 2:1 in order to represent the shoulders

4.2.2.2 Testing Approach

Scan parameters used on the two CT scanners are shown in table 4-1. These correspond to ATCM options used in the routine CAP protocols, and these were compared with a fixed tube current setting. Five different standard ATCM modes are available on Aquilion scanners that correspond to the selection of different pre-selected image noise levels (Angle 2009; Soderberg and Gunnarsson, 2010), which are given in brackets; a) high quality (standard deviation (SD)=7.5 HU), b)

quality (SD=10 HU), c) standard (SD=12.5 HU), d) low dose (SD =15 HU), and e) very low dose (SD=17.5 HU). Four modes of operation were assessed on the two scanners 1) ATCM inactivated, 2) with the high quality option, 3) with the standard option and 4) with the very low dose option, as carried out in chapter 3. Gafchromic film measurements were made in all positions previously identified for each scan. For each, the length of scan was 395 mm covering the whole phantom, excluding the endplates. The direction of scan for the torso phantom is shown in figure 4-3.

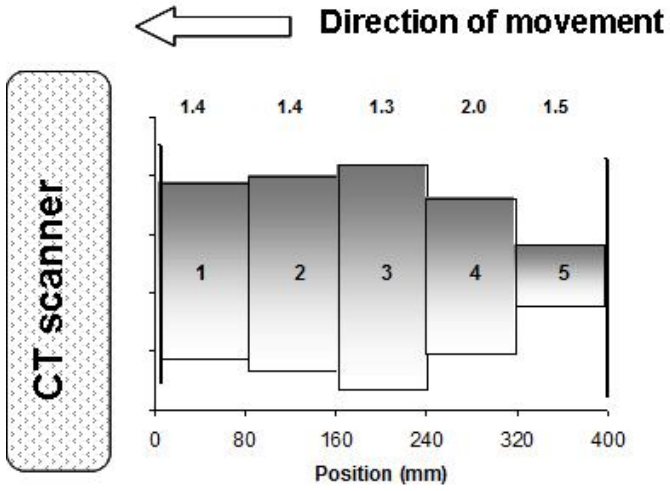

Figure 4-3 Scan direction of the torso phantom
(Note: the numbers above the sections of the phantom are ratios of the AP and lateral diameters)

Table 4-1 Scanning Parameters used for the present study

	Tube Voltage (kV)	Rotation Time (s)	Collimation	Field of View (mm)	Pitch	Recon. kernel	Tube Current	
							ATCM	Fixed mAs technique
A	120	0.5	64x0.5	400 (L)	0.828	FC13	50-240 (100-480mA)	200 (400 mA) CTDI= 30.4 mGy DLP=1.36Gy.cm
B	120	0.5	64x0.5	450 (LL)	0.828	FC13	50-240 (100-480mA)	240 (480 mAs) CTDI= 36.5 mGy DLP=1.85Gy.cm

4.2.2.3 Tube current variation and image noise

The variation in tube current (mA) for the two axes of the ellipse is displayed on the screen at the time of scan and was recorded photographically as only information on the average was contained in the DICOM header. Data on the tube current × rotation time product in terms of mAs per image, which is recorded in the DICOM header, were read out by an "Auto mA plugin", and were plotted against scanning position in terms of distance from the start of the scan.

The image noise was analysed using Image J (Ferreira and Rasband 2011). The image quality was evaluated by measuring the mean standard deviation in CT number from each image within 500 mm^2 regions of interest (ROIs). As a general rule, these were placed as close as possible to the centre of the phantom and at 1 cm from the edge in the four positions (Anterior, Posterior, Left and Right Lateral) for all images. However, the noise measurement at the lateral positions of the smallest section 5 was done at 3 cm from the edge to exclude the holes for the supporting rods, and the noise at the centre of the torso section phantom was measured by drawing eight ROIs around the central hole through the phantom (figure 4-4). The 'Measure Track plugin' from Image J was used to measure the z-profile of the ROI through a stack (Nicolai, 2009). The mean image SD values from all positions and the percentage variation were calculated.

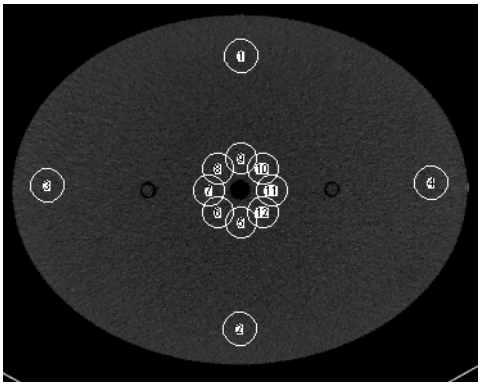

Figure 4-4 Positions of image noise measurement for torso phantom

4.3 Results

4.3.1 Measurement of ESAKs and central axis dose in the torso phantom

Measurements of ESAK for all sections of the phantom is shown in figure 4-5. The profiles with the fixed tube current had the highest ESAKs for the small section 5, and the ESAK for the lateral exposure through section 4 was the lowest. Figure 4-6a compares the average ESAKs across each section for the anterior and the sides of the phantom for each mode of operation to doses in the centre for scanner A. Figure 4-6b shows data for scanner B which followed a similar pattern to scanner A. The high quality mode showed reductions in ESAKs at the anterior for section 1 and the smaller section 5 of 42% and 33% respectively, and 17% to 25% for section 2-4. But there were virtually no reductions in the ESAKs in the lateral positions for sections 2-4. There were substantial reductions in the ESAKs of 33% to 48% for sections 1-4 with the change to the standard option, and further small reductions for all sections with the move to the very low dose option. The changes in the dose along the central axis with different programs are shown in figure 4-7. The doses were highest in section 5 and lowest in section 1 for all options. The changes followed those in the anterior ESAKs with the implementation of the high quality mode giving the greatest reduction for the smaller sections 5 and section 1, but greater reduction for sections 2-4 occurred with the move to the standard mode and a smaller reduction on the move to the very low dose option. The ratios of the ESAKs to the central axis doses in the same sections are given in table 4-2 to provide information on the dose distribution. The doses along the central axis were higher than the ESAKs at the lateral positions and higher than the anterior doses for sections 2 and 3 with fixed tube current and section 2-4 when the ATCM was operational (figure 4-6, table 4-2).

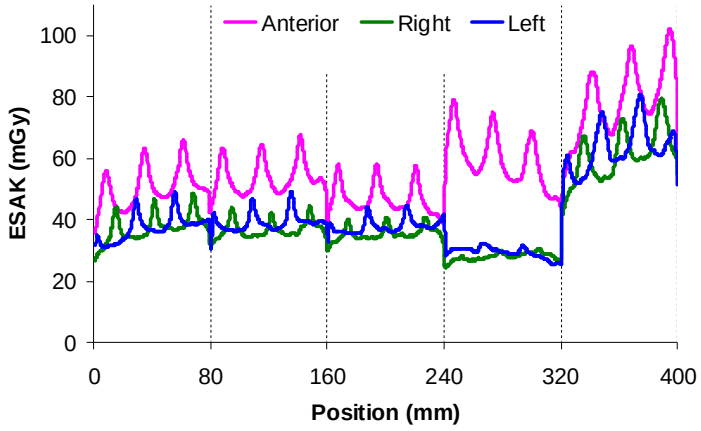

(a)

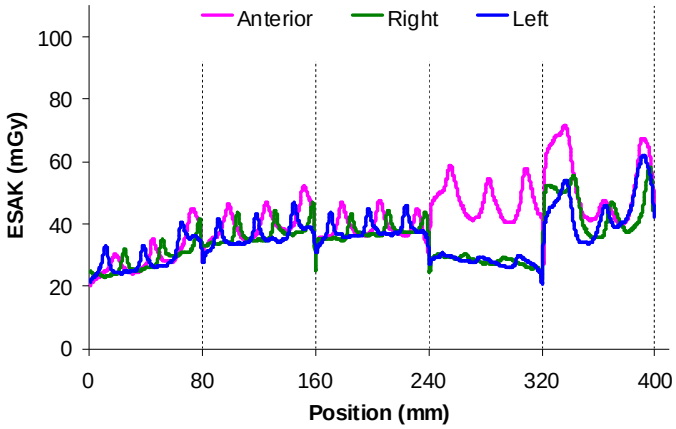

(b)

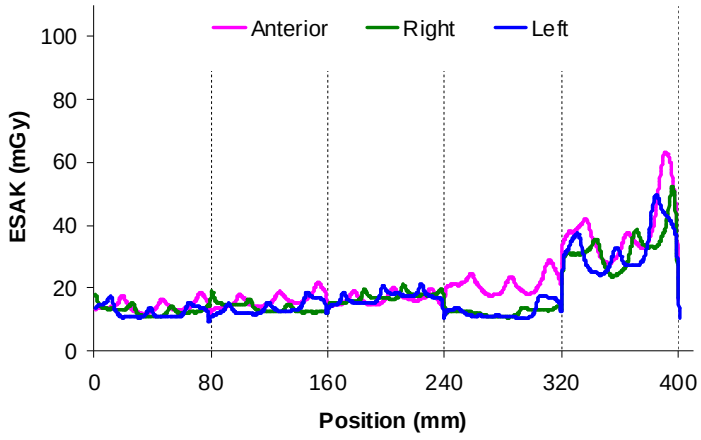

(c)

Figure 4-5 ESAK measurements along the length the torso phantom at different positions for (a) fixed tube current technique, and ATCM options (b) high quality and (c) very low dose. Measured from scanner A

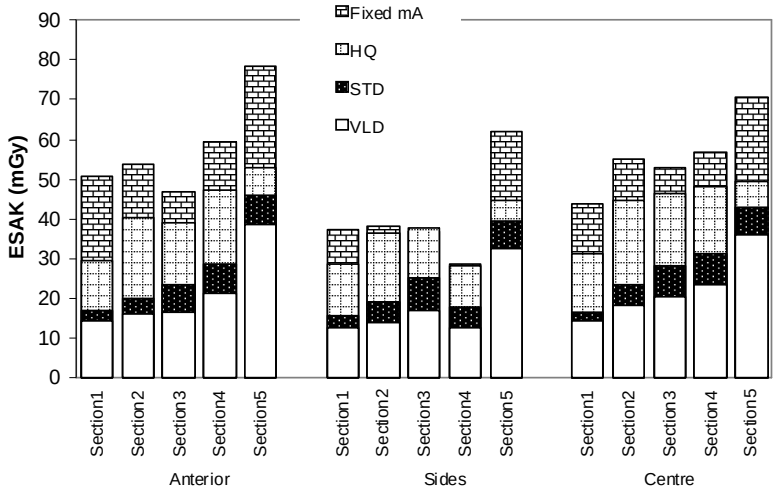

(a)

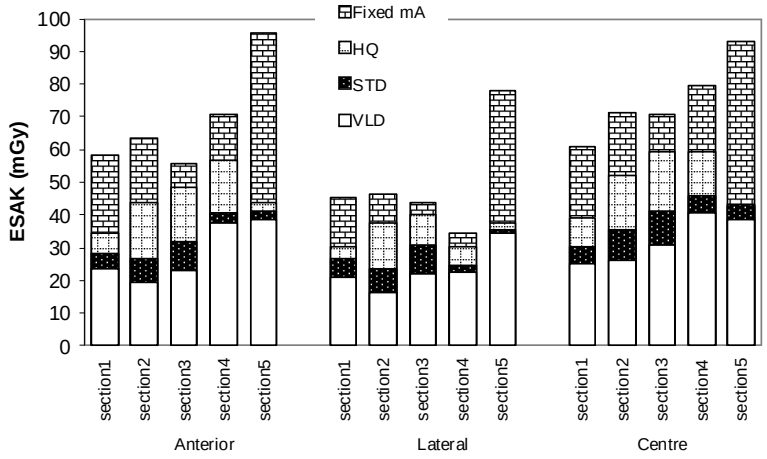

(b)

Figure 4-6 Average ESAK at the anterior and sides, and the central doses across each 80 mm section of the torso phantom for fixed mA and ATCM modes; HQ - high quality, STD - standard and VLD - very low dose. (a) Measured from scanner A, (b) Measured from scanner B

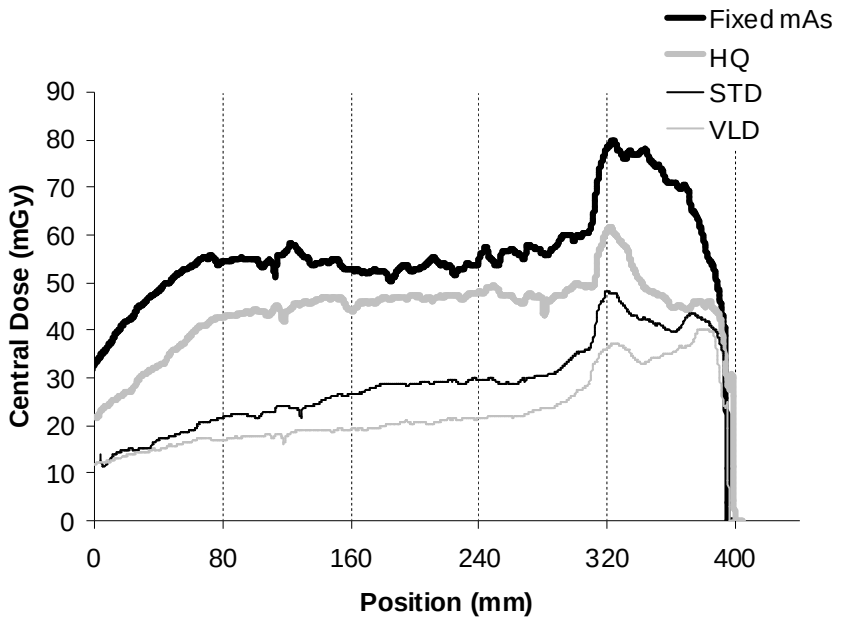

Figure 4-7 Dose along the central axis of the torso phantom; section 1 (0-80mm) to section 5 (320-400 mm), for fixed mA and ATCM modes; HQ - high quality, STD - standard and VLD - very low dose, measured from scanner A

Table 4-2 Mean central axis dose along the 80 mm width of each section in the CT torso phantom, and ratios of Anterior and Lateral ESAK and ratios of ESAK to the centre dose in each section. Measured from scanner B

		ATCM option			
		Fixed mA	HQ	STD	VLD
Section1	Centre Dose (mGy)	44.22	32.39	16.32	14.18
	Ratio of ESAK				
	$\frac{Ant.ESAK}{Lat.ESAK}$	1.29	1.14	1.07	1.13
	Ratio of ESAK to Centre dose				
	$\frac{Ant.ESAK}{CentreDose}$	1.14	0.91	1.03	1.00
	$\frac{Lat.ESAK}{CentreDose}$	0.85	0.88	0.94	0.89
Section2	Centre Dose (mGy)	54.91	44.72	23.07	17.90
	Ratio of ESAK				
	$\frac{Ant.ESAK}{Lat.ESAK}$	1.37	1.17	1.13	1.18
	Ratio of ESAK to Centre dose				
	$\frac{Ant.ESAK}{CentreDose}$	0.98	0.90	0.87	0.89
	$\frac{Lat.ESAK}{CentreDose}$	0.69	0.81	0.83	0.76
Section3	Centre Dose (mGy)	52.93	46.60	28.23	20.01
	Ratio of ESAK				
	$\frac{Ant.ESAK}{Lat.ESAK}$	1.28	1.20	1.03	1.05
	Ratio of ESAK to Centre dose				
	$\frac{Ant.ESAK}{CentreDose}$	0.89	0.83	0.83	0.82
	$\frac{Lat.ESAK}{CentreDose}$	0.70	0.81	0.90	0.85
Section4	Centre Dose (mGy)	56.93	48.40	30.84	22.85
	Ratio of ESAK				
	$\frac{Ant.ESAK}{Lat.ESAK}$	2.06	1.89	1.64	1.65
	Ratio of ESAK to Centre dose				
	$\frac{Ant.ESAK}{CentreDose}$	1.04	0.97	0.93	0.93
	$\frac{Lat.ESAK}{CentreDose}$	0.51	0.58	0.57	0.54
Section5	Centre Dose (mGy)	70.50	48.04	42.72	35.10
	Ratio of ESAK				
	$\frac{Ant.ESAK}{Lat.ESAK}$	1.23	1.17	1.17	1.12
	ESAK : centre dose				
	$\frac{Ant.ESAK}{CentreDose}$	1.11	1.10	1.08	1.10
	$\frac{Lat.ESAK}{CentreDose}$	0.88	0.93	0.92	0.93

ATCM modes; HQ - high quality, STD - standard, VLD - very low dose

4.3.2 Evaluation of automatic tube current modulation

The variations in tube current with position along the torso phantom during scans with different ATCM options are shown in figure 4-8 for AP and lateral projections. The standard and very low dose options have substantially lower mA values with adjustments in rate of change that lead to regular fluctuations of 100 mA to 200 mA throughout the length of the phantom. Close examination of the tube current data in figure 4-8 suggested that the rate of change in prescribed mA for AP and lateral remained constant during each 26.5 mm section of scan, which equates to one complete rotation for the 32 mm beam width and pitch of 0.828. as illustrated in figure 4-9. The rate of change in tube current was then adjusted to take account of the attenuation for the next section of the phantom.

The link between image noise levels and mAs per image is shown in figure 4-10 for three ATCM options. The noise in section 5 of the phantom was low in all sequences, because the tube current values were high and the dimensions of section 5 of the phantom are small (figure 4-12), and a similar pattern in tube current change is followed for the last 100 mm of the scan with all ATCM options. Figure 4-11 illustrates that as expected the average noise increased as the setting was changed from high quality to low dose. Whilst in the high quality mode the noise was relatively constant in each section of the phantom, in the standard and low dose modes the noise level varied considerably. The noise level for the fixed tube current was 8.3±2 HU for sections 1 to 4 and increases to 9.9±1.3 HU with the high quality option.

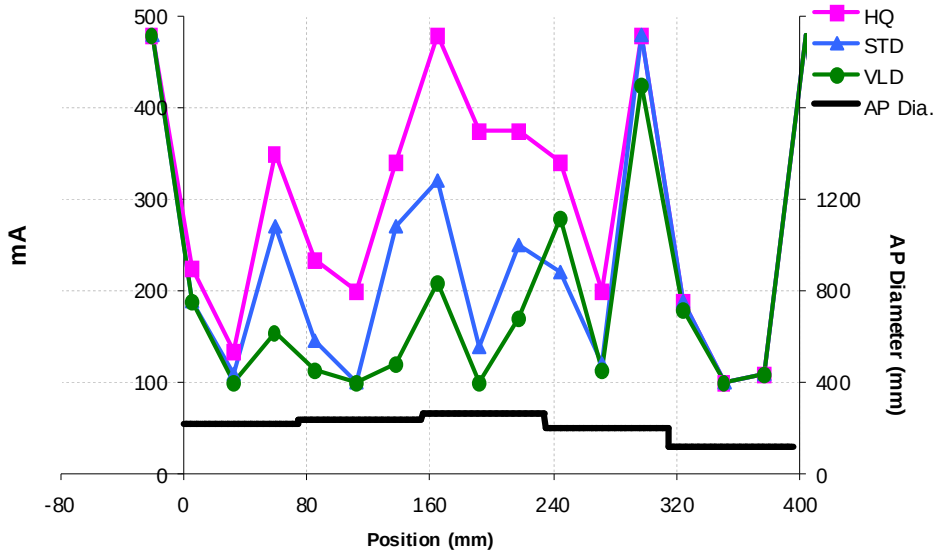

(a)

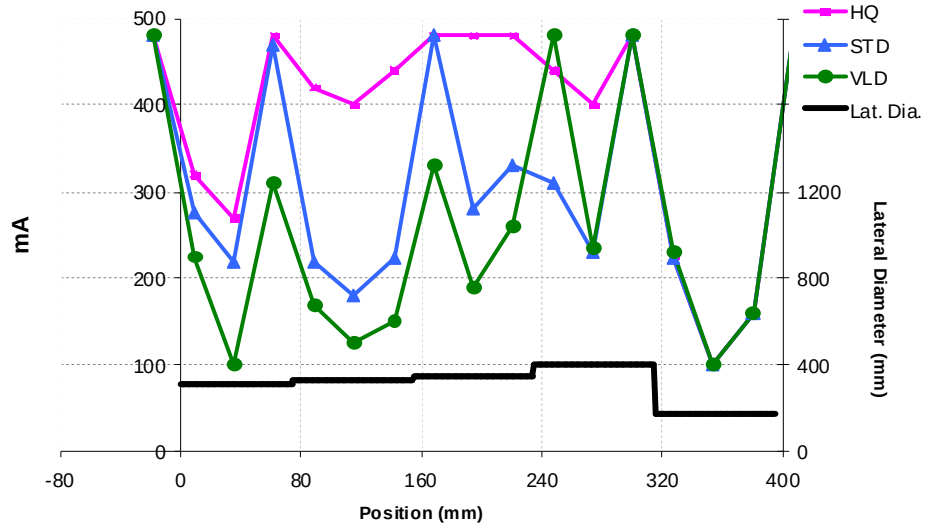

(b)

Figure 4-8 Tube current (mA) per slice against position along the torso phantom for (a) in AP direction, (b) in lateral direction from the Toshiba Aquillion scanner B

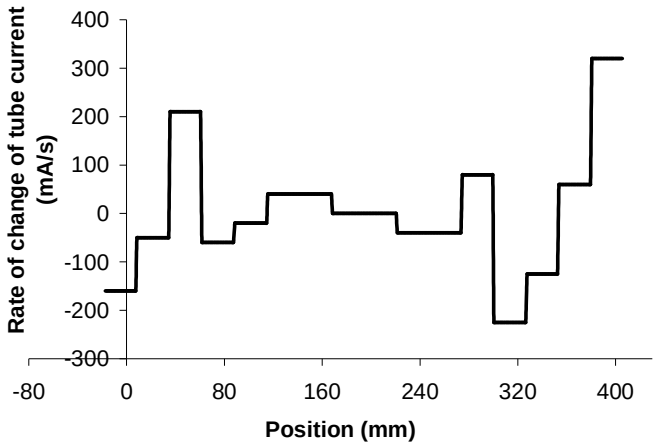

Figure 4-9 Diagram illustrating the rate of change in mA for the AP scanning orientation with the high quality setting

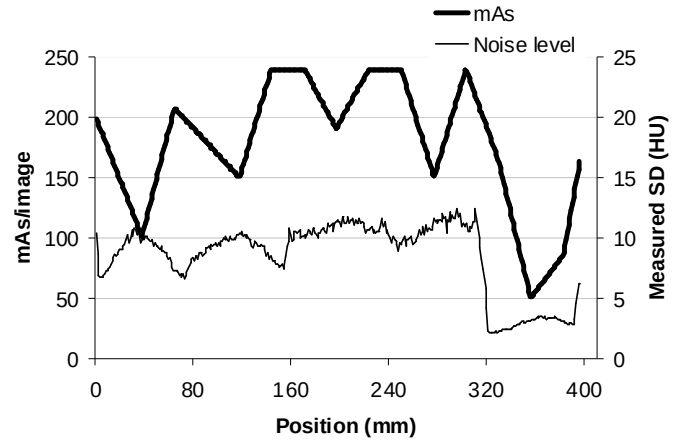

(a)

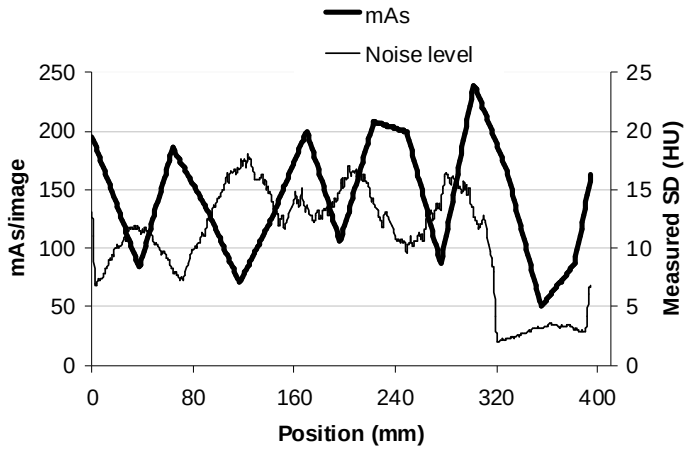

(b)

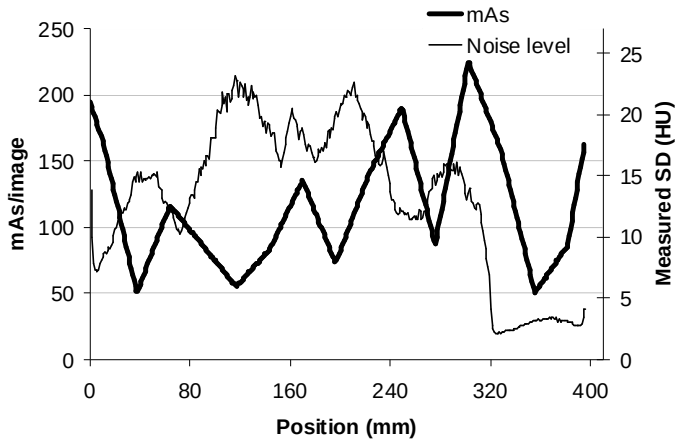

(c)

Figure 4-10 Average mAs per slice and noise along the legnth of the torso phabntom for Toshiba Aquiliion scanner B with ATCM options; (a) high quality, (b) standard and (c) very low dose.Measured from scanner B

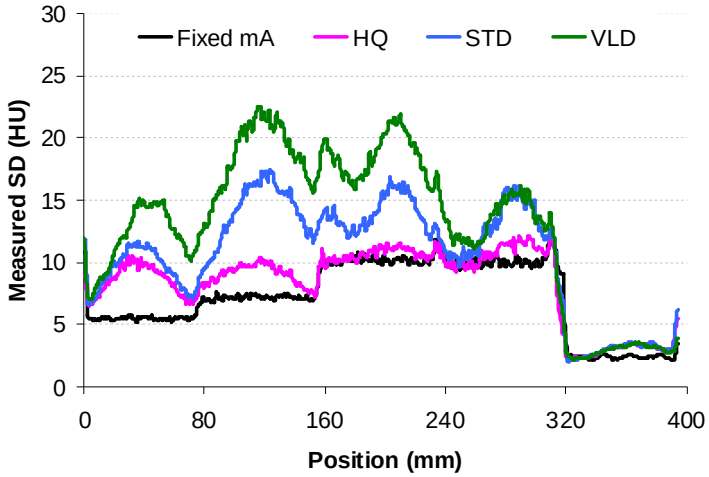

Figure 4-11 Comparison of noise values with a fixed mA technique, and HQ, STD and VLD ATCM options, measured from scanner B

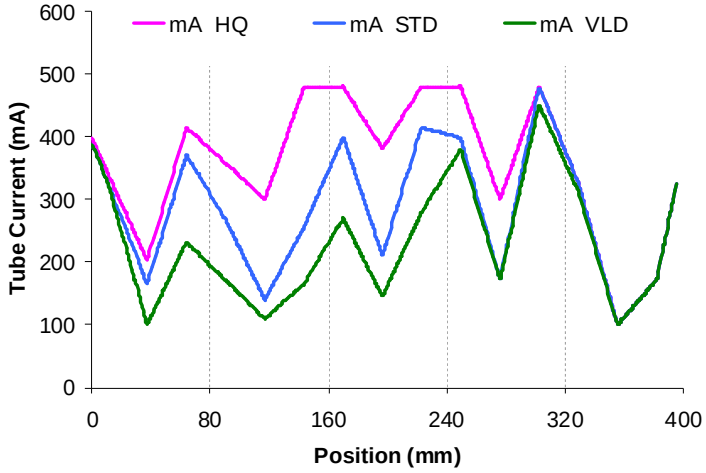

Figure 4-12 Comparison of mA values with a fixed mA technique, and HQ, STD and VLD ATCM options, measured from scanner B

4.4 Discussion

4.4.1 Dose distribution within the torso phantom

The ESAK and the air kerma along the central axis were made with the torso phantom and results compared with variations observed in tube current and image noise. The sharp peaks in the ESAK on the anterior of the phantom result from overlap of beams from adjacent rotations. These are not seen in the ESAK measured at the sides of section 4 (figure 4-5) because there is less beam overlap with the shorter focus to surface distance. The degree of overlap for

adjacent X-ray beams depends on the beam profile, pitch and scanner geometry (Dixon, 2003).

The ESAK levels were closely related to the diameter of the phantom with a fixed tube current. Section 4 which has the largest lateral dimension, but a smaller AP dimension than section 3 had the lowest ESAK at the lateral, but a comparatively high anterior ESAK (figure 4-5a). The ESAKs for section 5, the smallest section of the phantom, were greatest. The variation is linked to the position of the surface with smaller ellipse diameters being close to the isocentre, so that more of the radiation comes from nearer the centre of the bowtie filter.

The ESAKs on the anterior surface of the phantom were the highest for all sections with a fixed tube current but the differences were much smaller when the ATCM was in operation, as described in section 3.3.6 (figure 4-6). The doses at the centre of the torso phantom were similar to the ESAKs at the anterior of the phantom, and as much as double the ESAKs at the lateral positions for section 4 (figure 4-6, table 4-2). The doses along the central axis of the torso phantom were similar in sections 2-4, higher in the smallest section 5 and lowest in section 1 (figure 4-7). The high dose in section 5 results from the lower attenuation of the smaller section of the phantom. The peak adjacent to section 4 probably results from direct scatter within the large adjacent section (figure 4-7). The lower dose at the start and the end of the scan results primarily from the reduced backscatter from beyond the end of the section. The dose distribution in the ellipse of the torso phantom is different from that in the elliptical phantom, for which the ESAKs were higher (compare with results in chapter 3, figure 3-21). The difference probably results from the lighter density of the material used for the torso phantom, as polyethylene (density 0.95g/cm^3) has a lower density than PMMA (density 1.18g/cm^3). The dose distribution within the human body will be influenced by the lower density of tissue with respect to PMMA, although this will also be affected by the higher density of the bone component.

4.4.2 Tube current modulation with the torso phantom

Initial implementation of the high quality ATCM mode reduces dose levels in the less attenuating regions, namely both orientations in sections 1 and 5, and the anterior surface for all the sections. This can clearly be seen in change in ESAK (figure 4-6). The difference between the anterior ESAK and that at the lateral position was reduced from 41% with a fixed tube current to 9% when the ATCM was in operation (figure 4-6, table 4-2). Reductions for all parts of the phantom are similar when the mode is changed from high quality to standard. Further reductions in ESAK and central dose occur when the very low dose option is implemented but are relatively small (figure 4-6). This may be due to restriction in further modulation by the minimum tube current limit.

The calculated percentage variation of the doses compared to a fixed mA technique was based on the 240 mAs of scanner B. The mAs value was the upper limit of the mAs range default for the ATCM option. However, these dose variations will critically depend on the fixed mA chosen and whether this is representative of the mAs that would be chosen for a CAP examination of a standard sized patient. For routine scanning techniques with manually selected tube load, mAs values will be varied depending on patient size.

The ATCM for the Toshiba Aquilion is determined from the SPR recorded prior to the scan. When selecting the high quality ATCM mode, tube currents were reduced by up to a quarter in sections 1-4 and a half in section 5 (figure 4-11), resulting in the ESAKs being reduced by up to one third (figure 4-6b). During each rotation, the tube current changes at a constant rate and the rate of change is adjusted at the end of each rotation (figure 4-8). The initial tube current value was linked to the attenuation of the part of the phantom to be scanned during the first rotation. The tube current is calculated to have started at a higher level because the more attenuating polycarbonate end plates were included in the SPR. The adjustment to the rate of change in current was based on the attenuations for the sections of the phantom to be scanned.

A noise level of about 10HU was achieved in the thicker sections 3 and 4 of the phantom with the fixed mA, while the noise level was lower in the remainder (figures 4-10 and 4-11). The high quality ATCM mode brought the noise level to

10±1 HU throughout sections 1 to 4. The noise for the smaller section 5 was about 3 HU for all ATCM settings because the tube current being used was high, and since the minimum mA setting was 100 mA, tube current could not decrease further. There are significant fluctuations in the noise level of 5 HU to 10 HU linked to the changes in tube current for some ATCM options (figures 4-10b and 4-10c). The adoption of an ATCM system that gives large rates of change in tube current enables the scanner to be responsive to variations in attenuation and ensures that the required average noise level and a lower dose are achieved. However, the variations in noise level through the scan raise the question of whether this is the most appropriate method and whether different settings for factors such as the limiting tube current values should be selected for patients of varying size.

For the noise value and mA curve which are shown in figures 4-11 and 4-12, the mA and noise values among three different ATCM options were similar at smallest section 5. The mA and noise values between standard and very low dose and between high quality and standard modes were similar in section 4 and 1, respectively. Comparing noise values at the AP and lateral axes (table 4-3) showed that the noise measured at the lateral positions were similar to those at the centre but slightly higher than those at the AP position. This may be due to the increased thickness of the phantom and, therefore, higher attenuation for the lateral axis. The use of ATCM would result in more uniform noise values across all positions in the phantom.

Table 4-3 Noise levels and variations measured at section 1-4 of the phantom from scanner B

			ATCM Option		
		Fixed mAs	HQ (Target noise 7.5)	STD (Target noise 12.5)	VLD (Target noise=17.5)
All Positions	Mean SD (range)	8.2 (4.3-14.9)	9.8 (5.4-16.1)	12.6 (5.2-21.6)	15.7 (6.0-25.4)
	%CV	24%	13%	21%	24%
Centre	Mean SD (range)	9.3 (5.8-12.6)	11.1 (7.1-14.1)	14.3 (7.8-19.9)	17.6 (7.9-26.2)
	%CV	23%	13%	21%	25%
AP	Mean SD (range)	6.6 (4.3-10.4)	8.1 (5.4-10.5)	10.7 (5.2-16.6)	13.0 (6.0-19.9)
	%CV	25%	15%	24%	30%
Lateral	Mean SD (range)	9.4 (5.3-14.9)	10.7 (6.6-16.1)	13.7 (6.9-21.6)	17.4 (7.6-25.4)
	%CV	29%	19%	23%	21%

%CV is variation of the mean image SD

There were small sharp peaks in the mAs/image at the junction between the sections of the phantom (figure 4-10). This may be because of the rapid change in attenuation at the edges of the phantom and the beam overlapping with more than one section of the phantom for a significant proportion of time. The attempt to include a wide range of phantom dimensions to fully test the ATCM proved too complex for routine performance testing. However, some assessment is required to enable an understanding of factors that determine the performance of ATCM systems. For more routine performance testing, a phantom with fewer longer sections covering the range of sizes within an examination of the trunk is perhaps more appropriate. Use of phantom of different designs for ATCM tests, and carrying out in other CT scanner manufacturer will be discussed further in the next chapter.

4.5 Conclusion

Dose distributions for Toshiba Aquillion 64 scanners measured in a custom built torso phantom showed that the ATCM first reduced the tube current for the AP projection, so that the dose distribution around the periphery of the body was more uniform. Subsequent reductions to achieve lower noise levels involved proportionate changes in both AP and lateral values. Since the changes were linked to achieving a set noise level, the pattern of change for particular options varied with the size of each section of the phantom. Results demonstrated that the fluctuations in tube current for the Toshiba Aquilion scanner may be large, because of the way in which the rate of change is set for the next section of the phantom to be scanned. This can produce significant variations in noise along a phantom with sections of varying dimension. Since other medical physics centres are using stepped phantoms of varying design, the torso phantom and other phantoms of different shape were used to evaluate options for the design of ATCM phantoms on other CT scanners in the next chapter.

5 Comparison of Automatic Tube Current Modulation (ATCM) systems using phantoms of different design

5.1 Introduction

A multi section elliptical phantom in a shape of a torso was developed and preliminary tests with the Toshiba ATCM system are described in the previous chapter 4. The advantage of a phantom of this type is that it is significantly less expensive to manufacture compared with a conical phantom. There is, however, a limitation to the use of the phantom when testing the ATCM systems, as the abrupt changes in attenuation provoke a typical ATCM response for toshiba scanner. For this chapter, the torso phantom was used with other CT scanner manufacturer ATCM systems. The study was performed using four different CT scanner manufacturers; Toshiba, GE, Philips and Siemens scanners and the results were compared with ones obtained using the ImPACT conical phantom.

A second prototype stepped phantom was developed from the results of the first which provides a test of the ATCM system that is more effective when used with the Toshiba scanners. The study will show assessments of ATCM systems in terms of the dynamic changes in tube current and the image noise using the new phantoms as well as giving evaluations of both phantoms. The aims of the study are to evaluate options for the design of phantoms, suitable for checking that ATCM systems are functioning correctly and to investigate the modes of operation of the ATCMs on different scanners, in order to gain knowledge on optimisation of image quality and patient dose. The study focused on adjustments of tube current made along the z-direction or scanner axis.

5.2 Materials and Methods

5.2.1 Materials

5.2.1.1 Phantom design

The conical phantom (Keat *et al.,* 2005) developed by ImPACT and the first prototype custom built of torso phantom which was introduced in Chapter 4 were used. The ImPACT conical phantom (figure 5-1a) is 300 mm long, increases

from 61.2 X 40.8 to 428.7 x 285.8 mm (figure 5-1b). The diameters of the x and y axes are in the ratio of 3:2 throughout the phantom (figures 5-1c and 5-1d), which is approximately equal to that for an abdomen. The phantom has a mounting lip that hooks over the edge of the wooden carrying case from a Catphan phantom (The phantom laboratory incorporated, New York, USA), which is a standard phantom widely used for assessment of CT image quality in the UK.

(a)

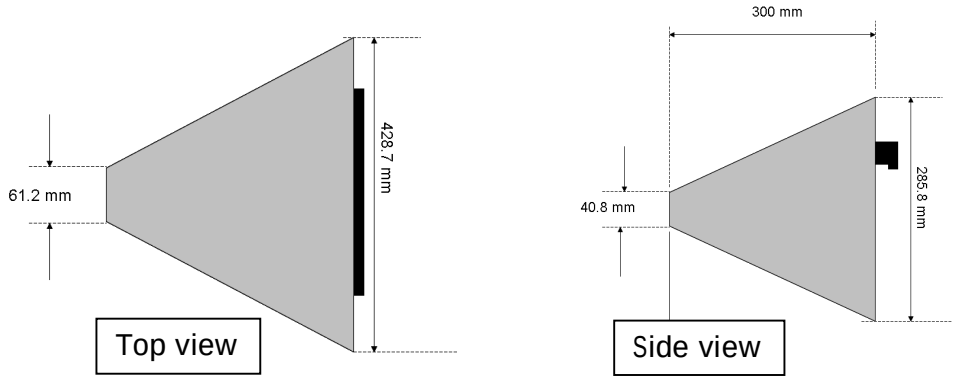

(b)

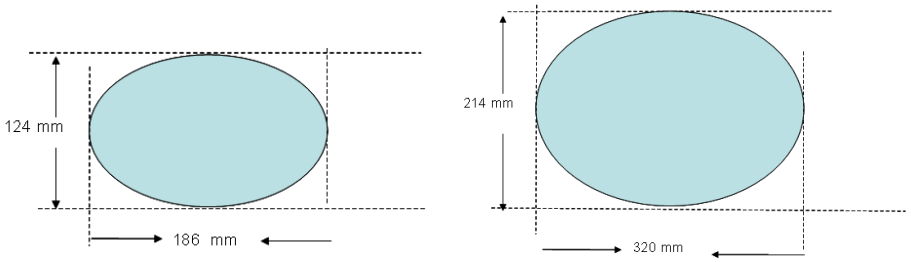

(c) (d)

Figure 5-1 (a) ImPACT conical phantom and diagram illustrating diameters at the minor and major ends of the phantom for (b) top view and and side view and cross-sectional diameter at (c) 100 mm and (d) 200 mm from the minor end

5.2.1.2 CT scanner measurements

Measurements were performed using a 64 slice CT scanner from each manufacturer. Because of the variation in the design and operation of the ATCM systems that were being tested (Söderberg and Gunnarsson 2010), it was not possible to use a standard testing protocol. The protocols used in the study were the routine CAP protocols, which were based on recommendations from the company applications specialists, with slight modifications for Toshiba and GE to increase the range of tube current. All measurements were performed using 120 kV. The available minimum and maximum tube current values were set for the Toshiba and GE scanners, while the ranges of the tube current being used for the Philips and Siemens scanners were set by the scanners. Comparisons were made with results for a fixed tube current. For the ImPACT conical phantom, a fixed tube current time product of 200 mAs was used, but for the torso phantom the fixed value was defined as the maximum tube current applied to achieve the standard or reference noise level of the CAP protocol of each manufacturer. The fixed mAs values being used for Philips, Siemens, GE and Toshiba scanners were 124 mAs/slice, 110 effective mAs, 443 mAs and 250 mAs, respectively.

Details of the testing approach for different CT scanners are summarized in table 5-1, which were recommended settings for each scanner. However, image quality options availabled for individual scanners were changed manually in order to evaluate the ATCM system. For the GE scanner, smart mA was used in the majority of the experiments as it is recommended for scan of trnk, but comparisons of tube current and image noise levels between SmartmA and AutomA settings were also tested.

For the scan direction and scan length, the length of scan for the torso phantom was 395 mm covering the whole phantom, excluding the endplates and for the conical phantom was 300 mm covering the length of the phantom. The directions of scan for both phantoms plotted in the figures throughout this chapter are shown in figure 5-2.

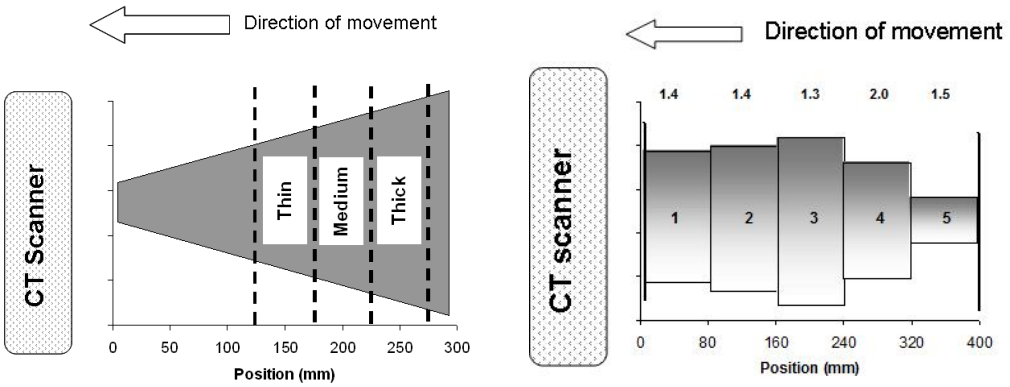

(a) (b)

Figure 5-2 Diagram illustrate scan directions for the (a) ImPACT Conical Phantom and (b) Torso phantom

(Note: figure 5-2a shows sections of the conical phantom referred to thin, medium and thick regions for purpose of noise measurement analysis)

Table 5-1 ATCM systems and standard scanning parameters used in CT scanners from different manufacturers

	Model	ATCM system	Tube current stored in DICOM	Phantom	kVp	Rot. time (s)	Beam	Pitch	Image quality	Reconstruction kernel
Philips	Brilliance	Z-DOM ACS	mAs/slice	ImPACT	120	0.75	64x0.625	0.921	188 mAs/slice	B Body
		D-DOM		Torso	120	0.75	64x0.625	0.921	124 mAs/slice	B Body
Siemens	Somatom	Caredose4D	Effective mAs	ImPACT & Torso	120	0.5	64x0.6	1.4	110 effective mAs (average decrease/ strong increase)	B31f medium
GE	Discovery	SmartmA	mA/rotation	ImPACT	120	0.6	16x0.625	1.375	NI=11.57 min mA=10, max mA=800	Standard
				Torso	120	0.6	16x1.25	1.375	NI=11.57 min mA=10, max mA=800	Standard
Toshiba	Aquilion	SureExposure 3D	mAs/rotation	ImPACT	120	0.5	64x0.5	0.875	SD=12.5 min mA=10, max mA=500 QDS+	FC 13
				Torso	120	0.5	64x0.5 32x0.5** 16x0.5**	0.828	SD=12.5 min mA=10, max mA=500	FC 13
				Wedding Cake	120	0.5	64x0.5 16x0.5	0.828	SD=12.5 min mA=10, max mA=500 QDS+	FC 13

*Quantum Denoising Software , ** used for extra experiments in section 5.3.4.3

5.2.2 Methods

5.2.2.1 Data analysis

All scan images were sent to PACS to allow the tube current values per image slice to be read, so that the effect of the ATCM systems on image quality could be evaluated. The tube current (mA) or mAs per slice or rotation values, as stored by each scanner in the DICOM header, were read out by an "Auto mA plugin", and were plotted against scanning position in terms of distance from the start of the scan.

The tube currents for the Philips and Siemens scanners were displayed in terms of the product of tube current in mAs per slice and effective mAs, respectively. Both are the same in calculation, when the pitch factor is taken into account. The effective mAs is defined as equation 5-1.

$$\text{Effective mAs} = \text{mAs}/\text{Pitch} \quad \textbf{Equation 5-1}$$

The GE and Toshiba scanners use mAs value rather than effective mAs; GE scanners quote the mA, rotation time (s) and pitch separately. The Toshiba scanner shows average mA, rotation time (s) and effective mAs on the screen console together with plots of the variation in mA but the quantities stored in the DICOM header are average mA/rotation and mAs/rotation.

The quantities provided from the scanners are plotted in the figures, in the form of tube current per image or slice against position along the phantom. The mA and mAs per rotation values from GE and Toshiba scanners are corrected to give the effective mAs for the purpose of the comparisons. $CTDI_w$ values were measured in the body CTDI phantom (32 cm in diameter). The effective mAs values were multiplied by the $CTDI_w$ in the unit of mGy/mAs to derive an effective body $CTDI_{vol}$. The new concept of effective body $CTDI_{vol}$ was developed for this study in order to normalise and compare dose distribution between different scanners.

The image noise was analysed using Image J. The method for measuring the image noise has been explained in chapter 4. Average noise levels for the ImPACT phantom were derived from three sections; 125-175 mm, 175-225 mm and 225-275 mm from the minor end of the phantom and these are referred to as thin, medium and thick (figure 5-2). The reason for selecting these regions for noise measurements is because they are regions containing full tube current modulation i.e. no saturation of the tube current at the minor end of the phantom.

5.2.2.2 ESAK measurement

For the torso phantom, positions for ESAK measurement are shown in figure 5-3b which was similar to those explained in section 4.2.2.1. For the Impact phantom, strips of Gafchromic XR-QA film were taped on the AP and lateral surfaces of the phantom along the longitudinal scanning axis (figure 5-3a). The results for right and left sides were averaged to represent the ESAK for the lateral. Gafchromic film strips were scanned with the Epson scanner 24 hour later and analyzed using ImageJ (Ferreira and Rasband, 2011). Details of the analysis of the Gafchromic film have been explained in section 3.2.1.2, chapter 3.

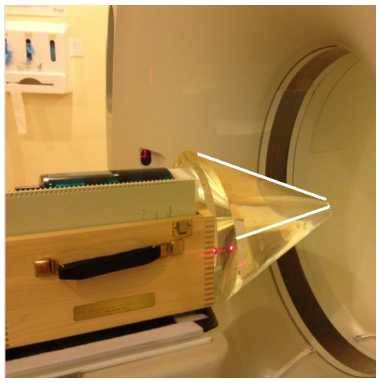

(a)

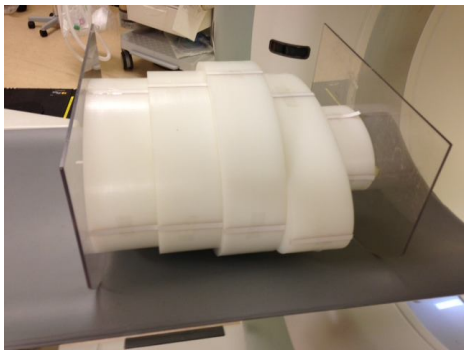

(b)

Figure 5-3 ESAK measurements for the (a) cone and (b) torso phantoms

5.3 Results

Variations in tube current have been recorded along the length of the different phantoms operating under ATCM. These are plotted together with the variations in noise levels that result. Mean noise levels and ESAK in different sections of each phantom have been derived to allow comparisons to be made.

5.3.1 Experiments on the Philips scanner

5.3.1.1 Tube current and image noise variations on the Philips scanner

The tube current modulations for different mAs/slice settings of the Philips scanner followed similar patterns within their own limited maximum and minimum tube current values for, both Z-DOM and D-DOM settings (figures 5-4 and 5-5). Under the Z-DOM setting, the tube current remained at the minimum value set for the first 100 mm of the ImPACT phantom, which was about 20% the maximum value for each setting (figure 5-4a). For the D-DOM setting the tube current remained relatively constant along the whole phantom length (figure 5-5a), because ratios of attenuation level between the AP and lateral diameters are similar (section 2.4.1.3). Comparisons of mAs/slice and image noise values between recommended settings of the Z-DOM and D-DOM are shown in figure 5-6.

Changes in mAs along the length of the torso phantom for different settings are shown in figures 5-4b and 5-5b. Overall for the Z-DOM setting, the mAs values were highest at section 3 and lowest at section 5 corresponding to the largest and smallest AP diameters of the phantom. The dynamics of the tube current modulation of all settings followed similar patterns and were limited by their maximum and minimum tube current values. For the D-DOM setting, tube current remained constant for sections 1-3 but declined at section 4 the shoulder region, where the ratio of the AP and lateral diameters of the phantom changed from 1.3-1.4 to 2, despite the higher relative attenuation in the lateral direction. Tube current started and ended toward the end plates with higher values.

The image noise associated with the different ATCM settings increased substantially towards the larger diameter of ImPACT phantom for both Z-DOM and D-DOM settings (figures 5-4c and 5-5c), but there was less variation than with the fixed current. For the torso phantom, noise levels of individual settings varied in relation to the diameters of each section with the lowest value in section 5, the smallest one. This was also because the tube current was high during the final part of this section (figures 5-4d and 5-5d). The average noise increased as the settings were changed from 405 mAs/slice to 124 mAs/slice. The percentage variation in noise over sections 1 – 4 which was 17% for a fixed mA decreased to 11.2% for the recommended Z-DOM setting (as shown in table 5-1), but with D-DOM the 16.4% change was not significantly different from that for a fixed mA. It was not possible to compare the overall noise values in both phantoms directly since the diameters were different. However, there were decreases in noise levels by factors of 1.2-1.3 in both phantoms when the Z-DOM settings were changed from 250 mAs/slice to 300 mAs/slice and from 300 mAs/slice to 405 mAs/slice.

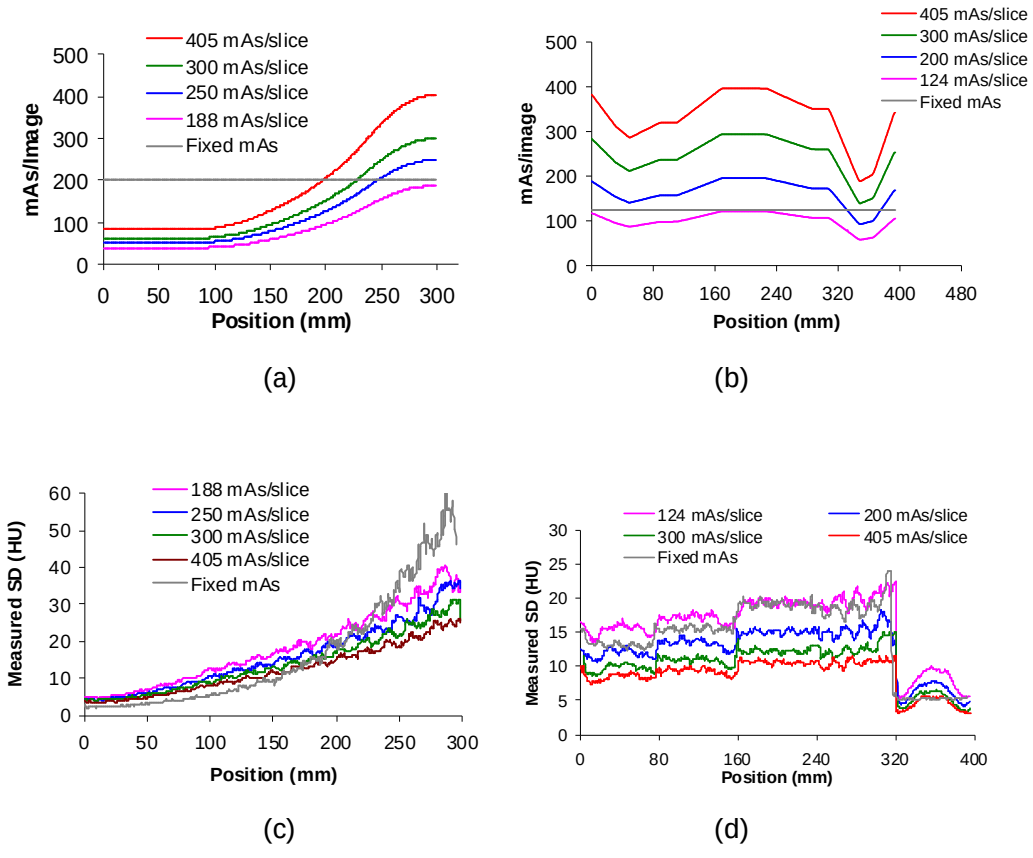

Figure 5-4 Comparisons of the effective mAs/slice values (a) ImPACT Conical Phantom (b) Torso Phantom and image noise (c) ImPACT Conical Phantom (d) Torso Phantom as a function of distance for the fixed tube current and different mAs/slice settings of the Z-DOM, Philips scanner

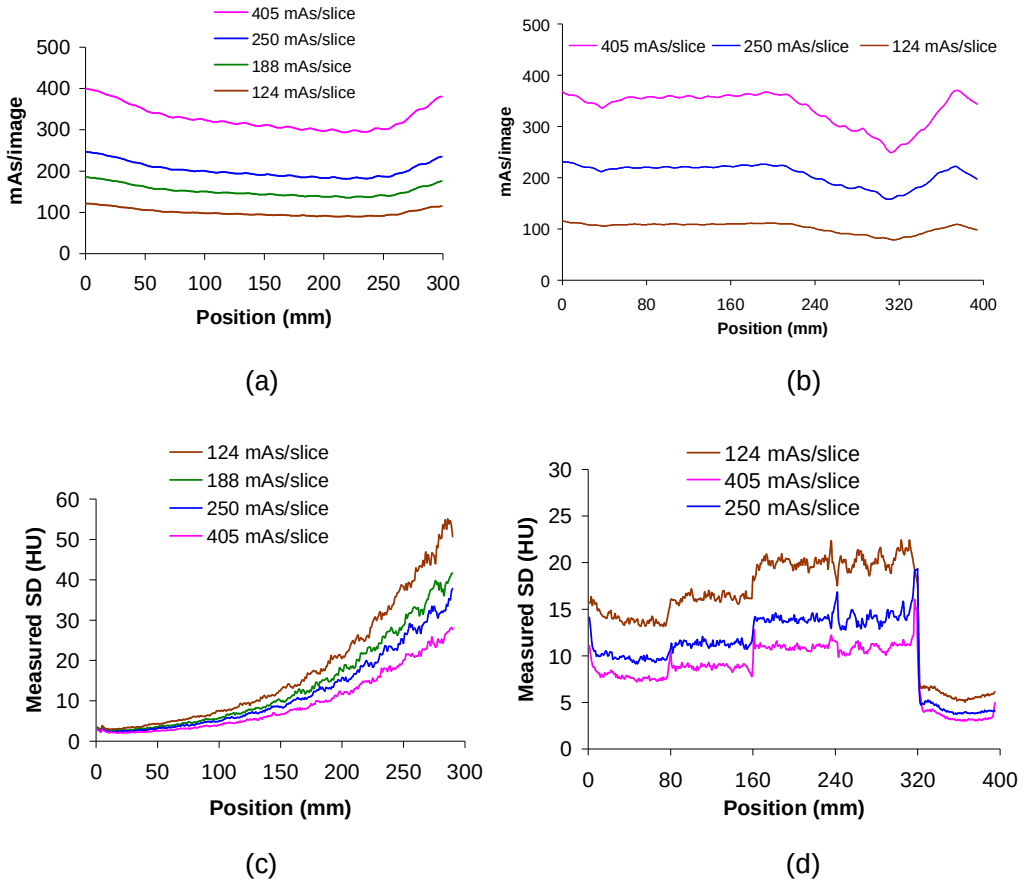

Figure 5-5 Comparisons of the effective mAs/slice values (a) ImPACT conical phantom (b) torso phantom and image noise (c) ImPACT conical phantom (d) torso phantom as a function of distance for the fixed tube current and different mAs/slice settings of the angular (D-DOM) Philips scanner

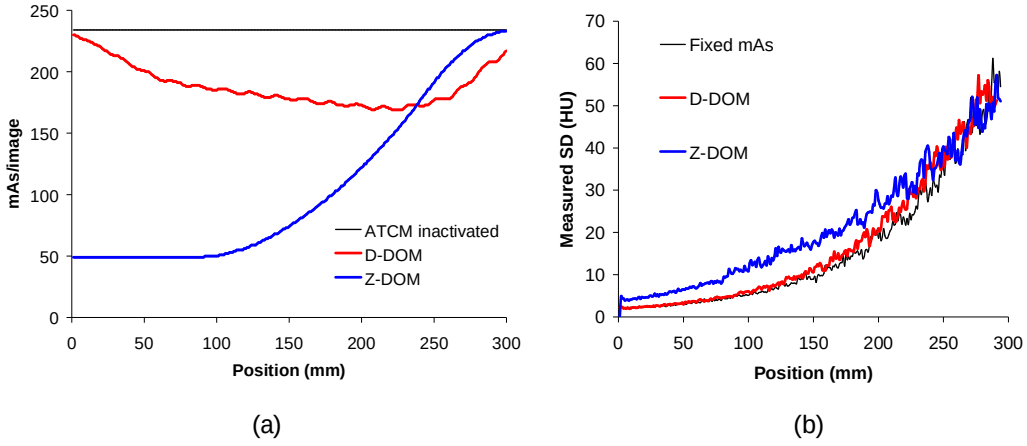

Figure 5-6 Comparisons of (a) the effective mAs/slice and (b) image noise values between recommended settings for Z-DOM and D-DOM, measured from ImPACT Conical Phantom, Philips scanner

5.3.1.2 ESAK on the Philips scanner

ESAK profiles measured on the anterior and lateral surfaces using recommended settings for both phantoms and a fixed mA technique in the torso phantom are shown in figure 5-7. For the ImPACT phantom, ESAKs at the anterior surface were 1.3 times higher than those at the lateral position, after 100 mm from the start of the scan (figure 5-7a), ESAKs were approximetly doubled for both AP and lateral positions, but with the same pattern, when the mAs/slice was changed from 188 mAs/slice to 405 mAs/slice. For the torso phantom, the average ESAKs of sections 1-3 from the fixed mA technique were 7%-17% and 5%-14% higher at the anterior and lateral surfaces respectively than those obtained from the 124 mAs/slice (figures 5-7b and 5-7c). The ESAK at section 4 obtained from the fixed mA technique was only 4% higher for both AP and lateral positions, compared with the recommended setting. The ESAKs at the smallest section 5 showed the largest difference between the two settings. The settings which were changed from 124 mAs/slice to 200, 300 and 405 mAs/slice resulted in increases of the ESAKs by 1.8, 2.6 and 3.4 times at the anterior surface and 1.7, 2.5 and 3.4 times at the lateral surface.

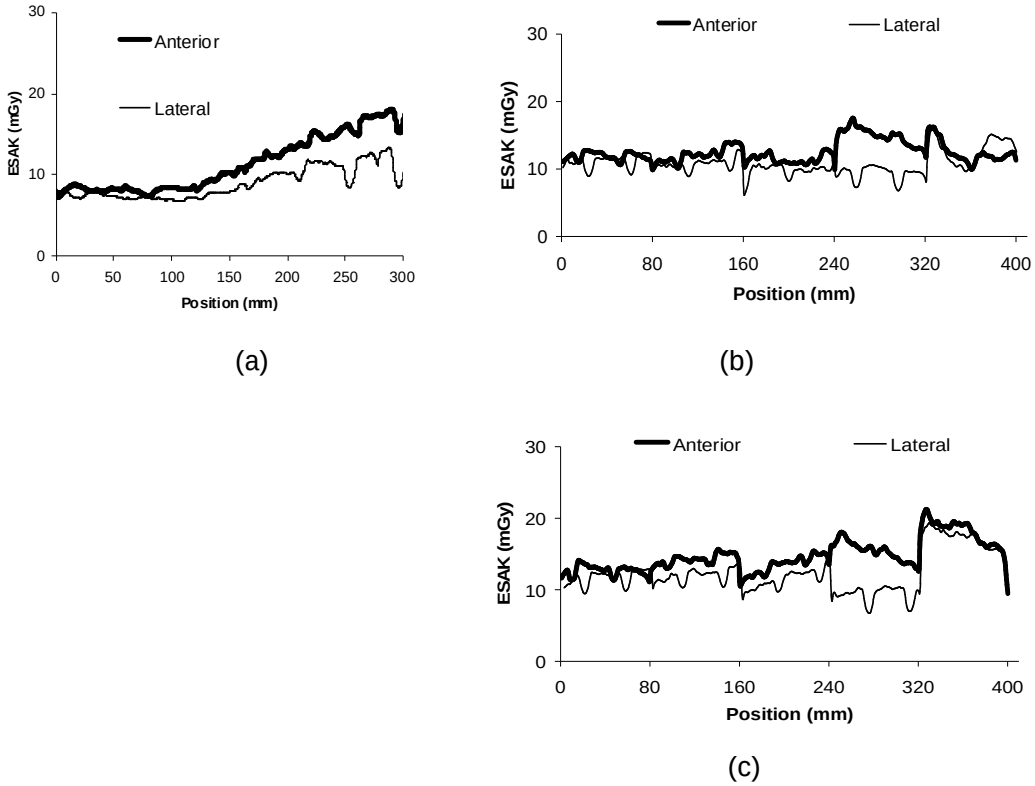

Figure 5-7 ESAK profiles measured on the anterior and the lateral surfaces measured from the Z-DOM ATCM settings of (a) 188 mAs/slice for the ImPACT phantom, (b) 124 mAs/slice for the torso phantom and (c) a fixed 124 mAs/slice for the torso phantom on the Philips scanner

5.3.2 Experiments on the Siemens scanner

5.3.2.1 Tube current and image noise variations on the Siemens scanner

Changes in effective mAs values followed a similar pattern for each setting (figures 5-8a and 5-8b). The effective mAs per slice increased with phantom diameter for the ImPACT phantom (figure 5-8a). However for the torso phantom, the mAs started and ended at a higher value (figure 5-8b). The tube current was saturated in the most attenuating parts of both phantoms for the highest effective setting.

The image noise followed a similar pattern for all ATCM settings in both phantoms (figures 5-8c and 5-8d), except where the tube current saturated. There were large variations in image noise along the whole length of the phantom although the ATCM was in operation, as with the Philips scanner. The measured SD values for both phantoms decreased by a factor of 1.2 when the settings were changed from 80 effective mAs to 110 effective mAs and from 110 effective mAs to 150 effective mAs. The percentage variations in the image noise along the whole length of the ImPACT phantom were about 45%-60% for ATCM settings, while the variation was 87% with the fixed mA technique (figure 5-8c). For the torso phantom, the image noise varied by 35% with the fixed tube current technique, and 23%-26% for the ATCM (figure 5-8d).

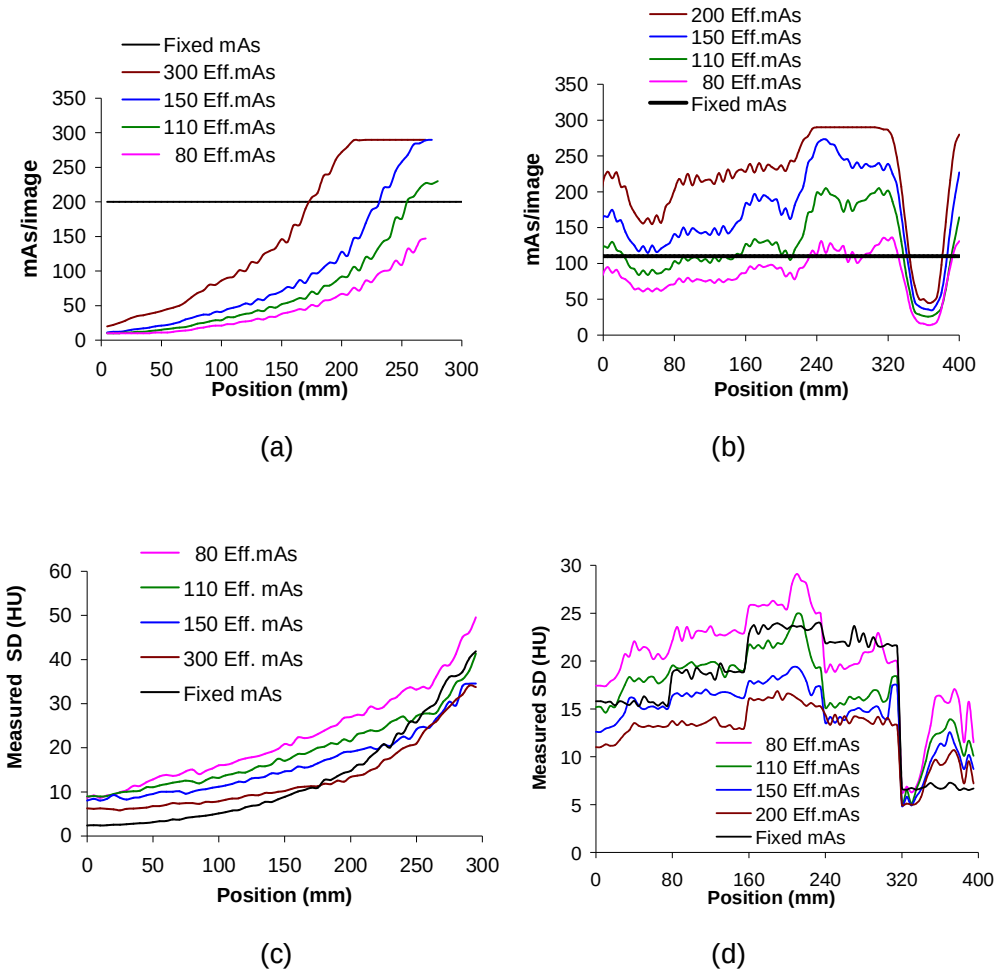

Figure 5-8 Comparisons of the effective mAs/slice values obtained from (a) ImPACT conical phantom (b) torso phantom, and comparisons of the image noise obtained from (c) ImPACT conical phantom (d) torso phantom as a function of distance for the fixed tube current and different QRM settings of the CareDose4D, on the Siemens scanner

5.3.2.2 ESAK on the Siemens scanner

ESAK profiles measured on the anterior and the lateral surfaces using the recommended QRM setting of 110 effective mAs for both phantoms are shown in figure 5-9. Those measured from a fixed 200 mAs from the ImPACT phantom are also shown. For the Siemens scanner, the measurement of ESAKs for various effective mAs settings were only carried out for the ImPACT phantom, comparisons of the ESAKs for different effective mAs settings measured in the ImPACT phantom are shown in figure 5-10.

The ESAKs decreased as phantom diameter increased and those at the anterior were higher than those at the lateral surfaces when the ATCM was not operated (figure 5-9c). They increased with phantom diameter and were more similar, with slightly higher values for the lateral ESAKs, when the ATCM was in operation (figures 5-9a and 5-9b). The exception was for section 4 of the torso phantom and the 300 effective mAs setting in the ImPACT phantom in which the ESAK at the anterior was 16% higher because of saturation of the tube current at the position of 200 mm onwards (figures 5-8a and 5-8b). The ESAK values increased by 46% and 33% for AP and lateral surfaces when 150 effective mAs was used, compared with the recommended setting (110 effective mAs) (figure 5-10).

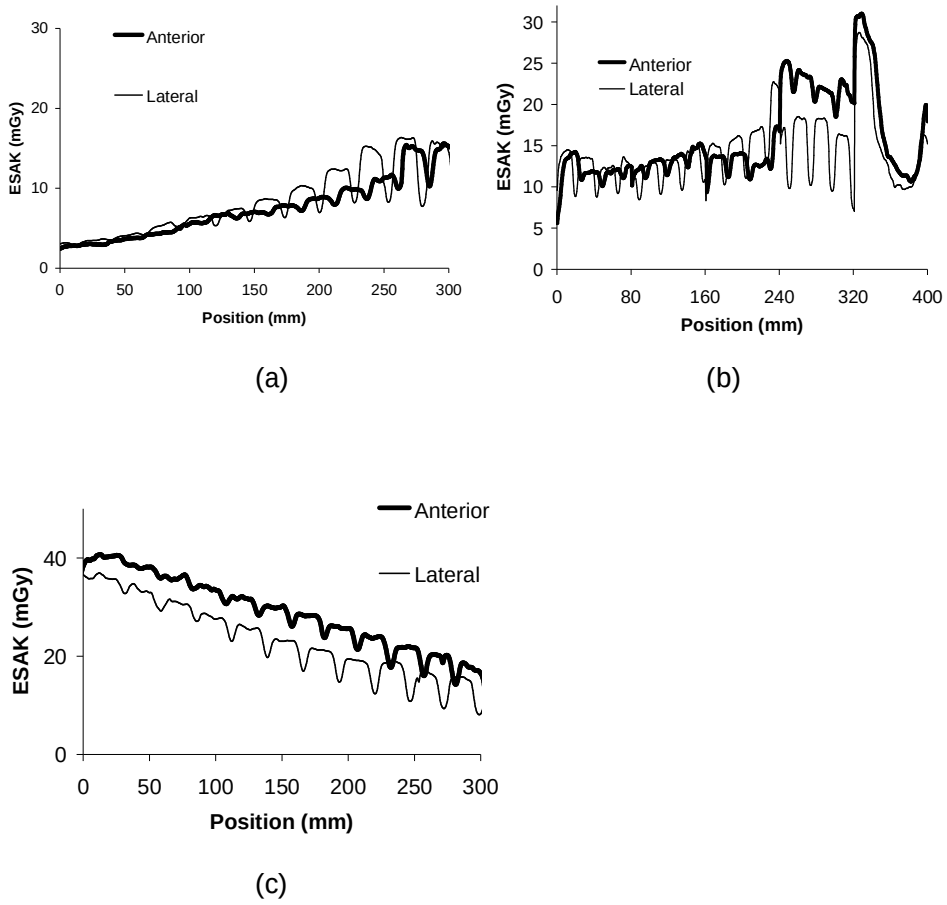

Figure 5-9 ESAK profiles measured on the anterior and the left and right surfaces of the phantom, measured from the 110 effective mAs setting on (a) conica and (b) torso phantoms, and (c) those measured from the fixed 200 mAs/slice technique in the ImPACT phantom, on the Siemens scanner

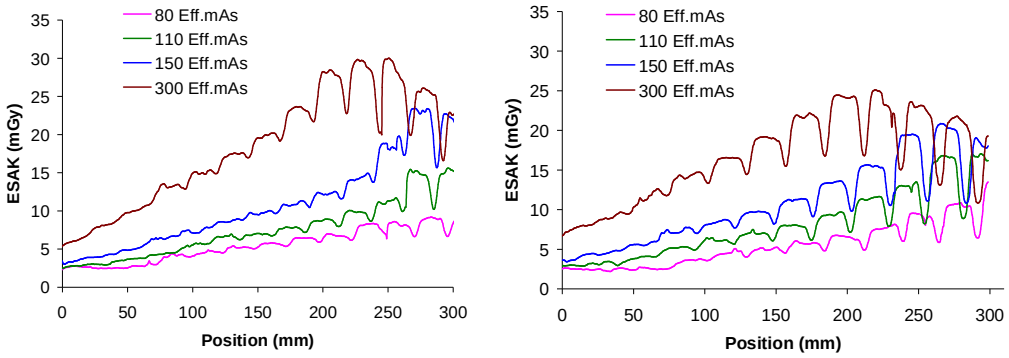

(a) (b)

Figure 5-10 Comparisons of ESAK profiles between different effective mAs settings (a) at the anterior and (b) at the lateral surfaces of ImPACT phantom, on the Siemens scanner

5.3.3 Experiments on the GE Scanner

5.3.3.1 Tube current and image noise variations on the GE Scanner

Comparisons of mAs/image from various NI settings, using 'Smart mA' are shown in figures 5-11a and 5-11b. The mAs values for the ImPACT phantom started close to the maximum setting for the lateral direction, because the lateral tube current started at the maximum (figure 5-12a). This was due to the rapid change in attenuation when the edges of the phantom were included in the SPR. However, they did not appear in results for the other manufacturers.

The tube currents in the lateral direction (figure 5-12) were not much greater than those in the AP direction for either phantom except in section 4 of the torso phantom; for which the ratio of the ellipse diameter was 2:1 rather than 3:2. This confirmed findings in figures 5-13 that the tube current value obtained from the AutomA was not different from that of the Smart mA. The variations in mA/slice for different NI settings follow a similar pattern over the middle parts of both phantoms. The tube currents were modulated within the same minimum and maximum values for all NI settings. However, although the range of the tube current was set at 10-800 mA, the maximum values allowed were substantially lower, as they were limited by heating of the x-ray tube. The tube currents along the entire lengths of both phantoms, before saturation were 50% and 70%

lower compared with those for the reference settings for the NI settings of 16.20 and 20.83, respectively.

Figures 5-11c and 5-11d show the effect of the ATCM system on the image noise measured along the length of both phantoms. Since the GE ATCM system aims to achieve a constant noise value, similar to the NI setting, the image noise for each NI setting remained relatively constant from about 30 mm from the beginning of the ImPACT phantom up to 160-220 mm, as the tube current increased proportionally with the diameter of the phantom (figure 5-11a). When the tube current reached the maximum, the image noise increased with increasing phantom diameter. For the torso phantom, overall image noise levels were similar to the NI settings however, there were variations in image noise from different NI settings, with fluctuations related to the tube current and relative attenuation of each section. The absolute image noise levels for the NI settings of 16.20 and 20.83 were 40% and 80% higher than those of the reference settings of NI of 11.57 in both the ImPACT and torso phantoms.

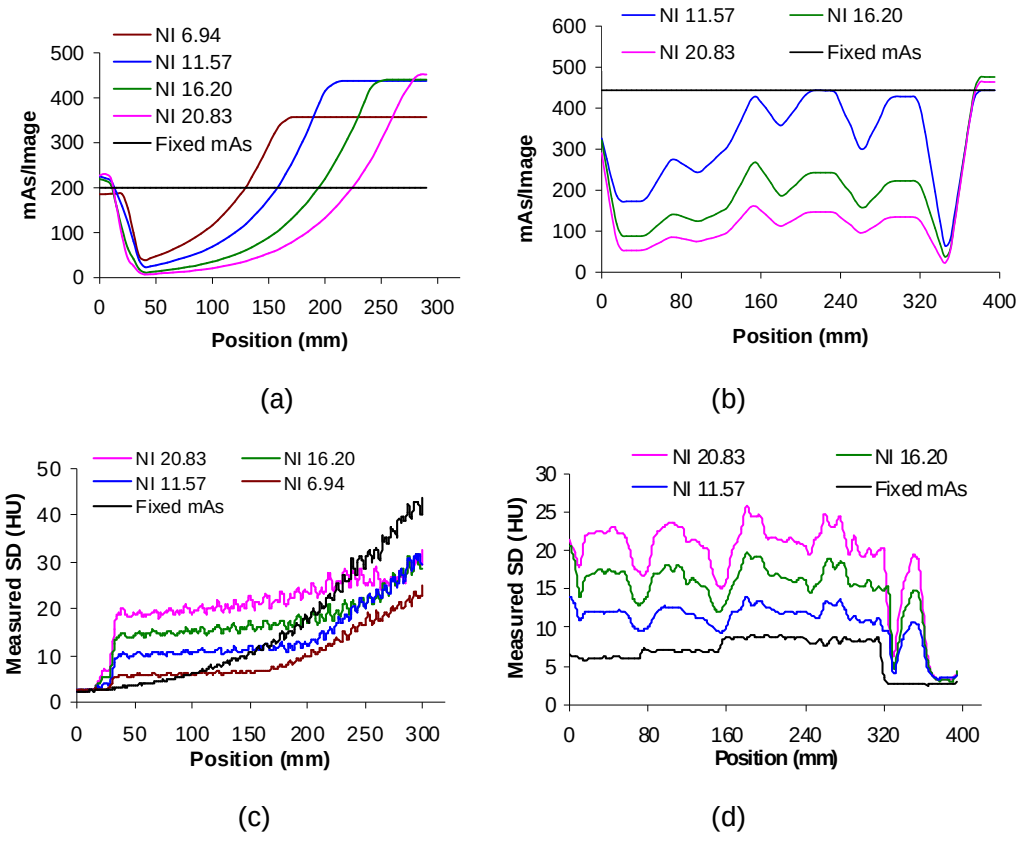

Figure 5-11 Comparisons of the effective mAs/slice values (a) ImPACT Conical Phantom (b) Torso Phantom and image noise (c) ImPACT Conical Phantom (d) Torso Phantom as a function of distance for the fixed tube current and different NI settings of the smart mA, GE scanner

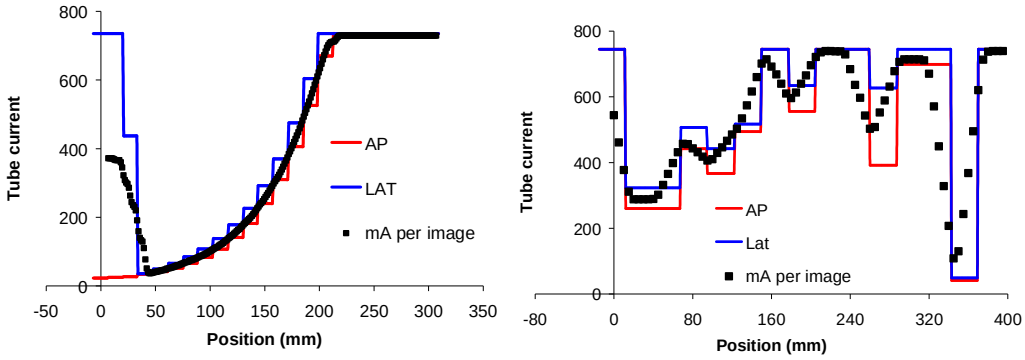

(a) (b)

Figure 5-12 Tube current modulations for the AP and the lateral directions for the reference NI setting of 11.57 of the Smart mA for the (a) ImPACT and (b) torso phantoms, GE scanner

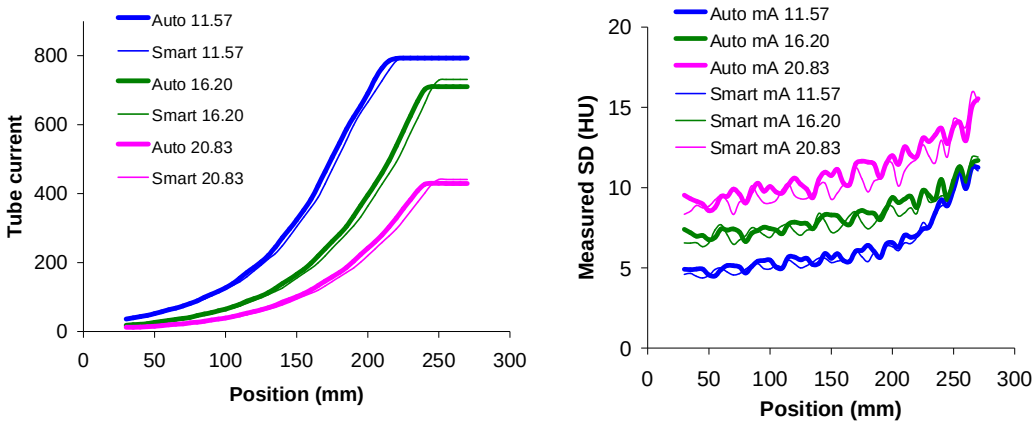

(a) (b)

Figure 5-13 Comparisons of (a) mA per rotation and (d) image noise for various NI settings for Smart mA and Auto mA settings, GE scanner

5.3.3.2 ESAK on the GE Scanner

ESAK profiles measured on the anterior and the lateral surfaces using the recommended setting for both phantoms are shown in figure 5-14. For the ImPACT phantom, the mA and ESAK dropped at the beginning of the scan in the case of ATCM operated (figures 5-14c). At the position of 35 mm from the beginning, the tube current and ESAK had increased significantly. ESAK dropped substantially after 200 mm as the major diameter of the phantom increased. This occurred because the tube current reached the maximum and stayed constant, but the ESAK declined as the distance from the isocentre increased. This also happened to the ESAK profile of the NI setting of 16.2 but not for the NI setting of 20.83 (figure 5-15) since the tube current was not saturated at the major end of the phantom (figure 5-11a).

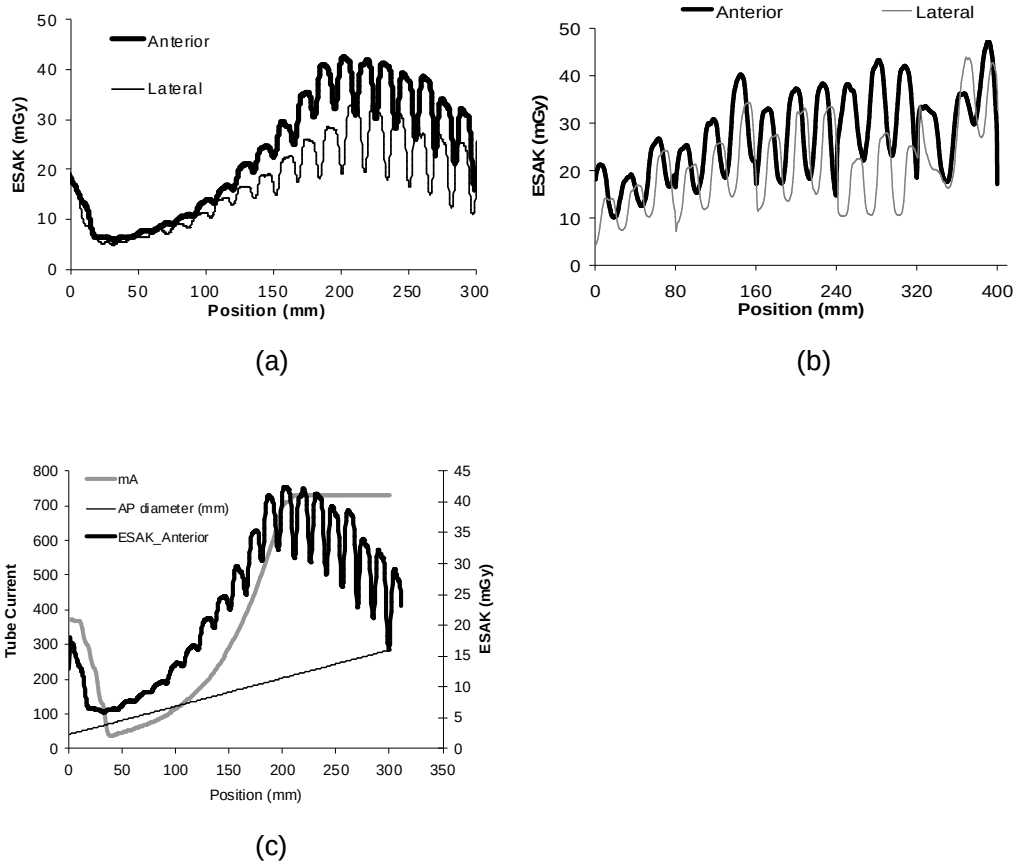

Figure 5-14 ESAK profiles at the anterior and the lateral surfaces from NI settings of 11.57 for the (a) ImPACT and (b) torso phantoms and (c) relationship between the AP diameter of the ImPACT phantom, the tube current and ESAK profile at the AP position of the phantom

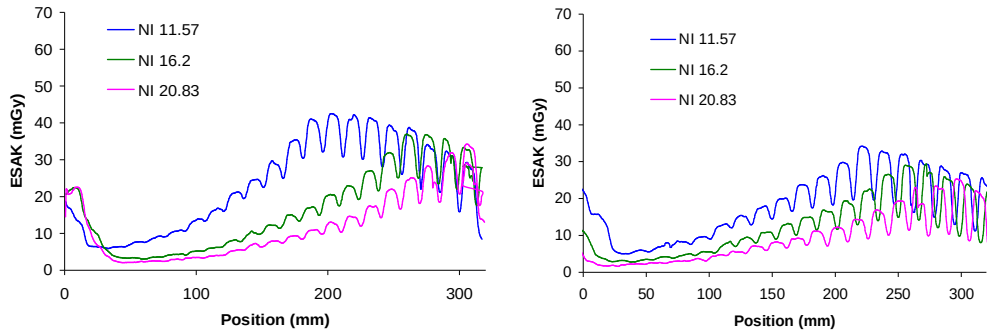

Figure 5-15 Comparisons of ESAK profiles between different mAs/slice settings at the (a) anterior and (b) lateral surfaces of the ImPACT phantom, GE scanner

5.3.4 Experiments on the Toshiba scanner

5.3.4.1 Tube current and image noise variations on the Toshiba scanner

For the ImPACT phantom, the mAs remained constant up to 40 mm to 90 mm from the start of the scan this because the minimum mAs values were high enough to archieve the target noise values, after which it increased significantly with the larger phantom diameter and reached a peak near the end of the phantom. Tube current reached the maximum setting of 250 mAs for all image quality options except the low dose ++, for which the maximum tube current was about 200 mAs (figure 5-16a).

The pattern of change in tube current for the torso phantom resulted in large oscillations in tube current which were much greater than for other scanners (figure 5-16b). In addition the tube current value in the AP direction was substantially lower than that in the lateral direction (figure 5-16f). For the high quality mode the tube current used for the lateral direction stayed constant at the maximum limit until section 4 of the phantom. Tube currents for both AP and lateral directions of the standard option and also the AP direction of the high quality option fluctuated between sections 1 and 4. All declined rapidly in section 5 linked to the small dimension of the phantom. The tube currents went up at the junctions between sections of the phantom.

For the ImPACT phantom the noise reached the selected target value between 40 mm and 120 mm from the start of the scan for the different options (figure 5-16c). Noise levels, then remained constant within 8%-10% for all ATCM options, except that for the high quality option (SD=7.5) the noise increased in the final part (figure 5-16c) because of the limitation on the maximum tube current. Figure 5-16d shows the image noise level with the different ATCM settings for the torso phantom. In sections 1 to 4 the average noise levels increased as the setting was changed from high quality to low dose++. The noise variations were about 10%-11% for the high quality, standard and low dose options and varied by 13% for the low dose++ setting. The noise level was lowest at the start of section 5 due to the high tube current value in the small diameter. The noise rose once the tube current was decreased by the modulation.

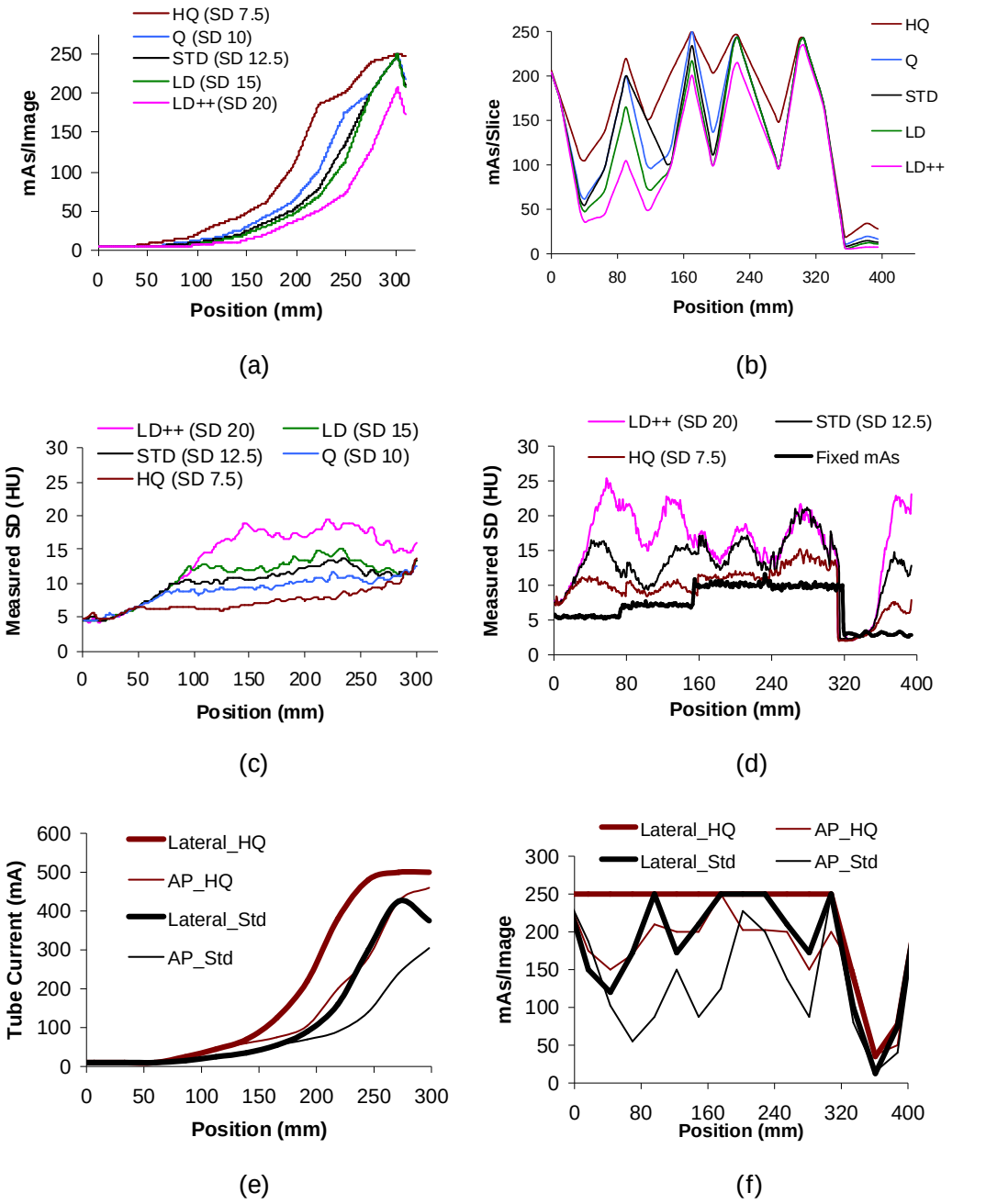

Figure 5-16 Comparisons of the effective mAs/slice values for (a) ImPACT conical phantom (b) torso phantom and image noise for (c) ImPACT conical phantom (d) torso phantom as a function of distance for the fixed mA techniques and different target noise settings of the SureExposure, Toshiba scanner, and Tube current modulations for the AP and the lateral directions for high quality (HQ) and standard (STD) settings for (e) the ImPACT phantom and (f) the torso phantom, Toshiba scanner

5.3.4.2 ESAK

ESAK profiles in the anterior and lateral surfaces obtained from fixed mA techniques and standard ATCM option (SD=12.5) for both phantoms are shown in figure 5-17. When the ATCM was operated within the full mA range, the ESAK varied less along the phantom but rose gradually at the end of the scan when the tube current increased. Comparisons of ESAKs for AP and lateral directions from different target noise setting are shown in figure 5-18. There were substantial reductions in the ESAKs with the changes from HQ to the STD and LD++ options. There were no differences between ESAKs from the three ATCM options for smallest section 5 because the tube current values were similar (figure 5-16b). As reported in section 3.3.6, chapter 3, there were differences in the AP and lateral peripheral doses with the fixed mA, due to the narrower bow-tie filter. However, there were reduced by operation of the ATCM and so did not have a significant effect upon the results.

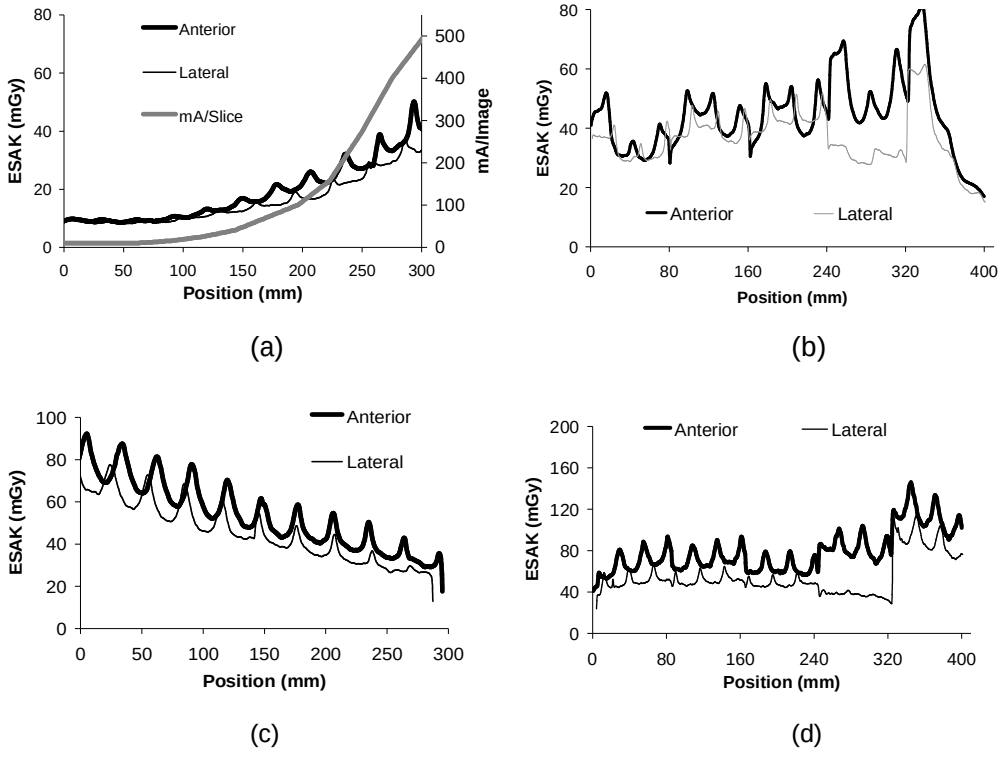

Figure 5-17 ESAK profiles at the anterior and the laterals surfaces measured from standard ATCM option (SD=12.5) of the (a) ImPACT, (b) torso phantoms and those for fixed mA techniques of the (c) ImPACT and (d) torso phantoms. Measured from Toshiba scanner

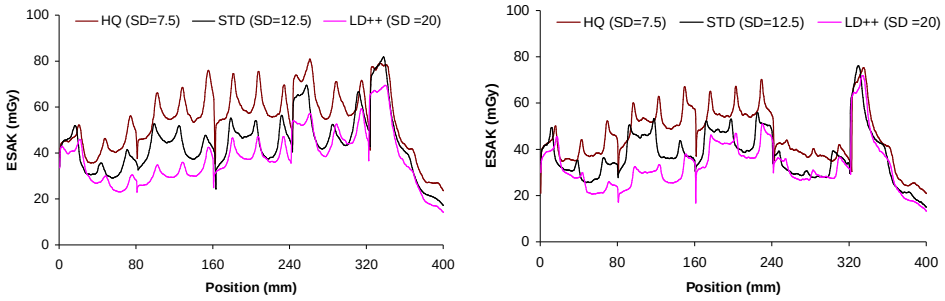

Figure 5-18 Comparisons of ESAK profiles between different ATCM settings for the torso phantom (a) at the anterior and (b) at the lateral surface of the phantom, Toshiba scanner

5.3.4.3 Investigation of the mA oscillation with the Toshiba ATCM

The magnitudes of the variations in tube current for the torso phantom did not appear to be linked entirely to differences in phantom attenuation. An initial hypothesis was that the sharp peaks between phantom sections occured because of air gaps between sections, therefore the air gaps were reduced by inserting rubber sheets between the sections. Experiments were carried out to investigate this using beam widths of 16 mm (32x0.5) and 8 mm (16x0.5). In addition, 2 mm thick natural rubber sheets (density 1.2 g/cm^3) cut to the shapes of the ellipses were inserted between sections of the phantom in order to reduce the air gaps (figure 5-19).

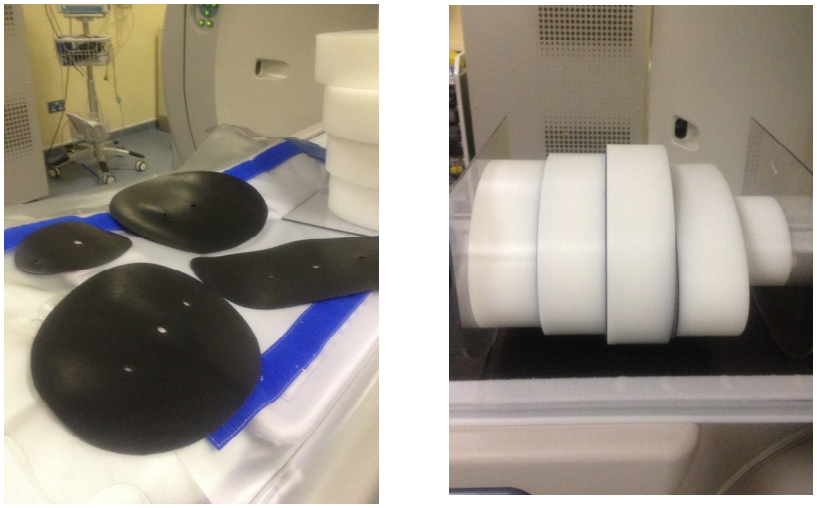

Figure 5-19 Rubber sheets and the torso phantom inserted with the rubber sheets between each phantom section

Use of the narrower beam width gave a better defined link between tube current and phantom thickness, but the sharp peaks in the tube current were still present after the air gaps had been filled (figures 5-20a and 5-20b). Therefore the peaks appear to result from increases in tube current trigged by step changes in attenuation. When the end plates were excluded from the SPR the tube current was no longer higher at the beginning and end of the scan (figure 5-20c).

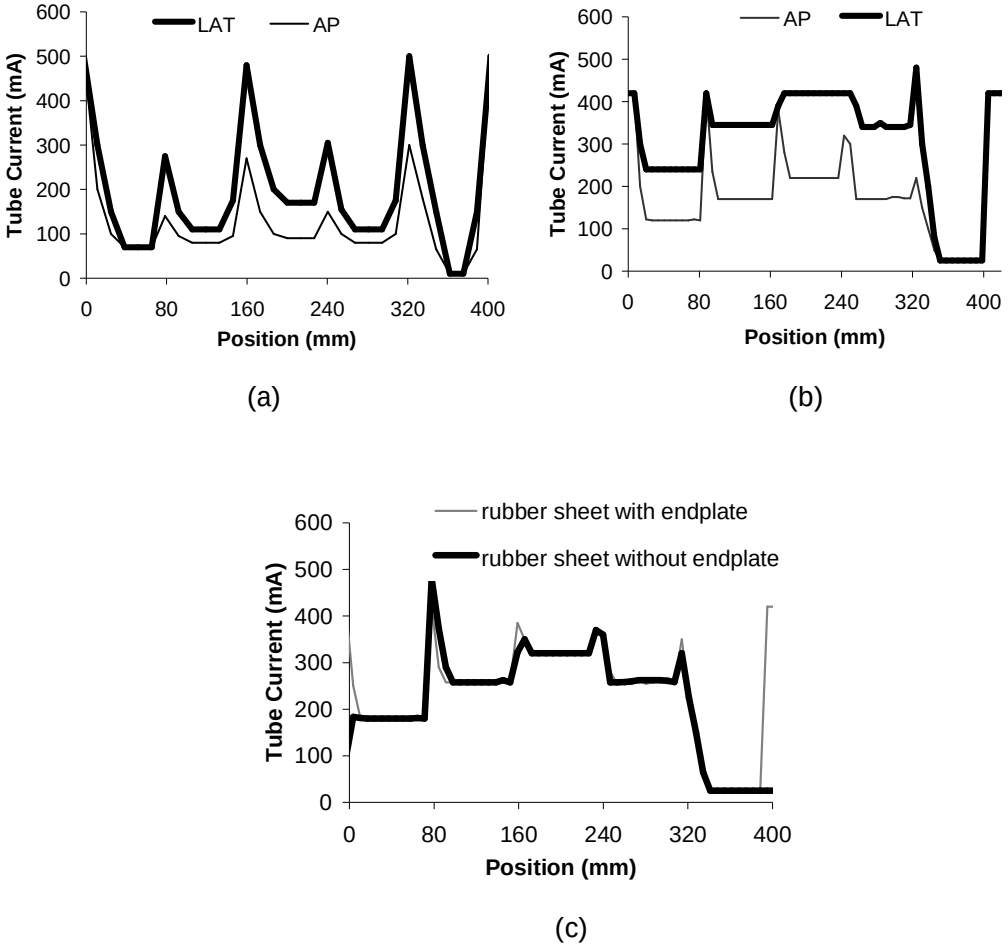

Figure 5-20 Plots of the tube current (mA) against position from sections 1 to 5 of the torso phantom for the AP and lateral directions for the standard setting from the Toshiba Aquilion scanner with a mA range of 10-500 mA with, (a) 16 mm beam width and (b) 8 mm beam width with rubber sheet inserted between sections and (c) comparison of mAs/image values from the 8 mm wide beam with endplates included and excluded from the SPR

5.3.5 Comparison of ATCM systems for different CT scanners

5.3.5.1 Comparison of tube current for different CT scanners

The ATCM for CT scanners for all manufacturers increases the tube current with phantom diameter, but the pattern of implementation for each manufacturer was slightly different. Figure 5-21a shows comparisons of the tube current modulation pattern in the ImPACT phantom from the standard setting of each manufacturer. The effective body $CTDI_{vol}$ for the GE scanner rose more rapidly than those for the Toshiba, Philips and Siemens scanners reaching a maximum at a comparatively small phantom lateral diameter.

Average effective mAs values used for each section of both phantoms from different CT manufacturers with their recommended or standard ATCM options for the CAP protocols are shown with $CTDI_w$ values in tables 5-2 and 5-3, The $CTDI_w$ of the Toshiba scanner is slightly higher than that of the Philips, Siemens and GE scanners. In addition to the recommended ATCM options, the results from the 405 mAs/slice setting of the Philips and 300 effective mAs setting of the Siemens scanners are shown in table 5-2, as these gave similar ranges of image noise to the recommended settings of the GE and Toshiba scanners.

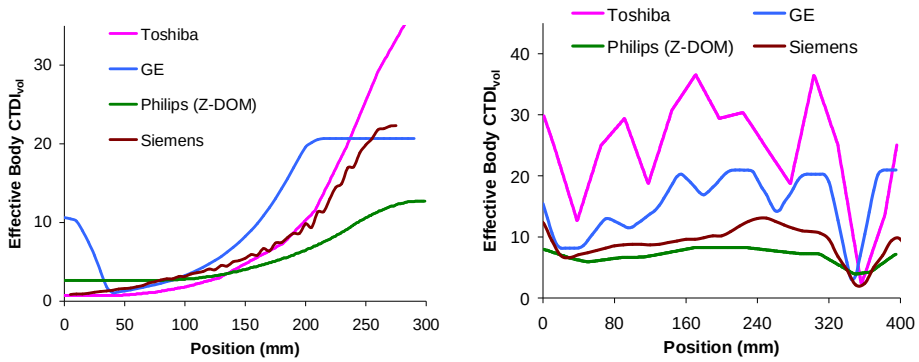

Figure 5-21 Comparisons of the effective body $CTDI_{vol}$ for (a) in the ImPACT conical phantom and (b) the torso section phantom, with the standard settings of different CT scanner manufacturers shown in table 1. Effective body $CTDI_w$ values were calculated for the purpose of relative comparisons

The patterns of tube current modulation for the torso section phantom were similar in the GE and Toshiba scanners, and in Siemens and Philips scanners. The tube current started and ended at a higher value which was associated with the attenuation of the end plates. The modulations of tube current were smooth in the Philips, and the Siemens scanners, while there were large fluctuations in the tube currents in the Toshiba and GE scanners. The fluctuations of the tube currents were wider for the Toshiba scanner compared with the GE. This is partly because of the use of a wider beam for the Toshiba scanner, but also linked to the manner in which the tube current was adjusted for sudden changes in phantom attenuation.

Table 5-2 $CTDI_{vol}$, effective mAs and ESAK values in different regions of the ImPACT phantom for the four CT scanners

Manufacturer	Image Noise* (HU)	$CTDI_w$ (mGy/mAs)	Average effective mAs ** (Average effective body $CTDI_{vol}$)			Average ESAK (mGy)*** (Ant and Lat.)		
			125-175 mm	175-225 mm	225-275 mm	125-175 mm	175-225 mm	225-275 mm
Philips Z-DOM (188 mAs/slice)	22.2±2.2	0.068	60 (4.08)	96 (6.53)	154 (10.5)	9.9±0.9 7.9±0.3	13±1.2 9±0.5	16.4±1.4 10.8±1.2
Philips Z-DOM (405 mAs/slice)	15.1±1.5		129 (8.77)	208 (14.1)	331 (22.5)	21.4±2 17±0.7	28±2.6 19.3±1.1	35.4±3.1 23.3±2.5
Siemens (110 Eff. mAs)	22.2±1.6	0.077	52 (4)	92 (7.08)	180 (13.9)	7±0.4 7.4±0.7	8.5±0.8 10±1.6	11.5±2.1 13.3±2.8
Siemens (300 Eff. mAs)	13.5±1.8		148 (11.40)	261 (20.1)	290 (22.3)	19±1.6 18.5±1.7	25.5±2.4 22.2±1.8	26.6±3.3 20.3±1.9
GE (NI=11.57)	13.2±1.5	0.065	129 (8.39)	284 (18.5)	318 (20.7)	26.1±4.8 18.4±2.8	37.5±4.1 26.1±3.6	35±4.9 26.3±3.2
Toshiba (SD=12.5)	12.2±0.7	0.121	29 (3.51)	66 (8.0)	168 (20.3)	15.4±1.9 13.3±1.3	22±1.9 17.6±1.5	30.2±3.8 26.4±3.2

* Average image noise at regions of 175-225 mm

** Effective mAs values which were calculated from (mA x rotation time) ÷ Pitch

*** Upper lines are average ESAKs at the anterior surfaces, lower lines are average ESAKs at the lateral surfaces

Table 5-3 $CTDI_{vol}$, effective mAs and ESAK values in different regions of the Torso phantom for the four CT scanners

Manufacturer	$CTDI_w$ (mGy/mAs)	Average effective mAs ** (Average effective body $CTDI_{vol}$)					Average ESAK (mGy)*** (Ant and Lat.)				
		Section 1	Section 2	Section 3	Section 4	Section 5	Section 1	Section 2	Section 3	Section 4	Section 5
Philips (124 mAs/slice)	0.068	97 (6.60)	104 (7.07)	121 (8.23)	109 (7.41)	75 (5.1)	11.9±0.7 10.2±1.3	12.1±1.1 10±1.3	11.5±0.8 9.4±1.2	14.9±1.3 8.6±1.9	12.4±1.6 11.8±2.4
Siemens (110 Eff. mAs)	0.077	107 (8.24)	117 (9.01)	143 (11.01)	148 (11.40)	76 (5.85)	11.3±1.6 11.8±1.7	12.6±1.2 11.7±1.8	12.7±1.5 14.9±3.1	21.4±1.7 14.7±3.3	17.8±7.3 15.4±6.7
GE (NI=11.57)	0.065	162 (10.53)	231 (15.02)	299 (14.89)	278 (18.07)	209 (13.59)	17.9±4.6 14.5±4.6	26±7.3 19.7±4.9	28.2±7.4 23.7±6.9	33.4±7 18.1±10.2	32.4±7.8 29.5±10.2
Toshiba (SD=12.5)	0.121	178 (21.54)	220 (26.62)	259 (31.34)	219 (26.50)	119 (14.40)	36.7±6.7 33.1±5.7	42.9±5.4 39.9±5.7	44.7±6.4 44.1±5.9	48.3±9.1 31.7±3.9	43.7±21.7 36.7±18.6

** Effective mAs values which were calculated from (mA * rotation time) ÷ Pitch

*** Upper lines are average ESAKs at the anterior surfaces, lower lines are average ESAKs at the lateral surfaces

5.3.5.2 Comparison of image noise for different CT scanners

Noise levels in different sections of the ImPACT conical phantom, as illustratred in figure 5-2, are compared in table 5-4. For the fixed mA option, for all scanners the noise in the thickest region was about double that in the medium, which in turn was double that in the thin region. Implementation of the ATCM systems for all the scanners reduced the variation in noise along the phantom. For the Philips and Siemens scanner, the noise levels for the medium and thick sections increased about 30% compared with that of the thin and medium sections, respectively, except for the 300 effective mAs setting for the Siemens scanner in which the noise level in the thick section doubled compared with that in the medium thick section, due to the saturation of the tube current at the major axis of the phantom. For the GE scanner, there was less variation along the phantom for higher NI values (about 60% for the NI setting of 6.94 while 12% for the NI setting of 20.83). However, saturation of the tube current affected the results. There was less variation in noise levels for the Toshiba (10%) than for other scanners. The noise levels for the recommended settings of the Toshiba and GE scanners were similar in the thin and medium sections, while there were greater variations for the Philips and Siemens scanners.

Noise levels in the five sections of the torso phantom are compared in table 5-5. The magnitudes of the variation along sections 1-4 were similar for the Philips, GE and Toshiba scanners (about 14% when ATCM systems were in operation, but 17% for D-DOM). The GE scanner showed the least variation in noise in sections 1-4 (within 4%), while the Siemens scanner had the greatest variation (14%), apart from Philips D-DOM for which the only modulation related to the ratio at the elliptical cross section axes. The noise increased from sections 1 to 4 for the Philips and Toshiba scanners, but declined at section 4 for the Siemens scanner. The noise levels were lowest in the smallest section number 5 for all scanners.

Table 5-4 The noise level in different parts of the ImPACT phantom for different ATCM settings for the four CT scanners

Manufacturer	ATCM option	Average noise (HU)from three different regions		
		125-175 mm	175-225 mm	225-275 mm
Philips	ATCM Off	10.1±2	19±3.5	35.8±7.2
Z-DOM	188 mAs/slice	16.7±1.8	22.2±2.2	29.9±2.7
	250 mAs/slice	14.3±1.4	19.3±1.7	25.5±2.4
	300 mAs/slice	12.7±1.1	17.1±1.7	22.8±2.2
	405 mAs/slice	11.3±1.1	15.1±1.5	19.7±1.8
D-DOM	124 mAs/slice	12.8±2.2	22.1±3.7	38.1±5.4
	188 mAs/slice	10.3±1.7	17.9±3.1	30±4.5
	250 mAs/slice	8.9±1.4	15.4±2.4	25.9±3.9
	405 mAs/slice	6.9±1.1	12±1.9	20±2.8
Siemens	ATCM Off	8.9±1.5	15.4±3	26.9±5.1
	80 Eff. mAs	20.5±1.9	26.6±2.1	33.8±3
	110 Eff. mAs	17.4±1.6	22.2±1.6	27.5±2.1
	150 Eff. mAs	14.6±1.1	18.8±1.3	24.2±3.2
	300 Eff. mAs	10.3±0.8	13.5±1.8	22.4±4.1
GE	ATCM Off	10.5±1.6	18.1±3.1	30.3±3.8
	NI=6.94	6.6±0.4	10.1±1.7	16.7±2.1
	NI=11.57	11.4±0.6	13.2±1.5	21.2±2.6
	NI=16.20	16.1±0.7	17.7±1.1	21.8±2.2
	NI=20.83	21.1±1	23.6±1.5	26.3±1.2
Toshiba	SD=7.5	6.8±0.4	7.7±0.2	8.9±0.7
	SD=10	9.3±0.2	10.3±0.6	10.7±0.4
	SD=12.5	10.7±0.4	12.2±0.7	12.3±0.9
	SD=15	12±0.3	13.6±0.8	13.2±1.1
	SD=20	17.4±0.8	17.6±0.9	17.7±1.2

Table 5-5 The mean noise levels in different sections of the torso section phantom for different ATCM settings

CT Scanner	option	Average noise (HU) from five different regions					
		Section 1	Section 2	Section 3	Section 4	Section 5	Sections 1-5
Philips	ATCM Off	13.4±0.9	15.6±0.6	19.1±0.5	18.1±3.3	5.4±0.8	14.4±5.1
Z-DOM	124 mAs/slice	15.4±0.8	17±0.7	19.3±0.5	19.9±1.2	7.7±1.6	15.9±4.5
	250 mAs/slice	11.9±0.9	13.4±0.7	15±0.4	15.4±1.1	6.2±1.4	12.4±3.4
	300 mAs/slice	9.8±0.7	10.9±0.6	12.3±0.4	12.7±1.1	5.1±1.1	10.2±2.8
	405 mAs/slice	8.5±0.6	9.3±0.5	10.6±0.3	10.5±0.5	4.4±0.9	8.7±2.3
D-DOM	124 mAs/slice	14.1±0.8	16.3±0.5	20±0.6	20.6±2	5.9±0.9	15.5±5.3
	250 mAs/slice	10±0.8	11.3±0.3	14±0.4	14.4±1.4	4.3±0.7	10.9±3.7
	405 mAs/slice	7.9±0.7	8.8±0.3	11±0.4	11.1±1	3.6±0.7	8.5±2.8
Siemens	ATCM Off	15.7±0.3	18.8±0.4	23.5±0.3	22±0.6	6.8±0.2	17.6±5.9
	80 Eff. mAs	19.8±1.6	22.9±0.5	26.4±1.3	20.1±1.1	12.2±4.1	20.6±4.9
	110 Eff. mAs	17±1.4	19.4±0.4	21.9±1.6	16.2±1	10.1±3	17.2±4.1
	150 Eff. mAs	14.4±1.2	16.5±0.2	18.1±0.8	14.8±1.2	8.8±2.5	14.7±3.3
	200 Eff. mAs	12.4±1	13.4±0.3	16±0.5	13.8±0.4	7.8±2.1	12.8±2.7
GE	ATCM Off	6.1±0.4	7.1±0.6	8.7±0.2	7.9±1.2	2.6±0.1	6.6±2.2
	NI=11.57	11.6±1.2	11.4±1.1	12.4±0.7	11.6±1.1	6.2±2.9	10.7±2.7
	NI=16.20	16.3±2	15.7±2	17.2±1.4	16.2±1.5	7.9±4.9	14.8±4.2
	NI=20.83	20.6±2.2	20.5±2.9	22.1±1.7	21.3±1.9	9.1±6.1	18.9±5.7
Toshiba	ATCM Off	5.6±0.4	7.4±0.8	10.1±0.3	9.7±1.1	3±0.2	7.2±2.7
	SD=7.5	9.6±1.2	9.5±0.6	11.3±0.3	12.4±3.1	4.6±2	9.5±3.2
	SD=12.5	12.4±3.0	12.7±2.1	14.5±1.6	16.5±4.2	7.4±4.7	12.7±4.5
	SD=20	16.2±6.2	18.9±2.5	15.8±1.7	16.1±4.6	10.7±8.5	15.6±5.8

5.3.5.3 Comparison of ESAK for different CT scanners

ESAKs at the anterior and lateral surfaces measured along the length of the phantom for each scanner using the settings recommended by the manufacturer are shown in figure 5-22 and tables 5-2 and 5-3. For the ImPACT phantom, ESAKs increased slightly along the length of the phantom for all CT scanners, with more rapid increases with phantom diameter after 80 mm for the Toshiba and GE scanners (figures 22a and 22b). The increases in ESAK profiles relate to the effective body $CTDI_{vol}$ values (also tube current and $CTDI_{vol}$). This is because the AK level increases as the isocentre is approached, through lower attenuation in the central region of the bow tie filter. Therefore the incident AK per mAs rises as the phantom diameter declines. In addition, towards the thinner end of the phantom there are greater contributions from more penetration of the x-ray photons at the measurement point from other angles of the x-ray tube. The higher ESAKs at the thick end of the ImPACT phantom result from the higher effective mAs values. The net results are that the ESAKs at the narrow end of the ImPACT phantom are not substantially different from those at thicker end for the Philips scanner. For the GE scanner, ESAKs peak at about 200 mm from the beginning and drop slightly in the final part of the scan. The reason for the decline is that with the tube current remains constant over the final part of the phantom. As a result the ESAKs fell, as the measurement points were further from the iso-centre (Sookpeng *et al.,* 2013b). A similar argument applies to the cases with the fixed mA techniques. In the case of the Toshiba scanner, ESAKs increased slightly after 80 mm and increased rapidly after 200 mm from the start of the scan. The extremely high ESAKs and effective body $CTDI_{vol}$ values particularly at the final part of the scan are thought to be due to the effect of the phantom boundary edge discussed earlier.

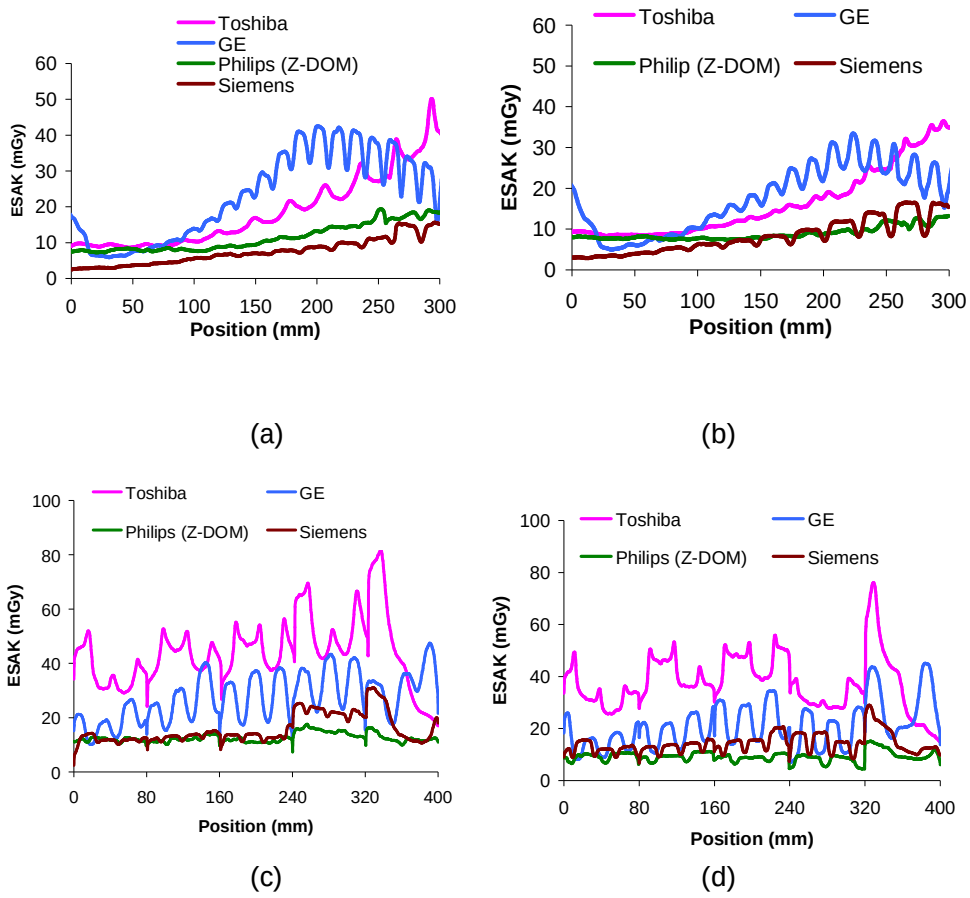

Figure 5-22 ESAK profiles (a) at the anterior and (b) at the lateral surfaces of the ImPACT conical phantom, and (c) at the anterior and (d) at the lateral surfaces of the torso phantom with the standard settings of different CT scanner manufacturers shown in table 5-1

For the torso phantom (figures 5-22c and 5-22d), ESAKs remained relatively constant for each section and also along the whole length of the phantom for the Philips scanner, but there were larger fluctuations in the ESAKs for both GE and Toshiba scanners which related to the effective body $CTDI_{vol}$ values. ESAKs and effective $CTDI_{vol}$ values for sections 1-4 for the Toshiba scanner were about two to four times higher than those of the other scanners (table 5-3). The ratios between the ESAKs at the anterior and lateral surfaces for the Philips and GE scanners were higher than those for the Toshiba and Siemens scanners with both the ImPACT and torso phantoms.

5.3.6 Results with the wedding cake phantom in the Toshiba scanner

A second prototype phantom comprising three elliptical segments of differing dimensions like a wedding cake has been developed. It was constructed from polyethylene (density 0.95 g/cm^3). Each section of the wedding cake phantom is 120 mm in length and the diameters of the major and minor axes respectively were: 1) 270 mm × 400 mm, 2) 260 mm × 385 mm, 3) 220 mm × 330 mm to reflect variations in the diameter of the trunk (figure 5-23). Recesses were cut into the second and the third sections of the phantom to allow the adjacent section to slot in and so minimise any gaps. Holes were included in the phantom to allow central and peripheral dose measurements. The SPRs and scan lengths were 300 mm excluding both edges of the phantom and the direction of scan was from the large section to the small section, as ahown in figure 5-23c. All scans were carried out in a similar direction along the phantom.

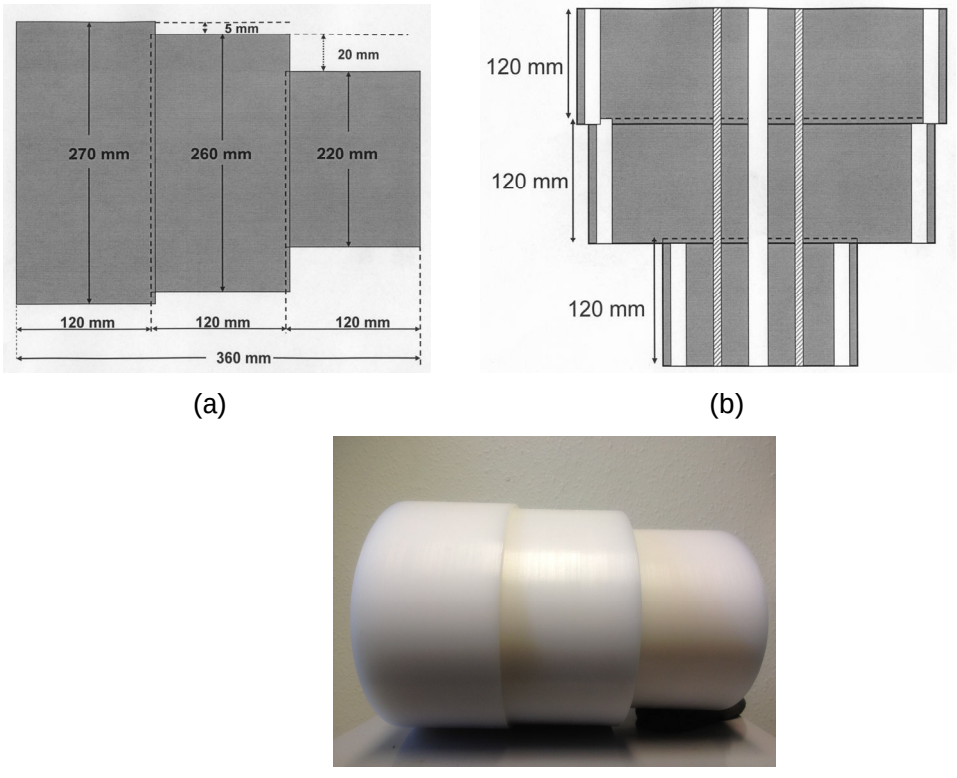

Figure 5-23 Second prototype ATCM wedding cake phantom (a) the side view and (b) the top view of phantom and (c) the phantom, the ratios of lateral and AP diameters of all sections are 3:2

The tube current oscillations apparent in scans of the torso phantom on the Toshiba scanner appear to be associated with the large step changes in attenuation. Observations of the tube current changes for scans of patients with implants, although exhibiting greater than normal changes in current did not show a similar behaviour. The next prototype phantom was made up from three longer sections with smaller changes in diameter between sections. It also had insets to avoid any air gaps between sections and did not require supporting endplates

Figure 5-24 shows the changes in tube current along the phantom, from different lengths of SPR and beam widths. The right hand side figures were obtained with a narrower beam of 8 mm and shorter SPR excluding both edges of the phantom. There were no sharp peaks and the tube current remained relatively constant within each section. Profiles obtained with a wider beam and a longer SPR including the edges of the phantom, still had sharp peaks in tube current at the beginning and the end of the scan but only small oscillations within the length of the phantom. Also, profiles obtained with a wider beam and a longer SPR had higher tube current values for each section of the phantom.

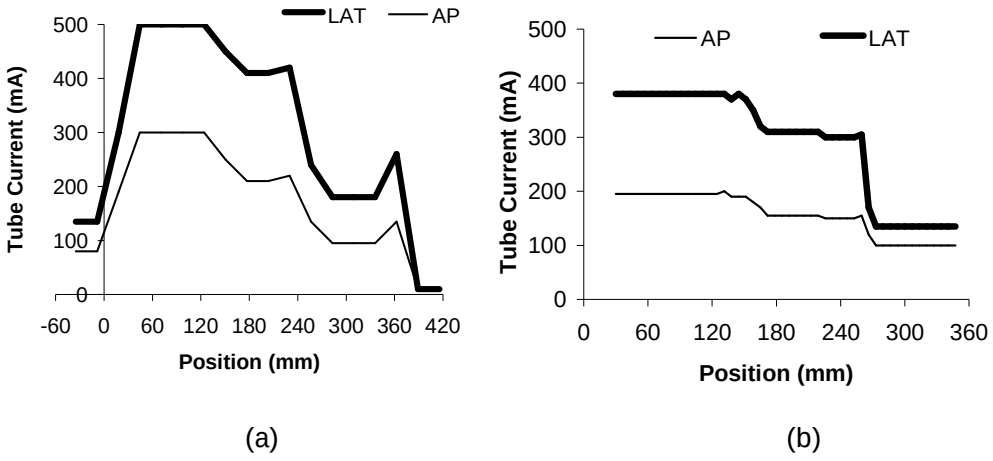

Figure 5-24 Tube current modulations for AP and lateral directions with Standard (SD=12.5) setting in a Toshiba scanner using (a) 32 mm wide beam and SPR covering both phantom edges and (b) 8 mm wide and SPR excluding both phantom edges

5.4 Discussion

5.4.1 Comparisons of the operation of ATCM systems

Direct comparison of the ATCM system functions from the various manufacturers is complicated because they employ different solutions for the tube current adjustment and define the image quality in different ways. The Toshiba and GE scanners allow users to select the minimum and maximum tube current values and the tube current is modulated within that range, while in the Philips and Siemens scanners the ranges of the tube current are determined by the scanners and depend on the image quality settings.

The ATCM system of the Toshiba displays two line graphs on the monitor to portray the tube current modulation in the AP and lateral axes prior to the CT scan. Similarly the GE scanner lists the tube currents in the AP and lateral directions in a table before the scan is performed. However, for the Philips scanner, the maximum and range of mAs/slice to be used are displayed, but the tube current modulation plan is not available prior to the scan. The tube current values used in the Toshiba, GE and Philips scanners are based on attenuation levels derived from SPRs, while the Siemens scanner uses the SPR to plan the tube current range, based on the selected QRM and the stored reference size of patient, and the tube currents are then adjusted based on real time measurements of patient attenuation made during the scan.

5.4.2 Comparison of the ImPACT conical and Torso stepped phantoms

The ImPACT conical phantom provides a smooth variation in size over a wide range of attenuations and enables the full range of tube current to be assessed. It is more difficult to quantify performance in term of specific markers as there is no region of constant geometry. The thinnest quarter of the phantom does not modulate the tube current in the Philips and Toshiba scanners because the minimum mA setting is higher than that required to provide the level of image quality selected. But commencing the scan in this part of the phantom provides a reproducible initial phase, minimising any end effects. The phantom only tests operation of the ATCM as the attenuation is either increased or decreased. In

addition, the phantom only tests operation of the ATCM for a fixed ratio of diameters.

The torso phantom had been designed to provide a series of uniform ellipses simulating the dimension at various positions along the human torso. This could provide a set of positions at which performance could be assessed. The responses for the Philips and Siemens scanners followed a recognisable pattern, except that in the small fifth section, representing the neck, the noise level fell in the Siemens scanner and then rose again when the tube current was reduced in response to the smaller diameter.

For the GE and Toshiba scanners, there were wide fluctuations in the tube currents throughout each section of the phantom (figure 5-11b and 5-16b). Large changes in the tube currents were triggered by the sharp boundaries. The fluctuations arose because the beams overlapped more than one of the 80 mm wide sections of the phantom for a significant proportion of time, and only irradiated a single section for a short period. As a result, the tube current did not achieve a constant value for any single section, as the ATCM response was influenced by adjacent sections. A constant tube current can be achieved in each section for beams that are narrow compared to the length of the section (e.g. figure 5-20b). Pronounced peaks in current modulation occurred at the boundaries between sections in the torso phantom for the GE and Toshiba scanners even for narrow beams. These resulted from increases in tube current triggered by step changes in phantom attenuation. Consequently tube current modulation adjacent to sharp boundaries for these scanners will not represent the performance of the ATCM in normal clinical applications where such large abrupt changes rarely occur.

Another unusual feature of the tube current variation for the GE and Toshiba scanners was the large tube current value at the start and the end of the scan (figures 5-11b and 5-16b). Initially, it was thought that the presence of the polycarbonate end plates which supported the torso phantom were entirely responsible. However, further investigation identified that higher tube currents still occurred when the end plates were removed due to the rapid changes in attenuation at the edges of the phantom. When the SPR that was used to plan

the scan included the edges of the phantom, the tube current began at its maximum value for all ATCM options, in the case of the wedding cake phantom (figure 5-24). This effect is not seen when the SPR starts within the boundary of the phantom. However, the sharp rises in tube current towards the ends of scans with the Siemens and Philips scanners were associated with the end plates. The boundary effects have a profound influence on the overall scanner performance.

The torso phantom provides the broad range of attenuations required to test the ATCMs. However, the large abrupt changes in attenuation induce an exaggerated response in some scanners, which makes the phantom unsuitable for assessment of these models. In addition the large change in attenuation from the shoulder (section 4) to the neck (section 5) provokes such a large ATCM response; that it is difficult to gain any useful information from this part of the scan.

5.4.3 Alternative design of stepped phantom

The polyethylene phantom in the form of the tiered wedding cake has been developed to overcome problems with the torso phantom. The phantom has a smaller number of broad sections, with smaller differences in attenuation between sections. Recesses were cut into the second and the third sections of the phantom to allow the adjacent sections to slot together and so minimise any gaps. Each section is 120 mm wide to enable the ATCM to stabilise the mA and to support measurements on wider beams. The phantom also incorporates holes which could be used for dose assessment during ATCM operation. The wedding cake phantom is relatively simple and inexpensive to manufacture. As the phantom is close to human body shape and attenuation, it can be used to study how image noise and patient dose are related, to compare the dose and image quality for different protocol settings, for the purpose of optimisation (Sookpeng *et al.,* 2013a).

5.4.4 Comparison of tube current, image noise and ESAK for different scanners

5.4.4.1 Tube Current

The results of the tube current modulation can be separated into two groups, the Philips and Siemens scanners and the GE and Toshiba scanners. The tube current changed gradually with the phantom diameter along the length of both phantoms for Philips and Siemens scanners, all ATCM options followed the same pattern and there were no fluctuations in the tube current along the phantom lengths. This can be seen from figures 5-4 and 5-5 (Philips scanner) and figure 5-8 (Siemens scanner).

In contrast, the changes in tube current for the Toshiba and GE scanners were more irregular at each image quality setting, this is especially true for the torso phantom (figure 5-11 (GE), figure 5-16 (Toshiba)). For the GE scanner, the pattern of variation in tube current was similar over the middle of the phantom (figure 5-11b) for all settings, although the values were different, but for the Toshiba scanner all image quality modes reached the maximum current at the same point resulting in more variation in image noise (figures 5-16b and 5-16d). These larger changes will make the ATCM more responsive, but result in the phantom irradiation being less uniform.

The performance of the ATCMs in the most attenuating parts of both the ImPACT and torso phantoms is affected by the maximum tube current available. For the Philips scanner, the range of the tube current was determined by the scanner for the option chosen. The modulation followed a similar pattern for all results and never saturated at the maximum limit (figures 5-4a and 5-4b). For the Siemens scanner, the maximum tube current achieved during tube current modulation is limited by the scanner tube capacity and the image noise in these regions increased, if the estimated tube currents exceed the scanner limit there will be a warning message displayed to the user, stating that the image noise will be increased locally. The user can choose to increase kV or rotation time, or to decrease pitch.

For the Toshiba scanner, the tube current is limited by the maximum value set by the users, therefore image noise rises above the target noise for images of high quality setting (figure 5-16). A lower noise level may be achieved by increasing the tube current or the rotation time to achieve higher mAs values but this will of necessity increase dose. The GE scanner follows a similar pattern with the tube current limited by the mAs range selected by the user and tube loading. The position at which the tube current saturates and noise level starts to rise depends on the selected NI (figures 5-11a and 5-11b). For the lowest NI the mAs appeared to reach a limit for the average tube current at a lower value, but the SD remained below the levels for the other options (figure 5-11c, NI setting of 6.97). The reason for this is uncertain, but may be associated with the relative values of the current for the AP and lateral directions.

5.4.4.2 Image Noise

The ATCM of the GE and Toshiba scanners maintained a constant noise level (within 10%) for the first 150-200 mm of the ImPACT phantom (figure 5-11c and 5-16c) over which the tube currents were modulated according to ImPACT phantom diameter (figures 5-11a and 5-16a, table 5-4). Once the target noise was reached, the ATCMs for both Toshiba and GE scanners were able to maintain the absolute noise levels close to the target noise values, for all phantom sizes because of the more aggressive tube current modulation. On the other hand, the Siemens and Philips scanners, for a given protocol, try to maintain a constant level of overall diagnostic quality linked to patient sizes relating to a reference image, as illustrated in figure 5-25. Siemens and Philips ATCMs can be considered as 'acceptable noise' systems. They do not maintain constant image noise for all patient sizes but decrease tube current for small patients and increase tube current for large patients less than those of the Toshiba and GE scanners. The manufacturers do not provide a definition of acceptable image quality, but suggest that it is based on the assumption that larger patients who have more fat layers between organs have better image contrast and can accept more noise, compared to small patients. This produced greater variations in noise with phantom size, with variations of 50% and 30% for Philips and Siemens respectively (figures 5-4c and 5-8c). These results are similar to those reported by Muramatsu *et al* (2007).

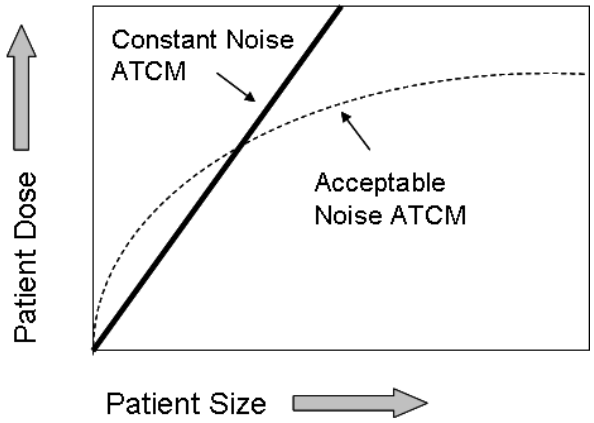

Figure 5-25 Comparison of patient dose with patient size between constant noise based ATCM system (Toshiba and GE scanners) and manufacturer 'judged' acceptable noise based ATCM system (Philips and Siemens scanners)

The overall results of image quality measurements between the ImPACT and torso phantoms were similar. Image noise levels for the Siemens and Philips scanners varied with phantom size (16% and 11% for sections 1-4, for recommended settings) (figures 5-4, 5-5 and 5-8), in contrast to those for the Toshiba and GE scanners. The ATCM systems of the GE and Toshiba scanners aimed to preserve a constant noise along the length of scan and these were similar to the target values at the middle of each section of the phantom, but for the comparatively narrow sections in the torso phantom, there was insufficient time for the modulation to take effect, when a wider beam was used, and this resulted in fluctuations in image noise (figures 5-11d and 5-16d).

5.4.4.3 ESAK

ESAK profiles along the ImPACT and torso phantom lengths between the AP and lateral directions were more uniform when the ATCM systems were in operation compared with fixed mAs techniques (eg. figures 5-17a and 5-17c). However, section 4 of the torso phantom was in exception (figure 5-17b, table 5-3). This may be explained in terms of the tube current being attenuated by the longer lateral axis of section 4. Comparison of ESAKs for the recommended settings for the ImPACT phantom from each scanner (table 5-2) shows that results at the lateral surface for the Philips scanner were lower than those for the Siemens scanner, while the ESAKs at the anterior surface were higher. The overall EASK values along the phantom length for the Philips were lowest (figures 5-22a and

5-22b). The ratios between the ESAKs at the anterior and lateral surfaces for the Philips scanner were higher than those for the Siemens scanner because only z-axis modulation is operational for the Philips scanner (table 5-2). However, the ratios between the ESAKs at the anterior and lateral surfaces for the GE scanner were also high even when both x-y and z-axis modulation was used. This is because the tube currents for AP and lateral directions of the GE scanner were similar (figure 5-12). Comparison of ESAKs for different manufacturers that gave similar ranges of image noise (table 5-2) revealed that the ESAKs for the Toshiba scanner were lowest, except for the final part of the scan (225-275 mm) at which the ESAKs were extremely high because of the edge effect. This may result from the use of QDS software on the Toshiba scanner for the ImPACT phantom scan.

The ESAK profiles obtained from the torso phantom showed large fluctuations for the GE and Toshiba scanners (figures 5-22c and 5-22d), reflecting the tube current modulation because of the response of the ATCM systems to the sudden changes in attenuation, described earlier. The fluctuating ESAKs and effective $CTDI_{vol}$ values lead to large variations in image noise. Absolute ESAKs and noise for sections 1-3 were similar for the Philips and Siemens scanners (table 5-3), but the ESAKs were higher for both AP and lateral directions at section 4 for the Siemens scanner for which the ATCM operated with both x-y plane and z-axis dose modulation.

5.4.5 Options for the design of ATCM phantoms

Stepped phantoms were developed and used for tests of the ATCM stsyems for different CT scanners.The results were compared with those obtained from the ImPACT conical phantom. Results have shown substantial differences in the manner in which the ATCM systems for different CT scanners operate. Results from the cone phantom and the torso phantom were similar in the Philips and Siemens scanner, tube current modulations were smooth over the phantom length. However, application of the stepped phantom was limited for the Toshiba and GE scanners since the abrupt change in attenuation provoked an aggressive ATCM response. Any phantom used for testing should be able to deal with all available systems. Therefore number of recommendations can be made based on measurements carried out in this investigation.

Phantom design

1) Phantom should avoid sharp discontinuities in attenuation (section 4.3.2, chapter 4 and section 5.3.4.3).

2) Sectional phantoms should be constructed to exclude air gaps (section 5.3.4.3).

3) Thicknesses of individual sections within the phantom should not be less than three times the beam width at which measurements are to be made, in order to achieve a constant tube current over an area sufficient for measurement (sections 5.3.4.3 and 5.3.7).

4) Conical phantoms can provide the best overall indication of performance in terms of tube current modulation and image noise, but as the tube current varies continually along the phantom, they do not provide positions where factors are relatively constant for measurement of dose and image quality (section 5.3.5.1).

5) A phantom with a limited number of elliptical sections should be used for dosimetry and image noise measurement (section 5.3.7).

6) The phantom should cover the useful range of patient attenuation encountered routinely in clinical practice. A steady progression from the smallest to largest diameters is recommended to avoid unnaturally large change in attenuation which influence ATCM response (section 5.3.5).

7) A ratio of 3:2 provides a realistic cross section for much of the trunk, but a wider section (ratio 2:1) is required to mimic the cross section at the shoulder (section 5.3.1, Philips D-DOM).

ATCM testing

1) Use of small beam widths is recommended whenever possible unless the phantom has sufficiently large sections (section 5.3.4.3).

2) The SPR should be set within the boundaries of the phantom to avoid unrealistic tube currents at the start or end of a scan (section 5.3.4.3).

3) Scans of phantoms in directions of both increasing and decreasing attenuations may be useful in assessment of performance.

5.5 Conclusion

Evaluation of the CT ATCM system is important for routine quality control of CT scanners in order to manage patient dose and image quality. In this chapter, phantoms developed to evaluate CT ATCM performance have been tested and results compared. Results from the ImPACT conical and torso phantoms were in similar ways for the Philips and the Siemens systems, suggesting that the torso phantom could be used for ATCM systems testing for these scanners. The ATCM systems of the Philips and Siemens scanners modulate the tube current within a narrower range of allowed mA values, and the tube current changes were smooth and unaffected by the junctions between sections. The GE and Toshiba scanners, however, whose mA ranges are freely selectable by the user modulate the tube current more aggressively. This approach provides systems which are more responsive and able to maintain set noise levels more readily but results in patterns with large changes in the tube current when phantoms with larger discontinuities in attenuation are scanned. There were fluctuations in the tube current with the first prototype torso section phantom, which were exacerbated by the narrow width of the sections in comparison with the large beam widths. A elliptical wedding cake phantom designed with a smaller number of broader sections and smaller differences in attenuation between sections was more effective in determining the operational characteristics of the ATCM utilised by each CT manufacturer. The phantoms used in this chapter were designed to test ATCM performance. In order to understand how scanners perform in situation closer to clinical practice, experiments were carried out on an anatomical phantom of a small adult.

6 Investigation into performance of ATCM technique for abdomen and pelvis examination using anthropomorphic phantom

6.1 Introduction

Evaluation of ATCM system using custom made phantoms has been carried out and shown in chapters 3-5. For this chapter, to move closer to the CT optimisation required in clinical practice, a phantom representing a more realistic human shape that was available in the department has been used in order to understand the responses of the ATCM systems for different manufacturers.

ATCM is normally used for scans of the trunk. A main reason this project focusing on the CT examinations of abdomen and pelvis and CAP is because the patient dose received from these examinations were high and higher than DRL for some CT scanners. A scan of the abdomen and pelvis is the third most common CT examinations after CT head and CT CAP. The percentage of the total CT examinations performed in the UK in 2008 for the CT abdomen and pelvis examination was 10%, while that for the CT head and CT CAP was 33% and 12% (Hart *et al.,* 2010). Although the ATCM systems have been implemented in the majority of CT scanners, a CT patient dose survey in the West of Scotland in 2011 involving 23 CT scanners, for which data were collected from patients of any size, revealed that the patient DLP values for CT examinations of the abdomen-pelvis and the CAP were high. For CT abdomen-pelvis examinations, DLPs for almost all CT scanners were higher than the national diagnostic reference level (DRL) of 560 mGy.cm (Shrimpton *et al*., 2005), as illustrated in figure 6-1. This was not the case for the majority of other CT examinations.

The only dose related quantity that can be measured with an anatomical phantom of this type is ESAK. ESAK is the air kerma at the point that radiation enters the patient or phantom including backscatter radiation. Patient ESAK can provide an assessment of dose performance throughout a CT scan and is measureable using Gafchromic film.

This study has been carried out by scanning an abdomen pelvis phantom of below average size on different CT scanners to determine the levels of dose reduction that are being achieved. ATCM systems are designed to allow reductions in dose for less attenuating parts of a scan. The largest reductions should be achievable on smaller patients. The aims can be separated into three parts. The first objective was to measure the tube current, image quality in terms of image noise, and ESAK. The second objective was to evaluate the routine protocol of each scanner in order to identify reasons for any higher patient doses. The third was to analyze the dose reduction potential from the ATCM technique compared to the fixed tube current technique used on individual scanners.

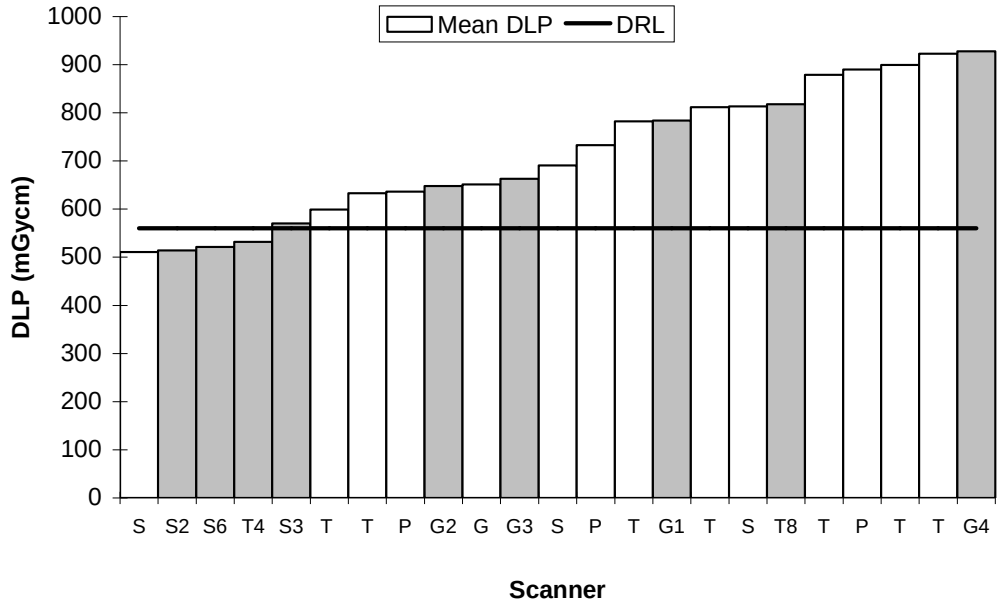

Figure 6-1 Average DLP from various scanners for the West of Scotland CT scanners, surveyed in 2011
(Shading refers to scanners involved in this chapter)

6.2 Materials and Methods

Ten CT scanners equipped with ATCM systems from three different CT manufacturers; GE, Toshiba and Siemens were recruited into the study. Specific CT scanner codes defined for this PhD project were used to represent each CT scanner (table 6-1). SureExposure 3D ATCM system was used for the Toshiba scanners. Auto mA which is the modulation of the tube current along the z-axis and is type of modulation routinely selected for all the GE scanners in this study. For the Siemens

scanners, the CareDose 4D which modulates tube currents in the x-y plane and along the z-axis was implemented in scanners S2 and S4, while the CareDose, which is a patient size based selection of tube current was implemented in scanners S3 and S6. These scanners select the tube current based on the SPR, but the value remains constant during the scan for individual patients. Details regarding principles of CT ATCM systems for different CT manufacturers are available in chapter 2. Scanning protocols and image quality parameters used for the routine adult CT abdomen-pelvis from the various CT scanners are shown in Table 6-1. All CT scans were performed with 120 kV. Scanners T4, T8 and G2 have saved reconstructed images of narrower slice thicknesses in the PACS. The reason for this is to allow 3D images in coronal and sagittal planes to be reconstructed in individual hospitals.

Table 6-1 Details of CT scanners and scan parameters for CT abdomen and pelvis examination

Manufacturer	Code	Slice	Collimation	Rot. Time (s)	Pitch	Protocol	Image Quality	Recon.Kernel	Slice Thickess*
Toshiba	T4	64	32x1	0.5	0.844	Routine	SD=12.5 (31.25), Min mAs=50, Max mAs=220	FC13	5 mm
						Modified	SD=12.5 (31.25), Min mAs=5, Max mAs=220		(0.8mm in PACS)
	T8	64	64x0.5	0.5	0.828	Routine	SD=13.5, Min mAs=40, Max mAs=240	FC03	5 mm
						Fixed mAs	75 mAs		(1 mm in PACS)
GE	G1	64	32x1.25	0.5	0.984	Routine	NI=28, Min mAs=100, Max mAs=325	Standard	1.25 mm
						Modified	NI=28, Min mAs=25, Max mAs=325		
	G3	16	16x1.25	0.8	1.375	Routine	NI=25, Min mAs=160, Max mAs=352	Standard	1.25 mm
						Modified	NI=25, Min mAs=40, Max mAs=352		
	G2	16	16x1.25	0.8	1.375	Routine	NI=14 (28), Min mAs=64, Max mAs=352	Standard	5 mm
						Fixed mAs	140 mAs		(1.25 mm in PACS)
	G4	16	16x1.25	0.8	1.375	Routine	NI=11.57, Min mAs=64, Max mAs=280	Standard	1.25 mm
						Fixed mAs	240 mAs		

Values for the SD (T4) and NI (G2) in brackets relate to the equivalent values for images sent to PACS (see section 6.4.2)

*Slice thickness for the first reconstruction

Table 6-1 (Cont.) Details of CT scanners and scan parameters for CT abdomen and pelvis examination

Manufacturer	Code	Slice	Collimation	Rot. Time (s)	Pitch	Protocol	Image Quality	Recon.Kernel	Slice Thickess*
Siemens	S2	64	64x0.6**	0.5	1.4	Routine	Reference mAs=200	B20f	1 mm
						Fixed Eff.mAs	160 effective mAs		
	S3	4	4x2.5	0.5	1.25	Routine	Effective mAs=121	B30f	3 mm
						fixed Eff.mAs	165 effective mAs		
	S4	64	64x0.6**	0.5	0.8	Routine	Reference mAs=150	B20f	1 mm
						Fixed Eff.mAs	150 effective mAs		
	S6	4	4x2.5	0.5	1.5	Routine	Effective mAs=141	B31f	3 mm
						fixed Eff.mAs	165 effective mAs		

*Slice thickness for the first reconstruction

**z-flying focal spot: double sample along z-axis; actual beam width is 32x0.6 mm

6.2.1 Materials

6.2.1.1 Gafchromic film

ESAK was measured by Gafchromic XR-QA radiochromic film (International Specialty Product, Lot No.A10071002A). The film is designed for radiology dose measurement (International Specialty Product 2010). The calibration methodology was described in chapter 3.

6.2.1.2 Anthropomorphic Phantom

The study was performed using a sectional transparent abdomen/pelvis phantom of a small adult. It is 40 cm long starting from the first lumbar vertebra to 10 cm beyond the symphysis pubis. The phantom comprises a skeleton encased in PMMA in the form of the body contour. The AP and lateral diameters measured between the two widest points along a line at right angles to the AP and lateral diameters and at the level of body of the first lumbar vertebra are 17 cm and 22 cm, respectively and those measured at the sacroiliac joint of the pelvis are 19 and 27 cm, respectively (figures 6-2c and 6-2d). This compares with average values of 24 cm (15cm-34cm) in AP and 32 cm (22cm-47cm) in lateral directions, measured at the first lumbar vertebra in 225 patients.

6.2.2 Methods

6.2.2.1 Testing approach

Radiographers who operate individual CT scanners were asked to scan the phantom with their routine abdomen-pelvis protocols with ATCM systems activated. For some scanners, the radiographers were also asked to scan the phantom with ATCM system inactivated using appropriate factors (fixed mA technique) in order to compare the patient ESAK and the image quality between the two techniques. For these cases, the radiographers were asked to select tube currents that would be used in clinical practice. In addition to these tests, the minimum tube current settings from the routine protocols were reduced for some Toshiba and GE scanners to assess the changes in tube current modulation patterns.

After SPRs, two strips of Gafchromic XR-QA film each measuring 10 mm x 300 mm were taped on to the surface of the phantom within the scanning region along the longitudinal scanning axis at the anterior and right lateral surfaces of the phantom as illustrated in figure 6-2b. The dose profile data were analyzed using ImageJ, as described in chapter 3. The scan direction for all figures in this chapter was from the abdomen to pelvis.

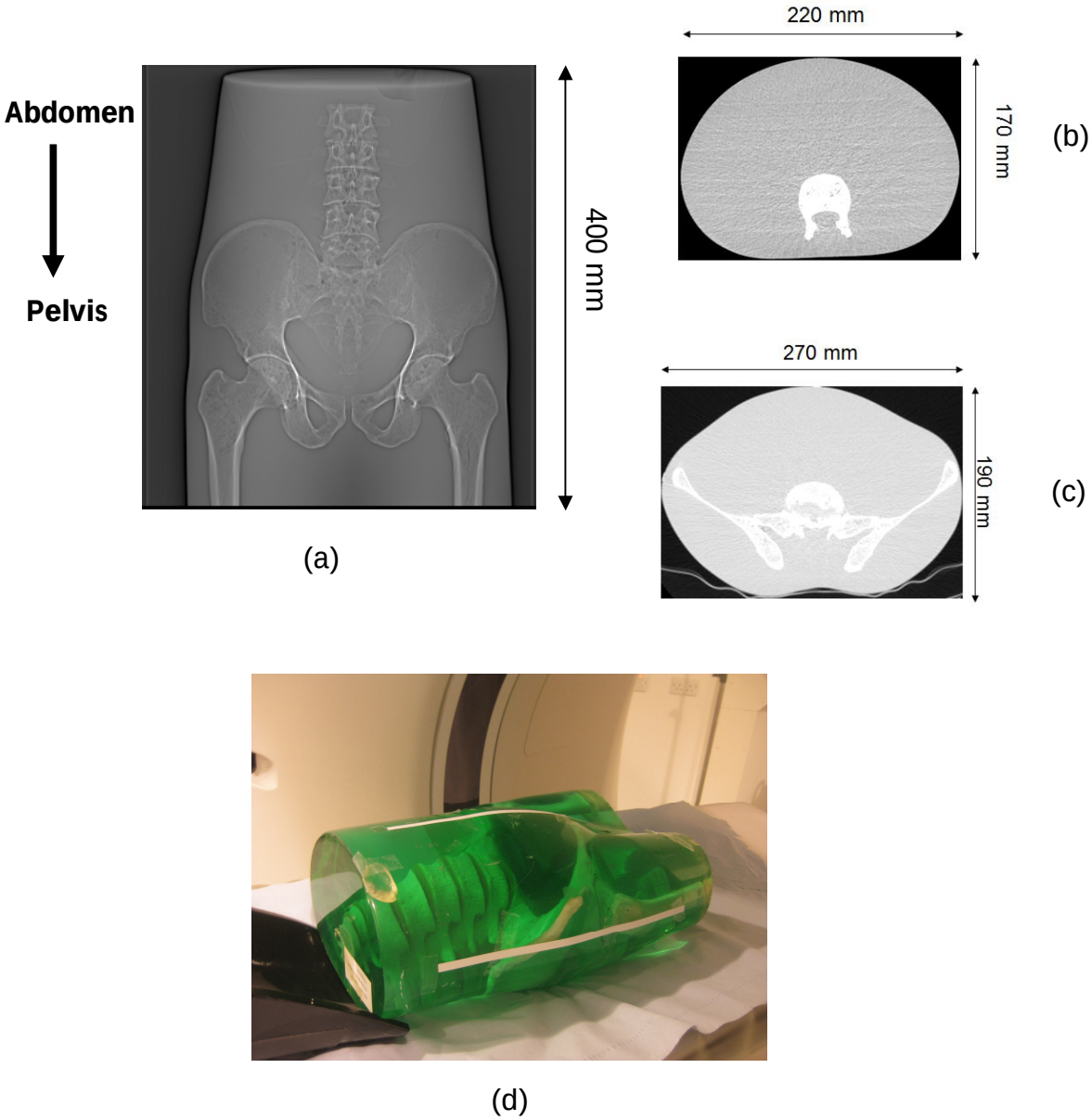

Figure 6-2 (a) Image of the abdomen-pelvis phantom in AP direction and cross-sectional diameters of the phantom at (b) the first lumbar vertebra and (c) the sacroiliac joint and (d) positions of Gafchromic film dose measurements

6.2.2.2 Data Analysis

Images were sent to the PACS and the tube current values per image determined from the DICOM header. An automA plugin was used to read out the mAs/image for the Toshiba and GE scanners and the effective mAs/image for the Siemens scanner. The tube currents per image values were plotted against scanning position starting from the lumbar spine to the head of femur (abdominal to pelvis).

An image noise value in terms of the standard deviation of the CT number was measured using ImageJ. Unlike measurements described in the previous chapters that used the circular ROI, for this study, rectangular ROIs of 500 mm^2 were placed on the PMMA matrix, avoiding the bones, at four different locations; anterior, right lateral, left lateral and central parts of the phantom. This shape of ROI was chosen because the phantom had been made by pouring layers of gelled resin while the phantom was laid horizontally, and the gel was not completely homogeneous. Drawing ROI with a rectangular shape within layers of resin was therefore a more reasonable approach for measuring the image noise, in order to avoid the inclusion of components from two layers.

Noise was measured along the image stack to evaluate the consistency of image quality throughout each scan. It was not possible to place the ROIs at exactly the same positions throughout the phantom because of the need to avoid the bones. Four sets of ROI for sections at the levels of the lumbar spine, the pelvic bone, the head of femur and the body of femur, as illustrated in figure 6-3, were chosen and the image noise values from the four measuring positions within each section were averaged. The image noise levels were separated into those for the abdominal and pelvis parts, the former referred to the noise measured at the lumbar spine and the latter referred to the noise measured from the pelvis bone onwards. The measured noise from individual ROIs were averaged and are shown in table 6-2.

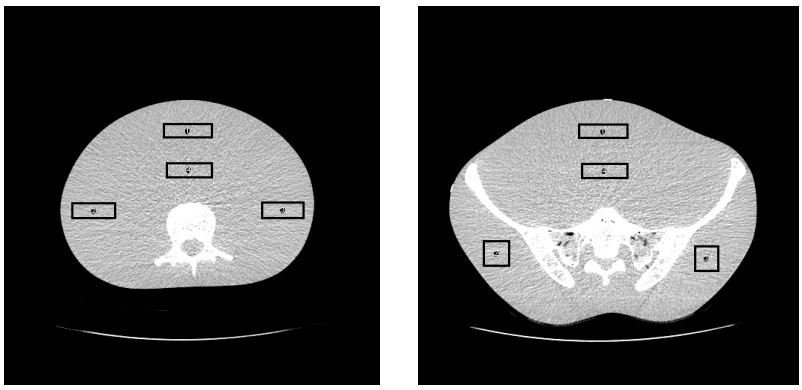

(a) (b)

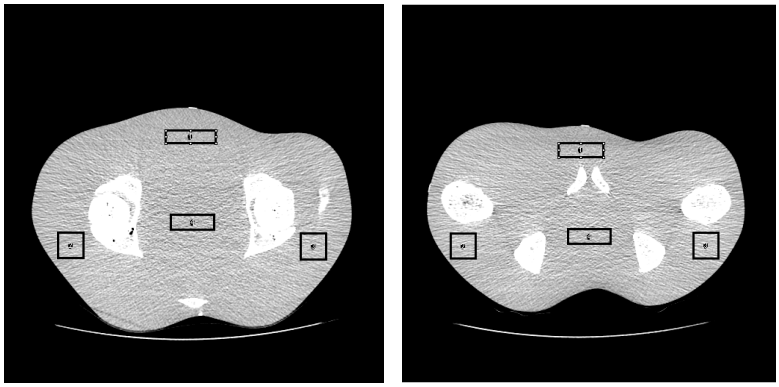

(c) (d)

Figure 6-3 Cross sectional view showing ROI placements throughout the abdomen-pelvis phantom, which were measured (a) between the beginning of the phantom and the fourth lumbar spine, (b) over the level of pelvis bone, (c) over the level of the head of femur and (d) between the body of femur and the end of scan
(Note: Rectangular ROIs, rather than circle, was used to avoid the inclusion of components from two layer)

6.3 Results

6.3.1 Tube current modulation

The changes in tube current values, starting from the abdomen for the routine ATCM system settings of individual scanners and manufacturers are illustrated in figure 6-4. Tube currents for the routine protocols remained constant at their minimum settings of 50 mAs and 40 mAs for scanners T4 and T8 (figure 6-4a). Similarly tube currents for the GE scanners G1 and G3 remained constant at the minimum limits set of 100 mAs and 160 mAs respectively. The tube current for scanner G4 remained constant at the maximum value of 280 mAs over the pelvic region, while the tube current stayed constant at the minimum value of 64 mAs at the abdomen for scanner G2. Scanning protocols were modified by adjusting the ranges of tube currents to 5 mAs-220 mAs for scanner T4 and 25 mAs-325 mAs, and 40 mAs-352 mAs for scanners G1 and G3, respectively (table 6-1). These were to allow tube current to be modulated over the full ranges. The modulation of tube currents along the phantom lengths for the modified protocols gave lower values at the abdomen as expected (figures 6-4a and 6-4c for Toshiba and GE scanners).

For Siemens scanners with CareDose '4D' ATCM (scanners S2 and S4), tube currents were lower in the abdominal part of the phantom, but the degree of modulation was less than for the modified protocols on the Toshiba and GE scanners. The scanners S3 and S6, were equipped only with a patient size-ATCM (figure 6-4d) based on the SPR that did not modify the tube current during the scans. Thus the tube currents were fixed at 121 effective mAs and 141 effective mAs along the entire scan lengths

Levels of modulation were classified into three, 1) no modulation where the tube currents remained constant along the entire length of the phantom 2) partial modulation where the tube current was varied by the ATCM and 3) fully modulated where tube currents were modulated along the entire length. Data sets are marked as no modulation, partial modulated or fully modulated by superscripts 1, 2 and 3, respectively.

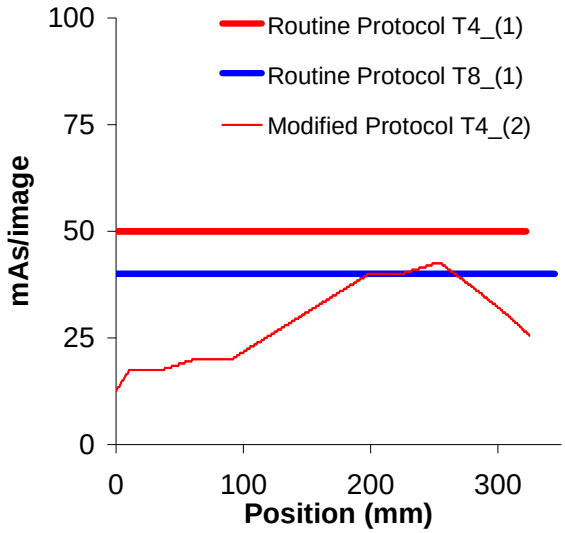

(a)

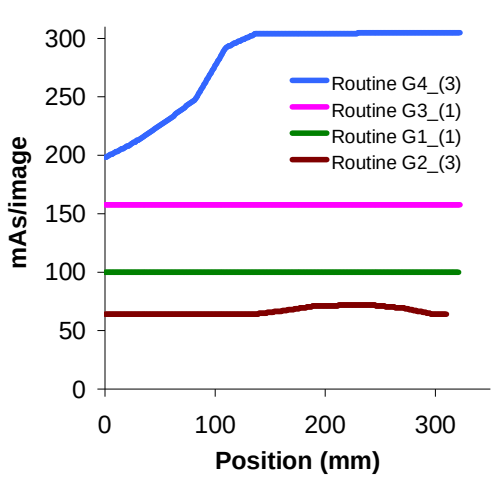

(b)

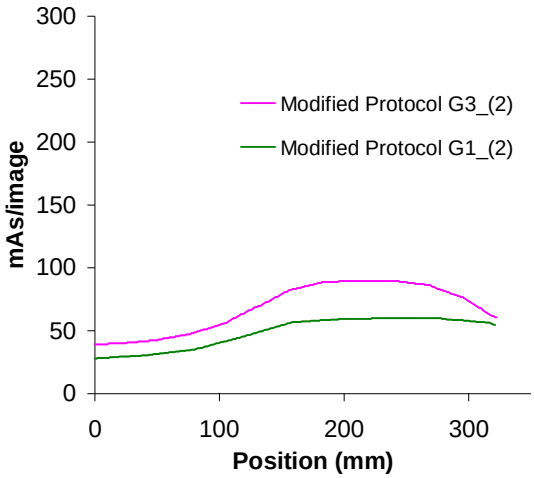

(c)

Figure 6-4 Comparisons of the mAs/image (Toshiba and GE scanners) and effective mAs/image (Siemens) values for (a) Toshiba scanners T4 and T8 (b, c) GE scanners and (d) Siemens scanners, the scan direction shown in figures started from abdomen to pelvis

N.B. (1) Protocols that tube currents were not modulated, (2) Protocols that tube currents were fully modulated, (3) Protocols that tube currents were partly modulated

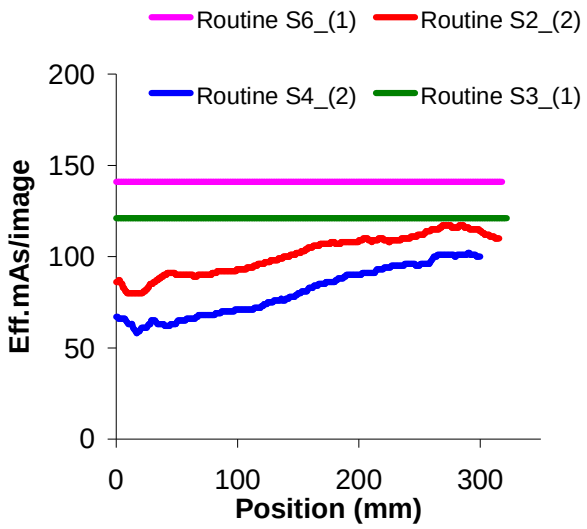

(d)

Figure 6-4 (Cont.) Comparisons of the mAs/image (Toshiba and GE scanners) and effective mAs/image (Siemens) values for (a) Toshiba scanners T4 and T8 (b, c) GE scanners and (d) Siemens scanners, the scan direction shown in figures started from abdomen to pelvis

N.B. (1) Protocols that tube currents were not modulated, (2) Protocols that tube currents were fully modulated, (3) Protocols that tube currents were partly modulated

6.3.2 Image Noise

Standard deviations of the CT number or image noise levels measured along the phantom length are shown in figure 6-5 and the absolute values are shown in table 6-2. For the Toshiba scanner T8 (figure 6-5a), the image noise increased with attenuation level along the phantom length. The absolute values obtained from the fixed tube current technique were lower since they were obtained from higher mAs values, but there were similar trends in the noise variation for both protocols because no tube current modulation occurred with the routine protocol of scanner T8. The noise patterns from the routine protocols of scanners T4 and T8 were similar with the noise level increasing from 10 HU in the abdomen to about 35 HU in the pelvis (figure 6-5b). When the minimum value of the tube current for the ATCM was reduced to 5 mAs for scanner T4 (or modified protocol), the image noise remained relatively constant and the variation of the noise level was 12% along the

length of the phantom. However, the absolute noise value appoximately doubled the target value.

For the GE scanners, higher NI values of 28 and 25 were set for scanners G1 and G3, but the minimum tube current settings were higher than the values required for this noise level. This resulted in the tube currents remaining at the minimum values along the whole length of the scan as shown earlier and therefore the image noise increased from the abdomen to the pelvic regions. Reductions in the minimum tube currents for scanners G1 and G3 resulted in less variations of the noise (11.2%) compared with the routine settings (21%-22%) (figure 6-5c), the absolute noise levels were higher because of the lower tube currents but close to their target NIs. The NI values set for scanners G2 and G4 were 14 and 11.57. The low NI setting for scanner G4 coupled with selection of a lower maximum tube current resulted in saturation of the tube current at the maximum value for the most attenuating part of the phantom (figure 6-4b), although this was still substantially lower than results for other scanners (figure 6-5d). In contrast to scanner G4, the slightly higher NI setting for scanner G2, which was coupled with a high minimum tube current, resulted in the tube current remaining the same at the minimum value for the less attenuating part of the scan (figure 6-4b). The noise level for this scanner was substantially greater along the whole length of the phantom (figure 6-5d).

Siemens scanners S2 and S4 were equipped with CareDose 4D, while the scanners S3 and S6 were equipped with CareDose using fixed tube currents for the entire phantom length. The noise levels for scanners S2 and S4 were between 12 HU and 20 HU, and for scanners S6 and S3 were between 7 HU and 15 HU (figure 6-5e). The lower noise levels of scanners S6 and S3 were achieved with higher average tube currents (figure 6-4d). The noise patterns with the CareDose4D and the fixed tube current techniques were similar, the noise levels increasing slightly from the abdomen to pelvis and decreasing after the pelvis bone (figure 6-5f). The variations in the image noise for the CareDose4D and for the fixed tube current techniques were 16% and 17%-18%, respectively (table 6-2).

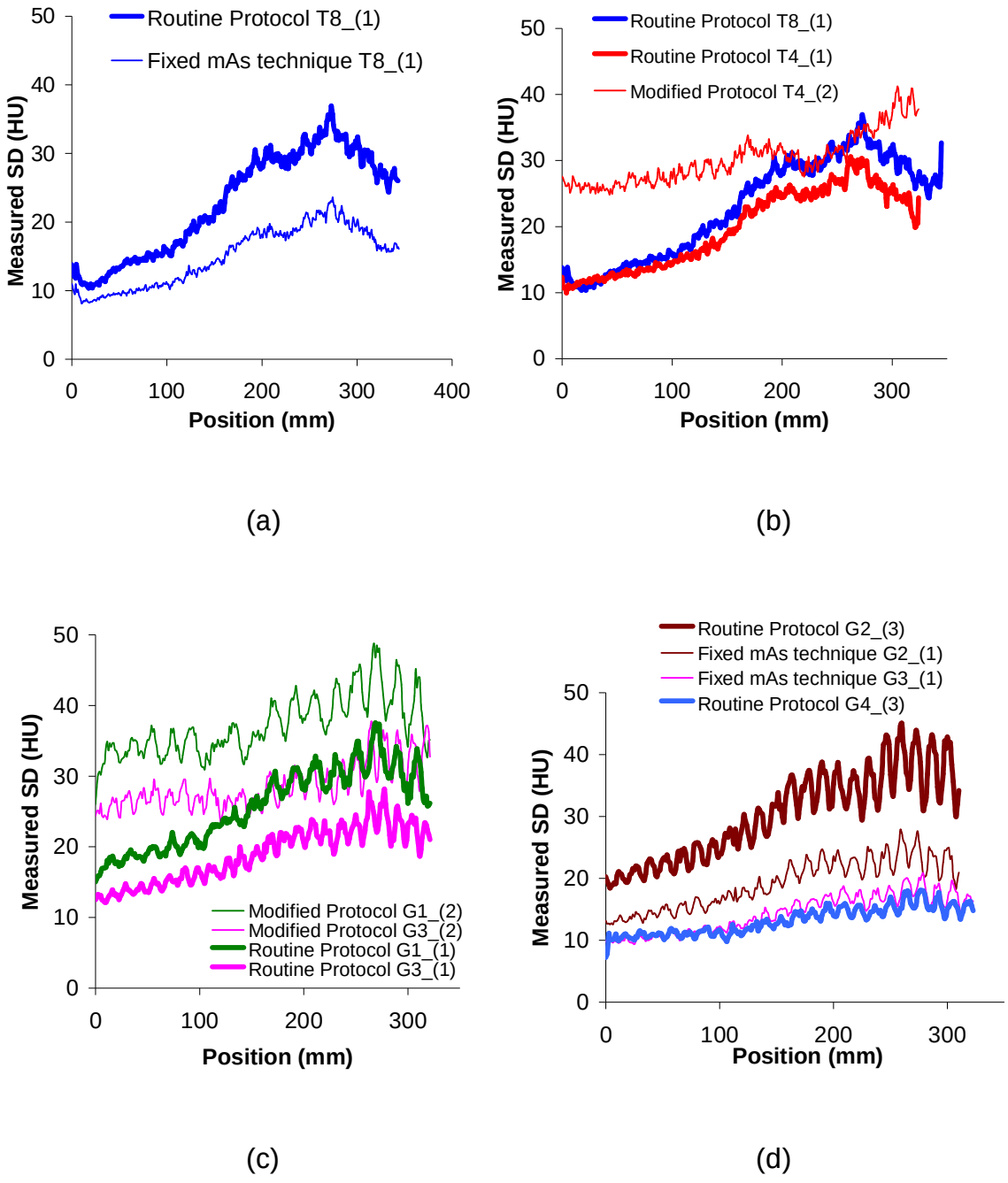

Figure 6-5 Comparisons of image noise throughout the phantom length for (a-b) Toshiba, (c-d) GE and (e-f) Siemens scanners, the scan direction shown in figures started from abdomen to pelvis

N.B. (1) Protocols that tube currents were not modulated, (2) Protocols that tube currents were fully modulated, (3) Protocols that tube currents were partly modulated

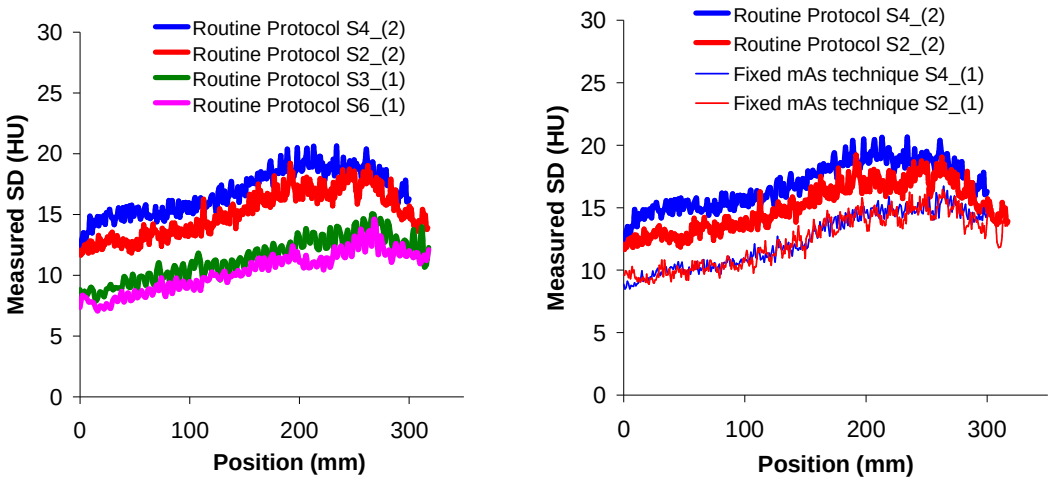

(e)

(f)

Figure 6-5 (Cont.) Comparisons of image noise throughout the phantom length for (a-b) Toshiba, (c-d) GE and (e-f) Siemens scanners, the scan direction shown in figures started from abdomen to pelvis

N.B. (1) Protocols that tube currents were not modulated, (2) Protocols that tube currents were fully modulated, (3) Protocols that tube currents were partly modulated

The absolute noise values depend on the average tube current being used. The image noise levels measured near the anterior of the phantom (figure 6-3) were lower than those measured at the lateral positions and centre because the smaller body thickness in the antero-posterior direction resulted in higher photon fluence (table 6-2).

For scanners T4, G1 and G3 (figures 6-5b and 6-5c and table 6-2), the variations in image noise were 21%-30% for the routine protocols. However, when the tube currents were fully modulated by the ATCM the variations in image noise were 11%-12% compared to 15%-16% for the Siemens scanner with full modulation. The absolute noise level for full modulation for scanner T4 of 30.6 was double the target noise of 12.5, while those for scanners G1 and G3 were close to the target NI with slightly higher values for scanner G1.

Table 6-2 Image noise levels measured at the abdominal and pelvis parts and the average values for the whole phantom
(Note: [1] Protocols that tube currents were not modulated, [2] Protocols that tube currents were fully modulated, [3] Protocols that tube currents were partly modulated)

Code	Setting	Measured SD (HU): Abdominal Part			Measured SD (HU): Pelvis Part			Measured SD (HU): Whole phantom	
		Ant	LAT	Centre	Ant	LAT	Centre	Mean	%CV
T4	Routine Protocol[1]	10.7	13.7	13.7	15.3	26.9	25.1	19.8	30.4
	Reduce min mA[2]	23.2	29.4	29.5	20.8	37.1	33.7	30.6	12.3
T8	Fixed mA[1]	7.3	10.8	10.6	11.5	19.8	19.4	15.0	28.8
	Routine Protocol[1]	10.1	14.9	14.8	16.9	31.7	30.0	22.9	33.1
G1	Routine Protocol[1]	16.8	19.4	21.9	22.1	30.7	33.1	25.6	21.6
	Reduce min mA[2]	29.0	34.1	37.4	29.0	42	43.5	37.2	11.2
G3	Routine Protocol[1]	12.5	14.7	16.6	17.0	21.8	24.6	18.9	20.7
	Reduce min mA[2]	22.7	26.7	30.1	22.8	31.2	33.8	28.6	11.2
G2	Fixed mA[1]	13.3	15.3	18.0	16.6	23.5	26.0	19.2	20.7
	Routine Protocol[3]	20.0	24.3	26.6	24.3	39.5	40.6	30.3	23.4

Table 6-2 (Cont.) Image noise levels measured at the abdominal and pelvis parts and the average values for the whole phantom
(Note: [1] Protocols that tube currents were not modulated, [2] Protocols that tube currents were fully modulated, [3] Protocols that tube currents were partly modulated)

Code	Setting	Measured SD (HU): Abdominal Part			Measured SD (HU): Pelvis Part			Measured SD (HU): Whole phantom	
		Ant	LAT	Centre	Ant	LAT	Centre	Mean	%CV
G4	Fixed mA[1]	9.1	11	12.5	12.8	17	18.4	14.3	21.5
	Routine Protocol[3]	9.2	10.9	12.4	11.6	15	16.4	13.2	16.9
S2	Fixed mA[1]	8.8	10.1	11.2	12.0	13.8	15.6	12.4	17.0
	Routine Protocol[2]	12.2	12.5	15.1	14.9	15.8	18.5	15.1	15.5
S3	Fixed mA[1]	9.7	10.2	10.9	9.9	10.2	12.3	10.3	13.5
	Routine Protocol[1] (CareDose)	11.0	11.2	11.9	12.1	11.8	13.5	11.4	15.3
S4	Fixed mA[1]	8.4	10.6	10.9	11.4	14.6	15.2	12.5	17.7
	Routine Protocol[2]	13.4	15.1	16.4	16.1	18.3	19.7	16.9	15.9
S6	Fixed mA[1]	7.2	8.5	9.0	9.2	10.7	11.4	9.7	14.0
	Routine Protocol[1] (CareDose)	7.9	8.4	9.4	10.5	11.3	12.4	10.3	16.2

6.3.3 ESAK and Dose reduction

ESAK profiles obtained from the scan presented a sinusoidal dose variation pattern related to helical scanning as shown in figure 6-6, while the absolute values are shown in table 6-3, the tail part of the curve was not included in the average measurement. The degree of periodic variation is determined by the relative values for the beam width at the phantom surface and the distance moved per rotation, it was 27 mm/rotation for scanner S2 (figure 6-6a). Figure 6-6a shows ESAK profiles at the anterior and lateral surfaces obtained from the routine protocol of scanner S2, the amplitude of the wave varies from one peak to another because of the tube current adjustment. Figure 6-6b shows the same profiles that have been smoothed by averaging the ESAK values over 27 mm in order to show the overall trend in dose variation more clearly.

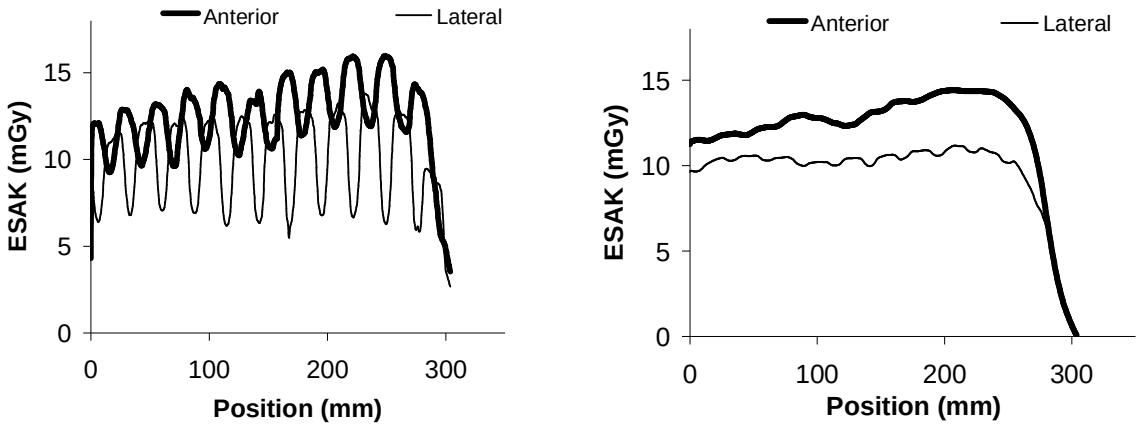

(a) (b)

Figure 6-6 (a) ESAK profiles at the anterior and right lateral surfaces of the phantom, measured from the routine protocol, Siemens scanner S2 and (b) the smoothed profiles

Smoothed ESAK profiles for some CT scanners are shown in figure 6-7. The pattern of ESAK profile was similar for the Toshiba and GE scanners (figures 6-7a to 6-7c) and the Siemens scanner (figures 6-7d and 6-7e). The EASK increased with the effective phantom diameter and phantom attenuation, while those for the fixed tube current technique decreased, the reason for this has been explained in section 5.4.3, chapter 5. The pattern of ESAK profiles with protocols for the Toshiba and GE

scanners where the ATCM was not activated were similar to fixed tube current techniques (figure 6-7b). The ESAK profiles for CareDose4D and the fixed effective mAs techniques were similar for Siemens scanners S2 and S4, but the ESAK profiles were close together for the CareDose4D, compared with the fixed effective mAs techniques (figure 6-7d). The absolute values of ESAK depended on the tube currents being used for each scan.

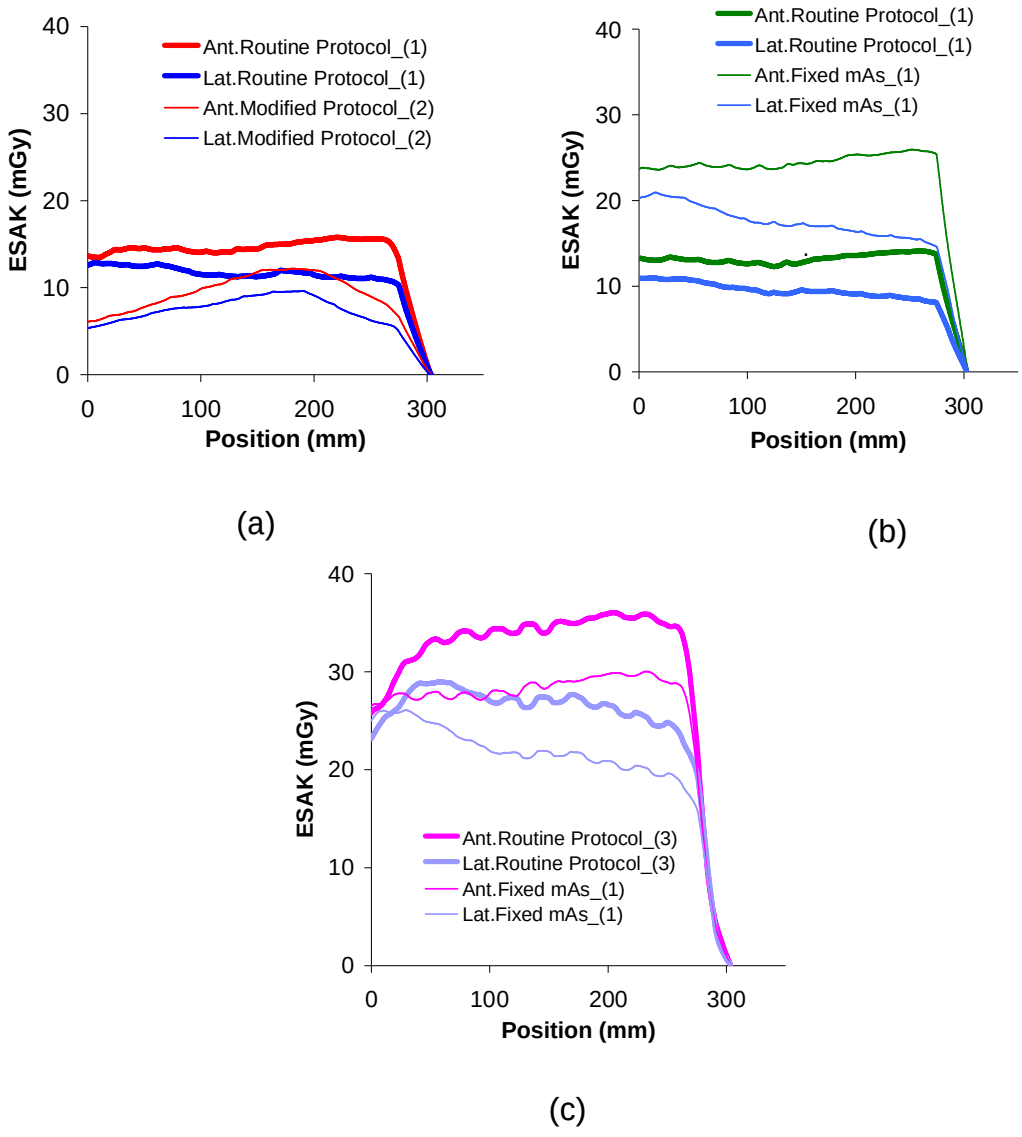

Figure 6-7 Smoothed ESAK profiles at the anterior and lateral surfaces of the phantom, measured from the routine and modified protocols and the fixed tube current technique for scanners (a) T4, (b) T8, (c) G4, (d) S2 and (e) S3, the scan direction shown in figures started from abdomen to pelvis

N.B. (1) Protocols that tube currents were not modulated, (2) Protocols that tube currents were fully modulated, (3) Protocols that tube currents were partly modulated

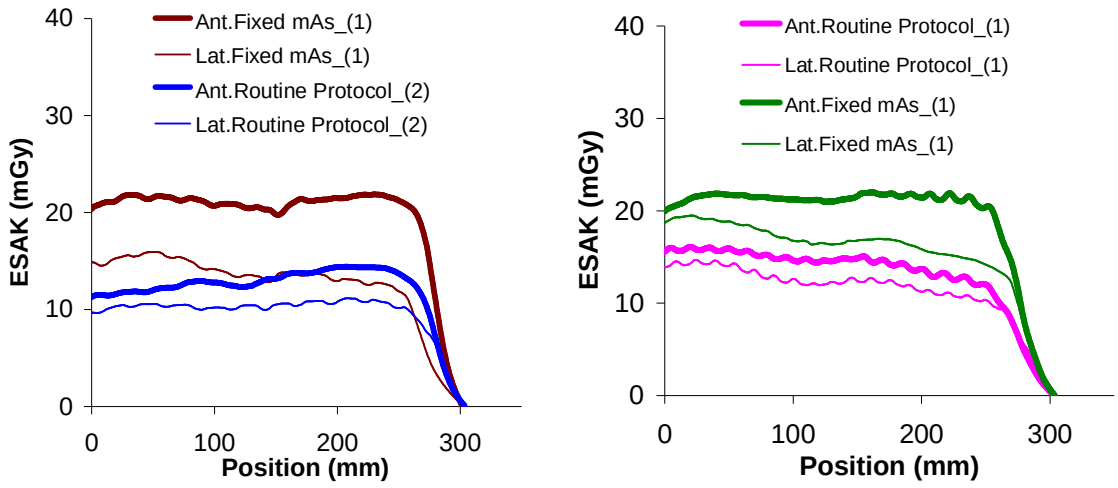

(d) (e)

Figure 6-7 (Cont.) Smoothed ESAK profiles at the anterior and lateral surfaces of the phantom, measured from the routine and modified protocols and the fixed tube current technique for scanners (a) T4, (b) T8, (c) G4, (d) S2 and (e) S3, the scan direction shown in figures started from abdomen to pelvis

N.B. (1) Protocols that tube currents were not modulated, (2) Protocols that tube currents were fully modulated, (3) Protocols that tube currents were partly modulated

The dose parameters averaged over the length of scan are shown in table 6-3. The values from the fixed tube current techniques and the routine protocols that essentially acted as fixed tube current techniques were higher than those from the ATCM systems. Reductions in DLP and ESAK values of 46%-51% were found for the Toshiba scanner T8 and GE scanner G2. However, for scanner G4 the DLP and ESAK values increased by 16% and 23% respectively. This is because the tube currents used for the fixed tube current technique was lower than the routine protocol using the low NI. The adjusted protocols for scanners T4, G1 and G3 when the minimum tube currents settings were reduced were significantly lower than the corresponding routine protocols (table 6-3).

For the Siemens scanners, the differences in dose between the fixed tube currents technique and the routine protocols varied with the fixed tube current settings used by different scanners, but the percentages differences in DLP and ESAK values between the two techniques were similar.

Table 6-3 Tube currents, DLP, $CTDI_{vol}$ and measured ESAK values at the anterior and lateral surfaces of the phantom
(Note: [1]Protocols that tube currents were not modulated, [2]Protocols that tube currents were fully modulated, [3]Protocols that tube currents were partly modulated)

Scanner	Setting	Mean Tube currents (mAs)	Effective mAs*	DLP (mGy.cm)	DLP Reduction **	$CTDI_{vol}$ (mGy)	ESAK (mGy)***		ESAK Reduction**	
							Ant	Lat	Ant	Lat
T4	Routine Protocol[1]	50	60	240		7.2	14.4	11.6		
	Reduce min mA[2]	30	36	143	40%	6.1	9.5	7.5	34%	35%
T8	Fixed mA[1]	75	91	435		10.8	24.2	17.5		
	Routine Protocol[1]	40	49	235	46%	6.8	13.1	9.5	46%	46%
G1	Routine Protocol[1]	100	102	308		8.4	17.3	14.7		
	Reduce min mA[2]	49	50	146	53%	4.0	9.3	7.7	46%	48%
G3	Routine Protocol[1]	160	116	375		10.8	19.3	14.5		
	Reduce min mA[2]	69	50	161	57%	4.6	9.9	7.2	49%	50%
G2	Fixed mA[1]	140	102	328		9.51	17.7	13.4		
	Routine Protocol[3]	67	49	154	53%	4.5	8.6	6.8	51%	49%
G4	Fixed mA[1]	240	175	566		16.2	27.7	22.2		
	Routine Protocol[3]	279	203	659	Increase 16%	18.7	34.2	27.2	+23%	+23%

Table 6-3 (Cont.) Tube currents, DLP, $CTDI_{vol}$ and measured ESAK values at the anterior and lateral surfaces of the phantom

(Note: [1] Protocols that tube currents were not modulated, [2] Protocols that tube currents were fully modulated, [3] Protocols that tube currents were partly modulated)

Scanner	Setting	Mean Tube currents (mAs)	Effective mAs*	DLP (mGy.cm)	DLP Reduction**	$CTDI_{vol}$ (mGy)	ESAK (mGy)***		ESAK Reduction**	
							Ant	Lat	Ant	Lat
S2	Fixed mA[1]	-	160	441		12.3	20.9	13.9		
	Routine Protocol[2]	-	102	274	38%	7.6	12.7	10.3	39%	26%
S3	Fixed mA[1]	-	165	436		12.5	20.5	17.2		
	Routine Protocol[1] (CareDose)	-	121	324	26%	9.12	15.2	12.8	26%	26%
S4	Fixed mA[1]	-	150	357		11.4	23.6	16.5		
	Routine Protocol[2]	-	82	181	49%	5.8	11.9	9.8	50%	41%
S6	Fixed mA[1]	-	165	428		12.5	20.3	17.5		
	Routine Protocol[1] (CareDose)	-	141	378	12%	10.8	17.8	15.9	12%	9%

* For Toshiba and GE scanners, there were calculated from the average mAs/rotation divided by pitch factor
**Compared with the fixed tube current techniques of individual scanners or routine protocols in cases of not modulate
*** The tail part of the curve in figure 6-7 was not included in the average measurement

6.4 Discussion

For a conventional CT examination, the tube current in a fixed mAs technique is normally selected to generate good quality images based on the region with the highest attenuation for the average patient size. Therefore smaller patients may be exposed to unnecessarily high doses, while the images for larger patients are of lower quality if the same protocol is used. With the ATCM system, the tube current values are adjusted automatically with patient attenuation. If ATCM systems are deployed correctly, they should give consistent image quality with reasonable patient dose reduction. In this study, the tube current modulations, patient ESAK and image quality in terms of noise were measured for routine protocols for ten CT scanners used to scan an anatomical phantom representing a small adult.

Sub-optimal protocols are currently in use on a number of CT scanners. The results from this study could serve as a lessons learned to CT users with an interest in the design, audit and development of CT scanner protocols. The study highlighted the importance of proper selection of the appropriate image quality level. It emphasized that the image noise can be different from that specified if the user does not pay attention to a regular system audit and protocol harmonisation.

6.4.1 Tube current modulation

The tube currents for all Toshiba scanners and GE scanners G1 and G3 remained constant even though the ATCM systems were activated. This is because the tube currents are only modulated within the ranges defined by the minimum and maximum tube current values set for the users. Thus, setting too high a value for the minimum tube current prevents reduction beyond the limit for the low attenuation regions and setting too low a maximum tube current value, in the same way, prevents the tube current from rising further for the higher attenuation parts. The minimum tube current settings for scanners T4 (50 mAs), T8 (40 mAs), G1 (100 mAs) and G3 (160 mAs) were higher than the tube currents required to give the selected image quality for the most attenuating part. This resulted in constant tube current levels along the entire phantom (figures 6-4a and 6-4b). Thus the tube currents on these scanners will saturate for small

patients. For scanner G2, the tube current remained constant over the abdominal or lower attenuating part of the phantom, because the minimum tube current was set too high, but increased at the pelvis or the higher attenuating part. For scanner G4, however, the tube current was lower over the abdomen but remained constant throughout the pelvis because the maximum tube current level was set was too low to allow the noise to decrease to the target NI. For an average size of patient which would be larger than the phantom used in this study, this would result in a fixed mAs technique and the noise being higher than required. When the minimum tube current settings were reduced, tube current modulation occurred over the entire scans (figures 6-4a and 6-4c). There is no option for the user to set the range of the tube current for Siemens scanners, in contrast to the Toshiba and GE ones. Tube currents used for all Siemens scanners depend on the QRM, which is installed by the application specialist and generally not adjusted by the user. Tube currents for scanner S2 were higher than those for scanner S4 because a higher reference mAs setting was selected (table 6-1). The tube currents were modulated in a narrower range for the scanners S2 and S4, compared with those for the modified protocols for the scanners T4, G1 and G3. This relates to the designs of the Toshiba SureExposure 3D and GE Auto mA ATCM systems. These manufacturers claim that the systems maintain the uniformity of image quality between different anatomic regions (Angel 2009, Bruesewitz *et al.,* 2008). For the Siemens CareDose4D, the tube current reductions for small patients and increases for large patients were less than was required to achieve the same image noise level (Flohr 2013).

6.4.2 Image noise

The Toshiba and GE scanner ATCM systems allow users to set the target noise for the image. They were able to maintain a constant noise level along the whole length of the phantom for scanners T4, G1 and G3 once the tube currents were fully modulated (figures 6-5b and 6-5c), as verified by the lower coefficients of variation (CV) (table 6-2). Moreover, the image noise levels were similar to the targeted NIs for scanners G1 and G3. This is especially true for the measured image noise levels at the anterior. The image noise measured at the lateral and centre were substantially higher than at the anterior. This can be explained as the x-ray beam is attenuated from the periphery to the centre of the phantom. There is an increasing reduction in relative photon fluence and therefore

increase in image noise. Although the tube current at the lateral axis was higher than that at the AP, the noise level in the lateral region was higher than those in the AP, this may due to the greater attenuation across the lateral axis.

When the range of tube currents was properly adjusted for the target noise selected, the image noise for scanner T4 increased to 30.6, which was higher than the target noise of 12.5. This difference occurred because the target noise level for Toshiba and GE scanners is related to slice thickness for the first reconstruction and this may not be the same as the image data set stored on the PACS. For scanner T4, the thickness of the first reconstruction was set at 5 mm but the volume reconstruction was for an image thickness of 0.8 mm and this was saved to PACS. The image noise for the 0.8 mm image thick slice is greater than that of the 5 mm thickness by $\sqrt{5/0.8}$ or 2.5. The image noise levels for the original reconstruction setting would be 7.9 HU, and 12.2 HU for the original routine and the adjusted protocols, respectively. A similar explanation can be applied for scanner G2, the image thickness for the first reconstruction is 5 mm (NI 14) but 1.25 mm thick images were sent to PACS and used to measure the image noise levels (table 6-2).

For GE scanners, as explained earlier, a lower NI setting requires a higher maximum tube current to achieve the full current modulation. A NI of 11.57 was set for scanner G4 but the maximum tube current setting was 280 mAs (350 mA) and this was slightly too low to achieve the target noise level for the higher attenuation regions. This resulted in a constant tube current for the pelvis section of the phantom (figure 6-4b) and the average image noise measured over the pelvis was about 14.5 (table 6-2), slightly higher than the target noise . The average noise for the three positions measured in the abdominal part of the phantom where the tube current was fully modulated was 10.8 (table 6-2). In contrast to scanners G2 and G4, significantly higher NI values of 28 and 25 were set for scanners G1 and G3. For G1 and G3 the minimum tube current values were 100 mAs and 160 mAs, respectively, which were too high to give the chosen noise level. The net result was that the scanner operated in a constant tube current mode along the entire length of the phantom, giving lower noise levels than those selected (25.6 and 18.9, from table 6-2). The NI should be selected based on the clinical experience of the radiologists. These high minimum tube current settings may give the radiologists a false indication of the image quality

associated with the NI 28 and 25 values. Thus the radiologists could make decisions on required image quality requirements based on misleading information. It is therefore recommended that a series of scans of an anatomical or other suitable phantom are made with different target noise settings and a full range of tube currents to allow radiologists to determine the level acceptable for clinical images at commissioning.

Variations in image noise between the fixed tube current techniques and CareDose 4D ATCM systems measured from scanners S2 and S4 were similar (figure 6-5f, table 6-2). Unlike the Toshiba and GE scanner ATCM systems, the approach for the Siemens system changes the level of noise for different patient sizes. Therefore, the range of the tube current used for the Siemens scanner was narrower than that for the Toshiba and GE. The pattern of tube current modulation for Siemens scanners does not differ as significantly from the fixed tube current technique for the range of attenuations within a small patient.

6.4.3 Dose reduction

There have been many studies of the dose reduction from ATCM systems compared with the fixed tube current operation. In this study the ESAK and DLP values were significantly reduced once the ATCM systems were fully operational. The results showed 38%-57% DLP reductions for ATCM similar to reports from Soderberg & Gunnarsson (2010) and Gutierrez *et al* (2007) that found the dose reductions of 35%-60% in anthropomorphic chest phantoms. The report by Papadakis *et al* (2008) shows 52% and 57% in tube current value reductions for an abdomen and pelvis phantom scan in a Siemens CareDose4D scanner, when SPRs of the AP and lateral directions were selected, respectively. This study found reductions DLPs in the range 38%-49% (table 6-3) for scanners S2, S3 and S4. However, these also depended on the value of tube current selected by radiographers, and these studies have been performed on patients of average size.

From the results of the GE scanners G1 and G3, when the minimum tube currents values were reduced the ATCM system worked more effectively, ESAKs dropped by 46%-50%, and the DLP dropped by 53%-57%. When the range of the tube currents selected was not appropriate for the NI value selected, this resulted in 16% higher DLP and 23% higher ESAK values, compared with the fixed tube current technique as shown for scanner G4 (table 6-3).

For all CT scanners, when the ATCM is implemented and the tube currents fully modulated there were substantial reductions in average tube current and DLP. The percentage reductions depended on the original values selected in the routine protocols. The percentage reductions in the tube current and DLP were similar, while the reductions in ESAK values were slightly lower than those for DLP (table 6-3). The differences may arise because the DLP is calculated from the average tube current along the whole scan, whereas the ESAKs were measured along a 300 mm region in the middle part of the phantom. The percent reductions in ESAK were similar between the AP and lateral directions for Toshiba and GE scanners. However, the reductions for the AP direction were higher than for the lateral direction for Siemens scanners S2 and S4. This may relate to the different way in which the tube current is modulated by the Siemens scanners, as the degree of modulation is different for the AP and lateral directions.

6.4.4 Limitation of study

This study highlighted the optimisation strategy focusing on the optimum selection of minimum and maximum mAs values to allow full ATCM to achieve the specified image noise. However, full optimisation strategies need to consider other patient based factors tailored to specific diagnostic requirements. Typically, the image contrast for slim patients is reduced due to limited fat delineation in slim patients. Therefore it should be possible to accept a higher dose in very small patients by capping the minimum mA , as it is unnecessary to achieve full modulation to maintain image noise.

6.5 Conclusion

An abdomen-pelvis phantom was used to assess the tube current modulation and changes in image noise and ESAK levels. Results were used to evaluate the potential for dose reduction on different CT scanner ATCM systems, through changes in the routine scan protocols. For the Toshiba and GE scanners that allow users to select a target noise level and then set the minimum and maximum tube currents, the ranges selected affected the degree of tube current modulation that could be achieved. The values set for the minimum tube current in standard protocols tended to prevent full modulation for the less attenuating parts resulting in lower image noise levels in the abdomen part of the phantom. When lower minimum tube currents were set, the ATCM systems modulation occurred throughout the length of the phantom and resulted in lower ESAKs and DLPs, and more consistent image quality. For one scanner a lower target noise coupled with a low maximum tube current setting prevented full modulation in the pelvis region. In order to use the ATCM of scanner maintaining image noise levels, care is required in setting the minimum and maximum tube currents to meet the requirements for the range of patients and image quality required. The interdependence of the target noise and limiting current values may result in a false impression of the noise level associated with a target value. The results from Siemens scanners followed a different pattern with a narrower range of the tube current modulation selected automatically. Full modulation was achieved, but image noise increased to some extent with phantom attenuation. A full assessment based on phantom images should be undertaken with the radiologists at commissioning to establish acceptable noise levels for clinical images on all CT scanner. The comparison of scans on an anatomical phantom allowed effects relating to a variety of setting, especially the maximum and minimum currents to be identified which were of assistance in understanding patient dose results.

7 Relationships between patient size, dose and image noise: a retrospective study from patient CT images

7.1 Introduction

As stated in the background of this project, CT patient doses for CAP examinations were high for some CT scanners and patients. The reason for the high dose was uncertain, whether or not these high doses related to the size of the patient was unknown. Conclusion that can be drawn from dose data without patient size are limited. There have been a number of studies of relationships between patient size and radiation dose received under ATCM systems (Castellano, 2013; Israel *et al*., 2010; Meeson *et a*l., 2010; Zarb *et al*., 2010) and on the optimisation of image noise and dose as a function of patient size (Siegel *et al*., 2004; Verdun *et al.*, 2004; Li *et al*., 2012), as explained in chapter 2. Patient size indicators including patient weight, height, body mass index (BMI), circumference, cross sectional diameter and cross sectional area have been used for these studies.

During the project while experiments on phantoms were being carried out, studies were undertaken at patient scans in order to assess the interrelationships between ATCM dose and image noise for patient examinations. Patient cross sectional areas were used for this study since they provide good estimates of patient size for study of the relationship with $CTDI_{vol}$ and DLP (AAPM Task group, 2011; Meeson *et al.*, 2010; Zarb *et al.*, 2010). Moreover they can be easily measured from CT images, since this study is a retrospective study and the patient weight and height are not available. There have been a number of studies evaluating relationships between radiation dose and image noise in phantoms or patients of different size in single CT scanners (Meeson *et al.*, 2010; Schindera *et al.*, 2008; Siegel *et al*., 2004). But none have investigated and compared these relationships for studies on patients with CT scanners from different manufacturers.

In this chapter, relationships between, CT dose parameters ($CTDI_{vol}$ and DLP), image quality (noise) and patient cross sectional area in different CT scanners

and manufacturers have been evaluated. The reasons why doses for patients on certain scanners were high have been investigated and changes that might be implemented to minimize the higher doses while maintaining an acceptable level of image quality have been determined to achieve optimisation of protection. The information from this chapter has been linked to results using phantoms to evaluate scanner ATCM performance. The main findings from this study have been published and are available from Sookpeng *et al*., 2014.

7.2 Materials and Methods

7.2.1 Materials

7.2.1.1 Patient data and dose data

West of Scotland Research Ethics Service (WoSRES) classified this study as an audit and did not require ethical review or approval, a letter was obtained confirming the status of critical data analysis (Appendix III). A survey of patient dose received from CT CAP examinations on 17 CT scanners was carried out. Radiographers were asked to complete a dose survey form using the data from 30 individual patients having CT CAP examinations. The data consist of $CTDI_{vol}$ and DLP received by individual patients and the patient accession number.

7.2.1.2 CT scanners and ATCM systems

The 17 CT scanners were from four different CT manufacturers; Toshiba (6 scanners), Philips, (4 scanners), Siemens (5 scanners) and GE (2 scanners). Details of the CT scanners and their routine CAP protocols are shown in table 7-1. All scanners were equipped with ATCM systems except scanner S3 that used a fixed tube current technique. For the Philips scanners, there are two types of the tube current modulation system, Z-DOM and D-DOM, the Z-DOM was used for scanners P1, P2 and P3 and the D-DOM was used for scanner P4. Scanner P3 is equipped with the latest software version and iterative reconstruction (iDose). The quantum denoising software (QDS) was used for all Toshiba scanners except scanner T5 which was equipped with the iterative reconstruction facility (Adaptive Iterative Dose Reduction: AIDR). There were two target noise settings for scanner T5; SD=9.2 and SD=11.50.

There were 2 data sets for scanner T2, the first data set was collected from patients who have normal body sizes as judged by radiographers, while the second data set was collected from patients of any size who were given CAP scans over the period for collecting data. Codes T2 and T2** refer to the first and second data sets, respectively.

Typically, scan lengths were between upper edge of the lungs and the symphysis pubis. The scans were separated into 2 sequences for scanners T1, T2, S1 and S5. In these scanners, the first sequence was the thorax scan and the second sequence was the abdomen and pelvis scan.

Table 7-1 Details of CT scanners and the routine CAP protocol

Code	Manufacturer/ Model	kVp	ATCM setting	Rotation time (s)	Beam width (mm)	Pitch	Start Position	Stop Position	Kernel (Recon.)	Image Thickness For first recon[a]
T1	Toshiba Aquilion 64	120	SD=12.5 SD=10	0.5	32x1	0.844	Lung Apices Above Diaphragm	Lung Base Symphysis pubis	FC17	5 mm (PACs 5 mm, 1 mm)
T2	Toshiba Aquilion 64	120	SD=15.0 SD=12.5	0.5	32x1	0.844	Lung Apices Top of Liver	Lung Base Lesser Trochanters	FC03 FC03	1 mm (PACs 1 mm)
T3	Toshiba Aquilion 64	120	SD=13.5	0.5	64x0.5	0.828	Sternal Notch	Symphysis pubis	FC03	5 mm (PACs 1 mm)
T4	Toshiba Aquilion 64	120	SD=12.5	0.5	32x1	0.844	Lung Apices	Symphysis pubis	FC11	1 mm (PACs 0.8 mm)
T5	Aquilion CXL	120	SD=9.2 SD=11.50	0.5	32x1	0.844	Lung Apices	Symphysis pubis	FC07 (AIDR 3D)	1 mm (PACs 1 mm)
T6	Toshiba Aquilion 64	120	SD=12.5	0.5	64x0.5	0.828	Lung Apices	Symphysis pubis	FC03	1 mm (PACs 1 mm)

[a] Data saved to PACs in brakets

Table 7-1 (Cont.) Details of CT scanners and the routine CAP protocol

Code	Manufacturer/ Model	kVp	ATCM setting	Rotation time (s)	Beam width (mm)	Pitch	Start Position	Stop Position	Kernel (Recon.)	Image Thickness For first recon
G1	GE Lightspeed VCT 64	120	Auto mA NI=28 mAs= 100-325	0.5	32x1.25	0.984	Apices	Symphysis pubis	Chest	1.25 mm
G2	GE LightSpeed 16	120	Auto mA NI = 12.73 mAs=64-352	0.8	16x1.25	1.75	Apices	Symphysis pubis	Standard	1.25 mm
P1	Philips Brilliance 64	120	Z DOM	0.75	64x0.625	0.797	Just Above Apices	Symphysis pubis	B	2 mm
P2	Philips Brilliance 64	120	Z DOM	0.75	64x0.625	0.797	Just Above Apices	Symphysis pubis	B	2 mm
P3	Philips Ingenuity 64	120	Z DOM	0.75	64x0.625	0.797	Top of shoulder	Symphysis pubis	B iDose4	1.5 mm
P4	Philips Brilliance 64	120	D DOM	0.75	64x0.625	0.908	Apices	Symphysis pubis	B	2 mm

Table 7-1 (Cont.) Details of CT scanners and the routine CAP protocol

Code	Manufacturer/ Model	kVp	ATCM setting	Rotation time (s)	Beam width (mm)	Pitch	Start Position	Stop Position	Kernel (Recon.)	Image Thickness For first recon
S1	Siemens Somatom Sensation 64	120	QRM 140 Eff.mAs	0.5	64X0.6	1.4	Lung Apices	Bottom of liver	B20f	1 mm
		120	QRM 160 Eff.mAs	0.5	64X0.6	1.4	Dome of Liver	Symphysis pubis	B20f	1 mm
S2	Siemens Somatom Sensation 64	120	QRM 150 Eff.mAs	0.5	64X0.6	1.4	Apices	Symphysis pubis	B20f	1 mm
S3	Siemens Somatom Sensation 4	120	165 with CareDose	0.5	4X2.5	1.25	Apices	Symphysis pubis	B30f	3 mm
S4	Siemens Definition AS	120	QRM 110 Eff.mAs	0.5	64X0.6	1.2	Apices	Symphysis pubis	B31f	1 mm
S5	Siemens Somatom Sensation 64	120	QRM 100 Eff.mAs	0.5	64X0.6	1.4	Lung Apices	Dome of Diaphragm	B20f	1 mm
			QRM 170 Eff.mAs	0.5		1.4	Diaphragm	Symphysis pubis	B20f	1 mm

7.2.2 Methods

CT images were accessed, using the patient accession number. First, the mAs per image (Toshiba and GE scanners) and effective mAs per image (Philips and Siemens scanners) values were read out. The DICOM files were then converted to 'Analyze' format images. The "Analyze' format consists of a header file (*.hdr) containing the raw binary data file (*.img) with all the header information, patient personal data and medical identification number removed. The patient cross sectional area and image noise were then measured.

Programs for drawing a contour of patient cross-section, and for image noise measurements were performed by Dr Maria del Rosario Lopez-Gonzalez. The programs were run on ImageJ. Patient $CTDI_{vol}$ and DLP and image noise were plotted against patient cross sectional area.

7.2.2.1 Measurement of tube current modulations

The mAs or effective mAs values were read out from the DICOM header using an "auto mA'' plugin. They were read out along the length of scan for patients who received the highest and lowest DLP values from each scanner, in order to see the ranges of values and patterns of modulations.

The attenuation varies substantially along the body, so the mAs and $CTDI_{vol}$ values displayed on the scanners represent averages. In order to allow dose levels in different parts of scan to be related to body size the average effective mAs values over the middle part of heart and liver were multiplied by the $CTDI_w$ values (mGy/mAs) for individual scanners to derive $CTDI_{vol}$ values for the heart and liver. The $CTDI_{vol}$ values for the heart and liver were then plotted against patient cross sectional area at the thorax and abdomen.

$CTDI_{vol}$ values displayed on the CT scanners were also recorded. However, the displayed $CTDI_{vol}$ for the Toshiba scanner is calculated from the maximum tube current value set and so does not represent the actual tube currents used in the scan, while those for the other scanners are derived from the average tube current value for the entire length of scan. Therefore $CTDI_{vol}$ values for Toshiba

scanners were calculated from DLP values divided by irradiated length, for comparison with those for other scanners.

7.2.2.2 Measurement of patient cross sectional area

The contour of the patient cross section was measured using the written macro mentioned above and the area of the cross section was measured using the 'area measurement' command from ImageJ (Ferreira and Rasband, 2011). The slice at the level of the seventh thoracic vertebrae was used as the reference for the Thorax and the slice at the level of the twelfth thoracic vertebrae was used as the reference for the abdomen.

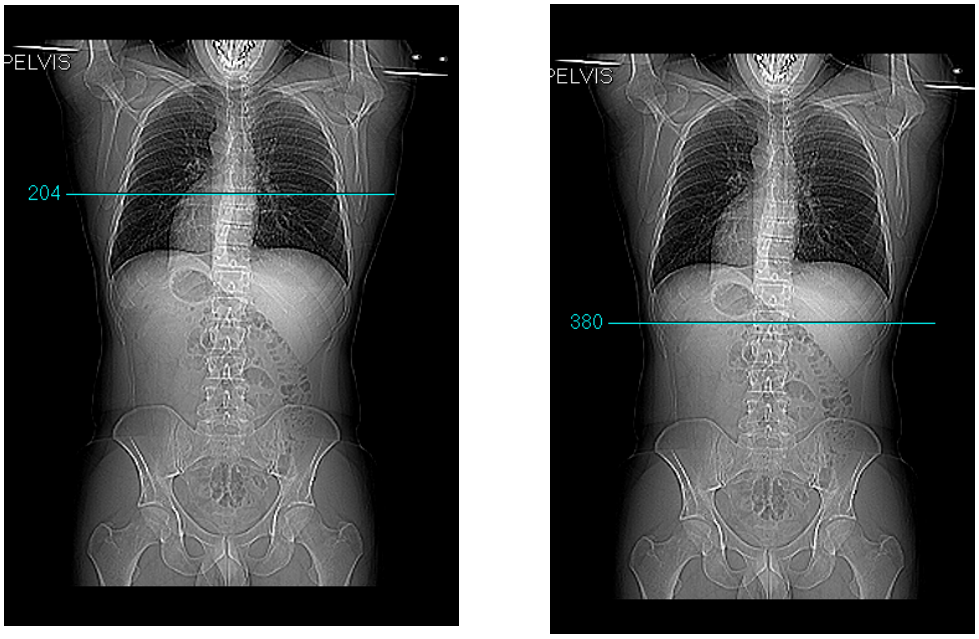

(a) (b)

Figure 7-1 Positions for measurement of patient cross sectional area at (a) thorax and (b) abdomen

7.2.2.3 Measurement of image noise across the CT image

Noise values were measured from CT images for individual patients within the heart and liver. The reason for selecting these organs is that they are relatively homogeneous and so the standard deviation in pixel values is unaffected by the presence of different types of tissue enabling measurement of noise levels relating to image quality. Where a scan was separated into two sequences, the

thorax and the abdomen-pelvis, the noise level in the heart was measured in the sequence for the thorax and that of the liver was measured in the scan sequence for the abdomen and pelvis.

The histogram of the CT number in Hounsfield Unit (HU) across the selected organ, which relates to the attenuation coefficient and is available on ImageJ, can be used for differentiation of the various tissues. The histogram of the CT number within the heart can be separated into three groups (figure 7-2); heart sac (pericardium and epicardium layers), heart septum (myocardium and ventricular septum), and heart cavity (chambers) which are referred to areas of a, b and c in figure 7-2. Three alternatives for assessment of image noise were analyzed, namely ROIs covering the whole heart, covering the heart cavity and interventricular septum, and covering only the heart cavity.

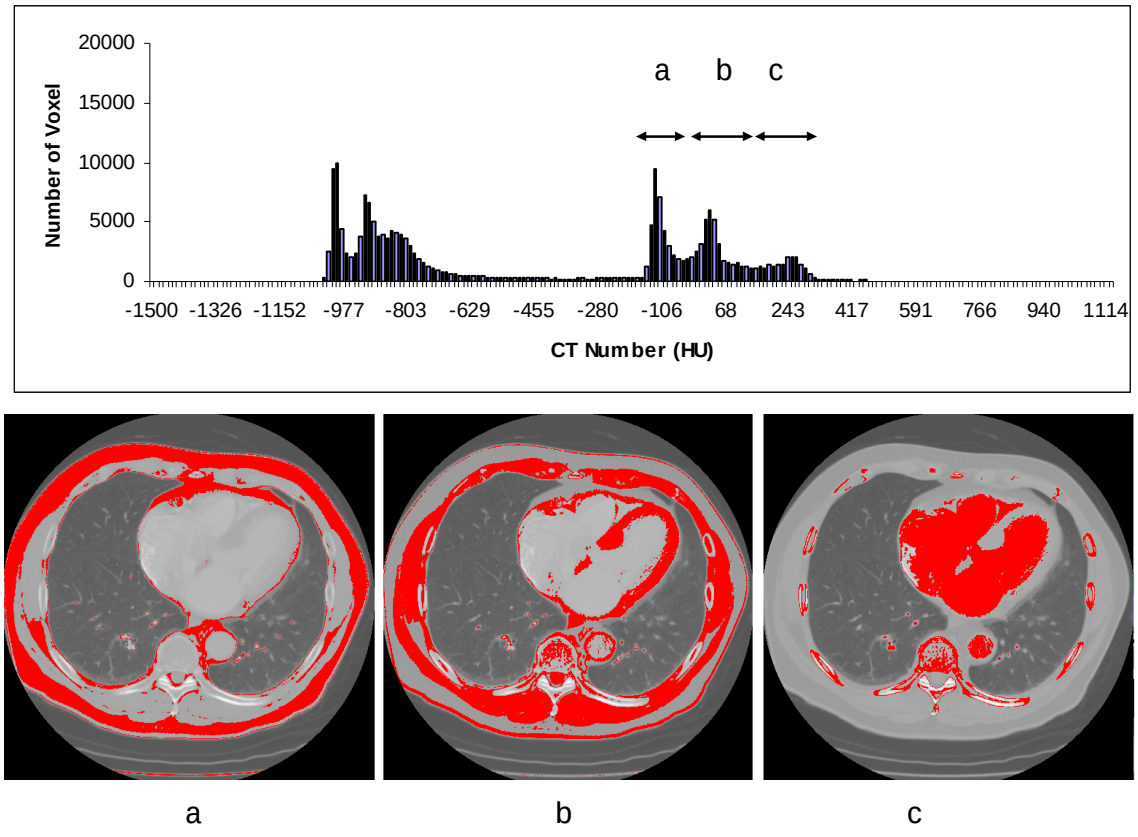

Figure 7-2 Histograms of the CT number at the heart, ranges of the CT number covering (a) heart sac (pericardium and epicardium layers) (b) heart septum (myocardium and ventricular septum), and (c) heart cavity (chambers)

Figure 7-3 shows comparisons of the selections of CT number range on SD of pixel values measurement at the heart (the result from scanner G1 was selected as an example). For the Toshiba, Philips, Siemens and GE scanners, when the heart septum was included the average SD of pixel values increased by 15%-50%, and by up to a further 60% when the heart sac was included in the range of measurement. However, in this study only the range in CT number of 100-150 HU that covers the heart cavity was used.

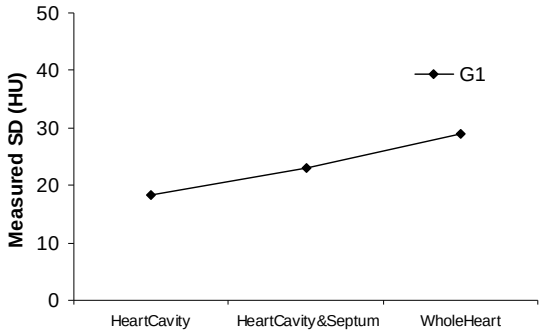

Figure 7-3 Comparisons of SD of the pixel values (image noise level) for different selected ranges of CT number, measured at the heart, from scanner G1

For the liver, there was a wide range in the CT number since it contains structures such as bile ducts and blood vessels. It was difficult to differentiate each structure, therefore the range in CT number of 100-150 HU covering the majority of the liver was selected (figure 7-4). The CT number values varied between patients, so it was not possible to use the same values for all patients and the ranges were selected patient by patient.

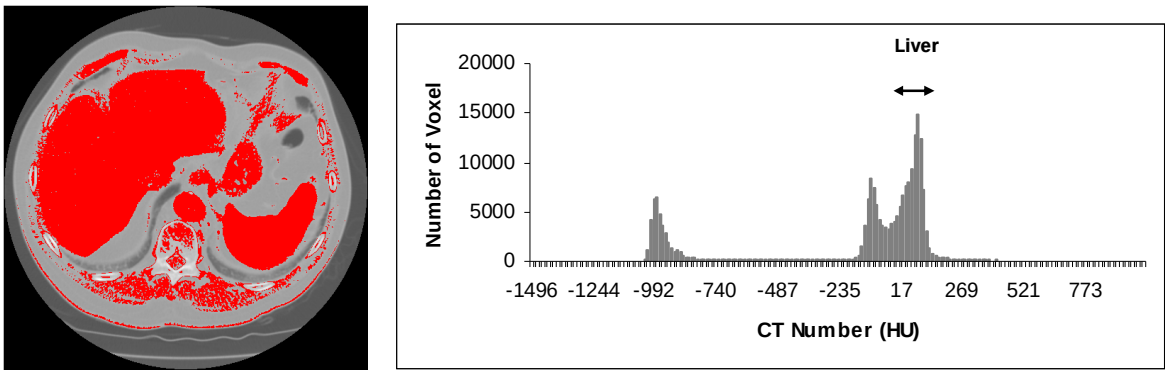

Figure 7-4 Histograms of the CT number at the liver

The written program, for noise measurement, displays the areas covering the selected range in CT number on each image slice, and these areas are used for SD measurement. The program then automatically moves a circular ROI of 200 mm^2 (16 mm in diameter) within each of those areas to measure the SD in the CT number at multiple ROI positioned for each slice. The size of ROI was smaller than that used for the noise measurements in phantoms as detailed in previous chapters. A circular ROI of 500 mm^2 was used for measuring noise in a homogeneous phantom, as recommended by ImPACT (Edyvean, 2003). However, for the measurement in human organs such as the heart and liver, the ROI should be made with the smaller circle, to avoid borders and edges of others structures (Reddinger, 1998). For individual patients, the noise was measured along about one third of the organ length and at the level of the middle of the organ (figure 7-5). The average noise values for each organ and patient were then plotted against the patient cross sectional area in order to evaluate the association between these parameters.

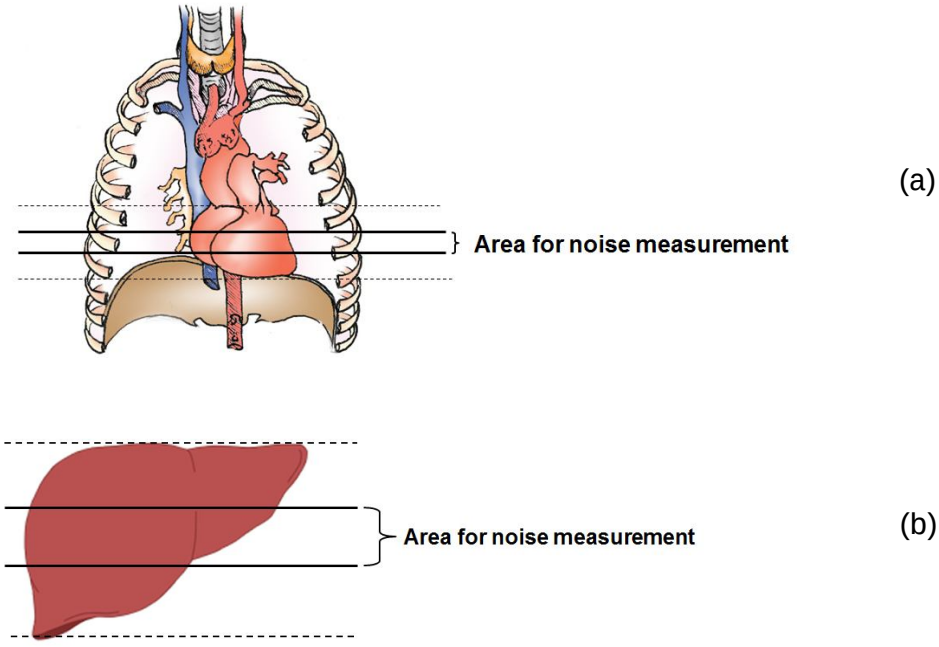

Figure 7-5 Diagram illustrating the areas for noise measurement at (a) heart and (b) liver

Statistic Package for the Social Sciences (SPSS Statistic 17.0 for Windows, IBM, New York) was used. A simple linear equation was fitted to the data to give an indication of the trends in results. Gradient values for a relationship between the patient cross-sectional area and the patient dose and the image noise level for each scanner were analysed using a linear regression model. The positive and negative values for slope of the regression line results in positive and negative correlations respectively. The strength of these relationships is given by the correlation coefficient (r) which can be calculated. Any r that is positive indicates a direct or positive relationship between two measured variables. Negative r indicates indirect or inverse relationship.The r values of 0-0.2, 0.2-0.4, 0.4-0.7, 0.7-0.9 and 0.9 to 1 were referred to no relationship, weak, moderate, strong and very strong relationships respectively.

7.3 Results

7.3.1 Tube current modulation pattern

The patient cross sectional area for individual CT scanners measured at the thorax and abdomen are shown in figure 7-6 and table 7-2. The values of patient cross sectional area for data from different CT scanners were in a similar range. This was except for the first data set for scanner T2 in which the average patient size was smaller. Two target noise values were used for scanner T5 as explained earlier, for smaller patients a lower target noise was used than for larger patients. The average patient size for the second data set of scanner T2 (T2**) was higher than that for other scanners, except for the group of larger patients for scanner T5.

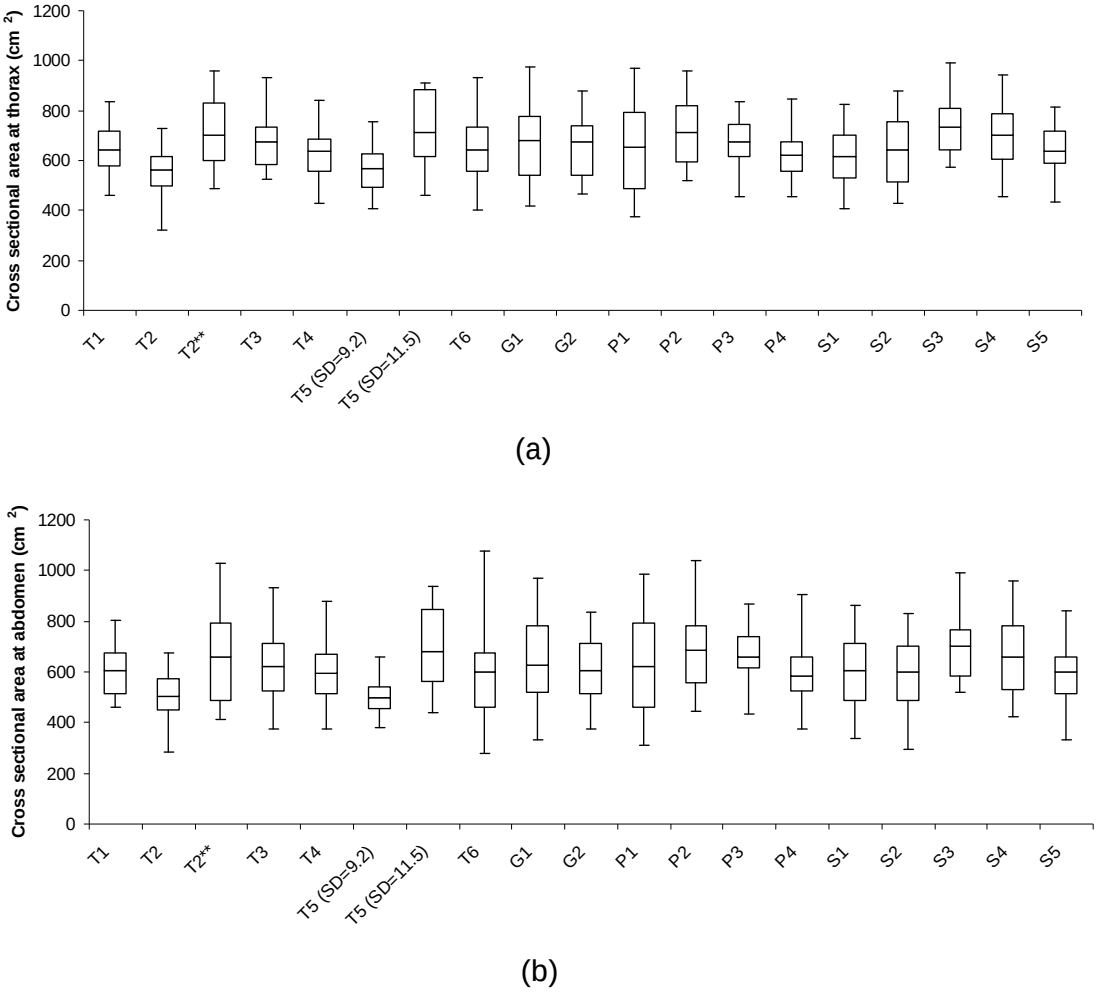

Figure 7-6 Box plots show the minimum, 25th percentile, mean, 75th percentile and maximum patient cross sectional area values measured from (a) thorax and (b) abdomen from different scanners and manufacturers

The tube current modulation patterns along the length of the scan for the patients who received the highest (H) and lowest (L) doses from some CT scanners are shown in figures 7-7 to 7-8. In some scanners, the scan was separated into two sequences, the thorax and the abdomen parts, and these are referred to as sequences 1 and 2 in brackets. The patterns of tube current modulation along the whole length of scan for the patients who received the highest DLP were similar in all scanners, the tube currents started at higher values at the shoulders, before falling towards the lung region, and rising again on entering the abdomen.

There were limitations in the minimum mAs/image of 50 mAs (100 mA), 40 mAs (80 mA), 60 mAs (120 mA), 40 mAs (80 mA) and 50 mAs (100 mA) for Toshiba scanners T2, T3, T4, T5 and T6 respectively, as set by users, therefore the mAs/image remained constant for the patients who received the lowest doses on these scanners (eg. figure 7-7b for scanner T4), except scanner T1 for which the minimum tube current setting was 5 mAs (10 mA) (figure 7-7a). For scanner G1, tube current was limited at the minimum of 100 mAs (200 mA), which was higher than the Toshiba scanners, therefore tube currents were constant and almost constant at 200 mA along the whole length of the scan for many patients (figure 7-7c). In contrast to scanner G1, tube current was limited at the maximum of 350 mAs (440 mA) for the patient who received the highest dose for scanner G2 (figure 7-7d). The NI for scanner G2 was set at 12.73 which was lower than that for scanner G1, and the maximum tube current setting for scanner G2 was 350 mAs.

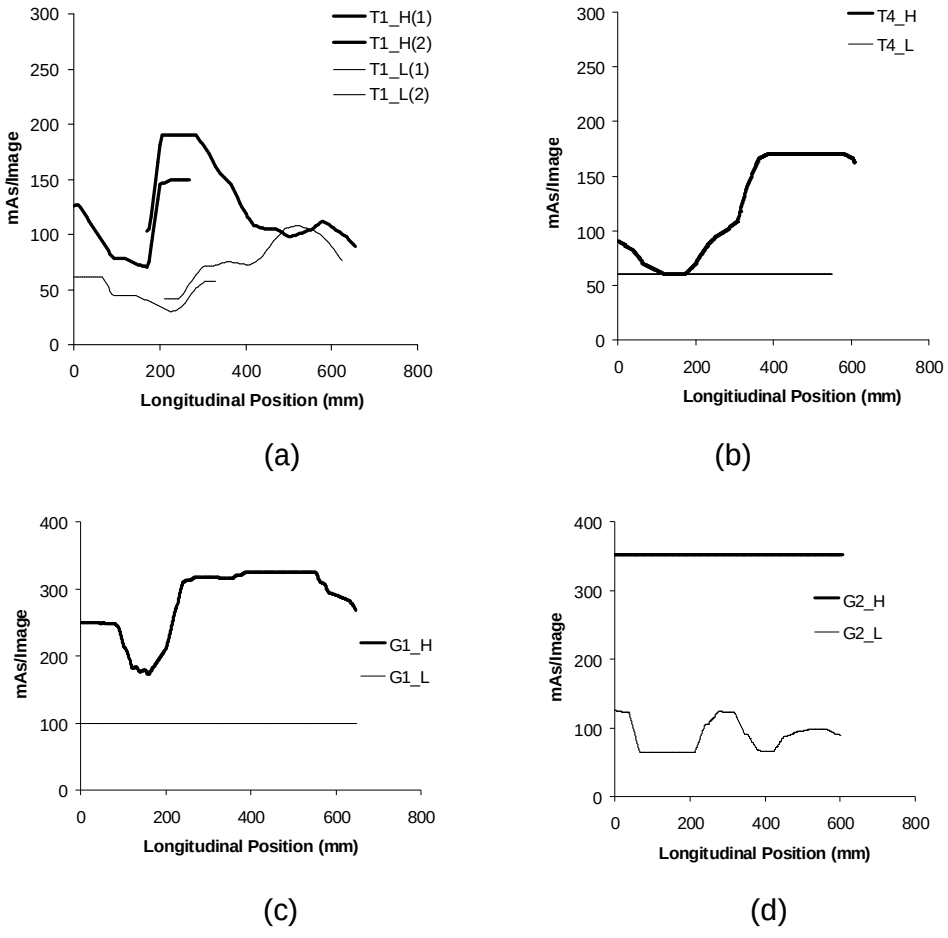

Figure 7-7 Values for mAs per image along the length of scan for the patients who received the highest (H) and lowest (L) doses from Toshiba scanners (a) T1, (b) T4 and GE scanners (c) G1 and (d) G2

For the Philips and Siemens scanners, there were no minimum and maximum settings of the tube current values. The tube current modulation patterns were similar for scanners P1 and P2 (figure 7-8a), the effective mAs/image values were between the minimum of 50 mAs and the maximum of 350 mAs, but the tube current was modulated within a narrower range for scanner P3. The tube current modulation patterns from scanner P4, which D-DOM was implemented, differed from the others, in having a wider range of tube currents and tube currents were higher in the region of the lung (figure 7-8b). The patterns of tube current modulation were similar for Siemens scanners (figure 7-8c and 7-8d).

The lengths of scans were about 600 mm for Toshiba, GE, Philips and Siemens scanners but were about 800-1,000 mm for scanners S1 and S5 (figure 7-8c and 7-8d). The scans were separated into two sequences for scanners T1, S1 and S5, with a long overlap region between both sequences for scanner S1. At the overlap regions, tube current values for the second scan sequence were higher because the QRM settings were higher.

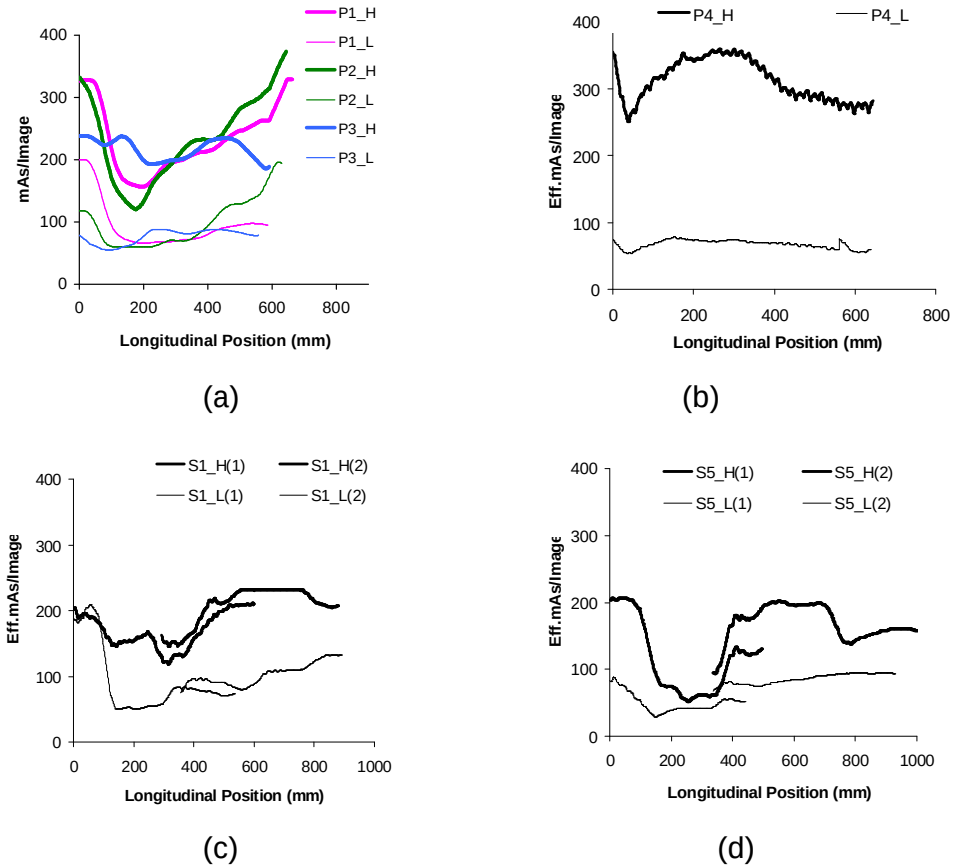

Figure 7-8 Values for effective mAs per image along the length of scan for the patients who received the highest (H) and lowest (L) doses from the Philips scanners (a) P1, P2, P3 (Z-DOM) and (b) P4 (D-DOM), and Siemens scanners (c) S1 and (d) S5

Table 7-2 DLP, $CTDI_{vol}$, cross sectional area and gradient values from regression line and the correlation coefficient (r) of patient cross sectional area and calculated CTDI values at the thorax (heart) and abdomen (liver)
Note *p<0.01 **p<0.05

Scanner	DLP	$CTDI_{vol}$			Cross-sectional area (cm^2)		Relationship Cross-Sectional Area Vs CTDI			
		One Sequence	Sequence 1	Sequence 2	Mean±SD		Thorax (Heart)		Abdomen (Liver)	
	Mean±SE (min-max)	Mean±SE (min-max)	Mean±SE (min-max)	Mean±SE (min-max)	Thorax (Heart)	Abdomen (Liver)	Gradient Mean± SE	correlation coefficient (r)	Gradient Mean± SE	correlation coefficient (r)
T1	883±70 (379-1608)	-	12.0±1.1 (4.3-24.0)	17.7± 7.6 (7.7-29.5)	642±91	606±109	0.014±0.003	0.723*	0.048±0.003	0.955*
T2	752±24 (486-972)	-	10.6±0.6 (5.6-16.1)	12.6±0.8 (5.6-23.2)	560±87	505±88	0.002±0.002	NS	0.025±0.002	0.836*
T2**	1198±109 (601-2232)		14.4±1.2 (8.5-25.4)	18.5±1.6 (8.8-34.5)	702±134	661±186	0.027±0.005	0.741*	0.037±0.003	0.933*
T3	770±66 (416-1706)	18.6± 1.6 (7.3-36.5)	-	-	679±123	629±136	0.022±0.005	0.679*	0.037±0.003	0.911*
T4	709±33 (345-1183)	16.1±1.1 (8.6-25.4)	-	-	639±99	595±123	0.000087±0	NS	0.013	0.763*

Table 7-2 (Cont.) DLP, $CTDI_{vol}$, cross sectional area and gradient values from regression line and the correlation coefficient (r) of patient cross sectional area and calculated CTDI values at the thorax (heart) and abdomen (liver)

Note *p<0.01 **p<0.05

Scanner	DLP	$CTDI_{vol}$			Cross-sectional area (cm^2)		Relationship Cross-Sectional Area Vs CTDI			
		One Sequence	Sequence 1	Sequence 2	Mean±SD					
	Mean±SE (min-max)	Mean±SE (min-max)	Thorax (Heart)	Abdomen (Liver)	Thorax (Heart)	Abdomen (Liver)	Thorax (Heart)		Abdomen (Liver)	
							Gradient Mean± SE	correlation coefficient (r)	Gradient Mean± SE	correlation coefficient (r)
T5 (SD=9.2)	354±26 (181-596)	5.6±0.4 (4.3-9.3)			568±92	500±74	0.005±0.004	NS	0.01±0.006	NS
T5 (SD=11.5)	444±35 (273-729)	7±0.6 (4.1-12.1)			711±139	682±152	0.005±0.002	0.622**	0.013±0.003	0.767*
T6	855±71 (372-1,682)	13.4±1.0 (6.23-24.1)			640±139	598±170	0.009±0.002	0.699*	0.015±0.01	0.902*
G1	803±65 (395-1,635)	11.8±4.7 (6.3-23.5)			679±155	629±173	0.016±0.004	0.657*	0.033±0.004	0.876*
G2	681±49 (301-1,193)	10.66±0.77 (4.7-18.6)			648±115	605±125	0.048±0.008	0.76*	0.055±0.008	0.804*

Table 7-2 (Cont.) DLP, $CTDI_{vol}$, cross sectional area and gradient values from regression line and the correlation coefficient (r) of patient cross sectional area and calculated CTDI values at the thorax (heart) and abdomen (liver)

Note *p<0.01 **p<0.05

Scanner	DLP	$CTDI_{vol}$			Cross-sectional area Mean± SD (cm^2)		Gradient of Relationship Cross-Sectional Area Vs CTDI			
		One Sequence	Sequence 1	Sequence 2			Thorax (Heart)		Abdomen (Liver)	
	Mean±SE (min-max)	Mean±SE (min-max)	Mean±SE (min-max)	Mean±SE (min-max)	Thorax (Heart)	Abdomen (Liver)	Gradient Mean± SE	Pearson correlation (r)	Gradient Mean± SE	Pearson correlation (r)
P1	806± 27 (427-1139)	11.3±0.4 (6.4-15.5)	-	-	710±125	684±150	0.004±0.002	0.394**	0.006±0.002	0.523*
P2	800±28 (481-1147)	11.0±0.4 (6.8-15.9)	-	-	654±172	619±192	0.005±0.002	0.502*	0.009±0.002	0.588*
P3	616±35 (319-977)	8.7±0.5 (4.6-14.1)	-	-	673±104	661±113	0.013±0.004	0.547*	0.012±0.003	0.66*
P4	806±65 (352-1467)	11.8±0.8 (4.54-21.41)	-	-	623±98	584±121	0.021±0.007	0.487*	0.02±0.006	0.544*

Table 7-2 (Cont.) DLP, $CTDI_{vol}$, cross sectional area and gradient values from regression line and the correlation coefficient (r) of patient cross sectional area and calculated CTDI values at the thorax (heart) and abdomen (liver)

Note *p<0.01 **p<0.05

Scanner	DLP	$CTDI_{vol}$			Cross-sectional area Mean± SD (cm^2)		Gradient of Relationship Cross-Sectional Area Vs CTDI			
		One Sequence	Sequence 1	Sequence 2			Mean±SE (min-max)		Mean±SE (min-max)	
	Mean±SE (min-max)	Mean±SE (min-max)	Mean±SE (min-max)	Mean±SE (min-max)			Gradient Mean± SE	Pearson correlation (r)	Gradient Mean± SE	
S1	958±43 (635-1340)	-	10.0±0.5 (6.8-15.7)	11.7±0.5 (7.8-16.1)	612±112	605±150	0.013±0.004	0.601*	0.011±0.001	0.842*
S2	737±34 (435-1281)	11.2±0.5 (6.9-18.7)	-	-	640±132	601±141	0.013±0.003	0.620*	0.015±0.001	0.915*
S3	824±7 (761-1029)	12.5	-	-	733±110	700±133	0	NS	0	NS
S4	633±42 (299-1014)	9.8±0.6 (5.4-16.6)	-	-	700±126	660±144	0.019±0.006	0.531*	0.027±0.003	0.891*
S5	697±26 (374-937)	-	7.4±0.3 (3.9-9.7)	10.1±0.4 (6.4-12.9)	636±98	601±119	0.004±0.002	0.486**	0.012±0.001	0.905*

7.3.2 Patient dose and distribution

The DLP and $CTDI_{vol}$ values obtained from scans are shown in table 7-2. A fixed tube current was used for scanner S3, therefore the $CTDI_{vol}$ values were similar for all patients, while the ATCM systems were operated for all other scanners and the average dose varied widely between patients and also scanners. The average DLP values from the majority of scanners were below the DRL of 940 mGy.cm except for scanners T2** and S1. The average DLP value for scanner S1 was within one standard errors of the DRL, while that for scanner T2** was higher due to the larger patient size.

Box plots showing distributions of $CTDI_{vol}$ and DLP, the minimum, 25th percentile, mean, 75th percentile and maximum values are shown in figure 7-9. Since DLP values involved scan lengths that can be varied between patients and CT scanners, $CTDI_{vol}$ is a better dose descriptor to compare the dose distributions relating to ATCM performance for different CT scanners. Results revealed smaller variations in $CTDI_{vol}$ and DLPs for the Philips (apart from for scanner P4) and Siemens scanners, compared with the Toshiba and GE scanners (except scanners T5) (figure 7-9).

Overall, ranges of $CTDI_{vol}$ of the Toshiba and GE scanners were wider compared with those of the Philips and Siemens scanners. However, the value for scanner T2 was less than those for other Toshiba scanners because the average patient size was smaller. But for the second data set of scanner T2 (T2**), which included patients of larger sizes, the $CTDI_{vol}$ and DLP covered a wider range. The $CTDI_{vol}$ values for both scan sequences for scanner T5 were significantly lower and in narrower ranges compared with the other Toshiba scanners, since it is equipped with iterative dose reconstruction.

Average $CTDI_{vol}$ values were similar in scanners P1, P2 and P4, with a wider range in scanner P4 and scanner P3 had the lowest value among the Philips scanners. For the Siemens scanners, the average $CTDI_{vol}$ values varied, and depended on QRM settings for each hospital protocol (table 7-1).

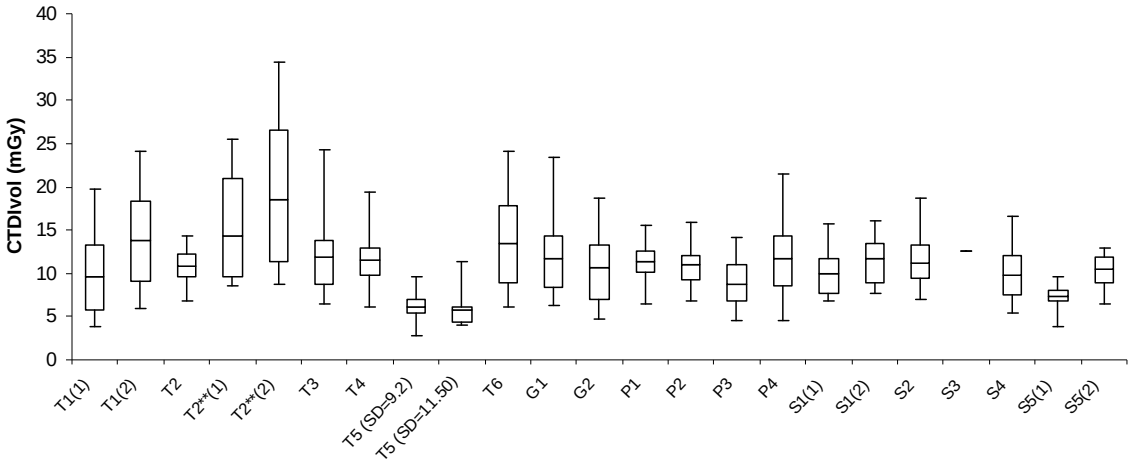

(a)

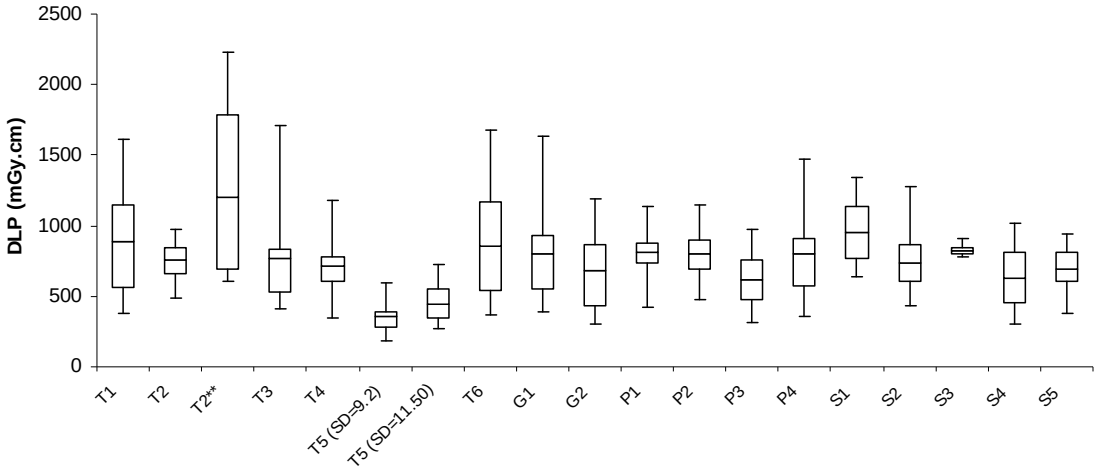

(b)

Figure 7-9 Box plots showing the minimum, 25th percentile, mean, 75th percentile and maximum (a) $CTDI_{vol}$ and (b) DLP values from different scanners and manufacturers
(Note: Numbers in brackets refer to scan sequences)

7.3.3 Relationship between patient size and CT Dose

The data set obtained from group T2** was used instead of T2 since it better represented a realistic clinical patient size distribution than those from group T2. Linear regression lines showed that the $CTDI_{vol}$ values increased with the patient cross sectional area at different rates for individual scanners and manufacturers (Gradient values, table 7-2). There were moderate correlations between the cross sectional area and $CTDI_{vol}$ at the thorax region for the Philips and Siemens scanners with the r values of 0.39-0.62 ($p<0.05$), while there were higher gradient values and stronger correlations for Toshiba and GE scanners (r values of 0.62-0.76, $p<0.01$). However, there was little correlation in the Toshiba scanners T2, T4 and T5 (SD=9.2) for the thorax region due to the saturation of tube currents at the minimum values. For the abdomen, there were higher gradient values with strong to very strong correlations between the patient cross sectional area and $CTDI_{vol}$ on the Toshiba, GE and Siemens scanners compared with the Philips scanner. However, $CTDI_{vol}$ values for the Toshiba and GE scanners increased at higher rates as can be seen from the gradient values compared with the Siemens scanners.

The relationships between patient cross sectional area at the thorax and abdomen and estimated $CTDI_{vol}$ values at heart and liver region are shown in figure 7-10. Results for scanner T5 were excluded from the figure, but shown in table 7-2, since they derived from a different reconstruction technique and $CTDI_{vol}$ were much lower. For the Toshiba scanners, $CTDI_{vol}$ increased strongly with patient size at the region of liver for scanners T1, T2 and T3 except scanners T4 and T6 (figure 7-10a). In addition, the $CTDI_{vol}$ increased slightly with patient size at the region of the heart for scanner T6, while the $CTDI_{vol}$ remained constant for scanner T4. Saturation of tube current dominated the relationships between the patient size and the $CTDI_{vol}$, otherwise $CTDI_{vol}$ values would be lower. Results for the GE scanner G1 were similar to those of the Toshiba, the minimum tube current of 100 mAs resulted in a constant $CTDI_{vol}$ for small patients who have cross sectional areas less than about 700 cm^2 and this dominated the weaker of overall relationships (figure 7-10b). For the Philips and Siemens scanners (figures 7-10c and 7-10d), $CTDI_{vol}$ increased slightly with patient size.

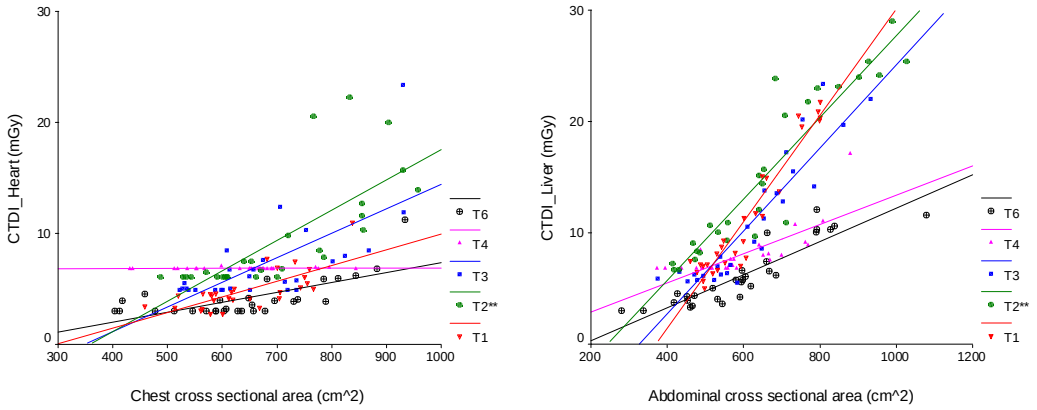

(a)

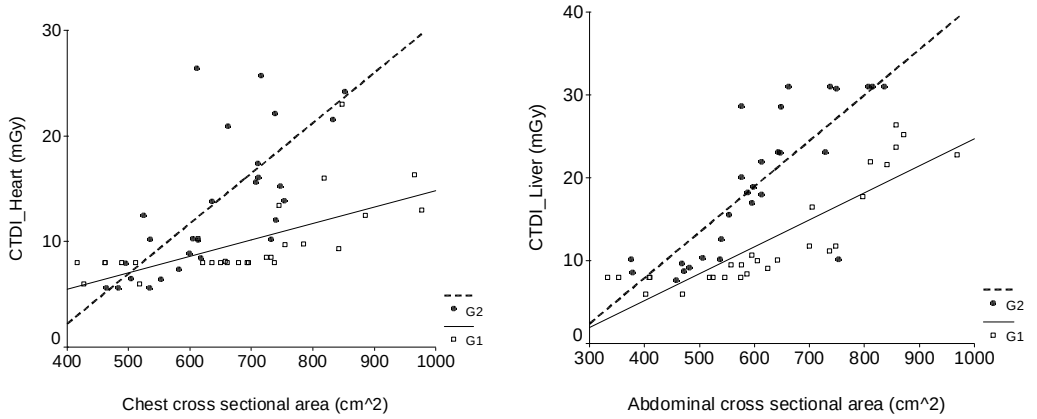

(b)

Figure 7-10 Relationships between patient cross sectional area, and calculated $CTDI_{vol}$ at the heart (left figure) and liver (right figure) regions in the form of the linear fit for (a) Toshiba, (b) GE, (c) Philips and (d) Siemens scanners

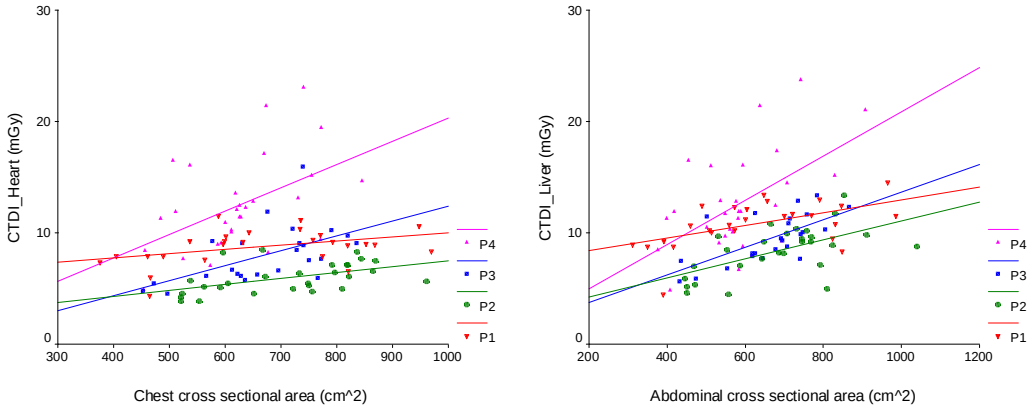

(d)

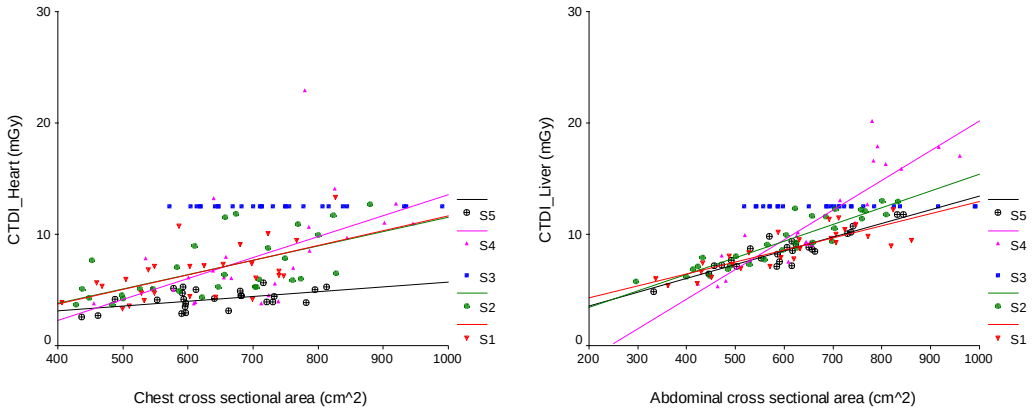

(e)

Figure 7-10 (Cont.) Relationships between patient cross sectional area, and calculated $CTDI_{vol}$ at the heart (left figure) and liver (right figure) regions in the form of the linear fit for (a) Toshiba, (b) GE, (c) Philips and (d) Siemens scanners

In order to evaluate the effect of the minimum tube current setting on the gradient of the curve, the patient data which were gained from scanners T4 were used as examples. When the constant tube current sections were excluded (figure 7-11) there were higher gradients and stronger relationships between the patient size and the $CTDI_{vol}$ for scanner T4 (gradient = 0.02, r=0.82, p<0.001 for the liver) so that larger patients required much more radiation doses than smaller patients.

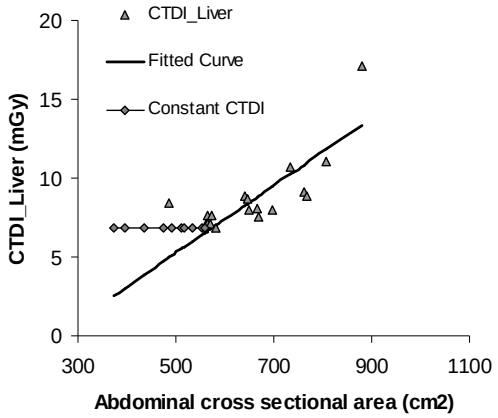

Figure 7-11 Relationships of $CTDI_{vol}$ and patient cross sectional area after excluding the effect of minimum tube current settings measured at liver from scanner T4

7.3.4 Noise measurement and relationship between the noise and patient cross sectional area

The mean values and the SD of the mean noise values across all patients from each hospital are shown in table 7-3. The image noise values measured from the Toshiba and GE scanners were more uniform compared with the other two manufacturers, as shown by the coefficient of variation. For the Siemens ATCM systems, the variations of image noise were less than with a fixed tube current (scanner S3). There were greater variations in image noise for the Philips scanners, except for scanner P3. Image noise levels are plotted against the patient cross sectional area in figure 7-12, for the Toshiba and GE scanners the image noise values remained relatively constant for all patient sizes in scanners T2**, T3 and G2 and at the abdominal part for scanners T6 and G1 since there were no relationships between patient and noise. But there was a moderate increase in noise with patient size for scanner T4 and at the thorax part for scanners T6 and G1 with r values of 0.42-0.52 ($p<0.05$). There were weak to moderate inverse relationships between noise and patient size at the thorax and abdomen for scanner T1 ($r=-0.43$, $p<0.05$ and $r=-0.37$, $p<0.05$). This would indicate that individuals with large body size tended to have less image noise.

There were strong to very strong positive correlations between patient size and noise at the thorax and abdomen parts for the fixed mAs technique of scanner S3 ($r = 0.82$, $p < 0.01$ and $r = 0.92$, $p < 0.01$). This would indicate that noise greatly increases with patient size. There were moderate to strong correlations between patient size and noise for all Siemens scanners operated with ATCM systems but at different rates with r values of 0.44-0.75 ($p<0.05$). However, there were no correlations between patient size and noise at the thorax and abdomen parts for scanners S5 and S4, respectively. For the Philips scanners, there were moderate to strong positive correlations between patient size and noise for scanners P1, P2 and P4 with r values of 0.42-0.87 ($p<0.05$), while there were no correlations between patient size and noise for scanner P3.

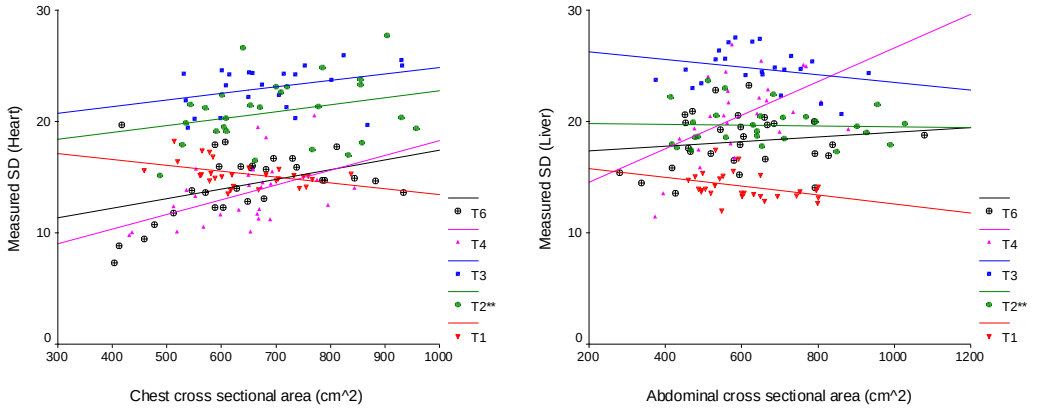

(a)

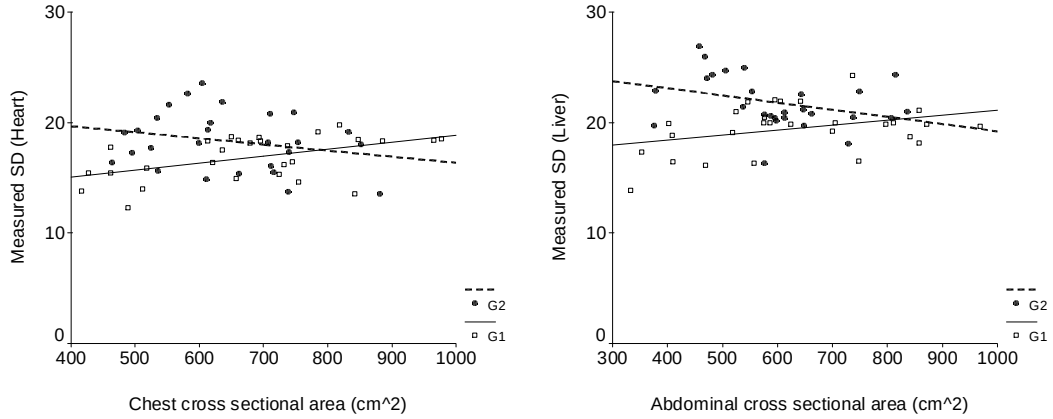

(b)

Figure 7-12 Relationships between patient cross sectional area, and image noise at the heart (left figure) and liver (right figure) regions in the form of the linear fit for (a) Toshiba, (b) GE, (c) Philips and (d) Siemens scanners

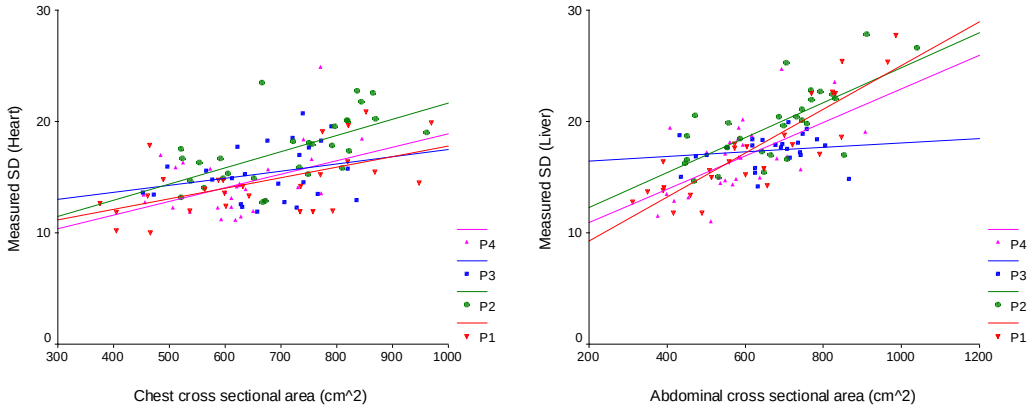

(c)

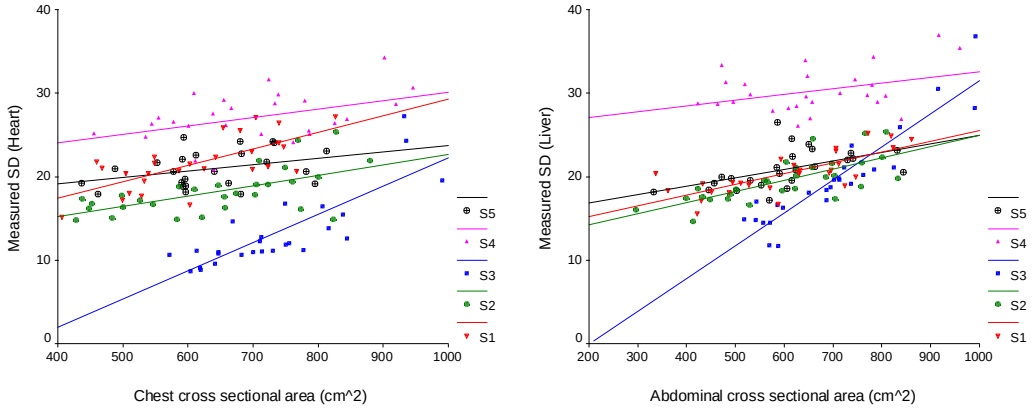

(d)

Figure 7-12 (Cont.) Relationships between patient cross sectional area, and image noise at the heart (left figure) and liver (right figure) regions in the form of the linear fit for (a) Toshiba, (b) GE, (c) Philips and (d) Siemens scanners

Table 7-3 Noise values, Coefficient of variation (%CV) of the noise values and gradient values from regression line and the correlation coefficient (r) of patient cross sectional area and noise values at the thorax (heart) and abdomen (liver)

(Note: *p<0.01 **p<0.05)

Scanner	Noise value (Mean±SD) (Min-Max)		%CV of noise		Gradient of Relationship Cross-Sectional Area Vs Noise			
	Heart	Liver	Heart	Liver	Thorax (Heart)		Abdomen (Liver)	
					Gradient Mean± SE	Pearson correlation (r)	Gradient Mean± SE	Pearson correlation (r)
T1	15.3±1.1 (13.6-18.3)	14.2±1.2 (12-17.5)	7.2%	8.3%	-0.005±0.002	-0.432**	-0.004±0.002	-0.372**
T2	17.2±2.0 (13.2-20)	21.3±2.3 (17.4-26.1)	11.6%	10.7%	0.006±0.004	NS	0.006±0.006	NS
T2*	20.9±3 (15.1-27.7)	19.7±1.7 (17.3-23.7)	14.4%	8.6%	0.006±0.004	NS	0±0.002	NS
T3	23.0±2.0 (19.4-26)	24.7±1.8 (20.7-27.6)	8.7%	7.3%	0.006±0.003	NS	-0.003±0.003	NS
T4	13.5±1.8 (9.7-20.5)	20.5±2.6 (11.4-26.9)	13.3%	12.7%	0.013±0.005	0.466**	0.015±0.005	0.520
T5 (SD=9.2)	15±2.5 (9.3-18)	16.4±1.3 (13.9-18)	16.6%	7.9%	-0.007±0.008	NS	0.005±0.005	NS
T5 (SD=11.5)	16±2.2 (11.8-19.3)	18±1.6 (14.2-21)	13.8%	8.9%	0.008±0.004	NS	0.007±0.002	0.638**

Table 7-3 (Cont.) Noise values, Coefficient of variation (%CV) of the noise values and gradient values from regression line and the correlation coefficient (r) of patient cross sectional area and noise values at the thorax (heart) and abdomen (liver) (Note: *p<0.01 **p<0.05)

Scanner	Noise value (Mean±SD) (Min-Max)		%CV of noise		Gradient of Relationship Cross-Sectional Area Vs Noise			
	Heart	Liver	Heart	Liver	Thorax (Heart)		Abdomen (Liver)	
					Gradient Mean± SE	Pearson correlation (r)	Gradient Mean± SE	Pearson correlation (r)
T6	14.3±2.9 (7.3-19.7)	18.2±2.5 (13.6-23.2)	20.3%	13.7%	0.009±0.004	0.416**	0.002±0.003	NS
G1	16.8±2.0 (12.3-19.8)	19.4±2.2 (13.9-24.2)	11.9%	11.4%	0.006±0.002	0.488	0.004±0.002	NS
G2	18.3±2.7 (13.6-23.5)	21.8±2.4 (16.3-26.9)	14.8%	11%	-0.005±0.004	NS	-0.006±0.004	NS
P1	14.5±2.9 (10.1-20.9)	17.5±4.3 (11.8-27.8)	19.9%	24.7%	0.009±0.003	0.56	0.02±0.002	0.872
P2	17.5±3.0 (12.8-23.5)	19.8±3.3 (14.7-27.9)	17.1%	16.9%	0.014±0.004	0.608	0.016±0.003	0.699
P3	15.4±2.5 (11.9-20.7)	17.4±1.4 (14.2-19.9)	16.3%	8.2%	0.006±0.005	NS	0.002±0.003	NS

Table 7-3 (Cont.) Noise values, Coefficient of variation (%CV) of the noise values and gradient values from regression line and the correlation coefficient (r) of patient cross sectional area and noise values at the thorax (heart) and abdomen (liver) (Note: *p<0.01 **p<0.05)

Scanner	Noise value (Mean±SD) (Min-Max)		%CV of noise		Gradient of Relationship Cross-Sectional Area Vs Noise			
	Heart	Liver	Heart	Liver	Thorax (Heart)		Abdomen (Liver)	
					Gradient Mean± SE	Pearson correlation (r)	Gradient Mean± SE	Pearson correlation (r)
P4	14.3±2.9 (11.1-24.9)	16.7±3.1 (11-24.6)	20%	18.9%	0.012±0.005	0.416**	0.015±0.004	0.579
S1	21.5±3.1 (15.3-27.2)	20.4±2.6 (15.7-25.2)	14.3%	12.5%	0.02±0.004	0.694	0.013±0.002	0.751
S2	18.2±2.7 (14.8-25.3)	19.6±2.6 (14.6-25.3)	15%	13.4%	0.012±0.003	0.6	0.013±0.002	0.722
S3 (Fixed tube current)	13.3±4.5 (8.7-27.2)	19.7±5.7 (11.7-36.8)	34.1%	29%	0.0339±	0.822	0.0394±	0.919
S4	27.1±3.0 (20.8-34.2)	30.3±2.7 (26-36.9)	11%	9%	0.01±0.004	0.441**	0.007±0.004	NS
S5	20.9±2.2 (17.9-24.7)	20.9±2.3 (17.1-26.5)	10.3%	11%	0.008±0.004	NS	0.01±0.003	0.525

7.4 Discussion

The study found that dose levels were indeed reduced for smaller and average sized patients, but for some scanners the dose levels were increased substantially for larger patients. This resulted in a lowering of image noise and improvement in image quality for these patients. Whether or not this improvement is necessary or appropriate and justifies the increase in dose level is difficult to prove. However, as a result, doses for larger patients were substantially higher on scanners operating on a fixed noise index, compared with those that allowed the acceptable noise level to increase with patient size. It should be noted that the maximum ATCM tube current level normally set is significantly higher than the tube current used for fixed mA techniques and it is for this reason that the increase in dose occurs.

7.4.1 Constant noise ATCM system (Toshiba and GE scanners)

The Toshiba and GE scanners ATCM systems aim to maintain constant image noise, the Toshiba uses a target noise and GE uses a NI to operate their ATCM systems. The tube currents and dose are dependent on patient size but noise levels are independent. The strengths of the relationships between patient cross- sectional area and DLP for Toshiba and GE scanners were higher than those for other manufacturers, and there were wide ranges in tube current to achieve the target noise (figure 7-10). The majority of mAs per image values were approximately the minimum values in the thorax region for the second data set of scanner T2 (T2**), scanners T4, T6 and G1. For the scanner G1, tube currents stayed the same at 200 mA throughout the scan length for patients who have the cross- sectional area of less than about 700 cm^2 (figure 7-10b). The range of tube current settings affects the image noise. The minimum tube current limits the current reduction for small patients for the second data set of scanners T2 (T2**), scanners T4, T6 and G1 and results in the lower image noise levels than required. As can be seen from figures 7-12a and 7-12b, the apparent increases in noise with patient cross- sectional area are due to the low noise levels for smaller patients. The overall noise value was similar to the target SD of 12.5 for scanner T1 (figure 7-12a). However, the image noise shows a steady decline with patient size, which implies that large patients have a higher level of image quality with higher doses. An ATCM test using the ImPACT conical

phantom confirmed the result for scanner T1 (figure 7-13), image noise decreased with the cross-sectional areas of the phantom greater than about 450 cm^2. Setting of adequate higher target noise settings may be an appropriate way to reduce the patient dose whilst preserving image quality for diagnosis for larger patients undergoing CT examinations on Toshiba and GE scanners.

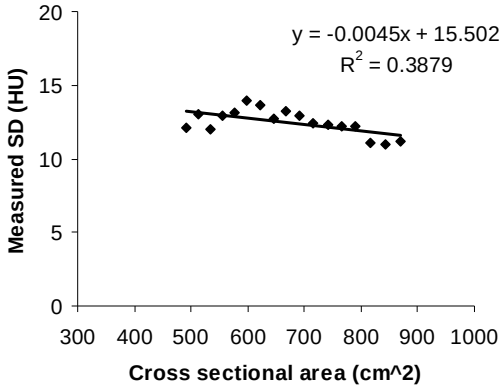

Figure 7-13 Measured SD (HU) against the cross- sectional diameter of the ImPACT Conical phantom showing linear regression and coefficient of variation

The $CTDI_{vol}$ values for the Toshiba scanners in this study (figure 7-9) were calculated from the DLP values to allow fair comparisons with those obtained from the other scanners. The $CTDI_{vol}$ shown at the Toshiba scanner monitor is based on the maximum mAs per rotation rather than average mAs being used for the entire scan length. A higher $CTDI_{vol}$ from a higher maximum tube current value could be from a large patient size or other contributing factors such as metal implantation in hip and other body areas.

The relationships between patient cross-sectional area and $CTDI_{vol}$ were limited by the minimum value settings of the tube currents. Any relationships between patient cross-sectional area and $CTDI_{vol}$ were limited in scanners T4, T6 and G1 (figures 7-10a and 7-10b). This was due to two reasons. The first reason was that the differences in the tube currents between large and small patient sizes were small, and this led to a narrower range of tube currents and $CTDI_{vol}$ values over the heart. The second reason was the minimum tube current settings which resulted in the saturation of the tube currents and $CTDI_{vol}$ values for small patients. As a result of these saturations patients of small size failed to show a reduction in $CTDI_{vol}$ due to minimum mAs values being reached.

The image noise from scanner T3 was higher than the target noise. This is because the Toshiba and GE scanner ATCM systems use the slice thickness of the first prospective reconstruction to estimate the tube current. Since the first reconstruction of scanner T3 was set at 5 mm but the second prospective reconstruction sent to PACS was 1 mm, with the same algorithm, then the noise level is increased by a factor of square root of a ratio between the image thicknesses of the first and second reconstructions. In this study the image noise levels for scanner T3 doubled the target noise.

7.4.2 Acceptable noise ATCM system

7.4.2.1 Philips scanner

There were D-DOM and Z-DOM ATCM systems for Philips scanners used in this study. Tube current modulation patterns from scanner P4, for which D-DOM was used, differed from those for the other scanners operated with Z-DOM. The tube currents for scanner P4 increased over the lungs. This related to the use of the angular dose modulation option (D-DOM) for scanner P4 and can be explained by results from a custom made phantom study in chapter 5, as shown in figure 7-17. Tube currents dropped significantly at a section of the phantom which represented the human shoulder, the section has a higher attenuation laterally than antero-posteriorly with an ellipse axis ratio of 2:1. Tube currents remained constant at other sections of the torso phantom (ratios between the AP and lateral are 1.3-1.5) as well as over the entire length of the ImPACT phantom (ratio between the AP and lateral is 1.5 through the phantom length). The mAs/slice is calculated from the ratio of the maximum and minimum patient attenuations; the higher the ratio the lower the mAs. For patient scans, the mAs is often lowest in the most attenuating parts, because the ratio is higher here (Wood, 2012). In thorax scans the mAs/slice values were lowest in the shoulders and highest in the lung (figure 7-8b).

For patients of similar size, the DLPs received from the scanner P4 were higher that those from the others (figures 7-9 and 7-10d). The finding confirms results described in chapter 5 (figure 7-14) and a report by Wood (2012) who states that there is a 14% higher dose in a CAP scan of an Alderson Rando phantom with D-DOM compared with Z-DOM. However, variations of image noise obtained from

D-DOM and Z-DOM ATCM systems were similar (table 7-3). Results indicate that it is not appropriate to use D-DOM for a CAP scan because of the higher patient doses.

.

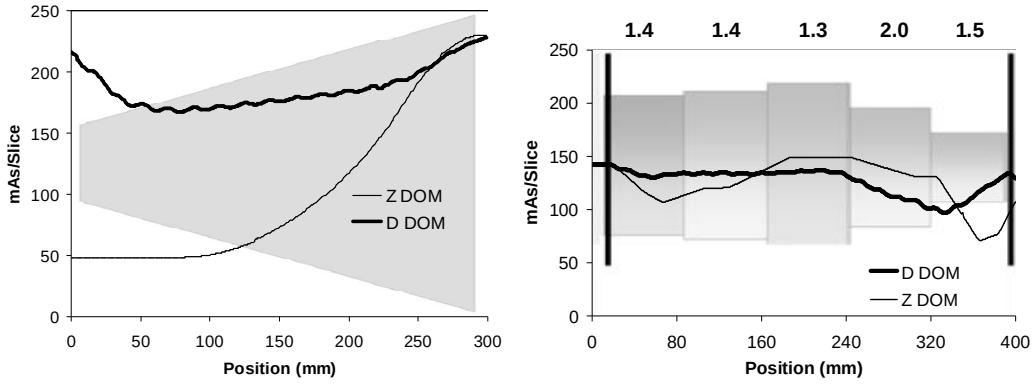

(a) (b)

Figure 7-14 Comparison of tube current modulation patterns between recommended mAs/slice values for D DOM and Z DOM in (a) ImPACT conical and (b) Torso section phantoms
(Note : A scan direction started from the minor end and section 1 for the conical and torso section phantoms (from the left to the right) and the numbers above the sections of the torso phantom are ratios of the AP and lateral diameters)

The dose from scanner P3 was 25% lower than that for other Philips scanners. Scanner P3 is the only Philips CT scanner in this study that incorporated the iterative reconstruction method iDose4. Philips Healthcare (2011) declared that iDose4 software helps to improve image quality and/or lower radiation dose. The Philips iDose4 improves the image quality whilst enabling dose reduction. However, the amount of radiation reduction and image quality improvement depends on which level of iDose4 is used (Hou *et al*., 2012 ; Olsson and Norrgren, 2012 ; Smyth and Doyle 2011).

The patient doses from Philips scanners P1, P2 and P4 have moderate relationships with the patient cross-sectional areas. The doses increase slightly with patient size but the noise increased more than for the Toshiba and GE scanners. The noise was relatively constant in scanner P3 that had iterative reconstruction and a more recent version of the ATCM software, and the gradient of the plot between the patient size and $CTDI_{vol}$ was lower. The older version of the ATCM calculation software on P1, P2 and P4 measured the average body size for all patients scanned with a specific protocol. The system

introduced images from previous studies into a database from which reference images for new examinations were derived (Nievelstein *et al*., 2010). As a result, the reference image changed gradually over time. Since the image noise is dependent on the tube currents used, image noise is also affected by the changes in the average patient size and this may explain why the relationships between image noise and patient size were more variable. Scanner P3, which has the more recent ATCM system, shows a stronger relationship between the $CTDI_{vol}$ and the patient cross sectional area (figure 7-10c, table 7-2) because the ATCM system compares the patient attenuation to the same reference patient size (personal communication from Philips CT application specialist, December 13 2012).

7.4.2.2 Siemens scanner

A fixed tube current technique was used for scanner S3, the tube current was not modulated along the length of scan therefore the $CTDI_{vol}$ remains constant and the DLP values were similar for all patients. The results showed a strong relationship between patient size and image noise. The relationship between image noise and cross- sectional area illustrates results expected from the fixed mAs technique. The Siemens scanners use the concept of reference mAs or QRM. The high setting of QRM results in higher $CTDI_{vol}$ and DLP. There were narrower ranges in tube current and the doses for larger patients were not as high as with the Toshiba and GE scanners. Both the tube current and the noise levels increased with patient size (figures 7-10d and 7-12d). Compared to the Toshiba and GE scanners, tube currents for slim patients are reduced less than constant image noise would require, while those for obese patients are increased less than a constant image noise would require. Overall absolute image noise values were related to the QRM settings. The lowest QRM setting of scanner S4 resulted in the highest noise value (tables 7-1 and 7-3) and the high settings of QRM resulted in higher $CTDI_{vol}$ and DLP (table 7-2). The DLPs from scanners using two scan sequences (scanners S1 and S5) are higher than those using a single sequence (scanners S2 and S4) because of longer scan lengths. The average DLP from scanner S1 was higher than the DRL, because there was more overlap between the two sequences, although the average $CTDI_{vol}$ was low. Moreover, the QRM settings of scanner S1 (140 and 160 effective mAs for the scan sequences 1 and 2) were higher than those for the other scanners.

7.4.3 Limitations of this study

There are some limitations to this study. Measurement of image noise should be within a uniform area of tissue. The heart cavity provided such an area, but in order to enable automatic identification in each image slice, a range of CT number covering only the heart cavity was selected. Since noise level depends on the selected range of the CT number (figure 7-3), a wider selected range of CT number may give greater variation in noise. When the range was increased to include different tissues within the heart, the standard deviation increased, and no longer reflected a realistic measure of noise. For the liver, although there was a wide range in CT number covering the liver, there was only one major peak. Another limitation of the noise measuring program was that because the area of measurement depended on the selected range of the CT number, another organ with a similar range of CT number to that for the organ of interest could be included in the assessment. This occurred on occasions when measurements of the noise in the liver included parts of the spleen.

7.5 Conclusion

Relationships between patient sizes, doses and image noise were examined in four different CT scanners. The results can be separated into two groups, constant noise ATCM system (Toshiba and GE scanners), and adequate noise ATCM system (the Siemens and Philips scanners). The first group; Toshiba and GE scanners use the concept of target noise and noise index to operate the ATCM system. The noise in the CT images was found to be constant in scanners for which the tube current values covered wide ranges. Here there were strong relationships between the patient size and dose received. These scanners are likely to have more significant dose variations and give larger doses for heavier patients. Setting of a higher target noise for larger patients in protocols is recommended. The selection of the minimum tube current value can also stop the tube current from decreasing further and affecting the image noise in some scanners. These settings lead to lower image noise levels but higher doses than expected. In this case, users should be aware of the range of tube current settings to ensure that adjustments are appropriate for all patients scanned.

The second group; Philips and Siemens scanners, use the concepts of the reference image and reference mAs to operate the ATCM systems. Relationships between the patient size and dose received were not as strong as the relationship with the Toshiba. There were narrower ranges of tube currents and the doses for larger patients were not as high compared with the Toshiba scanner. The exception was the scanner using D-DOM for which there was a wide range of tube current. In terms of the relationship between image noise and patient size, for the Siemens scanners, image noise values were increased slightly with patient size. However, for the Philips scanners, the image noise remained constant in the modern scanner, while it was not possible to identify the relationship for the older scanners because the older systems incorporated a learning process which meant that the average patient size changed when the operator changed the mAs from that which the DoseRight ACS had suggested. These results demonstrate that the performance of several scanners reviewed was far from optimal. Before optimization was undertaken, it was necessary to understand how different scan parameters affected both dose and image quality variable. Therefore, experiments were undertaken to investigate the influence of different scan parameters.

8 A study of factors influencing dose and image quality with CT ATCM system

8.1 Introduction

As reported in the previous chapter, patient $CTDI_{vol}$ values for the Toshiba and GE scanners covered wider ranges and resulted in substantially higher doses for larger patients than those for the Siemens and Philips scanners. Although the study also identified some of the factors contributing to the variation in patient dose, the high variations in patient dose for these constant noise based ATCM systems were not explained completely.

ATCM systems have options for users to set the desired image quality levels and other scanning options (Kalender, 2005; Kalra *et al.*, 2004b; Lee *et al.*, 2008), individual CT users can set up their own protocols. Variations from site to site in the user selected scanning parameters had a substantial influence on the radiation doses and image quality levels for individual patients, as discussed in chapter 7. One of the challenges facing CT users is to determine how modifications to scan protocols using ATCM will affect image quality and patient dose. Efficient use of the ATCM system needs a knowledge of ATCM options available on the scanner and an understanding of the effect of all user selectable parameters including, for example, tube voltage (kVp), pitch factor, rotation time, slice thickness and reconstruction filter, as well as the input value for image quality. The user requires to understand how these parameters interact, and how the ATCM changes image quality and exposure factors depending on the selections made. From the results of the previous study, the selected filter convolution (FC) had been thought to be a key parameter affecting patient dose under Toshiba ATCM.

There have been some studies to investigate effects of changing CT scan parameters on the tube current and image quality (Goo and Suh, 2006; Israel *et al.*, 2008; Keat *et al.*, 2005). However, these studies did not provide information about changes in the tube current and image quality or include changes in scan parameters over the full range used clinically including the selectable FC for the Toshiba CT scanners. The Toshiba ATCM system is the only one among the four most important CT manufacturers in which altering the reconstruction algorithm

for the first reconstruction affects the tube current modulation (Gudjonsdottir *et al*., 2010). For this chapter, the wedding cake phantom has been used to assess the tube current modulation and image noise under different ATCM settings and CT scanner parameters. In addition, high contrast resolution analysis through evaluation of the modulation transfer function (MTF) and low contrast resolution were measured in order to determine differences in image quality (Mahesh, 2009). The aim of this study is to investigate the effects of changes in scan parameter setting on tube currents, dose, image noise and image quality, and identify factors that need to be considered by the scanner operators. The outcome of this study will be suggested as practical optimisation methods in the West of Scotland.

8.2 Materials and Methods

8.2.1 Materials

8.2.1.1 CT ATCM scanners

Measurements were carried out primarily on a Toshiba scanner. Philips and Siemens scanners which have ATCM systems based on different principles were used as comparators. Details of the ATCM systems for these scanners are described in chapter 2. Routine CAP protocols were used as default settings and are shown in table 8-1.

8.2.1.2 Phantoms

The wedding cake phantom as detailed in chapter 5 was used to test the effects of changes in image quality levels and scan parameters for tube current modulation, dose and image noise. A Catphan600® (The phantom laboratory, New York) which is a routine phantom for CT quality control checks was used to provide measurements of the image quality for different FC settings. Details regarding the phantom have been explained in chapter 2.

8.2.1.3 Testing Approach

The scan parameters pitch factor, rotation time, collimator configuration, kVp, image thickness and reconstruction filter were varied for the Toshiba scanner

while the target noise was maintained at 12.5. Minimum and maximum tube current values of 10 mA-500 mA were selected. Since the pitch factor can vary with other scan parameters, for example changes in collimator configuration with the same beam width, an effective mAs, namely the mAs per rotation divided by the pitch factor, was calculated and used for comparisons of changes in scan parameters. The selected filters can be divided into four groups; FC01-FC05 and FC11-FC15 are body filters, FC07-FC09 and FC17-FC19 are soft tissue filters. The first number after FC indicates whether or not beam hardening correction (BHC) is used, e.g. FC01 and FC11 are the same reconstruction algorithm with and without the BHC. The lower the second FC number gives smoother images, and the higher the FC number gives sharper images.

The scan parameters varied on the Philips and Siemens scanners were pitch factor, rotation time, collimator configuration, image thickness and reconstruction filter. The behaviour of the Philips ATCM tool using AP and lateral scan projection radiographs (SPRs) and the influence of the iterative dose reconstruction (iDose) software were tested on the Philips scanner. The quality reference mAs (QRM) used for the Siemens scanner was 110 mAs. The tube current ranges for the Philips and Siemens scanners were determined by the scanner. The reconstruction filters for the Philips scanner can be separated into three groups, A, B and C, corresponding to very smooth, smooth and sharp respectively. In addition, each filter can be applied with standard or high levels of resolution. For the Siemens scanner, two reconstruction filters of smooth (B31f) and sharp (B50f) filters were compared.

The phantom was scanned with a 300 mm long scan over the middle part, excluding both edges. The reason for the edge exclusion is to avoid sharp peaks in tube current in Toshiba scanners associated with step changes in attenuation as explained in chapter 5. The image noise was evaluated by measuring the mean standard deviation of CT number from each image with 500 mm^2 ROIs located in the centre, anterior, posterior and right and left lateral positions of the wedding cake phantom, as explained in chapter 5. The image noise values from all positions were averaged. A paired-samples t-test was conducted to compare the tube current and image noise values obtained from different scan parameter settings.

Table 8-1 Details of CT scanners and the routine protocols

Scanner	Model	kVp	ATCM setting	Rotation time (s)	Collimation (mm)	Pitch	Reconstruction filter	Image Thickness (for the first recon.)
Toshiba	Aquilion 64	120	SD=12.5 (5-250 mAs)	0.5	32x1	0.844	FC11, QDS+	5 mm
Philips	Ingenuity 128	120	Z-DOM	0.75	64x0.625	1.014	Standard Body	0.9 mm
Siemens	Somatom 64	120	QRM 110 eff. mAs	0.5	64x0.6	1.2	B31f medium smooth	5 mm

QDS : Quantum Denoising Software

Note: Measurements on Philips scanners were based on use of a SPR in AP direction

8.2.1.4 Image quality analysis using Catphan®600

Image quality checks including calculations of MTF from bead point sources and low contrast detecability (LCD) were carried out using the Catphan600®. A trial web-based software provided by 'Image Owl©' was used to analyze the image quality. Theory and methods for analysis of the MTF and LCD are available on the Image Owl website (Image Owl, 2013). Since the tube current for scans under ATCM is varied depending on the target noise and other scan parameter settings, an experiment was designed and carried out in order to determine the MTFs with different mAs values selected (similar to the condition with the ATCM activated). For this experiment, both the absolute MTF values and the variation with mAs were derived, using mAs values of 25 mAs, 50 mAs, 100 mAs, 200 mAs, 300 mAs and 400 mAs. The middle part of the module CTP528 (line pair resolution and point source, as shown in figure 2-11a chapter 2) was scanned in an axial mode. Scan parameters were fixed at 120 kV, 1 s rotation time, collimator 1x4 mm, FOV 240 mm. In order to calculate the absolute values for the number of lp/cm (MTF) and target diameter (LCD) for different FC settings, the scans were repeated five times, mean and mode values were used for the MTF and LCD, respectively.

Changes in FC settings covering the filters used for body and soft tissue scans as mentioned earlier were tested. The results of MTF obtained from the upper bead point source of the module CTP528 were averaged. The module CTP515 of low contrast target was used for the LCD analysis (figure 2-11b in chapter 2). Results of MTF_{50}, MTF_{10}, MTF_5 and MTF_2 values or the frequencies corresponding to the 50%, 10%, 5% and 2% MTF values (in $lp.cm^{-1}$), and the diameters of the low contrast target for the contrast level of 1%, 0.5% and 0.3% were derived.

8.3 Results

8.3.1 Toshiba scanner

8.3.1.1 Variations in image noise and dose with scan parameter setting

Results showing changes in mAs and $CTDI_{vol}$ for the Toshiba scanner when different parameters were altered are summarised in Table 8-2. Image noise levels and patterns were relatively constant over the middle part of each section of the phantom. Alterations in pitch factor, collimation and rotation time all changed the $CTDI_{vol}$ by less than 20%. But a reduction in image thickness for the first reconstruction from 5 mm to 1 mm resulted in an increase in the mAs and dose by about 2.5 times, while an increase in the image thickness from 5 mm to 10 mm resulted in a decrease of about 1.4 times (figure 8-1, table 8-2).

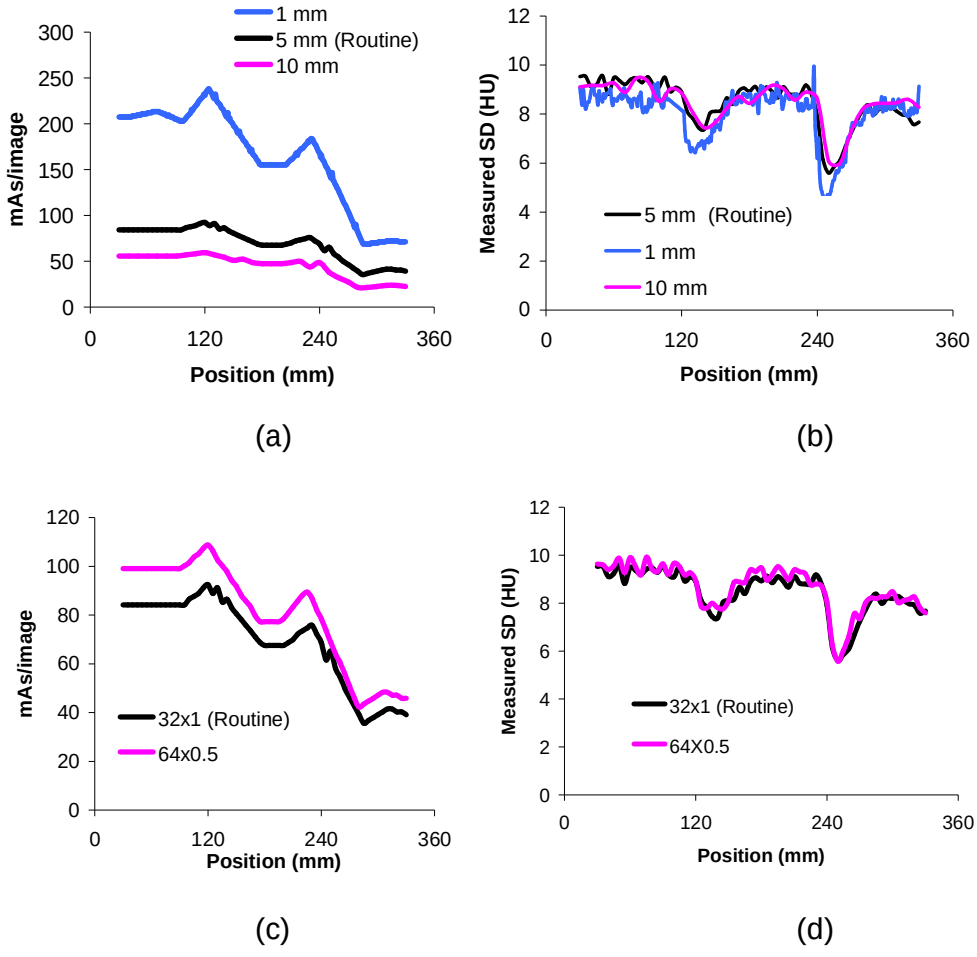

Figure 8-1 Comparisons of effective mAs and image noise over the entire length of the wedding cake phantom from different CT scan parameter settings ; (a-b) image thickness and (c-d) collimator configuration, measured from the Toshiba scanner and using the same target noise setting of 12.5

More substantial changes in effective mAs and $CTDI_{vol}$ occur with FC settings (figure 8-2, table 8-2), with tube current values increasing as filters were changed from smooth to sharp. For example the mAs values for FC03 and FC13 were double those for FC01 and FC11. The mAs remained constant at the maximum value of 200 mAs over the large and medium sections of the phantom for the sharpest filters of each group (FC05, FC15, FC09 and FC19). Both the magnitude and pattern of image noise were similar for various scan parameter settings, with the noise being relatively constant over the middle part of each section of the phantom, but with fluctuations at section junctions (figure 8-2b). The noise levels were higher where the tube currents saturated, at the large and/or medium sections of the phantom (figure 8-2a).

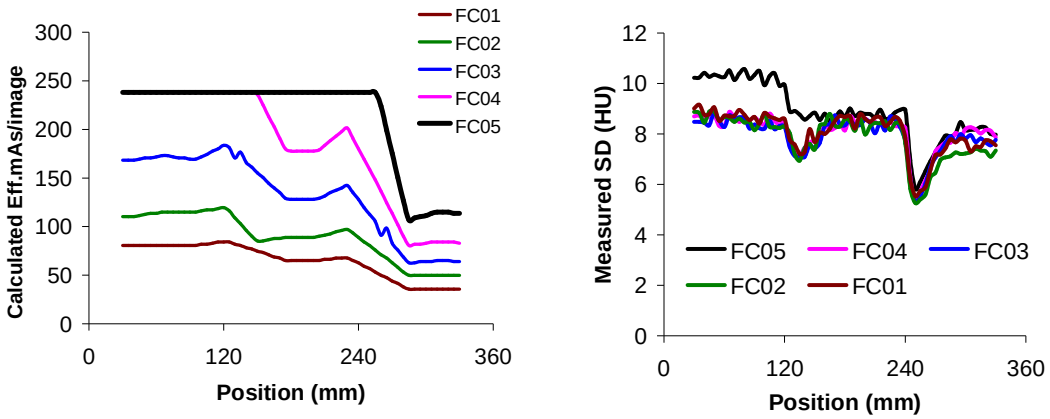

(a) (b)

Figure 8-2 Comparisons of (a) effective mAs and (b) image noise over the entire length of the wedding cake phantom from different FC settings for body scan with BHC (FC01-FC05), measured from the Toshiba scanner and using the same target noise setting of 12.5

Table 8-2 Values of effective mAs and estimated $CTDI_{vol}$ for different scan parameters, and % differences of these values compared with those for the routine setting, measured on the Toshiba scanner

(Note: Routine scan parameters were 120 kV, 32x1 mm beam, pitch=0.844, 0.5 sec rot. time, image thickness 5 mm, reconstruction filter FC11, QDS+ and target noise 12.5)

Parameter	Setting	Mean Effective mAs*				Estimated $CTDI_{vol}$ (mGy)	%Diff
		L	M	S	Average		
Routine setting		84	68	40	64	7.3	-
Vary Parameter							
Pitch Factor	0.656	93	79	46	73	8.3	14
	1.406	88	68	35	64	7.3	1
Rotation time	1sec	101	83	40	75	8.5	17
Collimator	64x0.5	99	77	48	75	8.5	17
kVp	135	65	56	30	50	5.7	21
Image Thickness	1 mm	207	155	72	145	16.5	126
	10 mm	55	47	23	42	4.8	35
Vary Filter							
Body filter (With BHC)	FC01	81	65	35	60	6.9	6
	FC02	110	88	50	83	9.4	29
	FC03	168	128	64	120	13.7	88
	FC04	238	178	83	166	19	160
	FC05	238	238	114	197	22.4	207
Body filter (Without BHC)	FC11	84	68	40	64	7.3	-
	FC12	118	88	52	86	9.8	34
	FC13	172	132	64	123	14	92
	FC14	238	195	87	173	19.8	171
	FC15	238	238	118	198	22.6	209
Soft tissue filter (With BHC)	FC07	124	92	52	89	10.2	40
	FC08	155	120	61	112	12.8	75
	FC09	238	238	100	192	21.9	200
Soft tissue filter (Without BHC)	FC17	124	92	52	89	10.2	40
	FC18	157	119	61	112	12.8	76
	FC19	238	238	100	192	21.9	200

L= Large, M=Medium and S=Small sections of the wedding cake phantom

Average value refer to average mAs over the middle part of the three sections

8.3.2 Philips and Siemens scanners

8.3.2.1 Effect of SPR direction on tube current and image noise on Philips scanner

Comparisons of the mAs and image noise between using the AP and lateral directions scanned projection radiography (SPR) for Z-DOM and D-DOM were performed on the Philips scanner, results were similar on Z-DOM and D-DOM (figure 8-3). The effective mAs values from the use of the lateral SPR were 15% higher than those of the AP SPR. The image noise levels were similar for both SPRs directions for the Z-DOM, while there was a 8% decrease in image noise for the lateral SPR for the D-DOM.

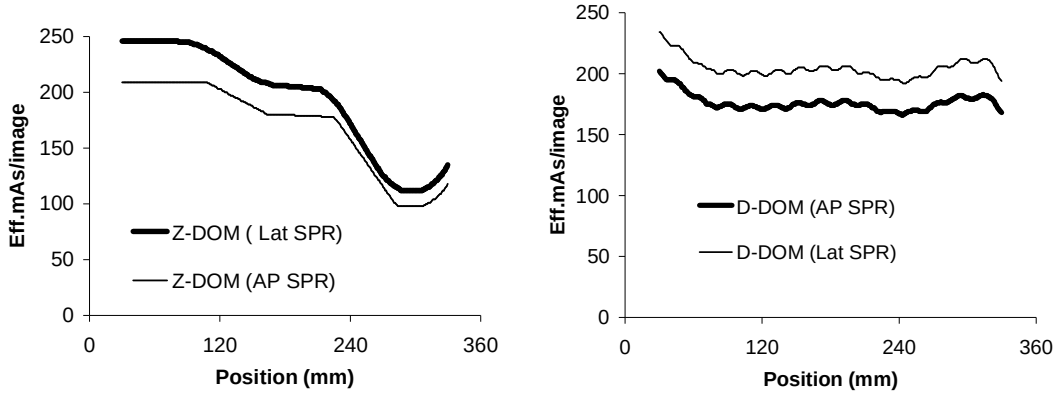

Figure 8-3 Comparisons of effective mAs/image value between using AP and lateral SPRs for (a) Z-DOM and (b) D-DOM, measured from the Philips scanner

8.3.2.2 Variations in image noise and dose with scan parameter setting

For the Philips scanner, the effective mAs values were not changed significantly, tube current modulation patterns were similar by altering the scan parameters (figure 8-4a). Unlike the Toshiba scanner, the tube current modulation on the Philips scanner does not saturate at a set value, as the maximumn is determined based on the region of highest attenuation within the SPR. The image noise levels were similar for all pitch factor, rotation time and collimator configuration settings. Use of high resolution coupled with sharp filters C increased the image noise values by 49%-58% ($p < 0.05$), compared with standard resolution coupled with filters A or B. Image noise level decreased significantly

(P<0.05) when iterative reconstruction software (iDose) was implemented, with a 27% decrease for iDose level 3 and 44% for iDose level 6, compared with the routine setting (figures 8-4b and 8-4c).

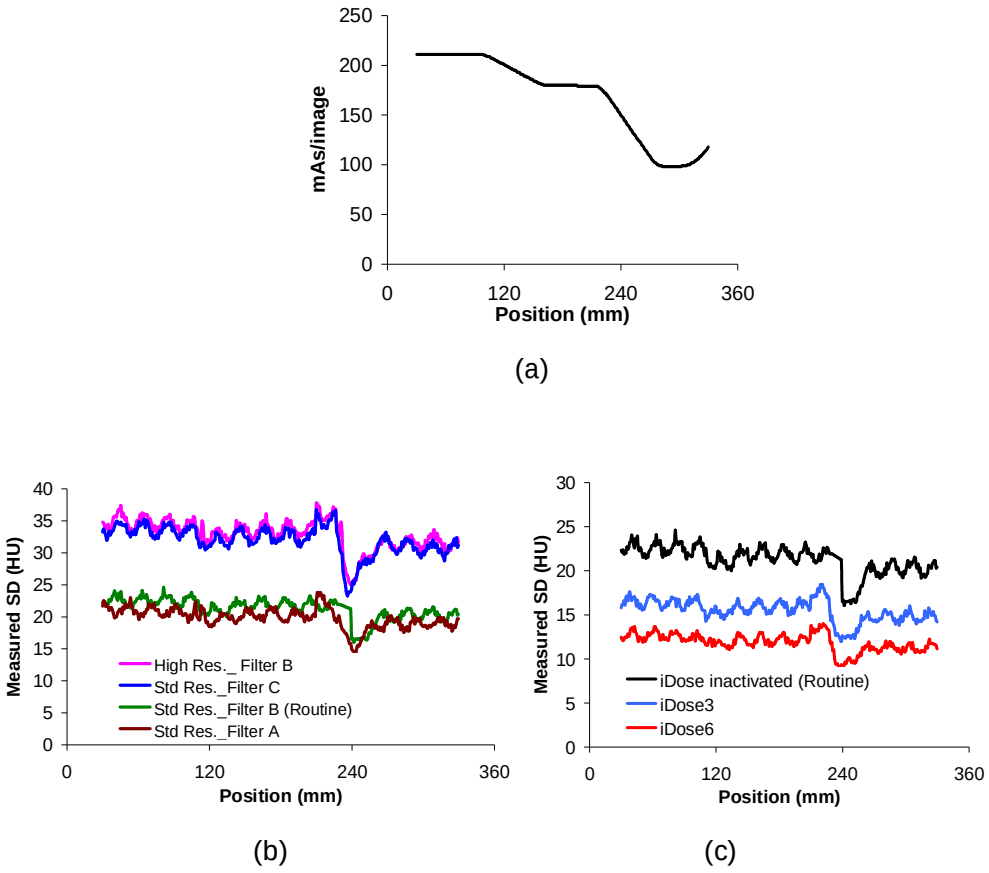

Figure 8-4 Effective mAs/image values which were similar for various scan parameter settings and image noise over the entire length of the wedding cake phantom from different scan parameter settings of (b) reconstruction filter and (c) use of iDose, measured from the Philips scanner

For the changes in scan parameter settings on the Siemens scanner, using the same QRM setting of 110 mAs (figure 8-9), the mAs decreased significantly for the lower pitch of 0.9 and longer rotation time of 1 sec ($P<0.05$) (table 8-3), There were significant differences in the noise level between different settings of pitch factor and rotation time, but only 4% changes in mAs. There was not a significant difference between mAs values used for B31f and B50f, but use of the B50f filter resulted in a 2.4 times increase in the image noise, compared with the default B31f filter ($p<0.05$). Values of effective mAs and estimated $CTDI_{vol}$ with scan parameters are shown in table 8.3.

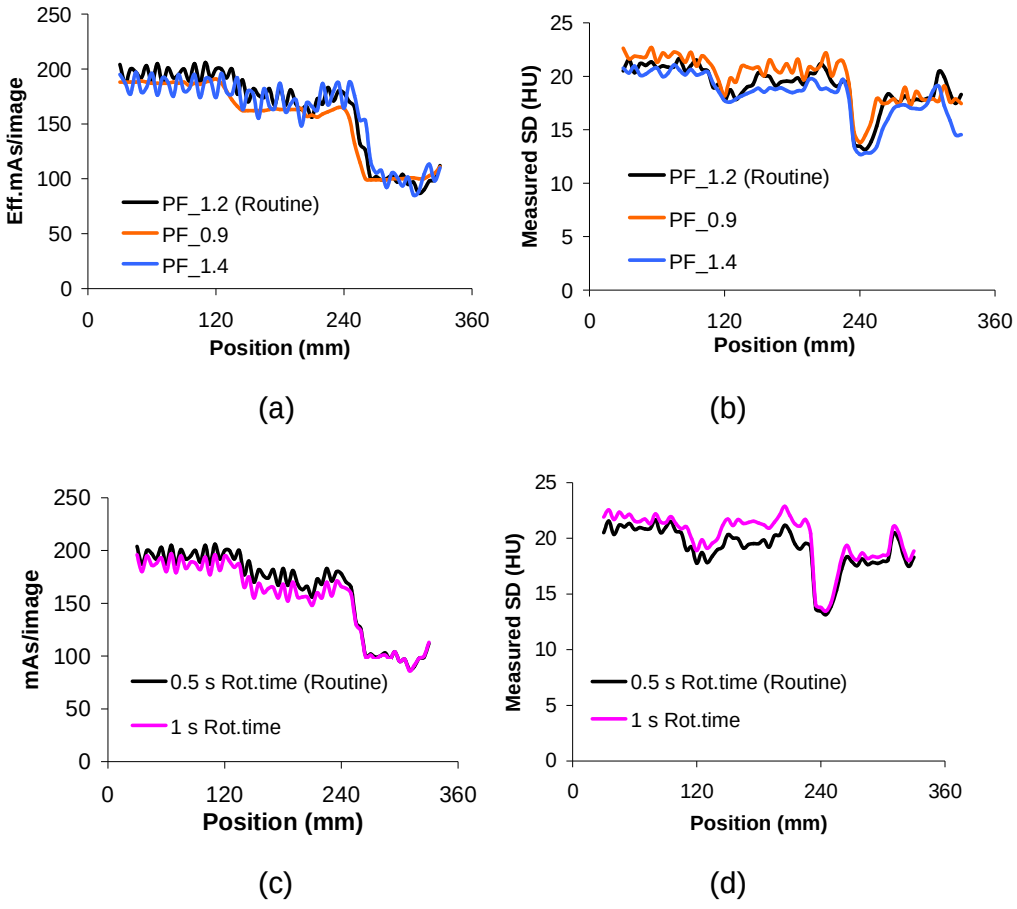

Figure 8-5 Comparisons of effective mAs and image noise over the entire length of the wedding cake phantom from different scan parameter settings of (a-b) pitch factor, (c-d) rotation time and (e-f) reconstruction filter, measured from the Siemens scanner

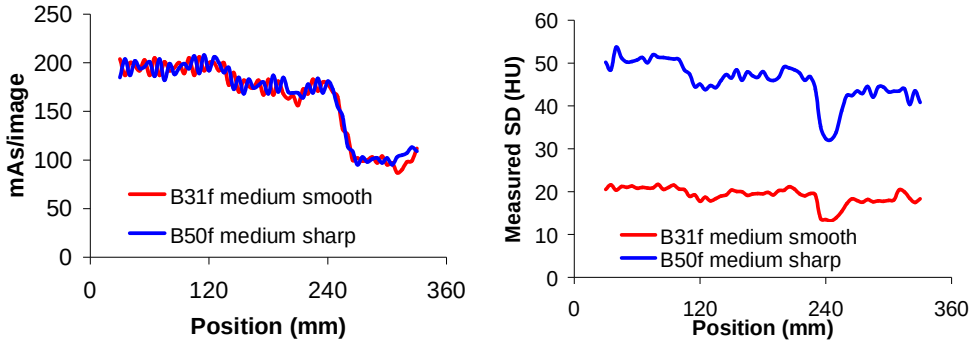

(e) (f)

Figure 8-5 (Cont.) Comparisons of effective mAs and image noise over the entire length of the wedding cake phantom from different scan parameter settings of (a-b) pitch factor, (c-d) rotation time and (e-f) reconstruction filter, measured from the Siemens scanner

Table 8-3 Values of effective mAs and estimated $CTDI_{vol}$ for different scan parameters, and % differences of these values compared with those for the routine settings, measured on the Siemens scanner

(Note: Routine scan parameters were 120 kV, 64x0.625 mm beam, pitch=1.2, 0.5 sec rot. time, image thickness 0.9 mm, reconstruction filter B31f)

Parameter	Setting	Mean Effective mAs*				Estimated $CTDI_{vol}$ (mGy)	%Diff
		L	M	S	Average		
Routine setting		196	177	110	161	11.4	
Vary Parameter							
Pitch Factor	0.9	188	164	107	153	10.9	4.4
	1.4	186	173	116	158	11.2	1.8
Rotation time	1 sec	188	165	109	154	10.9	4.4
Filter Reconstruction	B50f	195	179	113	162	11.5	0.9

8.3.3 Image quality with filter convolution for the Toshiba scanner

8.3.3.1 Modulation transfer function (MTF) with filter convolution

The absolute values of the spatial frequencies in lp cm^{-1} were relatively independent of mAs for a given FC setting, with coefficients of variation within 4%. The spatial frequencies measured using 200 mAs for filters used with BHC are shown as examples in figure 8-6. Values for the 0.5 level were 3.4-4.2 $lp.cm^{-1}$, while the number of $lp.cm^{-1}$ increased to 6.9-10.7 at 0.02. Overall, for individual groups of filters, a sharper filter has a higher number of $lp.cm^{-1}$. The FCs having the same reconstruction algorithm but different beam hardening correction, for example FC01 and FC11, and FC 02 and FC12, and so on, gave similar MTF curves. With the same FC settings, the values were relatively constant for various mAs settings.

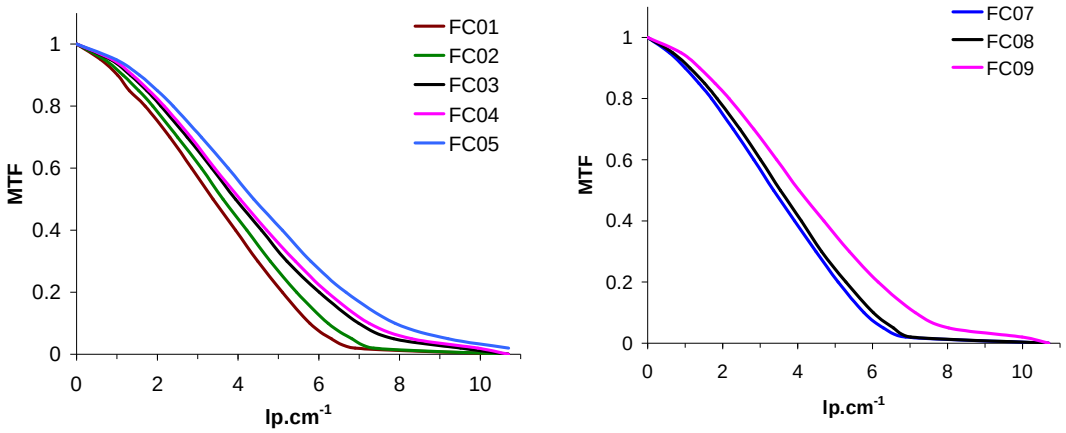

(a) (b)

Figure 8-6 Variation of spatial resolution with different FC settings for (a) body scan with BHC (FC01-FC05) and (b) soft tissue scan with BHC (FC07-FC09), measured from module CTP528, Catphan600®, using 200 mAs, and on Toshiba scanner

(Note: scan parameters were 120 kV, 0.5 s rotation time, FOV 240 mm, the mean values were derived from 5 times of measurement)

8.3.3.2 Low contrast detectability (LCD) with filter convolution

The detectable target diameter values for various FC and mAs settings are shown in figure 8-7. Overall, all FC settings had similar ability to detect the target diameter with the same mAs applied. With the same FC setting and contrast level, lower mAs settings tended to have lower abilities to distinguish between the two objects. For 1% contrast, detail diameters of 5 mm and larger could be detected with 25 mAs and the smallest detail diameter of 2 mm could be detected when the applied mAs was 200 mAs or above. For 0.3% contrast, 6 mm diameter detail could be detected at 200 mAs. The detectable detail diameter values declined with mAs but differences between FC settings were not significant.

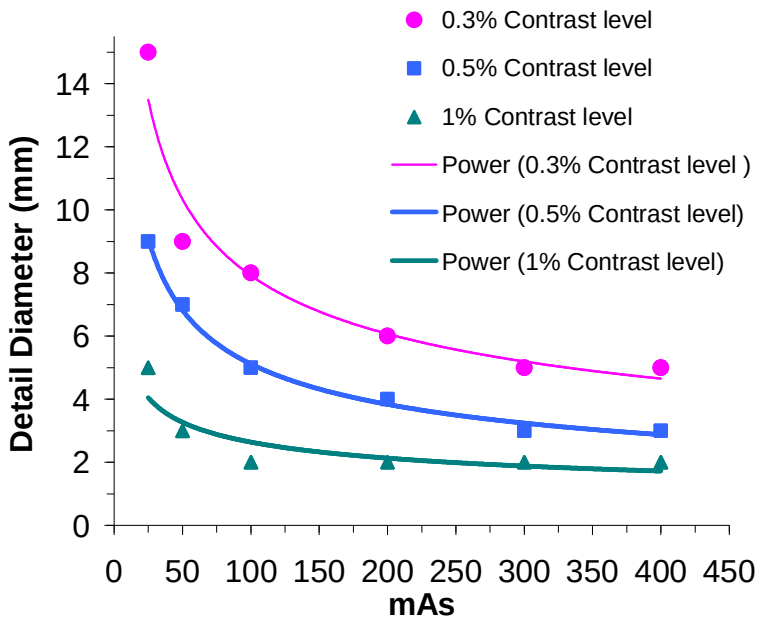

Figure 8-7 Variation of low contrast detail detectability with mAs values, for contrast levels of 1%, 0.5% and 0.3%. Measured from module CTP 515, Catphan 600®, using FC13 and on Toshiba scanner

8.4 Discussion

As an observation some countries such as USA require medical physicists to ensure each patient scan is optimised, in order to achieve this, it is important to understand the principles of different ATCM techniques and factors affecting the ATCM systems. The effects of altering scan parameters changes the response of the ATCM system and do not have the same consequences in all ATCM systems. Since the issue of larger variations in patient dose had been found with the Toshiba CT scanners, as shown in chapter 7, the study in this chapter paid more attention to the Toshiba scanner's dose and image quality optimisation. The Philips and Siemens scanners have been used as comparators since they have different principles of ATCM system operation.

8.4.1 Effects *of changes scan parameters*

The Toshiba ATCM system aims to achieve a constant image noise similar to the target set by users, while the Philips and Siemens scanners adjust scan parameters to achieve adequate image quality through comparison to a reference image and patient. For the Toshiba scanner, the image noise level obtained from scans of the wedding cake phantom using different scan parameter settings were all similar. The image noise remained constant for each section of the phantom, however, there were fluctuations in the noise at the section junctions, because the ATCM does not adjust the output immediately at the boundaries since the beam width overlaps two sections at the same time (figure 8-1b). The tube current remains higher than required to achieve the selected noise level for the smaller section until the beam width only incorporates the small section. As a result the noise level at the start of the smaller section is lower. The rise in tube currents at the edge of each section in the Toshiba scanner results from the step changes in radiation attenuation as explained in chapter 5.

Scan parameter protocols are typically set by CT application specialists, but users can adjust them. From the previous chapter 7, the pitch factor, collimation configuration, FC and image thickness setting for CAP protocols from Toshiba scanner users vary from site to site. Results have shown that tube current values and, therefore, patient dose, were affected by the changes in CT

scanner parameters. The mAs can rise by up to 17% for adjustments in the scan parameters (pitch factor, rotation time, collimator) within the range used clinically compared with the routine setting, and can be double when selecting a narrower image thickness for the first reconstruction (1 mm versus 5 mm) (table 8-2).

Use of a higher pitch factor (or faster table travel) and a faster rotation time reduces scan time but could also affect image quality, and consequently the ATCM system increases the tube current to maintain the image noise. As a consequence the dose should be the same when rotation time and pitch are changed, when other scan parameters are kept the same. However, from the results of this study, use of a lower pitch factor and longer rotation time led to slightly higher mAs and $CTDI_{vol}$ (table 8-2) and the result is similar to a report by the Toshiba company (Thomas, 2011) that stated a reduction of pitch factor from 0.828 to 0.641 results in a 15% increase in effective mAs. The reason for this is currently unknown. However, in the clinical situation, use of a lower pitch setting results in a reduction of the overranging spiral artefact due to interpolation and reconstruction process (Barrett and Keat 2004), and one obvious advantage for the short rotation time is eliminating a motion artefact caused by patient movement (Kumala, 2004).

When a higher tube potential is used, giving more highly penetrating photons, the ATCM can reduce the number of photons required to achieve the same noise level by decreasing the tube current (table 8-2). However, under clinical conditions, tube potential should be selected based on the requirement for a subject contrast enhancement in the image as well as patient size and clinical purpose of the CT examination (Strauss *et al.,* 2010). Tube potential other than 120 kV may be considered for some cases. Obese patients may require higher tube potential selections when mAs cannot be increased further to ensure a sufficient number of photons exit the patient. For slim or pediatrics patients where the mAs can not be reduced further, a lower kVp may be set (Nagel 2007). For CT examinations involving the use of iodinated contrast media with small size patients, a lower tube potential can give equal or better contrast to noise ratio than at a higher tube potential, at lower dose to the patient (McCollough *et al*., 2009).

The change in collimator configuration from 32x1 mm to 64x0.5 mm effectively alters the image slice thickness (figure 8-1, table 8-2), since the detector configuration used to acquire the desired slice thickness changes. In theory, in order to maintain image noise when reducing slice thickness by a factor of n, the mAs would need to be increased by a factor of n (as shown in equations 2-20 and 2-21, chapter2). However, the study found the mAs values were changed by approximately $\sqrt{n}$, as reported in other studies (Gudjonsdottir 2010, Kanal *et al*., 2007). In the clinical setting, the selected collimation should be as small as compatible with the aspect of overbeaming and overranging. A narrow slice thickness should be used only where limiting the partial volume effect is important. The wide beam collimation allows much faster z-axis coverage, while the narrow beam collimation acquisition is slower but allows retrospective reconstruction of narrower slices, the proper collimator should be selected that allows the desired slice thickness to be reconstructed.

The principles of the ATCM systems for the Philips and Siemens scanners, differ from that of the Toshiba. When scan parameters, including collimator configuration (32x1.25 versus 64x0.625) were altered, the effective mAs remained the same, while the image noise levels changed. Large variations in image noise occurred when sharper reconstruction filters were selected (figure 8-4b for the Philips and figure 8-5f for the Siemens scanners), so the user needs to be aware of the effect on the image quality when they select a filter which differs from the recommended one. The orientation of SPR is another factor affecting patient dose for the Philips scanner.

Use of the iterative reconstruction software (iDose) for the Philips scanner resulted in lower image noise levels which depended on their level (iDose3 or iDose6) (figure 8-4c). This has been confirmed by a study conducted by Olsson and Norrgren (2012) that reports that there are 15%-45% reductions in image noise from using iDose depending on which level of iDose. The response of different ATCM systems when scan and reconstruction parameters are varied is summarised in table 8-4.

Thus operators of CT scanners should be aware of how particular parameters affect ATCM performance when adjusting protocols for optimisation of protection. These factors will vary between manufacturers, as illustrated by the results of this study. For example:

Toshiba scanners

- Choosing a sharper filter will increase patient dose and image noise will remain the same.
- Selection of too high a minimum tube current or low a maximum current will limit the range of the ATCM and increase image noise
- The dose depends critically on the slice thickness selected for the first reconstruction
- The collimator configurations with narrower (64 x 0.5 mm, as opposed to 32 x 1 mm) will increase patient dose

Philips scanners

- Choosing a sharper filter will increase image noise, but have little affect on patient dose (also applies to Siemens scanners)
- Use of Philips iDose will reduce the noise with the same patient dose
- An SPR in AP direction as opposed to lateral direction for Philips scanner will save the patient dose

Table 8-4 Response of the ATCM systems for changes in tube current with variations of scan parameters within the range used clinically for CAP protocols

Parameter	ATCM Response with variations of scan parameters		
	Toshiba	**Philips**	**Siemens**
Pitch Factor (PF)	Yes A 25% higher mAs using PF 0.66 instead of PF 0.84	No	Yes A 4% lower eff. mAs using PF 0.9 instead of PF 1.2
Rotation time	Yes A 29% higher mAs using 1 s instead of 0.5 s	No	yes A 4% lower eff. mAs using 1 s instead of 0.5s
Collimator configuration	Yes A 23% higher mAs for using 65x0.5 instead of 32x1	No	n/a
Image Thickness	Yes A $\sqrt{n}$ higher mAs for reduction on image thickness by a factor of n	n/a	No
Reconstruction Filter	Yes Doubling of mAs for every two step change to sharper FCs	No	No
SPR	No Toshiba ATCM requires both AP and Lateral SPRs	Yes	n/a
Maximum Tube Current	Yes Will limit tube current at the values selected	No The range of tube current is set by the scanner and never hit the maximum limit	Yes Subject to the tube loading

n/a : this study was not performed

8.4.2 Image quality with different FC settings for the Toshiba scanner

Change in FC setting is another major factor affecting tube current and patient dose of the Toshiba scanner. From the Health Physics surveys, the selection of the FC for the CT CAP protocol varies with different Toshiba scanner users. The study has shown that the measured image noise levels are similar to that of the target value for all selections of scan parameter. However, in cases where the tube currents saturated at the maximum values for the large and medium sections (for example FC05, figure 8-2a), the image noise levels within these regions were higher. When a sharper filter was used, the mAs increased substantially.

Image noise is the standard deviation value of CT number which is measured from a homogeneous substance. It does not tell the whole story of the image quality. CT images can have the same image noise levels but different textures. MTF and LCD are the parameters most commonly used to assess image quality.

MTF is a parameter referring to spatial resolution on high contrast objects (measured resolvable lp.cm^{-1}) which is determined using objects having a large attenuation ratio. The higher spatial frequency (lp.cm^{-1}) a CT system can resolve, the better the spatial resolution (Mahesh, 2009). This means that the FC setting achieving higher lp.cm^{-1} is capable of separating smaller objects from one another than the FC setting having a lower lp.cm^{-1}. The results of this study showed that, the spatial resolution was influenced by FC setting (figure 8-6) but not by the tube current. The sharp filters, typically, enhance the spatial resolution at the detriment of increases in the image noise for the same tube current. However, when using the Toshiba ATCM, the tube currents will be adjusted to achieve the set target noise. Consequently, a higher tube current will be used for the sharp filters rather than the smooth ones. Different clinical tasks have different requirements for image quality. Solid nodule and emphysema identification are considered to be high contrast resolution tasks and may require the sharp filters (Boedeke *et al*., 2004). However if the same target noise was to be used with ATCM control then the patient dose would increase significantly.

The low contrast detectability of the system is the ability to differentiate objects in the CT image with small differences in attenuation. This is determined using test objects containing details which have small differences in attenuation from the surrounding material. Liver and kidney lesions and diffuse lung disease are examples of examinations that require good low contrast detectability. In these situations the pathology of interest has atomic numbers and densities that are nearly the same as the soft tissue. Noise is the most significant factor in determining detectability because the differences between the target and background are small. Consequently a reduction in mAs will increase the image noise and therefore, reduce the ability to detect an object with a low contrast difference (figure 8-7). In cases, with the same mAs value, the smooth filters produce lower noise and had a better ability to discriminate between two structures of low contrast difference. Since LCD is influenced by image noise, factors affecting image noise should also affect the LCD. However as the Toshiba ATCM preserves the image noise for all FC settings, then they should achieve similar LCD results.

8.5 Conclusions

Knowing and understanding how CT scan parameter options affect the ATCM system is important for patient dose and image quality optimisation. In the present study, changes in tube current, image noise and image quality with user selectable image quality options and scan parameters including tube voltage (kVp), pitch factor, rotation time, slice thickness and reconstruction filter were analysed. The subsequent dose reductions were found for options with higher noise levels. The minimum and maximum setting of the tube current in the CAP protocol affects the Toshiba ATCM. Ranges of the tube current for the Toshiba scanner should be adjusted based on patient size. For changes in the scan parameters using the same target noise in the Toshiba scanner, the tube currents were slightly different. However, changes in image thickness for the first reconstruction and FC setting were major factors affecting patient dose, since the ATCM system calculates the tube current being used based on the target value. Noise levels for all settings were in the same range and similar to the target setting. There is a trade-off between spatial resolution and tube current (or patient dose) for each filter under ATCM of the Toshiba scanner. A

smooth filter generates images with lower tube currents but with reduced spatial resolution. A sharp filter generates images with higher spatial resolution but increased tube currents. The selection of reconstruction filter should be based on each type of examination and clinical purpose. For the Philips and Siemens scanners, in contrast to the Toshiba scanner, user changes in CT scan parameter have less effect on patient dose, but change the image noise. This is especially true for changes of reconstruction filter for both scanners, and use of iterative reconstruction for the Philips scanner. The orientation of SPR is another key factor affecting patient dose for the Philips scanner. From the results of this study, use of the SPR in the AP direction is recommended. Knowing and understanding how CT scan parameter options affect the ATCM system is extremely important for optimising radiation protection and image quality in order to maximize the benefit to risk ratio. Protocols should be designed properly according to ATCM system's capacity and limitations of the ATCM system as well as patient size, clinical task and image quality requirement.

9 Conclusion and Future Work

Alternative techniques and phantoms for assessment of CT dose and scanner performance have been investigated. These were used to investigate the reasons why doses for patients on certain scanners are high and determine changes that could be implemented to minimise the high dose while maintaining acceptable level of image quality. The project can be divided into three phases linked together. The summary for individual parts is shown below.

9.1 Investigation of methodologies for CT dosimetry

Methodologies for practical implementation of proposed alternative CT dosimetry techniques have been examined at the beginning of this PhD project. The distributions of dose within a standard cylindrical body phantom and a specially constructed elliptical dosimetry phantom of similar dimension to the human trunk have been measured using Gafchromic film. Data sets have been combined to simulate helical scans from which values for cumulative doses in the middle of phantoms have been derived. The doses in the centre of the elliptical phantom were 70%-100% larger than for the cylindrical one and in the anterior were around 20%-40% larger, while the doses in the lateral positions were similar for the two phantom shapes. The differences between the anterior and lateral doses were larger for the Toshiba scanners and this is thought to be linked to the narrower profile of the beam produced by the bow-tie filter. When the ATCM mode for the Toshiba scanner was implemented, the doses in the anterior and posterior positions were reduced preferentially, bringing them closer to the doses in the lateral positions. The elliptical phantom will give a more realistic representation of the dose within the human trunk and has the potential to assess differences when ATCM is employed.

Results have shown that $D_L(0)$ reached an equilibrium value for L > 355 mm in the elliptical phantom confirming concerns that current CTDI measurements using a 100 mm pencil chamber and a 150 mm long phantom length significantly underestimate the total dose. Values of $\left(D_L(0)/D_{eq}\right)$ at the centre and periphery for each phantom could be used as correction factors in shorter phantoms to derive cumulative dose values.

9.2 Development and evaluation of phantoms of different designs for ATCM system tests

Evaluation of the CT ATCM system is important for routine quality control of CT scanners in order to manage patient dose and image quality. Two new phantom designs have been developed to evaluate CT ATCM performance. The concept of designing is to reflect the ATCM performance in varying dimensions along the possible length and based on the elliptical shape of the human body, with the length covering the equilibrium length of scan obtained from the first part of the project. The first torso phantom comprises five elliptical sections each with a wide range of different dimensions and the second of wedding cake phantom which has been developed from the results of the torso phantom has three sections that are more similar in size. The phantoms have been used to test ATCM systems for Philips, Siemens, GE and Toshiba scanners. The ImPACT conical phantom has been compared with two custom made phantoms.

Although the results of the tube current modulation patterns were similar for all CT scanners, the abrupt changes in attenuation for the torso phantom provoked an abnormal ATCM response for the GE and Toshiba scanners. The wedding cake phantom which was designed with a smaller number of broader sections and smaller differences in attenuation between sections was more effective for ATCM system testing and could be used for dose and image quality assessment in standard positions. However, the wedding cake phantom still has sharp discontinuities in attenuation although they are smaller, and use of narrow beam widths is recommended to avoid fluctuations in tube current and image noise at the section junctions. With the ImPACT conical phantom, there is no region of constant geometry therefore it is difficult to quantify performance in term of specific markers, but it provided the best overall assessment of performance in terms of tube current modulations and noise pattern.

9.3 CT optimisation of patient dose and image quality

In order to achieve the patient dose optimisation, as the final goal of the project, the analysis of patient dose and image noise data coupled with tests of factors affecting CT ATCM systems for CT scanners from four manufactures were

examined. The wedding cake phantom has been used to compare tube current modulation, dose and image noise from various protocol settings.

The results can be separated into two groups, Toshiba and GE scanners, and Siemens and Philips scanners. For the Toshiba and GE scanners, the image noise levels were constant for which wide ranges in tube current were set. These scanners had more variation in dose and gave larger doses for heavier patients. Setting of higher target noise for larger patients in protocols is recommended. The Philips and Siemens scanners had moderate correlations between the patient size and $CTDI_{vol}$. There were narrower ranges in tube current and $CTDI_{vol}$ for larger patients than for Toshiba scanners. The exception to this was the scanner using D-DOM for which there was a wider range in the tube current. In terms of the relationship between image noise and patient size, image noise values increased slightly with patient size. The scanner with a later version of ATCM software, showed less variations in the image noise, for the Philips scanner.

User selectable parameters such as image quality level, tube voltage (kVp), pitch factor, rotation time, slice thickness and reconstruction filter, within the range normally used clinically for CT CAP examinations, were varied and image quality factors (MTF and LCD) have been examined. The subsequent dose reduction was found for lower noise image quality option settings. The image noise was more constant in the ATCM compared with the fixed tube current technique. Selection of a lower tube current limit is likely to reduce doses for smaller patients in scans of chest and neck regions for the Toshiba scanner.

For the Toshiba scanner, changes in the image thickness for the first reconstruction and FC setting were the major factors affecting patient dose. A reduction in the slice thickness for the first reconstruction resulted in a higher tube current, and changes in every two step FC settings from smoother to sharper filters doubled the tube current. The increase of patient dose with the sharper filter is counterbalanced by an improvement in spatial resolution. The Philips and Siemens scanners, in contrast to the Toshiba, maintained tube current values similar to those used for a stored reference image, and the tube current and noise level varied only slightly for changes in individual CT scan parameters. The selection of sharper filters increased the image noise level for

these scanners. Scan parameters affecting patient dose and image quality on individual ATCM systems can be summarised in table 9-1.

Table 9-1 Summary of scan parameters affecting $CTDI_{vol}$ and image quality on ATCM systems of different CT manufacturers

Parameter	Direction of change	Toshiba		Philips		Siemens	
		$CTDI_{vol}$	IQ	$CTDI_{vol}$	IQ	$CTDI_{vol}$	IQ
Image quality	↑	↑	↑	↑	↑	↑	↑
Pitch factor	↓	↓	↓	↓	↓	↓	↓
	↑	↑	↔	↔	↔	↔	↔
Rotation time	↓	↓	↔	↔	↔	↔	↔
	↑	↑	↔	↔	↔	↔	↓
Slice thickness	↓	↓	↔	↔	↔	↔	↑
	↑	↓	↔				
Sharp kernel	↓	↑	↔				
	↑	↑	↔	↔	↑	↔	↑
Tube voltage	↓	↓	↔	↔	↓	↔	↓
	↑	↓	↔				
	↓	↑	↔				

Note: IQ = Image Quality
Image quality refers to image noise reduction

Key: ↑ Increase / Better
↓ Decrease / Worse
↔ No change

Knowing and understanding how CT scan parameter options affecting the ATCM system is extremely important for optimising radiation protection and image quality in order to maximize the benefit to risk ratio. Summary of strategies for dose and image quality optimisation for Toshiba, Philips and Siemens scanners is shown in figure 9-1.

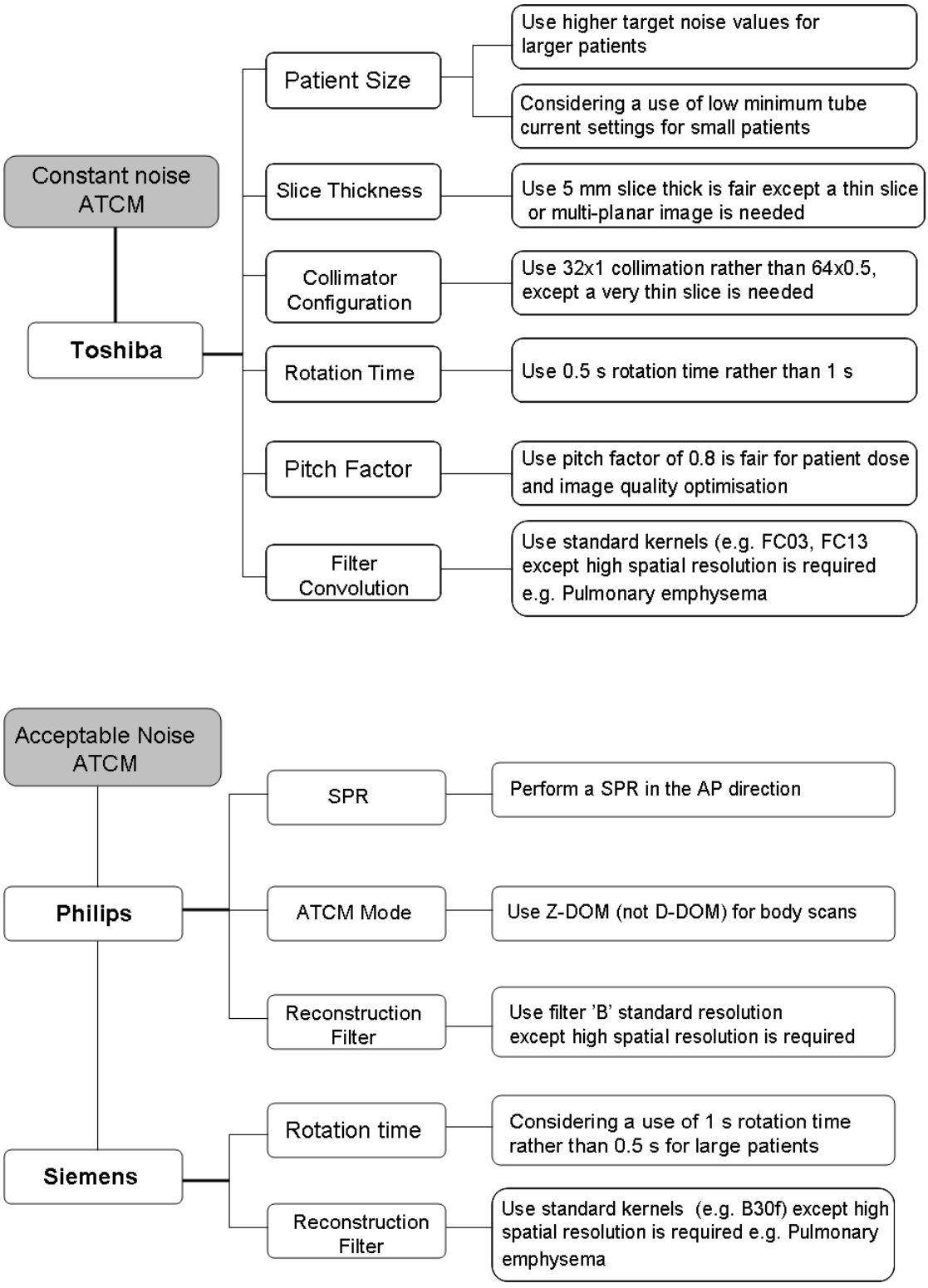

Figure 9-1 Summary of strategies for dose and image quality optimisation for constant noise and acceptable noise based ATCM systems

9.4 Future work

The conical shape phantom has proved better than the multi-elliptical sections in determining tube current and noise variation for investigation of ATCM performance. Contrast to noise ratio (CNR) is one of the image quality parameters used for interpretation of diagnostic image quality. Since the ATCMs aim to maintain a constant noise, it would be of interest to determine how the different manufacturer systems affect the CNR along the scan length.

Following on from this project, a modified conical phantom has been developed (figure 9-1). The concept of the design is to include an option for the image quality measurement of CNR, under ATCM. It consists of three conical sections; lower (largest), medium and upper (smallest) sections joined with a central tie bar. The phantom is 330 mm long with the individual sections each 110 mm long. The phantom is made from acrylic but the mounting bracket is made from acetal (delrin) and the nuts and screws are made from nylon. The individual lower and middle sections of the phantom contain four acrylic rods which are 20 mm in diameter positioned at 20 mm from each periphery side. The rods can be replaced by inserts of other materials. These materials can represent objects with different CT numbers and can be used to calculate the CNR. The different inserts are polypropylene (density 0.91 g/cm^3), nylon (density 1.1 g/cm^3), delrin (density 1.42 g/cm^3) and ultra high molecular weight polyethylene (UHMWPE) (density 0.94 g/cm^3). A phantom of this design will be used for comparison of responses for CT scanners from the four scanner manufacturers, it can also be used for comparisons of image quality for different CT scan protocols and image reconstruction techniques. Signal level and noise would be measured in preselected regions of interest in order to determine both the CNR and noise along the length of the phantom, using automated read-out systems.

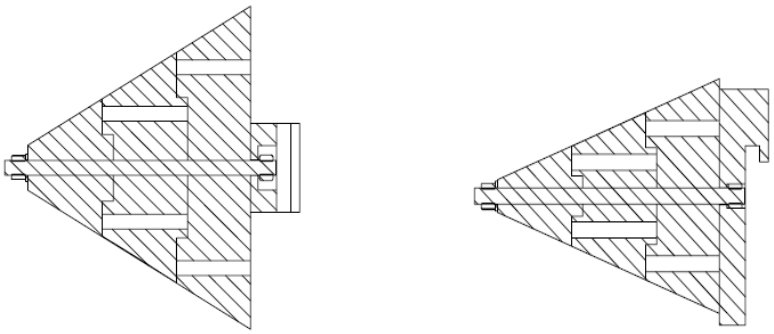

Figure 9-2 A modified conical phantom comprise of three sections and removable rods (a) top view and (b) side view

The torso and wedding cake phantoms developed in this project still have some flaws, especially when used for evaluation of the Toshiba and GE ATCM systems. The wedding cake phantom is suitable for measurement of dose variables at specific positions. However, an alternative phantom that could be used for dose measurements might be based on an elliptical conical shape coupled with a region of constant geometry for measurement of dose and image quality, avoiding sharp discontinuities in attenuation and air gaps. Any such phantom should cover the useful range of patient attenuations encountered routinely in clinical practice which includes those for human shoulder and body.

CT CAP is one of the more popular CT examinations. In most cases the clinical benefits of CT will outweigh the risks but patient dose optimisation should be carried out. From this study, reasons for the high patient doses in some CT CAP examinations in the West of Scotland have been determined. In order to implement changes in scanners having high doses, the appropriate levels of clinical image quality, especially noise settings have to be agreed with CT radiologists before changes to CT scanner protocols can be made. Since there are significant differences between scanners, it would be useful to obtain agreement on what was considered an ideal CAP protocol for a particular type of scanner. It would be good to start to set up a CT Optimisation Group with radiologists, radiographers, and medical physicists to discuss the approach and develop protocols, with input from CT applications specialists when required. After the implementation, the image quality should be assessed, dose audit undertaken, and the protocols reviewed periodically.

Appendix I: Diagrams of Phantoms

CTDI phantom

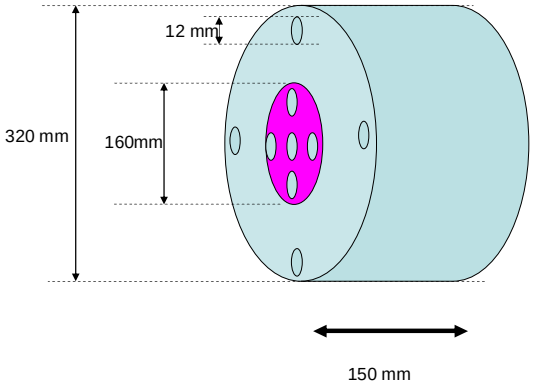

Overview : Head Phantom is fitted in to form the body phantom

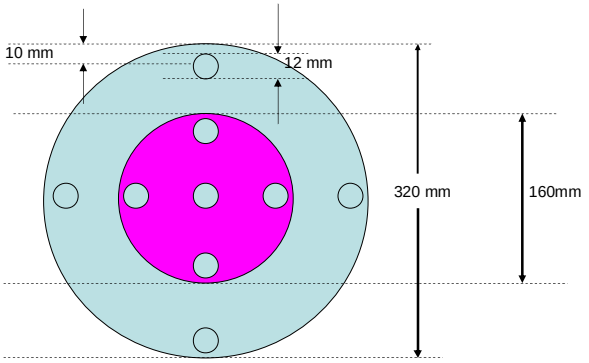

All 9 holes are 12 mm. in diameter;

- 4 holes of Body Phantom
- 5 hole of Head Phantom

Section View of Phantoms

Side view: when head phantom is fitted in

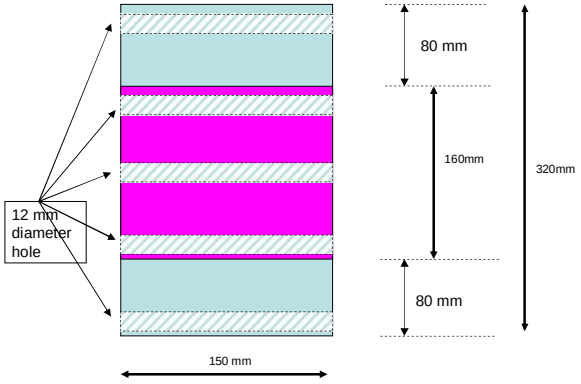

Cylindrical Phantom

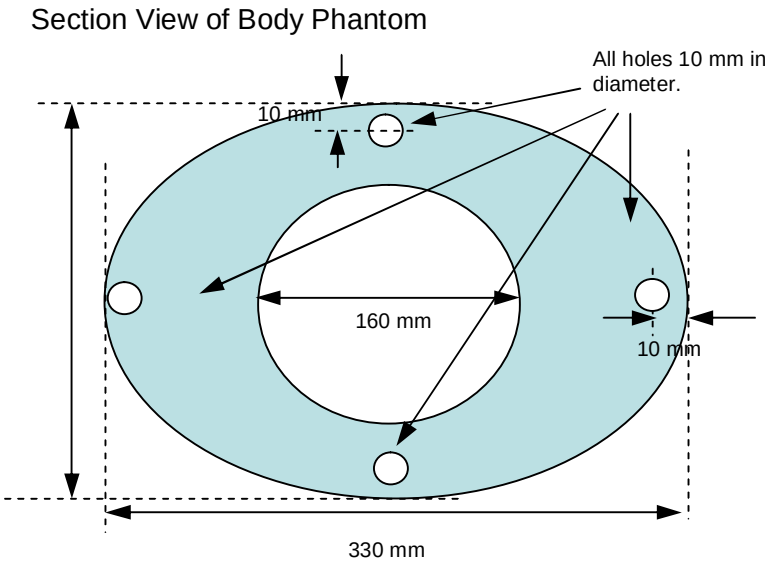

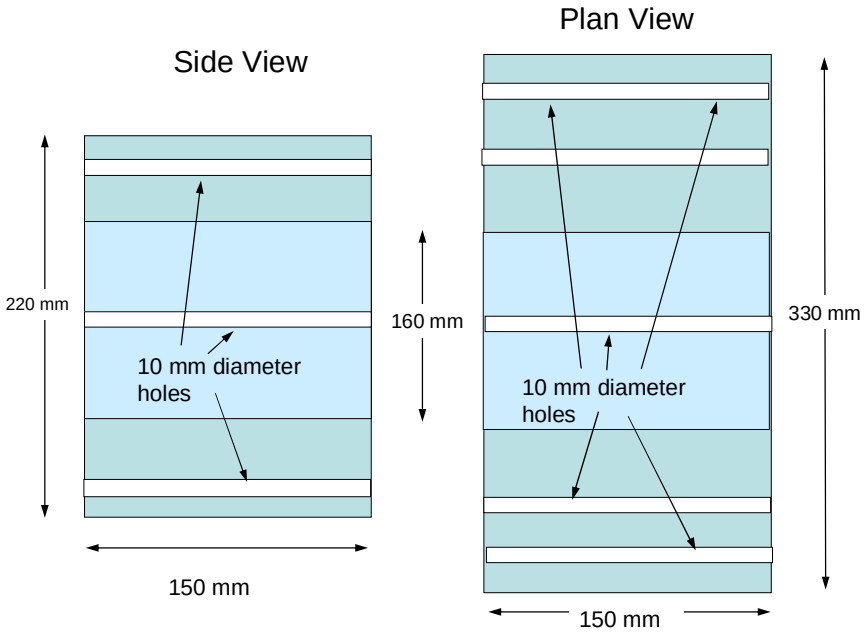

Elliptical Phantom

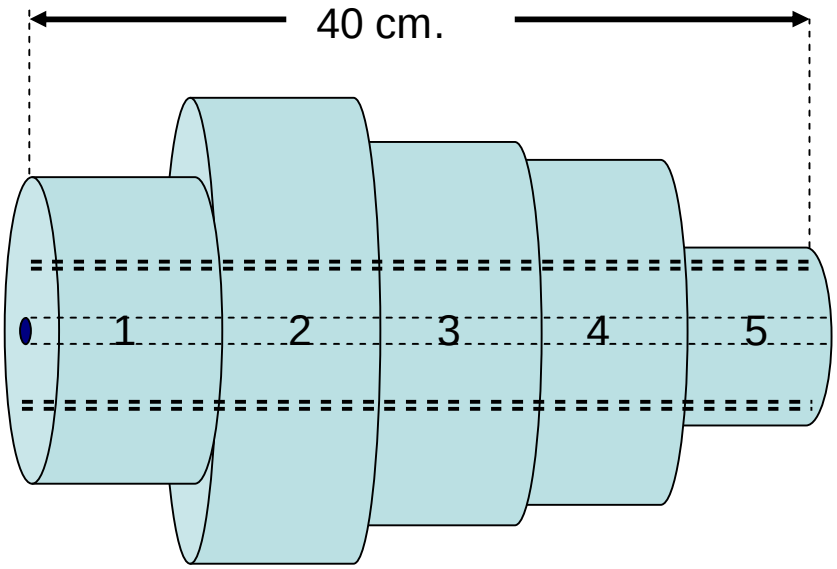

Section 1

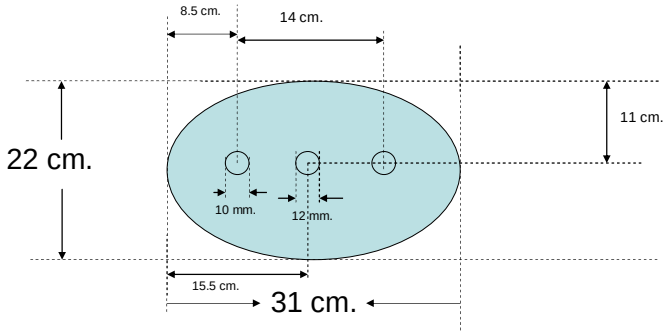

22 x 31 x 8 cm.

Section 2

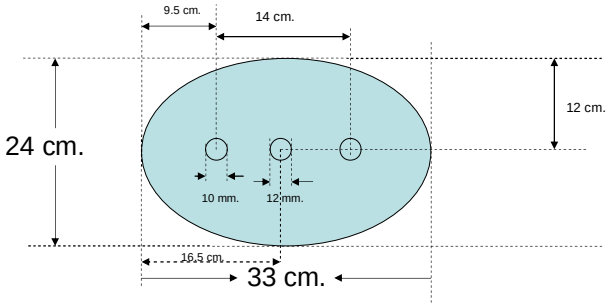

24 x 33 x 8 cm.

Torso Phantom

Section 3

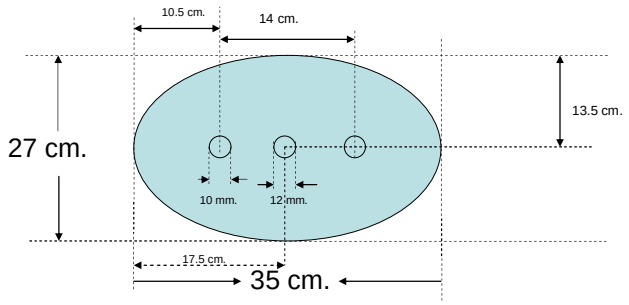

27 x 35 x 8 cm.

Section 4

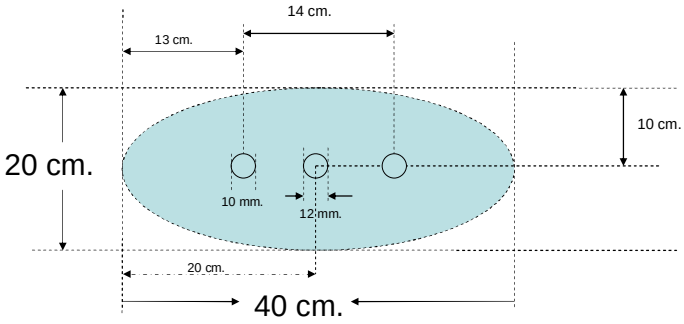

20 x 40 x 8 cm.

Section 5

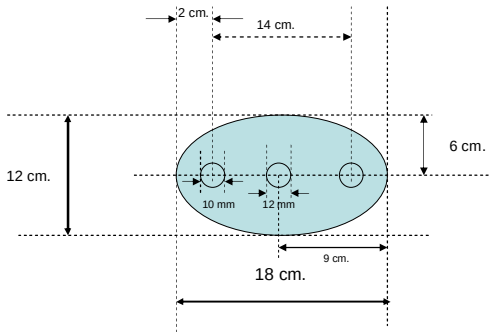

12 x 18 x 8 cm.

Torso Phantom

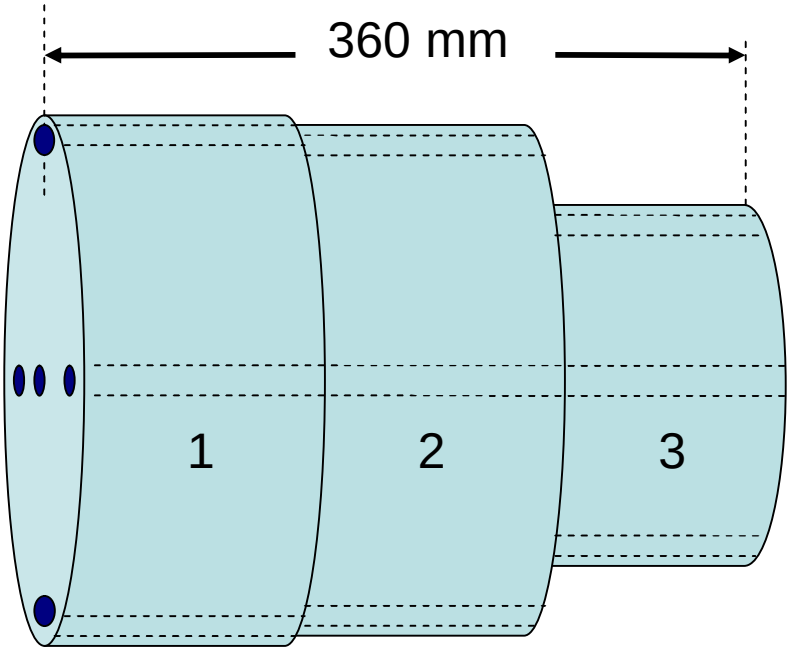

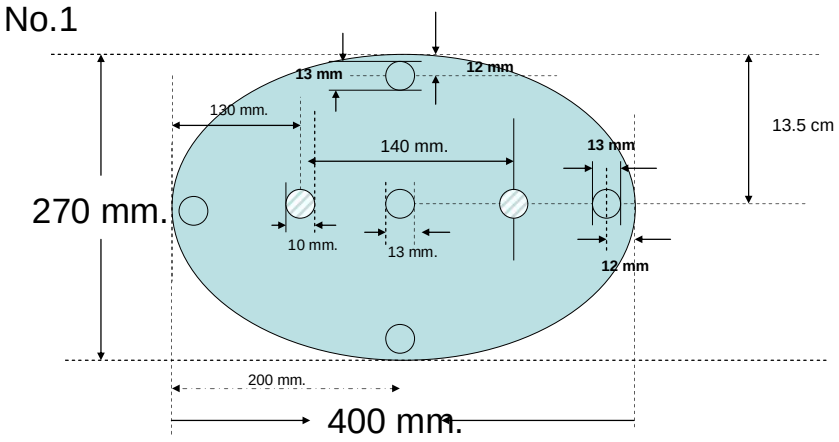

270 x 400 x 120 mm.

Wedding Cake Phantom

No.2

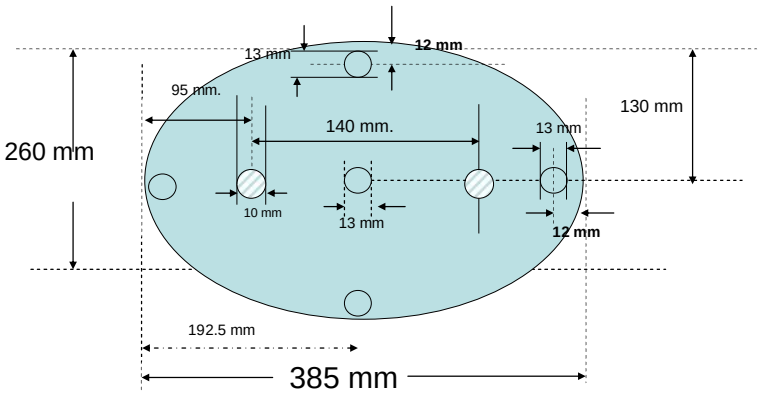

260 x 385 x 120 mm

No.3

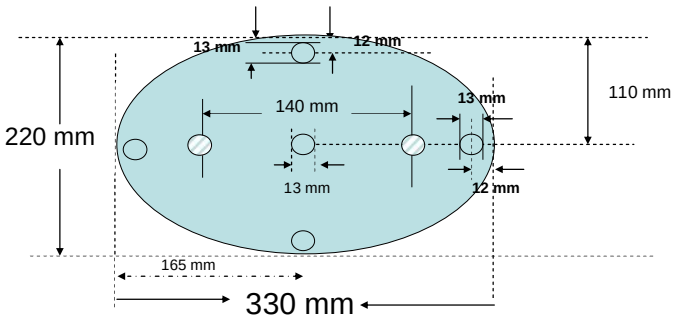

220 x 330 x 120 mm

Wedding Cake Phantom

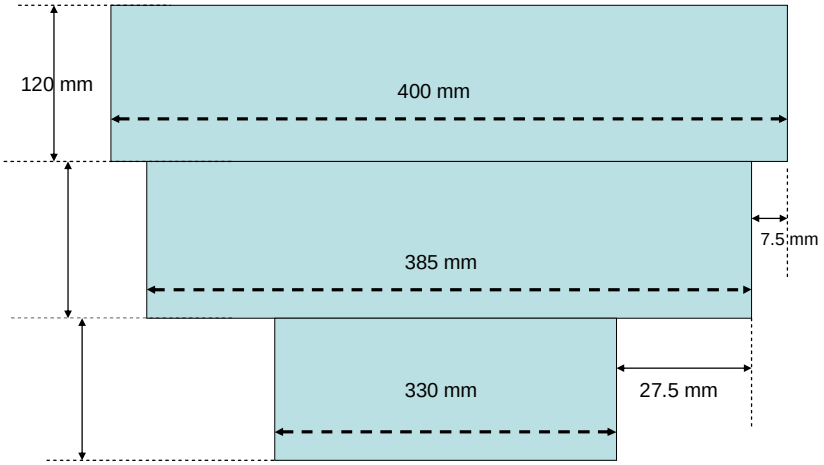

Top View

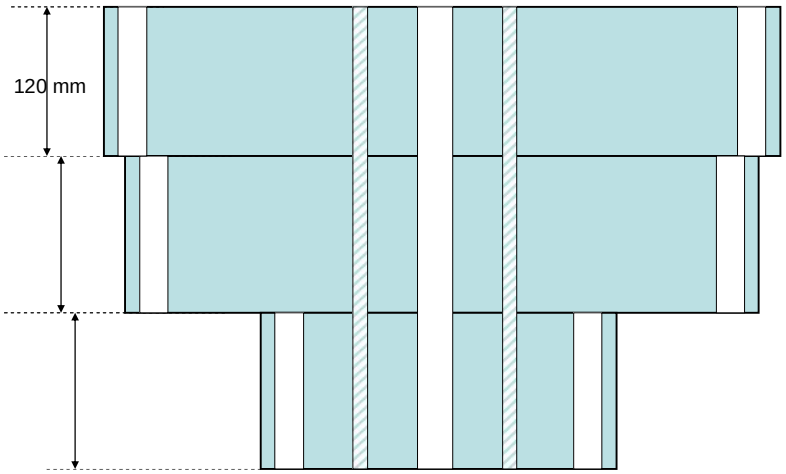

Top View

Wedding Cake Phantom

Appendix II: Calibration of Gafchromic film

HP-IRCAL-PROC-012	NHS Greater Glasgow and Clyde
Calibration of GafChromic Film	

Health Physics

PROCEDURE

CALIBRATION OF GAFCHROMIC FILM

SCOPE

This protocol covers the calibration of GafChromic film for use in CT dosimetry and measurements of patient entrance skin dose in interventional radiology.

EQUIPMENT

Gulmay superficial therapy unit using D3000 controller
Radcal dosemeter (6 cc chamber)
2 cm x 2 cm squares of GafChromic film; will usually 16 squares per calibration
4 x 1mm Al sheets
Clamp stand, boss and clamp
Sellotape
Foam blocks to rest film on at height of mid-chamber

PROCEDURE

1. Book machine a few days in advance at BWoSCC.

2. A formal handover using the relevant documentation should be carried with Radiotherapy Physics staff.

3. At handover it should be determined when the unit was last used. If the unit has not been used within the last few hours a 17-minute warm-up with a lead filter will be required.

4. In order to operate the Gulmay unit it is necessary to shut down and switch off the PC adjacent to the Gulmay control panel. If uncertain seek a member of Radiotherapy staff to assist with this.

5. if the. It may be necessary to run the D3000 controller with the verification system and then switch the unit back on without the verification system. A.

6. If a warm up has been necessary, replace the lead filter with the Al filter (filter 3). Additional filtration (as detailed below) can then be taped to the end of the cone.
   For CT film calibrations, add 4mm Al sheets to match the HVL of most CT units at 110 kV.
   For interventional radiology patient entrance dose film calibrations, add a 1mm Al sheet to simulate interventional radiology unit filtration at 70kV.

7. Insert the appropriate applicator into the unit using the insertion lever to the side of the slot e.g. use applicator G (100mm diameter circular, 200mm FSD). Again, if uncertain of how to attach the applicator seek a member of Radiotherapy staff to assist with this.

8. **For CT calibration**, use the clamp stand to position the ionisation chamber at some distance from the X-ray tube focus and at a height of 20cm from any scattering material.
For skin dose calibrations, position the chamber 15-20cm from the cone and 15-20cm above the couch.

9. Last Man Out button must be pressed on leaving the treatment room to enable the exposure.

10. Set up the RadCal controller with its display reading under the CCTV camera in the room. There is a screen at the radiographers' station where you can move the camera to a position where the display will be visible.

11. Determine the monitor units (MU) required to deliver the desired doses.
For CT calibrations, exposing the film to the following doses is recommended: 1, 2, 5, 10, 25, 50, 80, 100, 150, 200, 250 and 300mGy.
For skin dose calibrations, much higher doses will be required; the following approximate doses are recommended: 0.25, 0.5, 1, 2, 3.5 and 5.5Gy

12. Sit the film on foam cushions as close to the chamber as possible at the height of the centre of the chamber. Ensure they will intercept the beam.

13. Long exposure times will be required to deliver the doses required for the skin dose film calibrations, so it will be more efficient to expose several films at a time by surrounding the chamber with the film pieces. Remove each piece of film when it has been exposed to the desired cumulative dose.

14. To carry out an exposure:
    1. Select filter in use with the up and down arrows on the control panel
    2. Confirm
    3. Select applicator
    4. Confirm
    5. Press exposure button
    6. Use key-pad to enter the number of monitor units required
    7. Confirm
    8. Turn key
    9. Press green 'X-ray On' button

15. The dose delivered to each piece of film should be recorded and the films marked on the back for identification. Do not mark the rear of the film too heavily, as this may affect the optical density when the film is scanned.

16. When the work is complete, make sure the filter is returned to a location agreed with the Radiotherapy Physics staff. The lead warm-up filter should be re-inserted in the machine so the equipment is ready for the morning warm-up procedure.

17. Remove the key and return it to the appropriate member of staff.

ANALYSIS OF CALIBRATION RESULTS AND MEASUREMENT OF FILM DOSES IN IMAGEJ

1. Leave the films overnight before they are scanned in order for the optical density to reach equilibrium values.

2. Scan the film on the Epson Perfection Scanner. The scanning software is installed on DR, GS and CP's computers.

3. The settings on the Epson scanner should be Photo, 75dpi, .tif format.

4. Save to the relevant location on P:drive.

5. On your computer, start up ImageJ from the Start Menu and you will be prompted to open an image.

6. Your image will appear surrounded by a red border.

7. Go to Image -> Colour -> Split Channels and three new images will appear in red, green and blue. Close the blue and green images and use the red image to make red pixel value measurements.

8. Cross-hairs will appear as the mouse cursor when you hover over the image. Click and drag to create rectangular regions of interest over the film squares.

9. To obtain the red pixel value for your region of interest, press Ctrl+M. A results window will appear, showing: area of ROI, mean, std dev, max and min. Move the ROI with your mouse to another section of the image (or create a new ROI). You can add to the first measurement results by pressing Ctrl+M over the next ROI, and so on. The results in the Results Window can be copied and pasted into a spreadsheet if preferred, or you can just note the mean values.

10. Plot pixel values and/or optical density (see step 11) against known exposed dose. These will form your calibration curves, from which you can read a dose value for an exposed film, when you measure its red pixel value and/or optical density.

11. You can calculate optical density for a particular region of interest by comparing the red pixel value from that region to the red pixel value of the unexposed film. The formula is: $OD = \log_{10}(RPV_{unexposed}/RPV_{exposed})$.

Appendix III: Ethical review by west of Scotland research ethics service

WoSRES
West of Scotland Research Ethics Service

NHS
Greater Glasgow and Clyde

West of Scotland Research Ethics Service
Ground Floor – The Tennent Institute
Western Infirmary
38 Church Street
Glasgow G11 6NT

Dr Colin J Martin
Head of Health Physics
Department of Clinical Physics and Bio-engineering
West House
Gartnavel Royal Hospital
1055 Great Western Road
Glasgow
G12 0XH

Date	09 March 2011
Your Ref	
Our Ref	WoS ASD 549
Direct line	0141 211 2126
Fax	0141 211 1847
E-mail	Judith.Godden@ggc.scot.nhs.uk

Dear Dr Martin

Full title of project: Analysis of CT patient dose data for the purpose of optimisation

You have sought advice from the West of Scotland Research Ethics Service Office on the above project. This has been considered by the Scientific Officer and you are advised that it does not need ethical review under the terms of the Governance Arrangements for Research Ethics Committees (REC) in the UK. The advice is based on the following.

- The project is an audit using only data obtained as part of usual care but note the requirement for Caldicott Guardian approval to permit sharing or publication of anonymised data obtained from patient under the care of NHS Scotland

If during the course of your project the nature of the study changes and starts to generate new knowledge and thereby inadvertently becoming research then the changing nature of the study would necessitate REC review at that point, before any further work was undertaken. A REC opinion would be required for the new use of the data collected.

Note that this advice is issued on behalf of the West of Scotland Research Ethics Service Office and does **not** constitute a favourable opinion from a REC. It is intended to satisfy journal editors and conference organisers and others who may require evidence of consideration of the need for ethical review prior to publication or presentation of your results.

However, if you, your sponsor/funder or any NHS organisation feels that the project should be managed as research and/or that ethical review by a NHS REC is essential, please write setting out your reasons and we will be pleased to consider further.

Where NHS organisations have clarified that a project is not to be managed as research, the Research Governance Framework states that it should not be presented as research within the NHS. This letter has been copied to NHS Greater Glasgow & Clyde R&D Department for their information.

Kind regards

Dr Judith Godden
WoSRES Scientific Officer/Manager

List of References

AAPM Task Group 2010 Report No. III A new measurement paradigm based on a unified theory for axial, helical, fan-beam and cone beam scanning with or without longitudinal translation of the patient table. In: *Comprehensive methodology for the evaluation of radiation dose in x-ray computed tomography*: American Association of Physicists in Medicine)

AAPM TaskGroup 2011 AAPM Report No.204 Size-specific dose estimates (SSDE) in pediatric and adult body CT examination

Akbari S M, Ay M R, Kamali A R, Ghadiri H and Zaidi H 2010 Experimental Measurement of Modulation Transfer Function (MTF) in Five Commercial CT Scanners. XII Mediterranean Conference on Medical and Biological Engineering and Computing 2010, IFMBE Proceedings 29 351-4

Alnawaf H, Butson M, Cheung T and Yu P K 2010a Scanning orientation and polarization effects for XRQA radiochromic film *Phys Med* **26** 216-9

Alnawaf H, Cheung T, Butson M J and Yu P K 2010b Absorption spectra response of XRQA radiochromic film to x-ray radiation *Radiation Measurements* **45** 129-32

Amis E S, Butler P F, Applegate K E, Birnbaum S B, Brateman L F, Hevezi J M, Mettler F A, Morin R L, Pentecost M J, Smith G G, Strauss K J and Zeman R K 2007 American College of Radiology White Paper on Radiation Dose in Medicine *J Am C Radiol* **4** 272-84

Angel E 2009 Sure Exposure: Low dose diagnostic image quality [Brochure]

Barrett J F and Keat N 2004 Artifacts in CT: recognition and avoidance. *RadioGraphics* **24:** 1679-91

Bateman L and Hiles P 2008 A simple anthropomorphicphantom used to demonstrate the effectiveness of CT dose modulation functions [online] Available at <http://www.ctug.org.uk/meet08-10-21/A%20simple%20anthropomorphic%20phantom%20used%20to%20demonstrate%20effectiveness%20of%20CT%20dose%20modulation%20functions.pdf> (Accesses December 8, 2012)

Bateman L, Hiles P and Jones S 2012 New tools for new scanners- bringing physics testing into the 21st century[online] Available at https://www.dropbox.com/sh/hsjz8btj7dop0hv/bPzxfn1Z-n/Wednesday/E7%20Developments%20in%20CT%20dosimetry%20%26%20phantoms/E7%20Lynn%20Bateman.pdf(Accesses June 8, 2013)

Berrington G A, Mahesh M, Kim K P, Bargavan M, Lewis R, Mettler F and Land C 2009 Projected cancer risks from computed tomographic scans performed in the United States in 2007 *Archieves of Internal Medicine* **169** 2071-7

Boedeker K 2010 Noise reduction tools: Saving dose with QDS and Boots 3D [Brochure] Toshiba Medical Systems

Boivin J, Tomic N, Fadlallah B, DeBlois F and Devic S 2011 Reference dosimetry during diagnostic CT examination using XR-QA radiochromic film model *Med Phys* **38** 5119-29

Bongartz G, Golding S J, Jurik A G, Leonardi M, Meerten E v P v, Rodríguez R, Schneider K, Calzado A, Geleijns J, Jessen K A, Panzer W, Shrimpton P C and Tosi G 2004 European Guidelines for Multislice Computed Tomography [online] Available at http://www.msct.eu/PDF_FILES/Technical%20principles%20of%20MSCT.pdf (Accesses December 5, 2011)

Boone J M 2007 The trouble with CTDI100 *Med. Phys* **34** 1364-71

Bredenholler C and Feuerlein U Siemens medical proto-col, principles and helpful hints Softwere Version Syngo2006, Siemens AG, 2005.

Brenner D J, McCollough C H and Orton C G 2006 It is time to retire the computed tomography dose index (CTDI) for CT quality assurance and dose optimisation *Med Phys* **33** 1189-91

Brooks R A and Chiro G D 1976 Statistical limitations in x-ray reconstructive tomography *Med Phys* **3** 237-40

Bruesewitz M R, Yu L, Vrieze T J, Kofler J M and McCollough C H 2008 Smart mA-Automatic exposure control (AEC): Physics principle and practical hints [online document] Available at http://mayoresearch.mayo.edu/mayo/research/ctcic/upload/rsna2008-smart-ma.pdf (Accessed: January 10, 2012)

Castellano E 2013 Dose audit - size matters [Presentation to Optimisation in CT, London] October 4, 2013

DeLean A, Munson P and Rodbard D 1978 Simultaneous analysis of families of sigmoidal curves: application to bioassay, radioligand assay, and physiological dose-response curves *Am J Physiol* **235** 97-102

Denaro M d and Bregant P 2011 Dosimetric evaluation of a 320 detector row CT scanner unit *Radiology and Oncology* **45** 64-7

Dendy P P and Heaton B 2012 Tomographic imaging with X-rays, Physics for Diagnostic Radiology, Third Edition, 2012 CRC press Taylor &Francis Group, LLC, NW USA

Devic S 2011 Radiochromic film dosimetry: Past, present, and future *Phys Med* **27** 122-34

Dixon R L 2003 A new look at CT dose measurement: Beyond CTDI *Med Phys* **30** 1272-80

Dixon R L 2006 Restructuring CT dosimetry - a realistic strategy for the future requiem for the pencil chamber *Med Phys* **33** 3973-9376

Dixon R L and Ballard A C 2007 Experimental validation of a versatile system of CT dosimetry using a conventional ion chamber: Beyond CTDI100 *Med Phys* **34** 3399-413

Dixon R L, Munley M T and Bayram E 2005 An improved analytical model for CT dose simulation with a new look at the theory of CT dose *Med Phys* **32** 3712-28

Edyvean S 2004 Effects of ROI size on image noise [online] Available at <http://www.ctug.org.uk/meet04-01-13/roisizeimagenoise.pdf>(Accessed: September 8, 2013)

Edyvean S, Lewis M A, Keat N and Jones A P 2003 Measurement of the performance characteristics of diagnostic X-ray system used in medicine Part III : Computed tomography X-ray scanners (2 nd ed). York: York publisher

Ferreira T and Rasband W 2011 The ImageJ User Guide - Version 1.44 U. S. National Institutes of Health, Bethesda, Maryland, USA.

Field E 2010 Comparison of the function and performance of CT AEC systems. Twelfth CT users group meeting [online] Available at http://www.ctug.org.uk/meet10-10-14/Comparison%20of%20the%20function%20and%20performance%20of%20CT%20AEC%20systems.pdf (Accesses December 8, 2011)

Fisher R F 2006 Tissue equivalent phantoms for evaluating in-plane tube current modulated CT dose and image quality: Unpublished MSc Thesis, University of Florida

Flohr T 2012 CARE Dose4D Real-time Anatomic Exposure Control.

Geleijns J, Artells M S, Bruin P W d, Mather R, Muramatsu Y and McNitt-Gray M F 2009 Computed Tomography dose assessment for a 160 mm wide, 320 detector row, cone beam CT scanner *Phys. Med. Biol.* **54** 3141-59

GeneralElectricCompany 2008 GE Healthcare TiP Training in Partnership [Brochur] Available at http://www.gobookeee.com (Accessed October 10.2012)

Giaddui T, Cui Y, Galvin W, Yu Y and Xiao Y 2012 Characteristics of Gafchromic XRQA2 films for kV image dose measurement *Med Phys* **39** 842-50

Giles E R and Murphy P H 2002 Measuring skin dose with radiochromatic density film in the cardiac catheterisation laboratory *Health Physics* **82** 875-80

Goldman L W 2007 Principles of CT: Radiation Dose and Image Quality *J Nucl Med Technol* **35** 213-25

Goldman L W 2008 Principles of CT: Multislice CT *J Nucl Med Technol* **36** 57-68

Goo H W and Suh D 2006 The influences of tube voltage and scan direction on combined tube current modulation: a phantom study *Pediatr Radiol* **36** 833-40

Gorny K R, Leitzen S L, Bruesewitz M R, Kofler J M, Hangiandreou N J and McCollough C H 2005 The Calibration of experimental self-developing Gafchromic HXR film for the measurement of radiation dose in computed tomography *Med Phys* **32** 1010-6

Gudjónsdóttir J, Ween B and Olsen D 2010 Optimal use of AEC in CT: a literature review *Radiol Technol* **81** 309-17

Guibelalde E, Vano E, Gonzalez L, Prieto C, ernandez F J M and Ten J I 2003 Practical aspects for the evaluation of skin doses in interventional cardiology using a new slow film *Br J Radiol* **76** 332-6

Gutierrez D, Schmidt S, Denys A, Schnyder P, Bochud FO,Verdun FR 2007 CT-automatic exposure control devices: What are their performances? Nuclear Instruments and Methods in Physics Research Section A: Accelerators, Spectrometers,Detectors and Associated Equipment **580** 990–5

Hall E J and Brenner D J 2008 Cancer risks from diagnostic radiology *Br J Radiol* **81** 362-78

Hart D, Wall B F, Hillier M C and Shrimpton P C 2010a Frequency and collective dose for medical and dental X-Ray examinations in the UK 2008. In: *Report HPA-CRCE-012,* (Chilton: HPA)

Hart D, Wall B F, Hillier M C and Shrimpton P C 2010b HPA-CRCE-012 Frequency and collective dose for medical ans dental X-Ray examinations in the UK 2008. Health Protection Agency)

Hendee W R and Ritenour E R 2003 Computed Tomography, in Medical Imaging Physics, Fourth Edition, John Wiley & Sons, Inc., New York, USA.

Hiles P, Bateman L and Jones S 2011 Testing CT AEC systems with a purpose built object. (Abstract) European medical physics and engineering conference 2011

Hou Y, Liu X, Xv S, Guo W and Guo Q 2012 Comparisons of Image Quality and Radiation Dose Between Iterative Reconstruction and Filtered Back Projection Reconstruction Algorithms in 256-MDCT Coronary Angiography *Am J Roentenol* **199** 588 - 94

Huda W, Ogden K M and Korasani M R 2008 Converting dose-length product to effective dose at CT *Radiology* **248** 995-1003

Huda W and Mettler F 2011 Volume CT dose index and dose-length product displayed during CT: what good are they? *Radiology* **258** 236-42

Iball G 2013 mA modulation-What the patient gets [Presentation to Optimisation in CT , London] October 4, 2013

ImageOwl 2013 Image Owl Catphan® QA [Computer Program] Available at http://catphanqa.imageowl.com/ (Accessed: August 1, 2013)

ImPACT 2002 Technology Update No.1, 2nd Edition Multi-Slice CT Scanners

ImPACT 2009 *Comparative specifications 64 slice CT scanners* (London: Crown publisbling)

International Electrotechnical Commission (IEC) 2003 Medical Electrical Equipment Part 2-44. Particular requirements for the safety of X-ray equipment for computed tomography. IEC Standard 6061-2-44 Ed. 2 Amendment 1. (Geneva, Switzerland: IEC)

Israel G M, Cicchiello L, Brink J and Huda W 2010 Patient size and radiation exposure in thoracic, pelvic and abdominal CT examinations performed with automatic exposure control *Am J Roentenol* **195** 1342-6

Israel G M, Herlihy S, Rubinowitz A N, DCornfeld and Brink J 2008 Does a combination of dose modulation with fast gantry rotation time limit CT image quality? *Am J Roentgenol.* **191** 140-4

Joseph N and Rose T 2013 Quality Assurance and the Helical (Spiral) Scanner. Online Radiography Continuing Education for Radiologic X ray Technologist. [online] Available at <http://www.ceessentials.net/article33.html>(Accessed: September 8, 2013)

Kalender W A 2005 *Computed Tomography Fundamentals, System Technology, Image Quality, Applications* (Erlangen: Publicis Corporate Publishing)

Kalra M, Maher M, Toth T, Kamath R, Halpern E and Saini S 2004a Comparison of Z-axis automatic tube current modulation technique with fixed tube current CT scanning of abdomen and pelvis. *Radiology* **232** 347-53

Kalra M, Maher M, Toth T, Schmidt B, Westerman B, Morgan H and Saini S 2004b Techniques and applications of automatic tube current modulation for CT. *Radiology* **233** 649-57

Kalra M K and Brady T J 2006 CARE Dose4D New Techniques for Radiatioon Dose Reduction, Article from the customer magazine SOMATOM Session 19 [online] Available at http://www.medical.siemens.com/siemens/de_DE/rg_marcom_FBAs/files/news/CT_Dose_Reduction/DoseReduction_Sessions_19_RSNA_DRUCK.pdf

Kalra M K, Maher M M, Toth T L, Hamberg L M, Blake M A, Shepard J-A and Saini S 2004c Strategies for CT Radiation Dose Optimisation *Radiology* **230** 619-27

Kanal K M, Stewart B K, Kolokythas O and Shuman W P 2007 Impact of Operator-Selected Image Noise Index and Reconstruction Slice Thickness on Patient Radiation Dose in 64-MDCT *Am J Roentenol* **189** 219-25

Keat N 2005a Comparison of assessment techniques for CT scanner spatial resolution measurement [online] Available at <http://www.ctug.org.uk/meet05-10-06/assessment_techniques_ct_spatial_resolution.pdf> (Accessed: September 8, 2013)

Keat N 2005b Helical and multi slice principles, ImPACT Course October 2005 Programme, [online] Available at <http://www.impactscan.org/slides/impactcourse/helical_and_multi-slice_principles/img0.html> (Accessed: September 16, 2012)

Keat N 2006 Automated dose control in multi-slice CT [PowerPoint slides] Available at <http://www.impactscan.org/slides/ukrc2006/ukrc06_nk.pdf> (Accessed: September 16, 2012)

Keat N, Aplin M, Edyvean S, Platten D and Lewis M 2005 Assessment of automatic exposure control systems on CT scanners using a custom made phantom Available at http://www.ctug.org.uk/meet04-10-14/ct_aec_assessment.pdf<http://www.impactscan.org/slides/ukrc2006/ukrc06_nk.pdf> (Accessed: September 16, 2012)

Kulama E 2004 Scanning protocols for multislice CT scanners *Br J Radiol* **77** S2-S9

Kyriakou Y, Deak P, Langner O and Kalender W A 2008 Concepts for dose determination in flat-detector CT *Phys. Med. Biol.* **53** 3551-66

Lee C, Goo J, Ye H, Ye S, Park C, Chun E and Im J 2008 Radiation dose modulation techniques in the multidetector CT era: from basics to practice. *Radiographics* **28** 1451-9

Lee E, Lee S, Agid R, Howard P, Bae J and terBrugge K 2009 Comparison of image quality and radiation dose between fixed tube current and combined automatic tube current modulation in craniocervical CT angiography *Am J Neuroradio* **30** 1754-9

Lee S, Yoon S-W, Yoo S-M, Ji Y G, Kim K A, Kim S H and Lee J T 2011 Comparison of image quality and radiation dose between combined automatic tube current modulation and fixed tube current technique in CT of abdomen and pelvis. *Acta Radiologica*

Li X, Samei E, Williams C H, Segars W P, Tward D J, Miller M I, Ratnanather J T, Paulson E K and Frush D P 2012 Effects of protocol and obesity on dose conversion factors in adult body CT *Med. Phys* **39**

Lois R 2013 CT image quality [online] Available at <http://www.cewebsource.com/coursePDFs/CTimageQuality.pdf>(Accessed: September 8, 2013)

Mahesh M 2009 MDCT Physics: The basics-Technology, Image quality and radiation dose

MATLAB version 7.8.0. Natick, Massachusetts: The MathWorks Inc., 2009.

Martin C, Gentle D, Sookpeng S and Loveland J 2011 Application of Gafchromic film in the study of dosimetry methods in CT phantoms. *J. Radiol. Prot.* **31** 389-409

Martin C J 2008 Radiation Dosimetry for Diagnostic Medical Exposures *Radiat Prot Dosim* **128** 389-412

McCollough C H, Leng S, Yu L, Cody D D, Boone J and McNitt-Gray M F 2011 CT Dose Index and Patient Dose: They Are Not the Same Thing *Radiology* **259** 311-6

McCollough C H, Primak A N, Braun N, Kofler J, Yu L and Christner J 2009 Strategies for Reducing Radiation Dose in CT *Radiol Clin North Am* **47** 27-40

McNitt-Gray M F, Cagnon C H, Solberg T D and Chetty I 1999 Radiation dose in spiral CT: The relative effects of collimation and pitch *Med. Phys.* **26** 409-14

McNitt-Gray M F 2013 Tradeoffs in CT Image Quality and Radiation Dose [online] Available at <http://www.aapm.org/meetings/04AM/pdf/14-2328-89141.pdf> (Accessed: September 16, 2012)

Meeson S, Alvey C M and Golding S J 2010 The in vivo relationship between cross-sectional area and CT dose index in abdominal multidetector CT with automatic exposure control *J. Radiol. Prot.* **30** 139-47

Morgan H T and Luhta R 2004 Beyond CTDI dose measurement for modern CT scanners *Med Phys* **31** 1842

Mori S, Endo M, Nishizawa K, Tsunoo T, Aoyama T, Fujiwara H and Murase K 2005 Enlarged longitudinal dose profiles in cone-beam CT and the need for modified dosimetry *Med Phys* **32** 1061-9

Mori S, Nishizawa K, Ohno M and Endo M 2006 Conversion factor for CT dosimetry to assess patient dose using a 256-slice scanner *Br. J. Radiol.* **79** 888-92

Morin R L 2004 Computed Tomography Quality Control; Department of Radiology. Mayo Clinic. Jacksonville 3-23

Morrell R E and Rogers A T 2004 A calibration of Kodak EDR2 film for patient skin dose assessment in cardiac catheterisation procedures *Phys. Med. Biol.* **49** 5559-70

Muramatsu Y, Ikeda S, Osawa K, Sekine R, Niwa N, Terada M, Keat N and Miyazaki S 2007 Performance evaluation for CT-AEC(CT automatic exposure control)systems, Pubmed [Article in Japanese]

Nagel H D 2007 *CT Parameters that Influence the Radiation Dose : Radiation Dose from Adult and Pediatric Multidetector Computed Tomography*: Springer Berlin Heidelberg)

Nakonechny K D, Fallone B G and Rathee S 2005 Novel methods of measuring single scan dose profiles and cumulative dose in CT *Med Phys* **32** 98-109

Nicolai C 2009 Measure Track [Computer Program]. Available from http://rsbweb.nih.gov/ij/plugins/measure-track/index.html (Accessed February 9, 2012)

Nievelstein R A J, Dam I M v and Molen A J v d 2010 Multidetector CT in children: current concepts and dose reduction strategies *Pediatr Radiol* **40** 1324–44

Olsson M-L and Norrgren K 2012 An investigation of the iterative reconstruction method iDose(4) on a Philips CT Brilliance 64 using a Catphan 600 phantom In: *Conference on Medical Imaging - Physics of Medical Imaging* (San Diego, CA SPIE-Int Soc Optical Engineering)

Papadakis A, Perisinakis K and Damilakis J 2008 Automatic exposure control in pediatric and adult multidetector CT examinations: a phantom study on dose reduction and image quality. *Med Phys* **35** 4567-76

Peng Y, Li J, Ma D, Zhang Q, Liu Y, Zeng J and Sun G 2009 Use of automatic tube current modulation with a standardized noise index in young children undergoing chest computed tomography scans with 64-slice multidetector computed tomography. *Acta Radiologica* **50** 1175-81

Perisinakis K, Damilakis J, Tzedakis A, Papadakis A, Theocharopoulos N and NGourtsoyiannis 2007 Determination of the weighted CT dose index in modern multi-detector CT scanners *Phys. Med. Biol.* **52** 6485-95

Peter T 2002 CT Image Reconstruction American Association of Physicists in Medicine - 44th Annual Meeting.

PhilipsMedicalSystems 2008 Clinical Guide: Z Axis Dose Modulation (Z DOM)) [online document] Available at http://clinical.netforum.healthcare.philips.com/us_en/Operate/Application-Tips/CT/Z-Axis-Dose-Modulation-(Z-DOM) (Accessed: January 10, 2012)

Philips Medical Systems 2011 iDose4 iterative reconstruction technique: Breakthrough in image quality and dose reduction with the 4th generation of reconstruction [online document] Available at http://www.healthcare.philips.com/pwc_hc/main/shared/Assets/Documents/ct/idose_white_paper_452296267841.pdf (Accessed: January 4, 2013)

Rampado O, Garelli E, Deagostini S and Ropolo R 2006 Dose and energy dependence of response of Gafchromic XR-QA film for kilovoltage x-ray beams *Phys. Med. Biol.* **51** 2871-81

Rampado O, Garelli E and Ropolo R 2010 Computed tomography dose measurements with radiochromic films and a flatbed scanner *Med. Phys* **37** 189-96

Rego S L, Yu L, Bruesewitz M R, Vrieze T J, Kofler J M and McCollough C H 2007 CareDose 4D CT Automatic exposure control (AEC): Physics principle and practical hints [online document] Available at http://mayoresearch.mayo.edu/mayo/research/ctcic/upload/rsna2007-care-dose-4d.pdf (Accessed: January 10, 2012)

Rizzo S, Kalra M, Schmidt B, Dalal T, Suess C, Flohr T, Blake M and Saini S 2006 Comparison of angular and combined automatic tube current modulation techniques with constant tube current CT of the abdomen and pelvis *Am J Roentenol* **186** 673-9

Ruiz N, Katabathina V, Hatab M, Al-Senan R and Chintapalli K 2010 Use of GAFCHROMIC XR-QA Film for Entrance Skin Dose and Skin Dose Measurements during Computed Tomography-Guided Procedures; an Ongoing Study *Med. Phys* **37** 3463

Schindera S T, Nelson R C, Toth T L, Nguyen G T, Toncheva G I, DeLong D M and Yoshizumi T T 2008 Effect of patient size on radiation dose for abdominal MDCT with automatic tube current modulation: phantom study. *Am J Roentenol* **190** 100-5

Shrimpton P C, Hiller M C, Lewis M A and Dunn M 2005 Dose from Computed Tomography (CT) Examinations in the UK-2003 Review. (Chilton: National Radiological Protection Board)

Siegel M J, Schmidt B, Bradley D, Suess C and Hildebolt C 2004 Radiation Dose and Image Quality in Pediatric CT: Effect of Technical Factors and Phantom Size and Shape *Radiology* **233** 515-22

Siemens medical solution 2004 SOMATOMSensation 64 Application Guide:Protocols Principles Helpful Hints [online document] Available at http://www.medical.siemens.com/siemens/en_GB/gg_ct_FBAs/files/CIP/appl_guides/sensation/ApplicationGuide_Sensation64.pdf (Accessed: January 10, 2012)

Smith-Bindman R, Lipson J, Marcus R, Kim K-P, Mahesh M, Gould R, González A B d and Miglioretti D L 2009 Radiation Dose Associated With Common Computed Tomography Examinations and the Associated Lifetime Attributable Risk of Cancer *Arch Intern Med* **169** 2078-86

Smith S W 1997 - *Special Imaging Techniques / Computed Tomography in The Scientist and Engineer's Guide to Digital Signal Processing California Technical Publishing San Diego, CA, USA*

Smyth J and Doyle P Iterative Reconstruction with Philips iDose Characterising Image Quality in Attempting to Realise its Potential. Twelfth CT users group meeting [online] Available at http://www.ctug.org.uk/meet11-10-05/Iterative%20Reconstruction%20with%20Philips%20iDose%20characterizing%20image%20quality%20in%20attempting%20to%20realise%20its%20potential%20.pdf (Accessed December 1, 2013)

Söderberg M and Gunnarsson M 2010 Automatic exposure control in computed tomography--an evaluation of systems from different manufacturers *Acta Radiologica* **51** 625-34

Sookpeng S, Martin C J and Gentle D J 2013a Comparison of different phantom designs for CT scanner Automatic Tube Current Modulation (ATCM) system test *J. Radiol. Prot.*

Sookpeng S, Martin J C and Gentle J D 2013b A study of CT dose distribution in an elliptical phantom and the influence of automatic tube current modulation in the x-y plane *J. Radiol. Prot.* **33** 461-83

Sookpeng S, Martin C J and Gentle D J 2013c A study of dose distribution and image quality under an automatic tube current modulation (ATCM) system for a Toshiba aquilion 64 CT scanner using a new design of phantom [published conference paper] Available at <http://www.waset.org/journals/waset/v73/V73-17.pdf>

Sookpeng S, Martin C J, Gentle D J and Lopez-Gonzalez M R 2014 Relationships between patient sizes, doses and image noise under automatic tube current modulation (ATCM) systems *J. Radiol. Prot.* **34** 103-23

Strauss K J, Goske M J, Kaste S C, Bulas D, Frush D P, Butler P, Morrison G, Callahan M J and Applegate K E 2010 mage Gently: Ten Steps You Can Take to Optimize Image Quality and Lower CT Dose for Pediatric Patients *Am J Roentenol* **194** 868-73

The Phantom Laboratory 2006 Catphan® 500 and 600 user manual. Salem, NY: The Phantom Laboratory

Thomas M 2011 Dose optimisation. Presented at: Aquilion CT dose reduction-optimising your system 2011 Sep 27; Cumbernauld U.K.

Tsai H Y, Tung C J, Huang M H and Wan Y L 2003 Analyses and applications of single scan dose profiles in computed tomography *Med Phys* **30** 1982-9

Verdun F R, Lepori D, Monnin P, Valley J-F, Schnyder P and Gudinchet F 2004 Management of patient dose and image noise in routine pediatric CT abdominal examinations *Eur Radiol* **14** 835-41

Wood T 2012 Optimisation of the Philips CT automatic exposure control system [Presentation to Fourteenth CT users group meeting, Edinburgh] October 4, 2012

Zarb F, Rainford L and McEntee M F 2010 AP diameter shows the strongest correlation with CTDI and DLP in abdominal and chest CT *Radiat Prot Dosim* **140** 266-73

Zhou H and Boone J M 2008 Monte Carlo evaluation of CTDI¥ in infinitely long cylinders for water, polyethylene and PMMA with diameters from 10 mm - 500 mm *Med Phys* **35** 2424-31